Thesis to get the degree of a doctor of philosophy

Robust Damage Detection in Smart Structures

by

Fahit Gharibnezhad

Supervied by:

Dr. Jose Rodeallar Benede´

Dr. Luis Eduardo Mujica Delgado

Technical University of Catalunya

Department of Applied Mathematics III

CoDALabs

Barcelona, Spain

April 2014

International scientific reviewers to obtain international doctorate
Professor Dr. Mohammad Azarbayejani**,** University of Texas-Pan American, USA
Professor Dr. Andreas Kyprianou, University of Cyprus, Cyprus

Dean
Professor Dr. Alfredo Guemes, Technical University of Madrid, Spain

Referees
Professor Dr. Andreas Kyprianou, University of Cyprus, Cyprus
Professor Dr. Francesc Pozo, Technical University of Catalunya, Spain

Dedicated to my family,
my loving parents and my dear brother and sister
for they love, endless support and encouragement.

Contents

List of Figures

Abstract

This thesis is devoted to present some novel techniques in Structural Health Monitoring (SHM). SHM is a developing field that aims to monitor structures to make sure that they remain in their desired condition to avoid any catastrophe. SHM includes different levels from damage detection area to prognosis field. This work is dedicated to the first level, which might be considered the main and most important level. New techniques presented in this work are based on different statistical and signal processing methods such as Principal Component Analysis and its robust counterpart, Wavelet Transform, Fuzzy similarity, Andrew plots, etc. These techniques are applied on the propagated waves that are activated and captured in the structure using appropriate transducers. Piezoceramic (PZT) devices are chosen in this work to capture the signals due to their special characteristics such as high performance, low energy consumption and reasonable price. To guarantee the efficiency of the suggested techniques, they are tested on different laboratory and real scale test benchmarks, such as aluminum and composite plates, fuselage, wing skeleton, tube, etc. Because of the variety of tested benchmarks, this thesis is called damage detection in smart structures that are capable of sensing and reacting to their environment in a predictable and desired manner. This variety may promise the ability and capability of the proposed methods on different fields such as aerospace and gas/oil industry. In addition to the normal laboratory conditions, it is shown in this work that environmental changes can affect the performance of the damage detection and wave propagation significantly. As such, there is a vital need to consider their effect. In this work, temperature change is chosen as it is one of the main environmental fluctuation factors. To scrutinize its effect on damage detection, first, the effect of temperature is considered on wave propagation and then all the proposed methods are tested to check whether they are sensitive to temperature change or not. Finally, a temperature compensation method is applied to ensure that the proposed methods are stable and robust even when structures are subjected to variant environmental conditions.

Fahit Gharibnezhad, Technical University of Catalunya, 2014

Acknowledgments

Before any words, thanks to God almighty for the completion of this thesis. Only because of his blessing I could finish this work.

My sincere thanks must go to my supervisors Professor Jose Rodeallar and Dr. Luis E. Mujica whithout whom this work wouln't have been possible. I would like to thank them for encouraging my research and for allowing me to grow as a research scientist. I will appreciate all they have done for me forever.

I owe my deepest gratitude to the "Ministerio de Ciencia e Innovación" in Spain through the coordinated projects DPI2008-06564 and DPI2011-28033. Also thanks to the "Formación de Personal Investigador" of the "Ministerio de Ciencia e Innovación" for my FPI grant and the "Escola Universitaria d'Enginyeria Tecnica Industrial de Barcelona (EUETIB)" of the "Universitat Politecnica de Catalunya". Special thanks also to Control, Dynamics and Applications (CoDAlab) and its all members for all valuable days that I spent working in this group.

I would like to show my greatest appreciation to international reviewers of my thesis Professor Mohammad Azarbayejani from University of Texas-Pan American and Professor Andreas Kyprianou from University of Cyprus and for their brilliant comments, suggestions and feedbacks.

I am grateful to my committee members, professor Alfredo Guemes from Technical University of Madrid, professor Andreas Kyprianou from University of Cyprus and professor Francesc Pozo for serving as my committee members even at hardship.

I am deeply grateful to two SHM groups that warmly hosted me during my research visits in 2011 (Germany) and 2013 (USA) and allowing me to conduct my research and providing any assistance requested. Therefore, special thanks goes to Professor Dr.-Ing. Claus-Peter Fritzen and his group in "*Institut für Mechanik und Regelungstechnik, Universitat Siegen*", and all of its members, specially *Dr.-Ing. Maksim Klinkov* and *Dr.-Ing. Peter Kraemer* (for the test bed), *Mr. Gerhard Dietrich* (help with the experiment) and *Ms. Inka Buethe* and finally *Dr. Miguel Angel Torres-Arredondo* who his meticulous comments were an enormous help to me.

I would like to express my special appreciation and thanks to Professor Michael Todd and his group in university of California, San Diego (UCSD). And I would like to warmly appreciate the great support from the group and all of its members especially *Mr. Colin Haynes*, *Mr. Scott Ouellette, Mr. Richard Do, Mr. Eric*

Kjolsin and *Dr. Zhu Mao* for all of their supports and help during this stay. I also acknowledge and thank my dear friend, *Mr. Pouya Ghalei* for his friendly support during my stay in USA.

I am indebt to many friends, colleagues, students who assisted, advised, and supported my research and writing efforts over the years. Specially *Dr. Diego Tibaduiza*, for his collaboration during this project and *Mr. Edwin Santiago Baquero* for his friendly support in the group.

Fahit Gharibnezhad

Barcelona, Spain

13 April 2014

1. INTRODUCTION

1.1. Introduction

Nowadays, structures are an inseparable part of our life regardless of culture, religion, geographical location and economical development. It is almost impossible to imagine a world without man-made structures such as buildings, aircraft, bridge, vehicles, and so on. Their effect is obvious on all aspect of a society such as social, ecological, economical and cultural [1]. Due to the significant role that structures play, considering their health condition is a vital issue that needs a suitable attention. Regardless of their design, all of them have finite life spans and begin to degrade as soon as they are put into service. The better managed structure, the safer and more durable. There are mainly three reasons alter the state of structure from the domain specified in the design a) normal aging due to usage, b) action of environment and c) accidental events. For instance, processes such as corrosion, fatigue, erosion and overloads, degrade them until they are no longer fit for their intended use [2]. Depending on the value of a structure, the cost of its repairing and the consequences of its failing, a number of actions can be taken a) Wait until the structure breaks and dispose of it b) Wait until the structure breaks and repair it c) Examine it at periodic intervals and determine whether or not remedial action is needed. Many engineering structures, such as ships, bridges, aircraft, buildings, fall in to the latter category. For instance, collapse of certain structures, such as nuclear power plant, pipelines or aircraft, may provoke serious ecological pollution and irretrievable and catastrophic consequences. Examining periodically is the first solution that can be effective for important structures. This is what it called Time-Based maintenance and is the basic idea of Nondestructive Evaluation (NDE) that tries to develop some techniques and measurement technologies for the quantitative characterization of materials, tissues and structures by noninvasive means. The first problem of this method is lack of reproducibility of measurements due to variations in transducers and coupling conditions. Moreover, it is possible that the structure get to critical level earlier than the next session of monitoring that depending on the importance of structure can cause a catastrophic failure. Due to mentioned reasons, a much more reliable and trustable technology is needed to take care about safety of structures surrounding us. The solution for mentioned problem is to monitor the structure in any moment of its working life. It means implementing adequate hardwares in structure that beside the appropriate software can play a role very similar to the neural network in human. This helps somehow that health condition

of structure can be monitored almost online. It should be mentioned that successful structural monitoring techniques require information about the current behavior of the structure and methodology of analyzing this information for decision making. As a consequence extra sensors for monitoring the structural behavior should be hardwared on a structure. The measurements from these sensors constitute the data that is fed to the software for analysis and decision making about the structural health state. To achieve this goal, various methodologies in the field of SHM have been proposed to deal with this situation. SHM aims at real-time characterization of structural performance to enhance structural safety and to significantly reduce lifetime operating costs by early detection for maintenance. SHM has emerged as an important research area in recent years by early damage detection because of its strong links with structural safety and the need to monitor and extend the lives of existing structures. Many methods and approaches have been developed both in hardware and software area that presents a promising solution for having more reliable structures. For instance, damage detection and identification using guided waves is one of the main interests in this field. The majority of developed methods are satisfactory in laboratory environment where steady conditions prevail. As a consequence most of them are affected by a variety of interference sources including high-frequency ambient noise, outliers, low-frequency structural vibration, and environmental changes such as temperature fluctuation, inhomogeneity and anisotropy of materials. Therefore, there is a great demand to develop some kinds of algorithms that are more reliable in real conditions.

1.2. Motivation of work

Between $1990-2007$ there were 1502 commuter aircraft crashes in the U.S. of which 386 (26%) were fatal, resulting in 1104 deaths. The German Eschede train crash in 1998, the world's most serious high-speed train disaster, was caused by fatigue cracks in the wheel rims under repetitive load ($500,000$ cycles per day) (see Figure 1.1-c)[3]. Total of $5,657$ accidents since 1927 were identified as having fatigue fracture as a related cause, and these accidents resulted in 2240 deaths [4]. Figure 1.1 shows some examples of structural fatigues. The consequences of failing in this kind of structure are such irreparable that regular inspections are performed by skilled engineers to assess the health of structures and systems. This inspection process is necessary, costly and usually finds no faults. It is also subject to human error, meaning that some unnecessary maintenance is performed and some faults go undetected. For this reason, billions of dollars are spent every year maintaining and repairing buildings, bridges, aircraft, railroads, and other infrastructure. Early damage detection and eventual estimation of damage is an important problem to determine any decision for structural repair and prevention of disasters.

Conventional inspection methods are not only costly, but are not always effective in revealing appropriate safety concerns. Continuing failures which affect engineering

(a) Aircraft collapse [5] **(b)** Bridge collapse [6] **(c)** German train accident [7]

Figure 1.1.: Catastrophic consequences of collapsing structures

structures is the main reason for this claim. Therefore, more reliable systems are needed to ensure the integrity of structure and avoid happening catastrophes anymore. SHM is the most promising solution for mentioned problem. In many cases, an adequate health monitoring system installed on the structure can detect and isolate the damage before it becomes catastrophic, thereby reducing the likelihood of failures. On the other hand, SHM systems can reduce costs and save lives. As an example, the United State Federal Highway Administration (us FHWA) reported in 2006 that approximately $12 Billion was spent in the United States in 2004 on new bridge construction, bridge replacement, and bridge rehabilitation. It was also reported that 13.1 percent of bridges in the U.S. are structurally deficient, meaning that they show signs of deterioration and may have reduced load bearing capabilities, and that 13.6 percent of bridges in the United States are functionally obsolete, meaning that their geometry no longer conforms to current standards [8].

1.3. Objectives

The main objective of the current thesis is to develop a methodology for the detection and classification of damages in structures, focusing more on aeronautical structures. This aim is achieved by using the paradigm that any damage in the structure produces changes in the vibrational responses. Changes will be detected by means of different pattern recognition tools and signal processing such as Principal Component Analysis, Statistical Pattern Recognition, Wavelet transform, Fuzzy logic. Main attempt in developing the new methodologies goes to analyze their sensitivity against environmental changes such as temperature and applying compensation method if it is necessary. It leads to presenting new damage detection and classification methods as well as scrutinizing their stability against temperature change. This might help to obtain more reliable and trustable results in presence of condition variations.

To achieve the main objectives, some specific objectives are fulfilled

- To study the fundamental approach of wave propagation theory and dam-

age detection using lamb waves in different structures such as aluminum and composite plates, fuselage and tubes.

- To study the different pattern recognition techniques such as Principal Component Analysis, Wavelet, etc. and their application on damage detection.
- To present novel damage detection features based on the mentioned mathematical techniques.
- To analyze the sensitivity of the presented methods to environmental changes and enhancing the methods with the aim of robustification.
- To validate and implement the developed methods in different structures in laboratory scale.
- To validate and implement the developed methods in different structures in real scale.

1.4. Outline of the contribution

This work is dedicated to present new methods and strategies for damage detection in smart structure. To achieve this goal, a series of techniques are presented that are able to detect and classify damages in structures based on wave propagation method. The propose of new indices are based on different statistical and mathematical approaches such as Principal Component Analysis, Wavelet transform, Fuzzy logic etc. The presented indices are validated and tested on different structures such as aluminum and composite plates, aircraft fuselage, pipe tubes, aircraft wing and so on. The result of analysis show that new damage detection approaches that are presented in this work are able to distinguish between healthy of structure and the damaged one. After that, it will be shown that any damage detection method might be non-stable when environmental condition is changing. To show this, the effect of temperature effect, as one of the main environmental parameters, is tested on the wave propagation as well as the performance of the new indices. In this work it is analyzed, the sensitivity of the presented indices to the temperature fluctuation and in case where this phenomena can mask the effect of the real damage, it is compensated using an appropriate temperature compensation method.

1.5. Research Collaborators

Lately, the research group “Control, Dynamics and Applications Laboratory (CoDALab)” in the Department of Applied Mathematics III of Universitat Politecnica de Catalunya (UPC) has been working in SHM to aeronautical structures since 2008 through the project DPI2008-06564-C02-01/02 in coordination with the “Universidad Politécnica de Madrid (UPM)” supported by “Ministerio de Eduación y Ciencia

de España". In the subsequent project DPI2011-208033-C03-01, UPC, UPM and the new partner: IKERLAN are extending the developed methodologies to the other kind of structures such as wind energy plants. The current proposal is linked to this research and makes use of a series of statistical techniques for the detection, classification and localization of defects in such structures considering in some cases, variation in operational/environmental conditions.

Moreover 3 research visites were conducted to analyze the methodologies on different structures. The first one is one week visit to the Technical University of Madrid. The details of this visit and experiments are presented in Section 4.2. In addition, a six-month visit is done to collaborate with Siegen university that the detail of work is presented in Section 4.3 and Finally, a three-month stay is done collaborating with SHM laboratory in University of California, San Diego that more information can be found in Section 4.4.

1.6. Thesis organization

This dissertation is organized in seven chapters. Chapter 1 contains introduction and objectives of the work. Chapter 3 contains general information about Lamb waves, their mathematical description and some key points such as dispersion. In this chapter, the most applicable approaches for activation and detection of Lamb waves are presented. In addition, the theoretical background of methodologies that are applied in this work is presented in this chapter. Chapter 2 is dedicated to a general overview of Structural Health Monitoring. In this chapter some key points and definition such as "damage" and "damage type" and definition of damage detection is reviewed. Besides, a comprehensive overview on the SHM state of the art is presented in this chapter. Chapter 4 details the case studies and laboratory efforts on different structures that have performed in this survey. Chapter 5 discusses the result of new damage detection strategies and indices that are presented through this thesis. Chapter 6 is dedicated to analyze the performance and sensitivity of the novel approaches when there is a temperature fluctuation. Moreover, in this chapter the temperature compensation is presented for the indices that are highly sensitive to the temperature change. Finally, Chapter 7 contains a conclusion on the achievements of this thesis as well as some proposal for future research and main pursuing objectives to conclude this thesis.

2. STRUCTURAL HEALTH MONITORING REVIEW

This chapter present a literature review on Structural Health Monitoring (SHM). To do this, a brief review on SHM status of art is presented and moreover, different definitions such as damage, damage detection, major approaches for damage detection and finally environmental effects on SHM are described. To start, a brief review on the definition of SHM is presented and it is briefly compared with NDE/T. After that, the basic definitions in this area are presented. Next, the most commonly used damage detection approaches are reviewers. Then, a review on damage detection approaches on vibration based method is presented and finally a literature review on temperature effect on SHM techniques as well as temperature compensation techniques are presented.

2.1. Introduction

In engineering and architecture, a "structure" is a body or assemblage of bodies in space to form a system capable of supporting loads. The importance of structures in our lives is the difference between a safe house and an insane one or a reliable flight or daunting one. All man-made structures have finite life spans and begin to degrade as soon as they are put into service. Different processes such as fatigue, corrosion, erosion, wear and overloads degrade them until they are no longer fit for their intended use. Moreover, all materials used in engineering structures have some inherent initial flaws. Under environmental and operational loading, flaws will coalesce to form damage that produces component level failure and further loading causes system-level failure. Due to the significant role that structures play in our life considering their health condition is a vital issue that attracts a suitable attention. Structural Health Monitoring is one of the most promising solutions that could be chosen to deal with this issue. The first and the most obvious benefit of SHM is increasing human safety, indeed, much of research in this area is motivated by disasters where many lives have been lost [9]. Besides, a structural health monitoring system can provide engineers with some valuable information such as real-time monitoring. This could have various benefits such as reducing labor cost, system downtime and human errors. This also can improve safety and reliability of the structure.

Therefore, detecting these flaws, damages, in the early status is an important issue

that should be considered. Current developments in computation, sensing components and communications have led to a significant interest in developing new detection and diagnostic technologies for structures. This makes happen the design of on-line monitoring and real-time damage detection systems that minimize human involvement [10]. Indeed, the field of SHM developed through the combination of nondestructive evaluation/test (NDE/T) methods and novel sensing and actuation techniques to create intelligent monitoring systems permanently installed on structures. SHM can be applied to many sectors of infrastructure including civil, mechanical, and aerospace systems.

To be successful and competitive, a SHM system should have some specifications. For instance, Croxford *et al.* [11] consider a good sensitivity to defects, preferably with the capability of detection and localization, with a small number of sensors as one of important specification of a successful SHM system. SHM typically uses a sensor network that monitors the behavior of the structure. Typical sensors are optical fibers, electrical resistance, piezoelectric, strain gauges or acoustic devices. SHM should be viewed as a complementary method to available NDT/E methods. Indeed, as a first comparison between NDE/T and SHM, it should be mentioned that NDT/E is implemented offline and locally, whereas SHM is implemented online and globally which can be used to capture health monitoring data and perform more precise inspections of local areas of a component [12]. Figure 2.1 shows a simple comparison between NDE/T and SHM system. The next section presents a detailed review on SHM.

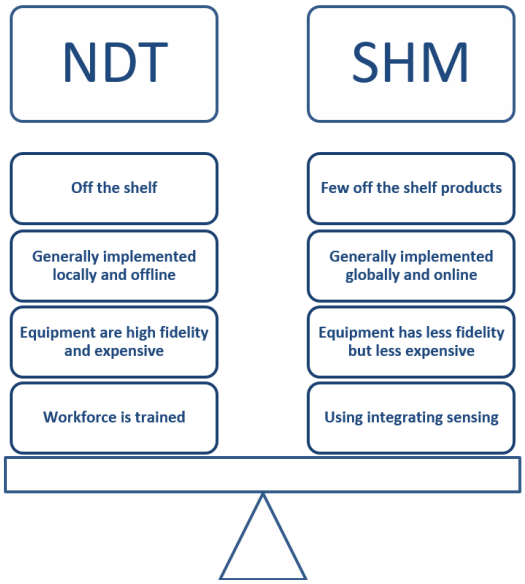

(a) SHM vs NDE/T [13]

Figure 2.1.: Comparison of NDE and SHM

Several reviews from different aspects are published about Structural Health Monitoring. Doebling *et al.* [14] present a comprehensive review on SHM from vibration

characteristic perspective. They summarize the application of SHM on different structures such as beam, plate, shell, bridge, offshore platform, aerospace structure and composite. They present another review on method based on vibration-based damage identification method in 1998 [15]. Three years later, in 2001, Los Alamos National Library publishes a report that covers the most important topics in SHM field such as feature extraction, data acquisition, statistical methods, etc [16]. Farrar *et al.* [17, 18] present two short reviews on vibration based methods from statistical pattern recognition perspective. Besides Carden *et al.* [19] summarize the vibration based SHM in structural engineering applications. Worden *et al.* [20] review different case studies on SHM from machine learning point of view. Fan *et al.* [21] present a comprehensive review on modal parameter-based damage identification methods for beam or plate-type structures. Other reviews on specific fields such as SHM in civil structures [22] or SHM in railway industry [23] are also useful to be alluded.

Beside the short reports, several authors have published fruitful books in this field. Here, a brief review on some of them is presented and they could be useful for the readers, specially the novices on this field. *Encyclopedia of Structural Health Monitoring* [13] is perhaps the most comprehensive book that consist of different reports and summaries that covers many aspects of SHM. Some other books pay attention to specific techniques For instance, Pawar *et al.* [24] have written a book that covers the latest achievements on SHM using genetic and fuzzy systems. In addition to the formulation of fuzzy and genetic systems they describe the application of these methods on different case studies such as beams, composite tubes and composite helicopter rotor. As a precise book on the usage of Wavelet transform in SHM, Gopalakrishnan *et al.* [2] is a valuable example. They first present a useful fundamental description about the structures behavior such as elasticity and also wave propagation rules. Then they present a review on different signal processing techniques on SHM such as Fourier transform and wavelet transform. They also describe finite element methods and spectral finite element method. Modeling of actuators and sensors is another topics that is covered in their book. Su *et al.* [3] present a book that is a very wise option as a starter for new researcher in SHM field. They present a comprehensive and easy-understandable review on wave propagation fundamental. Moreover, they cover different topics on Lamb waves such as activation and receiving, sensor and sensor location. In addition, they cover a brief review on signal processing on SHM on different case studies.

2.2. Structural Health Monitoring as a damage assessment approach

Generally speaking, there are three key multidisciplinary areas for which monitoring and damage assessing are principal concerns:

- Condition Monitoring (CM)

- Non-Destructive Testing / Evaluation (NDT/E)
- Structural Health Monitoring (SHM)

Condition monitoring (CM) is the process of monitoring a parameter of condition in machinery (vibration, temperature etc), in order to identify a significant change which is indicative of a developing fault. CM is relevant to rotating and reciprocating machinery, such as used in manufacturing. CM also uses on-line techniques that are often vibration-based and use accelerometers as sensors.

Nondestructive Testing/Evaluation (NDT/E) is a very broad, interdisciplinary field. The main goal of this field is to assure that structural components and systems perform their function in a reliable and cost effective fashion. These tests are performed in a manner that does not affect the future usefulness of the object or material. In other words, NDT allows parts and material to be inspected and measured without damaging them. The technologies that are used in NDT are similar to those used in the medical industry, but nonliving objects are the subjects of the inspections. As a comparison between NDE and NDT, it should be mentioned that NDE is used to describe measurements that are more quantitative in nature. For example, an NDE method would not only locate a defect, but it would also be used to measure something about that defect such as its size, shape, and orientation. NDE may be used to determine material properties, such as fracture toughness, form-ability, and other physical characteristics. NDE techniques in their various forms are crucial for the infrastructure, power generation, chemical and transport industries, and the use and applications of certain techniques are well-established. Technological development in the area means that new methods, based on the most varied natural phenomenon, are constantly being incorporated in routine industrial inspection and becoming one of the "traditional" NDE methods [25]. As some examples for NDT/E method, X-ray and electron microscopy could be mentioned.

SHM stands at the next level. Basically, the process of implementing a damage identification strategy for aerospace, civil and mechanical engineering infrastructure is referred to as structural health monitoring. SHM is necessary for various aerospace, mechanical, and civil engineering applications for evaluating the fitness of a structure to perform its prescribed tasks. The structure may change its performance based on a gradual or sudden change in state, load conditions, or response mechanisms. The difficulty of thorough visual inspection of structures has increased the need for complex SHM systems that can provide early and reliable damage detection in critical and historical structures [26].

The main objective of developing the SHM system is to enhance structural safety. However, SHM serves other economic benefits such as increased mission reliability, extended life of life-limited components, reduced tests, reduction in "down time", increased equipment reliability, customization of maintenance actions, and greater awareness of operating personnel, resulting in fewer accidents [27]. Pawar *et al.* [24] define the traditional SHM as a method based on manual feedback such as abnormalities reported by means of warning, caution, advisory, and/or maintenance

panels. The abnormalities were considered based on exceedance monitoring of various measurements such as vibration, temperature, pressure, strain, frequency, acceleration, displacement, and load. They define exceedance monitoring as some operations performed by the operators manually at various critical locations and for any critical components of the system to monitor that measurements do not exceed predefined thresholds. But recent years and because of development of different technologies and sensing techniques for damage detection in metallic and composite materials, this procedure gets more and more automatic. New techniques are capable of achieving continuous monitoring, integrated and on-line damage detection systems for aircraft maintenance [28]. It should be mentioned that hardware and software are both inseparable parts of SHM. The hardware elements are essentially the sensors and the associated instrumentation, while the software components consist of damage modeling and damage detection algorithms. Gopalakrishnan *et al.* [2] consider a general vision for SHM as developing structures with network of sensors, which periodically and continuously provide data. They mention that sensors may be active or passive, whereby passive sensors such as strain gauges only receive (or sense) signals, while the active sensors both receive (or sense) and transmit (or actuate) signals.

They summarize an SHM system encompassing the following components:

- The structure on which the SHM system will be placed
- Sensors, which can be of contact or non-contact type
- Data acquisition systems
- Signal processing
- Damage modeling and damage detection algorithms
- Data transfer and storage mechanisms
- Data handling and management

Worden *et al.* [29] have alternate way of looking at SHM as a discipline combination of the following four subjects:

- Condition based monitoring
- Non-Destructive Evaluation (NDE) technologies
- New modeling methods
- New sensor technologies

In health monitoring of some specific structures such as aircrafts, SHM can also be classified differently, namely on-line SHM and off-line SHM. In on-line SHM, the host of sensors is on-board the aircraft to provide outputs during its flight. The recorded data needs to be post processed to assess the state of the structures. This is indeed quite challenging. In off-line SHM, the aircraft is monitored when it is in the hangar [2].

From another point of view, SHM approach could be divided to two main categories, diagnosis and prognosis. Diagnosis aims to give, at every moment during the life of a structure, a procedure to determine the state of the structure. This procedure considers the structure in two levels. First, materials of the different parts, and second, the full assembly of these parts that constitute the structure as a whole system. Hence, the diagnosis procedure will notify the beginning of damages such as cracks, its location and its extent [2]. Damage prediction, or prognosis, requires that damage laws be used; model-based prediction uses physics laws to forecast the growth of damage, whereas data-driven prediction uses trends to forecast the growth of damage.

Farrar *et al* [18] considers the most important challenges of the SHM as follows. According to them, the damage is typically a local phenomenon and may not significantly influence the lower-frequency global response of structures that is normally measured during system operation. In addition, in many situations feature selection and damage identification must be performed in an unsupervised learning mode. That is, data from damaged systems are not available. Damage can accumulate over widely varying time-scales, which poses significant challenges for the SHM sensing system. Finally, a significant challenge for SHM is to develop the capability to define the required sensing system properties before field deployment and, if possible, to demonstrate that the sensor system itself will not be damaged when deployed in the field.

2.3. Smart structures

Structures that are capable of sensing and reacting to their environment in a predictable and desired manner, through the integration of various elements, such as sensors, actuators, power sources, signal processors, and communications network are referred to as “smart” [28]. Smart structures can respond adaptively in a predesigned useful and efficient manner to changes in environmental conditions, including any changes in their own condition. This is why they also could be called “adaptive structures”. Smartness ensures that the structure gives optimum performance under a variety of environmental conditions [30]. In addition to carrying mechanical loads, smart structures may alleviate vibration, reduce acoustic noise, monitor their own condition and environment, automatically perform precision alignments, or change their shape or mechanical properties on command [28]. Smart structures is a multidisciplinary definition that covers different topics such as energy harvesting, non-destructive evaluation (NDE), damage detection, structural health monitoring (SHM), dielectric elastomers, actuators, shape memory alloys and polymers, magnetorheological fluids, electroactive polymers (EAP), bioinspired and robotic systems, and smart materials, sensors, systems, and networks.

2.4. Damage detection

2.4.1. Damages

There are several definitions for "damage" in structures depending on the case. Pawar [24] defines damage as "a deficiency or deterioration in the strength of a structure, caused by external loads, environmental conditions, or human errors". Staszewski [28] defines damage as "material, structural or functional failure". Worden [29] defines damage as "when the structure is no longer operating in its ideal condition but can still function satisfactorily". Farrar [18] defines damage as "changes to the material and/or geometric properties of these systems, including changes to the boundary conditions and system connectivity, which adversely affect the system's performance". Cross et al. [9] consider any gradual or sudden change in structure as a damage. And generally speaking, damage can be defined as "changes introduced into a system that adversely affect its current or future performance". The term damage does not necessarily imply a total loss of system functionality, but rather that the system is no longer operating in its optimal manner. Physically, damages may be visible as a crack, de-lamination, de-bonding, reduction in thickness/cross section, or exfoliation. The damage may not be easily visible to the naked eye. For example, composite structures are susceptible to barely visible impact damage (BVID). Operational structures are designed to operate with some amount of damage; i.e., they are damage tolerant. But as the damage grows, it will reach a point where it affects the system operation to a point that is no longer acceptable to the user. This point is referred to as "failure". The term damage therefore, carries a very different meaning compared to the term failure.

2.4.2. Damage types

There are many different types of damage in metallic and nonmetallic structural material components such as plastic deformation, erosion, delamination, corrosion, fiber mission, matrix cracking, etc. In this section a brief review of some of them is presented.

Breaking Fasteners and Joints is the primary source of damage in bolted joints, especially under cyclic transverse loading. As a nut is rotated on a bolt's screw thread against a joint, the bolt extends. This extension generates a tension force (or bolt preload). The reaction to this force is a clamp force that causes the joint to become compressed (see Figure 2.2-a).

Cracks in homogeneous material components can initiate for a variety of reasons including sudden overloads and cyclic fatigue loading. Cracks initiate in areas of a component where there are anomalies (e.g. dislocations) in the material microstructure and/or geometrical stress concentrations (e.g. fillets, holes). Crack also

may change the dynamic characteristics of the structure. Figure 2.2-b shows a crack in a body of industrial oven.

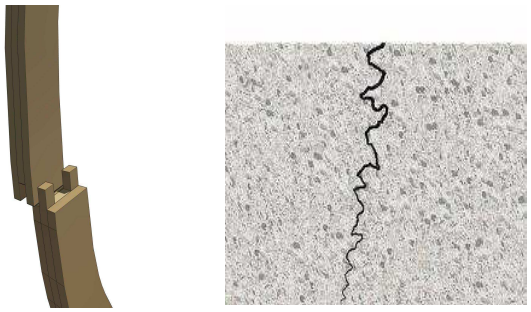

(a) Breaking fasteners and joints [31]

(b) Crack in material [32]

Figure 2.2.: Damage examples in structures and materials

Plastic Deformation is usually caused by impacts and other forms of overload, shock, or other foreign object impact (micrometeorites, birds, etc.). When the material is permanently deformed due to these impacts, the local geometry of the component changes leading to changes in local stiffness, damping and possibly even mass distribution (in the case of full penetration) [12]. For instance, Figure 2.3 (left) shows a sample of plastic deformation.

Erosion occurs due to repeated rubbing (abrasion) and impacting between two components. For example, erosion occurs between ball bearings and the inner and outer race of the bearing housing. As the balls and races erode, material flakes enter the lubricant and can be detected to identify this form of damage (often called Spalling) [33]. Figure 2.3 (right) shows an example of erosion.

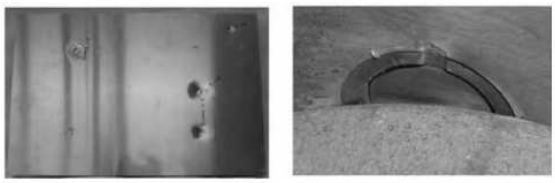

(a) (left) plastic deformation, (right) erosion[12]

Figure 2.3.: Example of plastic deformation and erosion

Delamination occurs when the layers of a laminated material component separate, the component does not resist bending moments as strongly. Laminated materials derive bending stiffness from the transfer of shear forces from one layer to the adjacent layers; therefore, if the layers separate, the bending stiffness goes down. The damping of the material increases at the location of separation as in the case of a crack because the material undergoes relatively large motions at that point,

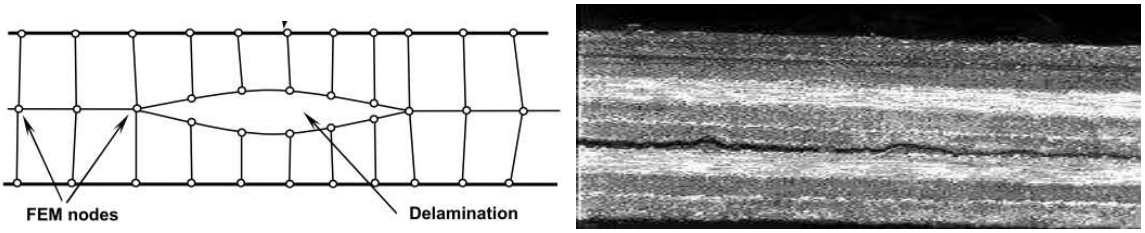

(a) schematic [3] **(b)** snapshot [34]

Figure 2.4.: Delamination in composite

increasing the local dissipation of energy. Figure 2.4 shows snapshot and a sample of delamination in a composite material.

Corrosion occurs due to environmental chemical loading, which causes pitting, exfoliation and other forms of corrosive damage including hydrogen embrittlement. Corrosion at low temperatures is primarily due to solid–liquid interactions and is accelerated by high temperatures. At high temperatures, however, solid–gas interactions are primarily responsible for material loss leading to oxidation. Corrosion in the form of pitting also introduces small holes in the surface of a material component (see Figure 2.5).

(a) corrosion [35]

Figure 2.5.: Example of corrosion

In composite material components, loads are carried primarily by the fibers or filaments. Fibers missing due to fiber pullout can occur during manufacturing or operation as high tensile loads along the fiber cause the fiber to debond and slide along the matrix. The region from which fibers have slide out is weaker than the bulk material leading to potential cracking in the plies (see Figure 2.6-a). Matrix cracking is relatively common in composite materials. Although this type of damage is less critical than broken fibers but it is still an important type of damages that should be considered. Composite elastic properties are a function of the fraction of matrix present in the material. If some of the matrix fails due to cracking, then the

elastic properties weaken (see Figure 2.6-b).

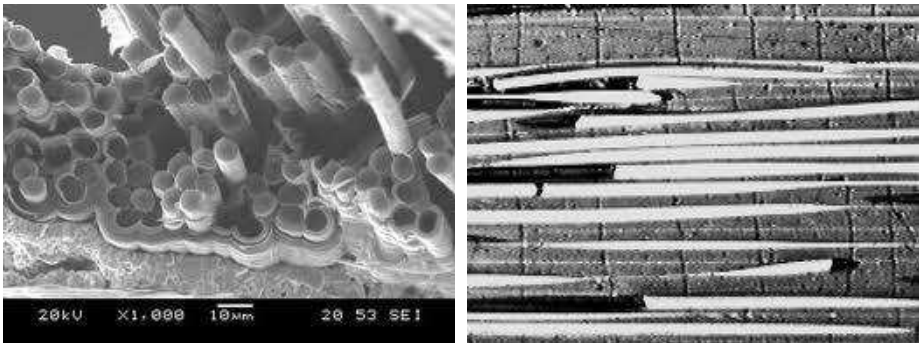

(a) Fiber pullout [36] **(b)** Matrix cracking [15]

Figure 2.6.: Examples of fiber pullout and, matrix cracking in composites

In spite of the type, early detection of damage is an important issue that can help to prevent failure of structures the same as early detection of heart disease and cancer can prevent premature death in a human. Once the damage is detected, appropriate action needs to be taken to repair the structure. This aim, understanding the state of damage, can be achieved either directly or indirectly. The first approach checks for the damage type (e.g. cracks, corrosion or delamination) by applying an appropriate inspection technique based on physical phenomenon. The established inspection techniques vary from visual inspection by the naked eye to passing the structure through a fully automated inspection. In the indirect approach structural performance or rather structural behavior is measured and compared with the supposedly known global response characteristics of the undamaged structure. If the effect of certain damages on structural response characteristics is known, this approach provides an indirect measure of damage and of structural health. Obviously, in both the direct and indirect approaches the sensitivity and the reliability of inspection are important quantitative performance measures [28]. One of the major problems in this area is to establish relevant parameters used for monitoring damage as well as subsequent damage accumulation. In next section damage detection's perspective is reviewed in more details.

2.4.3. Damage detection

According to Pawar [24], damage detection is defined as "the identification of existence of an anomalous condition in a system". Worden defines the damage detection as "method that gives a qualitative indication that damage might be present in the structure" [28]. Most damage detection and localization methods that have been proposed are based upon comparing monitored signals to baselines recorded from the structure prior to initiation of damage [37]. The simplest method is to subtract two signals and compute either the peak amplitude or the energy of the residual.

This approach is very effective if damage is the only factor causing the signals to change.

Detection includes different steps such as active and passive sensing, signal processing, feature extraction, and data fusion. Passive detecting systems are generally based on detecting changes in a chosen property which usually occur as a result of an event (e.g. strain [34] or acoustic emission [36]). Active SHM systems differ from passive systems in the sense that an excitation is applied to the structure, causing a response which is then measured and evaluated (e.g. modal analysis methods based on excitation [15] or ultrasound [38]). Passive approaches are relatively simple but more susceptible to measurement variability, while active approaches use actuation signals to better locate and quantify damage [12].

According to Rytter [39], it is possible to proceed with a four-level damage assessment scale if it is necessary to obtain more and more information on the damage (see Figure 2.7). While level I only gives the information that the damage is present in the structure, level II provides the location(s) of the damage. At level III, the extent of the damage is evaluated. Therefore, a parametric model is needed to describe the damage (crack length, the size of a delamination, stiffness decrease or else a loss of mass). It should be mentioned that the determination of the type of damage is sometimes included as an extra step between level II and III. The mentioned levels are considered as damage diagnosis, which generally means qualitative or quantitative identification and assessment of damage. The next level that is highest and most sophisticated is called prognostic step. Prognosis is the prediction of the amount of safe life left in a system. To achieve this, it is necessary to combine the global structural model with local damage models. This combination can describe the evolution of damage or fatigue crack growth [40].

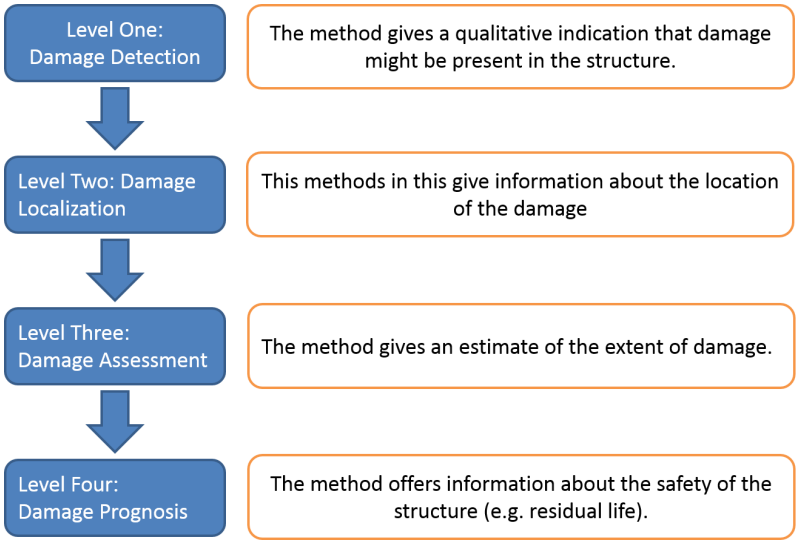

(a) [39]

Figure 2.7.: Damage detection hierarchy

In the next section the main approaches for damage detection are briefly described and then the state of art is presented for the main techniques that are used in this work for damage detection.

2.5. Damage detection major approaches

Several approaches have been implemented in SHM fields such as modal-data based approach, electro mechanical impedance, thermomechanical models, data interrogation approaches, thermal imaging methods, Eddy-current methods, finite element, vibration based damage detection, etc. In this thesis, the latest approach, vibration based damage detection, is used for damage detection. Therefore, in this section a brief review of this approach is presented.

2.5.1. Vibration based damage detection

The principle that uses vibrations as characteristics of solid bodies to test their quality or consistency and distinguish good or bad conditions is widely used in daily life. For example, when buying drinking glasses, it is commonly accepted that the bright sound indicates a flawless glass, and a dull tone refers to something that is different about a piece. Traditionally, experienced traders tested the quality of large cheeses by knocking on them and listening to the sound. The degree of ripeness of melons can also be tested by a similar procedure. Many other examples can be found in the literature [41]. The same basic principle can also be applied to technical structures. Research on vibration-based damage identification goes back to the late 1970s in the study of offshore oil and gas platforms as well as in the aerospace industry [26]. The classical way to gain information on the measurement of an existing structure (with respect to its dynamic behavior) is to retrofit this structure with a set of sensors, excite it with an actuator or use the natural forces of the environment to process the data on computers. Motivated by concepts of smart structure, modern approaches to SHM include sensors, actuators and computational intelligence, which process and control the information from the early design phase to an integral part of the structure. The aim of vibration-based structural health-monitoring (SHM) methods is to detect the appearance of damages by evaluating changes in the identified vibration characteristics. That way, the aim is to mimic the biological system, composed of a nervous system (sensing), muscles (actuation) and a brain (processing, storing and recalling information). Communication between the smart structure and the environment can be achieved via data networks, such as the Internet. To see if something has changed, the measurement data have to be evaluated and some characteristic features, such as means, variances, maximum/minimum values, spectral information, etc. have to be extracted by pure signal analysis. We can compare the actual values with the reference values which derive from the undamaged state of the monitored system, and apply the appropriate method [42]. Two main important

subsections of vibration based damage detection are Acoustic emission and Elastic wave based.

Acoustic emission

It is based on the fact that rapid release of strain energy generates transient waves, whereby presence or growth of damage can be evaluated by capturing damage-emitted acoustic waves. This method is able to triangulate damage in different modalities including matrix crack, fiber fracture, delamination, microscopic deformation, welding flaw and corrosion. It is also able to predict damage growth and it is surface mountable and good coverage. It is prone to contamination by environmental noise and therefore, the signals acquired are quite complicated. It could be used for locating damage only. This passive detection technique is unable to further evaluate damage severity. Because of high damping ratio of the wave, it is suitable for small structures only [43, 44, 45].

Elastic-wave-based

By using Lamb wave tomography and based on the fact that structural damage causes unique wave scattering phenomena and mode conversion, quantitative valuation of damage can be achieved by scrutinizing the wave signals scattered by damage. This method is cost-effective, fast and repeatable; able to inspect a large structure in a short time, sensitive to small damage, no need for motion of transducers, low energy consumption and able to detect both surface and internal damage. On the other hand, there is a need for sophisticated signal processing due to complex appearance of wave signals, multiple wave modes available simultaneously. It is difficult to simulate wave propagation in complex structures and, it is also strongly dependent on prior models or benchmark signals. It should be mentioned that a wave-based approach can quantitatively evaluate damage that is greater than half the size of its wavelength.

2.6. Damage detection strategies based on vibration analysis

To achieve the objectives of this thesis, different techniques are used such as Principal Component Analysis (PCA) and its robust counterparts, wavelet transform, etc. Therefore, in this section, a brief review is presented on the state of art of those major techniques which are used in this thesis. One of the main concentration of the thesis is on Principal Component Analysis (PCA) and its robust counter part. Both form a significant part of almost all techniques that are used in this work. After that the status of art for wavelet transform is briefly reviewed.

2.6.1. Principal Component Analysis (PCA)

Principal Component Analysis plays a vital role in statistical analysis; PCA, also known as Karhunen-Loève decomposition or Proper Orthogonal Decomposition (POD), is a multivariate statistical technique that was firstly introduced by Pearson [46], developed independently by Hotelling [47] and used for first time in the mechanics community by Lamley [48].

As it is mentioned before in the theoretical description (section 3.5), the central idea of principal component analysis is to reduce the dimensionality of a data set in which there are a large number of interrelated variables, while retaining as much as possible of the variation present in the data set [49].

In addition to its main usage as a dimension reduction tool, it can be used as pattern recognition, data interpretation, visualization, outlier detection and clustering tool [50, 51] in various engineering fields including Structural Health Monitoring. In the next few paragraphs, the latest application of PCA in SHM is reviewed. After that, the drawbacks of PCA are considered and it is mentioned why we need to reconsider the SHM techniques that are using PCA by changing to a robust variant.

PCA has been widely used in Structural Health Monitoring (SHM) in different ways. A brief general review of some applications is presented as follows. PCA is used as a clustering tool for acoustic emission (AE) transients in a composite laminate to detect matrix cracking and delamination in [52]. PCA is applied as visualization and clustering tool on acoustic emission data from box girder of a bridge for tracking crack development in [53]. Moreover, PCA is used as dimension reduction, classifier and visualization method for monitoring different operating conditions of automobile gearbox in [54]. Tong *et al.* [55] apply PCA on power spectral density (PSD) of impact-acoustic data to inspect defects assessment of tile-wall. Also they use a first two principal components as feature vectors of an artificial neural network (ANN) for classification purposes. Mustapha *et al.* [56] apply PCA on transmitted ultrasonic guided wave in hollow cylinder-like structure to classify undamaged conditions from damaged one. In another work, the same approach is applied on aircraft wing holder [57]. PCA is used beside wavelet transform for fatigue crack detection in [58]. References [59, 60] define a damage index as a comparison between the hyperplanes (subspace spanned by PCA) associated with healthy and damaged structure. [61] uses PCA as a monitoring technique for the diagnosis of bearing faults. In their works, they consider the effects of environmental condition changes as well as proposing a novelty criterion to isolate the area in which the faulty bearing stands. Reference [62] uses PCA to find out the intrinsic dimension of data in both "bad" and "good" conditions and claims that intrinsic dimension of data could be used as a damage index in machine condition monitoring. The work in [63] uses PCA as a machine conditioning tool on internal-combustion engine as well as automobile gearbox. Moreover, they propose a method to select the most appropriate representative PCs somehow that the selected low-dimensional PC representations respect the best statistical information of the machine. T^2 and Q statistic are implemented

on guided waves for damage detection in [64]. Their technique is based on the creation of a statistical data-driven PCA model for normal operation condition, so that any fault condition cause deviation from this model that can be detected using statistic indices. The work in [65] applies the same approach to detect, localize and identify the severity of very early tooth defects (deformation, breakage or fracture of the teeth) on industrial helical gearbox. PCA is implemented on hardware to establish a distributed system to achieve the goal of on-line monitoring and real-time damage detection in [10].

In a specific case of SHM, damage detection and localization, the way that PCA is used can be divided into two modes. In the first mode it plays the direct role to detect and localize the damages, while in the second mode PCA is used as a primary step for other algorithms. The works in [62, 61] are some examples that belong to the first type. As more examples, [66] first applies PCA to remove the effect of environmental changes and operational condition and then uses residual errors of PCA as a damage indicator for long term structural health monitoring. Besides, [67] applies PCA on frequency response function as well as transmibillities for an experimental damage detection of aircraft wing. The work in [64] is an example of the second type. As more examples, [68] implements two indices to detect and localize damages based on a model obtaining from projecting information using PCA.

2.6.2. Wavelet transform

Time-frequency evolution of the signal such as WT plays an important role in the analysis of transient non-stationary ultrasonic signals. Several factors, such as the change of the environmental conditions make the output signal of the structure contain non-stationary components [69]. WT has proven its ability to overcome many of the limitations of the other methods such as short-time Fourier transform, Gabor transform and Wigner distribution [70, 71]. The superiority of WT over other signal processing tools is its ability to decompose signals simultaneously both in time and frequency with adaptive windows. The advantage of algorithms based on the wavelet transform is that they may be able to reveal certain important temporal and spectral patterns in a signal. These patterns may constitute the signatures of the dynamic events in question and may be the key to the effective and reliable interpretation of the sensor signals [72]. WT is widely used in SHM in different fields: damage detection, singularity detection, denoising, system and parameter identification [73, 74] and vibration signal compression [75, 76, 77]; but major SHM research using wavelets is focused on feature extraction and pattern recognition. Readers are suggested to read a state of art about the usage of wavelet transform in structure health monitoring that is presented by Taha *et al.* [26] and also a comprehensive study on damage identification using wave-based approaches that is presented in [78].

The implementation of WT in damage diagnosis was started from about 1994 when Staszewski *et al.* [79] applied WT in machinery diagnostics to detect damaged tooth in a spur gear. In 1995, Masuda *et al.* [80] used WT to estimate the cumulative damage of a building with bilinear restoring force subjected to a real earthquake ground motion in terms of the accumulated ductility ratio, which is related to the number of spikes in the wavelet results. Deng *et al.* [72] process the wave propagation signals that are collected using arrays of piezoelectric transducers placed on or embedded in a structure and the final interpretation of the sensor signals is based on signal patterns uncovered by the wavelet transforms in correlation with elastic-wave propagation theory. Abbate *et al.* WT is used as signal detection and noise suppression to detect ultrasonic flaw in [81]. Legendre *et al.* [82] applies WT on Lamb wave captured by Electro Magnetic Acoustic Transducer (EMAT) and they compute the position of flaws in the structure under test from the time of arrival of the main peak of the reflected signal. They benefit the characteristics of WT dealing with the noisy nature of the received signal to extract the required time information. Piombo *et al.* [73] applies wavelet estimation technique for extracting modal parameters from transient time responses on a simply supported bridge in Northern Italy under traffic excitation. Sung *et al.* [83] applies WT to detect and localize the tooth defects in a gear system. Yan *et al.* [84] develop a method for online detection of initial damage in composite structures proposed based on energy variation of structural dynamic responses decomposed using wavelet analysis. They claim detection of extremely small cracks in composite plates. According to them, the smallest detectable crack may reach the dimension of width $0.1mm$ and length $2.3mm$, and the area containing this crack is only 0.06% of the total area of the plate.

The combination of PCA and WT is also presented in different works in SHM field. Browne *et al* [85] applies PCA for extracting parameters from raw empirical cumulative probability distribution of wavelet coefficient. Their study use this combination as feature extraction for visual sensor processing as an application to crack detection by a robot equipped with an infra-red camera. They use WT to transform the original image into a series of space-frequency subspaces and then apply PCA for dimension reduction and feature extraction. In another work, Ogaja *et al* [86] apply PCA on wavelet coefficients obtained from transform of GPS data for deformation monitoring. In their work, signal obtained from each individual sensor is first filtered using Finite Median Hybrid Filter (FMH). Then wavelet coefficients are obtained by applying DWT on filtered data and finally PCA is applied on the coefficients. To detect the deformation they use T^2 and Q statistic. Kesavan *et al* [87] applied PCA on energies of DB4 wavelet coefficients at fifth, sixth and seventh dyadic scales. For damage diagnostic, they compare features extracted by PCA from wavelet coefficient of any status of the structure with appropriate baseline signals. Damage detection is automated using the $k-$ means algorithm. Most recently, Tjirkallis *et al.* [88] applies a combination of decay lines of the Wavelet transform modulus maxima (WTMM) and Holder Exponent (HE) as damage detector on a

3-DOF system under temperature variation. They show that the decay lines are different when there is a damage in the structure while they stay identical when there is a temperature fluctuation in the structure.

2.6.3. Other techniques

In addition to the two important techniques, PCA and WT, that are applied in this work. In this part, other applied techniques in SHM is briefly reviewed. Soorgee *et al.* [89] presents a method to detect the location of a linear crack in a plate using piezoelectric actuator and sensor based on the time-of-flight of propagating waves. Sohn *et al.* [90] suggest a procedure based on enhanced time reversal method. They use this method to improve the detectability of local defects in composite structures. To improve the time reversibility of signal, they use wavelet-based signal processing techniques. They mention that time reversibility of Lamb waves can be violated if wave distortion due to wave scattering is caused by a defect along a direct wave path that leads to damage identification. In addition, Poddar *et al.* [91] present an experimental study of a baseline-free damage detection technique using time reversibility of Lamb wave for a woven-fabric composite laminate. They obtain the best possible reconstruction of the input signal by tuning various parameters of interest. They also use a finite element simulation to study the effect of amplitude tuning.

Michaels *et al.* [92] propose an integrated strategy for detection and imaging of damage by using a spatially distributed array of piezoelectric sensors. They claim that reduction of false alarms since signal changes due to benign variations will not be localized and erroneously identified as damage. Lu *et al.* [93] suggest a combination of the improved adaptive harmonic wavelet transform (AHWT) and the principal component analysis (PCA). They apply this method on the baseline signals to highlight the critical features of Lamb wave propagation in the undamaged structure. To purify the baseline dataset and quantify the deviation of the test data vector from the baseline dataset they employ Hotelling's T^2 statistical analysis.

Wang *et al.* [94] analyze the antisymmetric and symmetric contents of the wave propagation response in detail with respect to system parameters. Meruane *et al.* [95] propose parallel genetic algorithm (GA) for damage detection. They claim that parallel GA is faster than the normal counterpart. Furthermore, they are less sensitive to experimental noise or numerical errors.

Zhou *et al.* [96] propose integrating data fusion and random forests as damage detection method. To do this, they translate the original acceleration signals into energy features by wavelet packet decomposition. Then the processed energy features were fused into new energy features by data fusion. This is done to enlarge the differences among all types of damages. Finally, they apply random forests as an classifier is used to detect the multiclass damage. Haynes *et al.* [97] formulate a likelihood ratio based on a statistical model of the ultrasonic guided wave interrogation. They use

it to design an optimal detector for distinguishing damaged and undamaged states of the structure and found it to be a metric related to signal energy.

Casciati *et al.* [98] present a method based on a statistical comparison of models built from the response time histories collected at different stages during the structure lifetime. The damage detection and localization is performed by a comparison of the SSE (sum of the squared errors) histograms.

Autoregressive Models (AR), Autoregressive Moving Average (ARMA) and Autoregressive Integrated Moving Average (ARIMA) are other techniques that have been used widely in damage detection [99, 100, 101, 102, 103, 104].

2.7. Temperature effect on SHM

Environmental and operational variation of the structure is the one of the main obstacles for developing SHM solutions. In fact, these changes can often mask subtler structural changes caused by damage [105]. In other words, measured responses from a structure that demonstrate sensitivity to damage or structural degradation, will, in general, also exhibit sensitivity to any change in operational and environmental conditions [9]. Among various environmental conditions, temperature changes are of particular interest because temperature is a global environmental condition and its variations substantially alter the recorded waveform [106].

The effects of temperature variability on the measured dynamics response of structures have been addressed in several studies. It is intuitive that temperature variation may change the material properties of a structure. One the important examples is on the experiment has been done in [107] on the I-40 Bridge over the Rio Grande in New Mexico, (USA) to investigate if modal parameters could be used to identify structural damage within the bridge. Four different levels of damage were introduced to the bridge by gradually cutting one of the bridge girders. Investigation revealed that, beside the artificially introduced damage, the ambient temperature of the bridge played a major role in the variation of the bridge's dynamic characteristics [105].

In another work, the effect of temperature on the material stiffness has been reported by [108] due to a project working on five bridges in the UK. Daily and seasonal temperature variations also are an issue that should be noted. For instance, the change of first mode frequency of the bridge is approximately 5% during the 24h cycle. In another work a three span footbridge was tested for a 3-year period, a variation of 10% in the frequencies was observed every year because of seasonal changes. The authors concluded that the changes were partially attributed to the variation of ambient temperature.

Other authors such as Sohn *et al.* [104] also acknowledged potential adverse effects of varying operational and environmental conditions on vibration-based damage

detection. However, among the existing SHM methods, many of them neglect the effect of changing environmental conditions that include temperature, wind and humidity.

As many structures exhibit daily and seasonal temperature variations and SHM systems will need to operate across a variety of environmental conditions, understanding and considering the effect of temperature on SHM methodologies is critical. In another words, SHM systems will not be accepted in practical applications unless robust techniques are developed to explicitly account for environmental and operational constraints/conditions of the systems to be monitored [105].

Several investigations are performed to find out the reason of this adverse effect in SHM methodologies [109, 106, 110] and the main reason to such a effects are categorized as follows :

- Change in the properties of piezoelectric transducer (majority) such as piezoelectric constants [111, 112]. As a valuable reference, Schulz *et al.*[113] present a review on effect of temperature on PZT transducers.
- Alternation in properties of adhesive used to bond transducers to the host structures.
- Thermal expansion such as change in plate thickness, piezo dimensions and distances traveled by the guided wave in the structure [112].
- Change in elastic properties including density and Young modulus that cause changes in wave velocity [3].

Moreover, Rohrmann *et al.* [114] report the 10% change of natural frequencies due to temperature change in concrete structure. Besides, Xia *et al.* [115] report 0.13% change in reinforced concrete slab's natural frequency for every 1°C and they also mention some change in elastic modulus of asphalt. Peeters *et al.* [116] report a significant change in asphalt contributed to the stiffness of the Z-24 bridge if the temperature was under 0°C. Alampalli [117] reports a $50 - 70\%$ of change in natural frequencies of a bridge due to frozen hinge and roller supports. Sohn [105] conveys a survey on effect of damages on fundamental frequency of a bridge and he finds out that not only damage change those frequencies but also ambient temperature of the bridge played a major role in the variation of the bridge's dynamic characteristics. Cross et al. [118, 9] apply co-integration as a damage-sensitive features that is insensitive to environmental influence. They also investigate on effect of different environmental and operational factors such as wind, temperature, traffic loading on dynamic response of a long-span bridge in England. In their work, they suggest method that is based on incorporating environmental and operational condition into the definition of the normal condition. This leads to a successful damage detection unless the variation caused by damage is not smaller than that of daily variation. Besides, they demonstrate a comprehensive comparison between PCA and co-integration in the matter of damage detection under environmental changing. Manson et al. [119] mention the idea that instead of higher variance

principal components, minor components could be used as damaged detection as they might be less sensitive to the environmental changes.

Figueiredo *et al.* [99] do a test using autoregressive modeling with state-space embedding vectors for damage detection under operational and environmental variability. Yan *et al.* [120] present a method applied to vibration features identified during the monitoring of the structure under varying environmental and operational conditions. They underline the advantage of the method, consisting in the fact that it does not require to measure environmental parameters because they are taken into account as embedded variables. Bellino *et al.* [121] apply PCA to time-varying systems in order to eliminate the effects of external factors, such as temperature and humidity, supposed affecting the natural frequencies of a structure in addition to the damage. Blaise *et al.* [109] observed a decrease in wave amplitude and time of flight from ambient temperature to $-90°$C and they developed an empirical model to fit the experimental data. Lee *et al.* [122] measure a decrease in $S0$ amplitude with increasing temperature. Chambers *et al.* [123] report a drop in wave amplitude from room temperature using pulse-echo measurements in aluminum plates and it was justified by a degradation of the couplant between the plate and the clamp used to produce a wave reflection. Sohn *et al.* [124] suggest a unique integration of the AR-ARX time prediction model, the auto-associative neural network, and the sequential probability ratio test is developed to discriminate the changes of system responses caused by ambient operational conditions from those caused by structural damage. Lu *et al.* [106] perform a test on wave propagation under mild thermal variations from 20°C to 40°C. They report varying time-of-flight in this temperature range due to changing substrate elastic modulus and thermal expansion. Scalea *et al.* [125] suggest a model to predict $S0$ and $A0$ modes in aluminum plate for temperature range of $-40°$C to $+60°$C. Worden *et al.* [126] called the process of removing the effect of environmental variation in the observed data as a "*normalization*". They try to apply regression and interpolation approach to compensate the effect of temperature changes. Andrews *et al.* [127] consider the longitudinal and transverse wave speeds of aluminum 2024 under varying isothermal environments.

When environmental or operational conditions change, the propagating medium and guided wave behavior also change. Therefore, simple baseline comparison methods are unable to distinguish damage from benign environmental and operational effects [128]. Therefore it is necessary to compensate or mitigate the effect of temperature change in wave propagation strategy. Different methodologies are proposed to compensate the effect of temperature such as interpolation and extrapolation of baseline [33], baseline signal stretch (BSS) [106], optimal baseline selection (OBS) [37, 129] or combination of both BSS and OBS [130]. The most new methodology for temperature compensation is proposed by Harley [128], where applies scale transform is applied as a signal processing tool. It should be mentioned that these techniques are valid and limited for active guided ultrasonic wave approaches.

3. THEORETICAL BACKGROUND

This chapter presents the mathematical background for the methodologies that are used to pursue the main objectives of this thesis. The suggested methodologies in this dissertation are based on data driven analysis. In this method, all the information and the analysis is performed by using data gathered directly from case studies. In other words, no physical models are used to achieve damage detection. In order to capture appropriate data from structures, Lamb waves are produced into the structures through vibrational excitation signals generated by an active piezoelectric network. First section of this chapter is dedicated to review the mathematical background and the most important characteristics of Lamb waves that are necessary for SHM. After that, the mathematical background that is used in this work is presented and reviewed. The main mathematical concentration of this thesis is on statistical pattern recognition methodologies such as Principal Component Analysis (PCA). PCA is widely used in SHM in different aspects such as dimensional reduction and feature selection. A comprehensive review presented in section 3.5 highlights the important roles that PCA plays in SHM. It will be shown in this thesis that despite of the fact that PCA has many advantages, it possess some drawbacks such as sensitivity to outliers. Therefore, as a first contribution of the work, the effects of outliers on PCA are considered and, after that, the advantages of using robust PCA as an alternative for classical PCA to alleviate the outliers effect are presented. Theoretical background for different robust PCA algorithms are presented in this chapter. As the next contribution of this thesis, several new ideas are suggested that are closely related with PCA. For instance, a description about some new damage detection indices such as *Andrew plots*, *Similarity Classifier* and *PCA Orthogonal Distance* are presented. Besides, *Wavelet Ridge* is considered as an alternative to original signal to be used in damage detection algorithm (e.g. PCA, Robust PCA, etc.). After that and due to the importance of temperature fluctuation effect on wave propagation, a theoretical background for a series of temperature compensation methods are presented that could be used as a compensation tool with other methods to improve the reliability of SHM system. The presented methods in this chapter are scrutinized and tested in different case studies and results are presented in following chapters to prove their competence in SHM.

3.1. Guided waves for SHM

Among the technologies under investigation for SHM [13], the guided wave (GW) based approach is used in this thesis. In this method, the structure is excited with high frequency GWs and structural response is recorded, processed and compared with a baseline signal (pristine condition) using a testing algorithm to detect and characterize damage, if present. Guided waves can be defined as stress waves forced to follow a path defined by the material boundaries of the structure. For example, when a beam is excited at high frequency, stress waves travel in the beam along its axis away from the excitation source, i.e., the beam '*guides'* the waves along its axis.

Having advantages such as capability of propagation over a significant distance and high sensitivity to abnormalities and inhomogeneity near the wave propagation path, elastic waves can be energized to disseminate in a structure. Any changes in material properties or structural geometry created by a discontinuity, boundary or structural damage can be identified by examining the scattered wave signals. Guided waves are mainly used in pipes and plates and therefore aerospace and also they are recently used in wind turbines [9]. They are highly sensitive and they can evaluate damages that are greater than half size of their wavelength [131].

Two basic configurations are usually used in elastic wave based damage identification, 'pitch-catch' and 'pulse-echo'. In a pitch-catch configuration, elastic waves activated by a source (e.g., wave actuator) travel across a structure and they are then captured by a sensor at the other end of the wave path. In a pulse-echo configuration, both source and sensor are located at the same side of the structure, and the sensor receives the echoed wave signals from the structure. The first configuration is used for data acquisition in this dissertation.

Moreover, the active acoustic emission method is used in this work. Just as a brief comparison between the passive and active acoustic emission method, it could be mentioned that both are based on ultrasound waves which are known to propagate long distances in structures, often across several structural features, resulting in good coverage. Furthermore, both techniques use a permanently attached sparse-array of piezoelectric-based sensors and both have their range of coverage restricted by structural complexity and environmental conditions. Acoustic emission is a well-established technique which has been studied for many years, but interest in guided wave SHM of complex structures has increased significantly in recent years due to the commercial success of these systems for different engineering structures because of providing some features such as being permanently-attached and having relatively small size [132, 133].

3.2. Lamb waves

Lamb waves are mechanical waves whose wavelength is in the same order of magnitude as the thickness of the plate. These waves are related to other type of $2D$ vibrations such as Rayleigh waves which tend to occur on the surface of half spaces. Key aspects that should be kept in mind when working with Lamb waves are described briefly as follows :

- **Dispersion**: they are dispersive waves. This means that the wave phase velocity (Cph) depends on frequency (f) in a non-linear form.
- **Attenuation**: due to the material attenuation and the leakage effect (radiation into the surrounding media) the amplitudes of waves decrease with distance.
- **Non pure modes**: although some methodologies are suggested for "pure" mode excitation, in practice more than one mode can be excited [134, 135].
- **Mode conversion phenomena**: the existence of mode conversion phenomena in the test piece by the presence of defects, borders, impedance changes, etc. can produce other Lamb modes beside the excited one.

In addition, multiple symmetric and anti-symmetric Lamb wave modes are generated as the driving frequency for wave generation increases [105]. Su et al. [3] summarize the essential steps for a successful damage identification using Lamb waves as follows:

1. Activating the desired diagnostic Lamb wave signal using an appropriate transmitter and capturing the damage-scattered wave signals using a sensor or a sensor network in accordance with either the pitch-catch or the pulse-echo configuration.
2. Extracting and evaluating the characteristics of the captured wave signals with appropriate signal processing tools.
3. Establishing quantitative or qualitative connections between the extracted signal characteristics and the damage parameters (presence, location, geometric identity, severity, etc.) through some sort of physical or statistical model.
4. Figuring out the damage parameters of interest in terms of captured signals, based on the quantitative connections established in step 3.

Specific characteristics of Lamb waves, make them promising method for SHM. The most important characteristics of them are listed as following:

1. It is possible to capture a large area using a few transducers,
2. Both surface and internal damages can be detected due to the ability to examine the entire cross-sectional area of structures using multiple wave modes,
3. Different wave modes can classify different types of damage,
4. Waves are highly sensitive to damage, which leads to high precision damage identification,

5. Lamb wave can be excited in different structures such as plate, beam, pipeline, etc.,
6. Advances in transducer designing make it possible to integrate the SHM system in the structure,
7. Generally, it is a low energy consumption and also possibility of capture energy from the ambient thanks to energy harvesting methodologies.

3.2.1. Mathematical background

From historical point of view, it was Lord Rayleigh in 1889 who first explained wave propagation along a guided surface [136], and the waves are known as Rayleigh waves today. Following Rayleigh's work, Horace Lamb, a British applied mathematician, reported the waves discovered in plates in one of his historic publications. After his work called "*Waves in an Elastic Plate"*, in 1917 [137], the waves were named Lamb waves. With advances in computing devices, the period from the 1980s until the present day Lamb-wave-based engineering applications is increased dramatically, in particular Lamb wave based damage identification techniques in recent years.

Lamb wave mathematical description is described in different references [138, 139, 127, 8, 137] but Su *et al* [3] propose a simple review that is briefly described here. It is recommended to read mentioned sources for detailed information about Lamb waves and wave propagation.

In a thin isotropic and homogeneous plate (see Figure 3.1) the waves, regardless of the mode, can generally be described in a form of Cartesian tensor notation as:

$$\mu.u_{i,jj} + (\lambda + \mu)\,.u_{j,ji} + \rho.f_i = \rho.\ddot{u}_i \qquad (i,j = 1,2,3), \tag{3.1}$$

where u_i and f_i are the displacement and body force in the x_i respectively, ρ and μ are the density and shear modulus of the plate, respectively, and $\lambda = \frac{2\mu.v}{1-2v}$ (λ is the Lamé constant and v is the Poisson's ratio).

Using *displacement potentials method* based on *Helmholtz decomposition* [140], Equation 3.1 can be decomposed into two uncoupled parts under the plane strain condition as follows:

$$\frac{\partial^2\phi}{\partial x_1^2} + \frac{\partial^2\phi}{\partial x_3^2} = \frac{1}{c_L^2}\frac{\partial^2\phi}{\partial t^2} \tag{3.2}$$

for governing longitudinal wave modes, and

$$\frac{\partial^2\psi}{\partial x_1^2} + \frac{\partial^2\psi}{\partial x_3^2} = \frac{1}{c_T^2}\frac{\partial^2\psi}{\partial t^2} \tag{3.3}$$

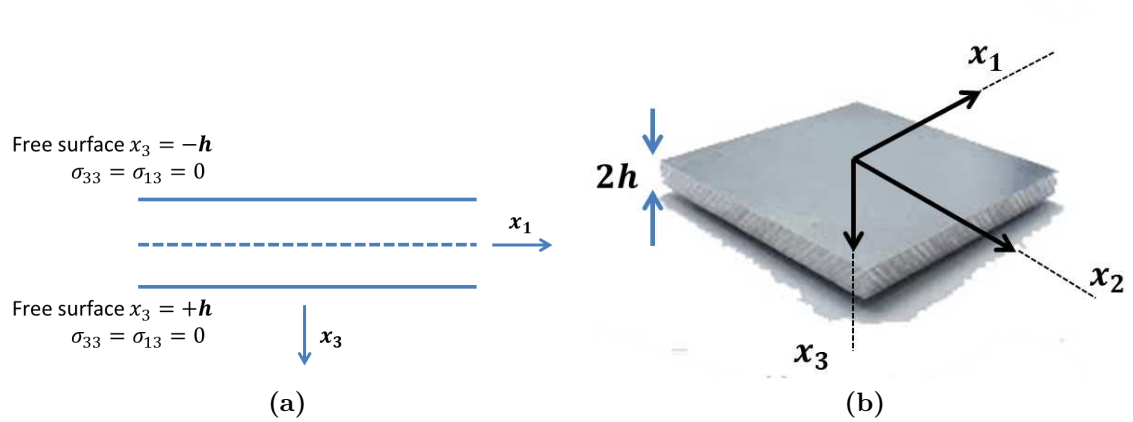

Figure 3.1.: A thin plate in thickness of 2h

for governing transverse wave modes, where

$$\phi = [A_1 \sin(px_3) + A_2 \cos(px_3)\,].e^{[i(kx_1 - \omega t)]}, \tag{3.4}$$

$$\psi = [B_1 \sin(qx_3) + B_2 \cos(qx_3)\,].e^{[i(kx_1 - \omega t)]}, \tag{3.5}$$

$$p^2 = \frac{\omega^2}{c_L^2} - k^2, \quad q^2 = \frac{\omega^2}{c_T^2} - k^2, \quad k = \frac{2\pi}{\lambda_{wave}}. \tag{3.6}$$

A_1,B_1,A_2 and B_2 are constants determined by the boundary conditions. k, ω and λ_{wave} are the wave number, circular frequency and wavelength of the wave, respectively and c_L and c_T are the velocities of longitudinal and transverse/shear modes (L stands for the longitudinal modes and T for the transverse/shear modes hereafter), respectively, defined by:

$$c_L = \sqrt{\frac{E(1-v)}{\rho(1+v)(1-2v)}} = \sqrt{\frac{2\mu(1-v)}{\rho(1-2v)}}, \quad c_T = \sqrt{\frac{E}{2\rho(1+v)}} = \sqrt{\frac{\mu}{\rho}} \tag{3.7}$$

where E denotes the Young's modulus of the medium ($E = 2\mu(1+v)$). It can be seen that Lamb waves are actually the superposition of the longitudinal and transverse/shear modes. An infinite number of modes exist simultaneously, superimposing on each other between the upper and lower surface of the plate, finally leading to well-behaved guided waves.

In transverse waves displacements are in a direction perpendicular to the direction of propagation of the wave while in longitudinal wave the disturbance produced as the wave passes is along the direction of wave propagation. For instance, the wave on a string is a transverse wave as well as light wave. On the other side, sound waves are longitudinal waves.

As a result of plane strain, the displacements in the wave propagation direction (x_1) and normal direction (x_3) can be described as

$$u_1 = \frac{\partial \phi}{\partial x_1} + \frac{\partial \psi}{\partial x_3} \ , \ u_2 = 0 \ , \ u_3 = \frac{\partial \phi}{\partial x_3} - \frac{\partial \psi}{\partial x_1}, \tag{3.8}$$

Therefore,

$$\sigma_{31} = \mu \left(\frac{\partial u_3}{\partial x_1} + \frac{\partial u_1}{\partial x_3} \right) = \mu \left(\frac{\partial^2 \phi}{\partial x_1 \partial x_3} - \frac{\partial^2 \psi}{\partial x_1^2} + \frac{\partial^2 \psi}{\partial x_3^2} \right), \tag{3.9}$$

$$\sigma_{33} = \lambda \left(\frac{\partial u_1}{\partial x_1} + \frac{\partial u_3}{\partial x_3} \right) + 2\mu \frac{\partial u_3}{\partial x_3} = \lambda \left(\frac{\partial^2 \phi}{\partial x_1^2} + \frac{\partial^2 \phi}{\partial x_3^2} \right) + 2\mu \left(\frac{\partial^2 \phi}{\partial x_3^2} - \frac{\partial^2 \psi}{\partial x_1 \partial x_3} \right). \tag{3.10}$$

For a plate with free upper and lower surfaces, by applying the following boundary conditions at both surfaces:

$$u\left(x,t\right) = u_0\left(x,t\right), \tag{3.11}$$

$$t_i = \sigma_{ji} n_j, \tag{3.12}$$

$$\sigma_{31} = \sigma_{33} = 0 \ at \ x_3 = \pm \frac{d}{2} = \pm h, \tag{3.13}$$

in Equations (3.8),(3.9) and (3.10), where d is the plate thickness and h is the half thickness, the general description of Lamb waves in an isotropic and homogeneous plate can be obtained:

$$\frac{\tan(qh)}{\tan(ph)} = \frac{4k^2 qp\mu}{(\lambda k^2 + \lambda p^2 + 2\mu p^2)(k^2 - q^2)}, \tag{3.14}$$

Substituting Equation (3.6) and (3.7) into the above Equation and considering that the trigonometric function *tangent* is defined with *sine* and *cosine,* which have symmetric and anti-symmetric properties, respectively, Equation (3.14) can be split into two parts with solely symmetric and anti-symmetric properties, respectively, implying that Lamb waves in a plate consist of symmetric and anti-symmetric modes [138],

$$\frac{\tan(qh)}{\tan(ph)} = -\frac{4k^2qp}{(k^2-q^2)^2} \quad \text{for symmetric modes,} \tag{3.15}$$

$$\frac{\tan(qh)}{\tan(ph)} = -\frac{(k^2-q^2)^2}{4k^2qp} \quad for\, anti-symmetric\, modes. \tag{3.16}$$

For brevity, it is stipulated that the symbols S_i and A_i $(i = 0, 1, \dots)$ stands for the symmetric and anti-symmetric Lamb modes.

Figure 3.2a and 3.2b show the symmetric and anti-symmetric part of wave mentioning motion related to each mode and Figure 3.3a and 3.3b show in plane and out of plane motion due to wave modes.

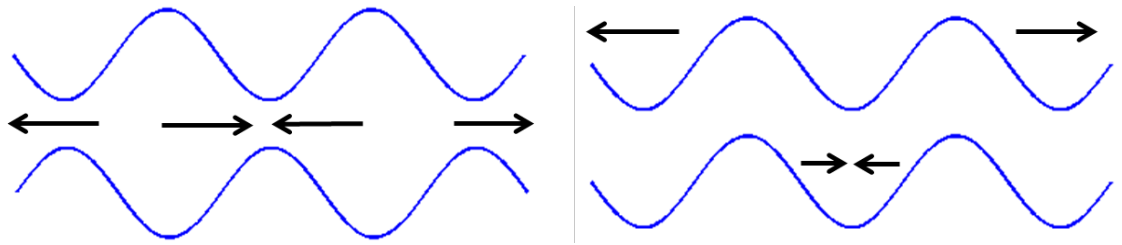

(a) Symmetric Lamb wave mode **(b)** anti-symmetric Lamb wave modes

Figure 3.2.: Symmetric and anti-symmetric Lamb wave modes

The propagation of Lamb waves can be characterized by the phase c_p and group c_g velocities. The former is referred to as the propagation speed of the wave phase of a particular frequency contained in the overall wave signals, which can be linked with the wavelength λ_{wave} as :

$$c_p = \frac{\omega}{2\pi}\lambda_{wave}. \tag{3.17}$$

The group velocity is referred to as the velocity with which the overall shape of the amplitudes of the wave propagates through space. The group velocity is dependent on frequency and plate thickness, formulated by

$$c_g(f.d) = c_p^2\left[c_p - \omega\frac{\mathrm{d}}{\mathrm{d}\omega}c_p\right]^{-1} = c_p^2\left[c_p - (f.d)\frac{\mathrm{d}}{\mathrm{d}(f.d)}\,c_p\right]^{-1}, \tag{3.18}$$

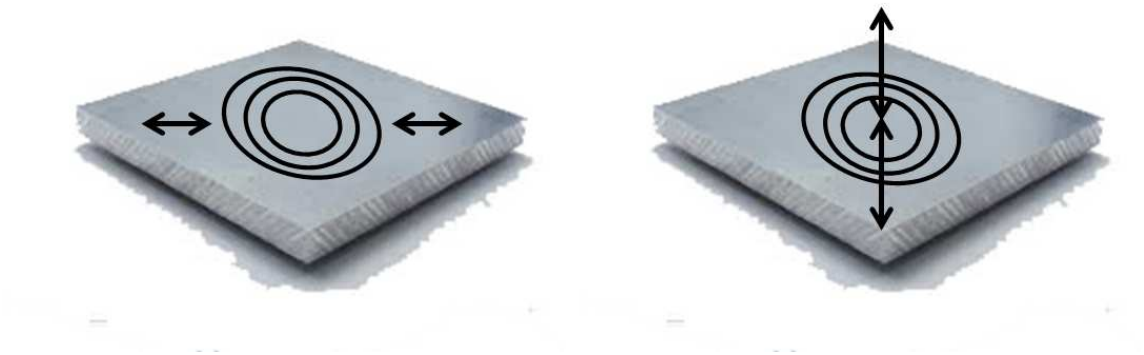

(a) Radial in-plane motion in symmetric mode **(b)** Out of plane motion in anti-symmetric mode

Figure 3.3.: In-plane and out of plane motions

where f is the central frequency and $f = \frac{\omega}{2\pi}$ [3].

Dispersion

Lamb waves are dispersive, where wave speeds are a function of frequency**,** and multiple modes co-exist and may interfere with each other [3]. Such a shift in the central frequency from the original excitation frequency is a key manifestation of wave dispersion.

In terms of Equations (3.6), (3.17) and (3.18), the phase velocity and group velocity can be related to the frequency and plate thickness, and also to the wave numbers k. Thus for a plate made of isotropic material, Equation (3.15) and (3.16) can be rearranged as

$$\frac{\tan(qh)}{q} + \frac{4k^2 p \tan(ph)}{\left(k^2 - q^2\right)^2} = 0, \tag{3.19}$$

$$q.\tan(qh) \; + \frac{\left(k^2 - q^2\right)^2 \tan(ph)}{4k^2 p} = 0. \tag{3.20}$$

The equations above are the dispersion equations of Lamb waves [138], and the graphic depiction of solutions of the dispersion equations is called the dispersion curves. Dispersion curves are used to describe and predict the relationship among frequency, phase/group velocity and thickness for each lamb mode ($A_i, S_i \; ; \; i = 0, 1, \ldots$) , see Figure 3.4.

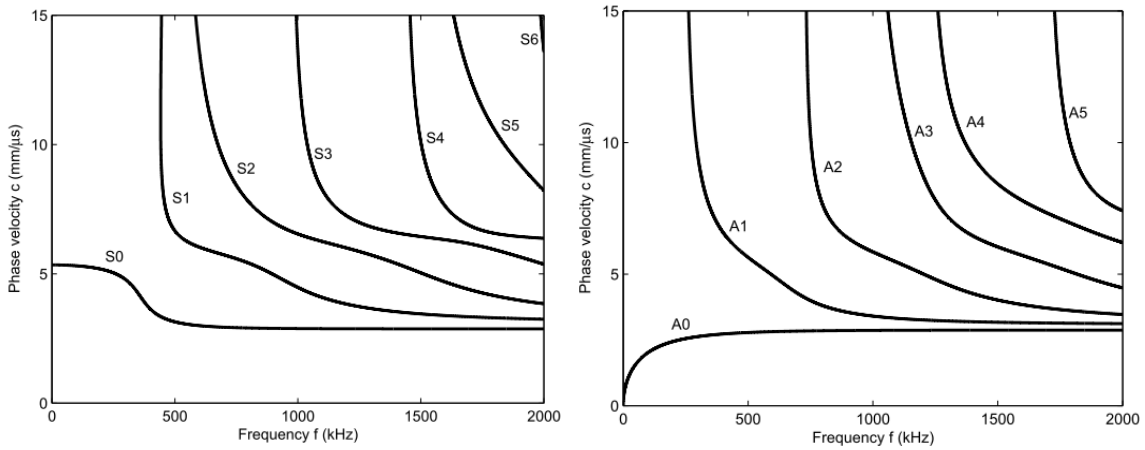

(a) Symmetric modes [141] **(b)** Antisymmetric modes [141]

Figure 3.4.: Dispersion curves for aluminum 7075 plate of thickness 6.35 mm

3.2.2. Generation and receiving

Lamb waves can be actively excited and collected by a variety of means, roughly grouped under four categorizes:

1. Ultrasonic probe,
2. Laser,
3. Optical fiber, and
4. Piezoelectric element.

Piezoelectric lead Zirconate Titanate (PZT) elements deliver excellent performance in Lamb wave generation and acquisition, and are particularly suitable for integration into a host structure as an in-situ generator/sensor, for their negligible mass/volume, easy integration, excellent mechanical strength, wide frequency responses, low power consumption and acoustic impedance, as well as low cost [3].

Since the piezoelectric effect exhibited by natural materials such as quartz, tourmaline, Rochelle salt, etc. is very small, polycrystalline ferroelectric ceramic materials such as barium Titanate and lead Zirconate Titanate (PZT) with improved properties have been developed. The piezoelectric effect may be direct piezoelectric effect in which the electric charge develops as a result of the mechanical stress or reverse or indirect piezoelectric effect (Converse piezoelectric effect) in which a mechanical force such as vibration develops due to the application of an electric field [142].

An optimal criterion for designing a disc-like PZT wave actuator was proposed [143], aimed at minimizing geometric effects and consequently avoiding uneven wave

propagation,

$$2R = \frac{v_{wave}}{f}\left(n + \frac{1}{2}\right) = \lambda_{wave}\left(n + \frac{1}{2}\right) \quad (n = 0, 1, 2, \dots), \tag{3.21}$$

where R is the radius of PZT disk; v_{wave}, f and λ are the wave velocity, frequency and wavelength of a concerned Lamb mode, respectively. Regarding to thickness selection, it has also been observed that the maximum voltage applied on a PZT, without depolarizing it, is 250–300 V/mm in the element thickness [144]. Figure 3.5 shows a typical PZT disk that is used in this work.

Figure 3.5.: Typical PZT disks

3.2.3. Lamb wave processing

Lamb waves captured by sensors are always carrying some features such as:

1. Signal is usually contaminated by some reasons such as random electrical and magnetic interferences, mechanical noise, temperature and humidity fluctuation.
2. Vibration of the host structure is affecting the damage scattered signal.
3. There are multiple modes in signal and also it is dispersed.
4. Huge amount of information exists due to high sampling frequency.

Therefore it is necessary to apply an appropriate signal pre-processing.

3.2.3.1. Averaging

Averaging a set of signals received repeatedly by an actuator-sensor path can reduce the data sensitivity with respect to uncertain fluctuation. Averaging also decrease experimental noise. To do this, usually a few observations are averaged to form an observation.

3.2.3.2. De-noising

Noise, measurements in a signal that are not a part of the phenomena of interest, is unavoidable even though precautions are taken. As a result, the damage-scattered wave components can easily be masked by the noise from a diversity of sources. In addition to the basic approach of de-noising such as averaging, other different approaches such as discrete wavelet transform could be used in order to denoise the signal [145]. The underlying model for the noisy signal is basically of the following form:

$$s(n) = f(n) + \sigma e(n) \tag{3.22}$$

where time n is equally spaced. In the simplest model, suppose that $e(n)$ is a Gaussian white noise $N(0, 1)$ and the noise level variance σ is supposed to be equal to 1. The de-noising objective is to suppress the noise part of the signal s and to recover f. The de-noising procedure proceeds in three steps:

1. Decomposition. Choose a wavelet, and choose a level N. Compute the wavelet decomposition of the signal s at level N.
2. Detail coefficients thresholding. For each level from 1 to N, select a threshold and apply soft thresholding to the detail coefficients.
3. Reconstruction. Compute wavelet reconstruction based on the original approximation coefficients of level N and the modified detail coefficients of levels from 1 to N [146, 147].

3.2.3.3. Feature extraction

Generally, any kind of changes that happen in either global or local properties of a structure can be associated with damage parameters. The process of identifying and selecting some properties and parameters that are sensitive to any probable damage in structure is called feature extraction. For instance, some features of a Lamb wave signal such as ToF (time of flight), magnitude, frequency, attenuation, phase, spectrum and others. These parameters can change to different degrees in signals captured before and after the presence of damage in structures. Though application specific, the basic principle in selecting signal features for damage identification is to extract those that are most sensitive to variation in damage parameters. Feature extraction may be performed in time domain, frequency domain or joint time-frequency domain depending on the situation [3].

3.3. A brief review on different domains from wave propagation perspective

3.3.1. Time domain

A time-series signal inherently records the propagation history of Lamb waves traveling in a structure, thereby providing the most straightforward information about the waves, such as existence of various wave modes, propagation velocity, attenuation and dispersion with distance, scattering from a structural boundary or damage. The characteristics contained in a time-series Lamb wave signal that may be beneficial to damage identification include the absolute value of magnitude, the root mean square (RMS) of the signal, standard deviation, Kurtosis, characteristic time moment, trend, cyclical component, time-of-flight (ToF), etc [28]. Figure 3.6 shows an example for excitation and response signal of a structure.

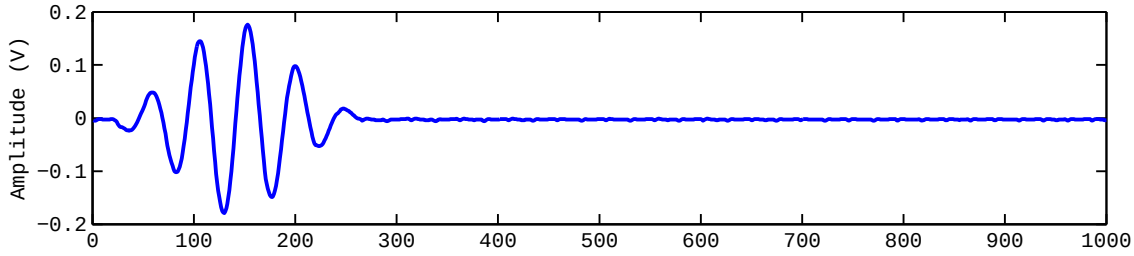

(a) Excitation Signal

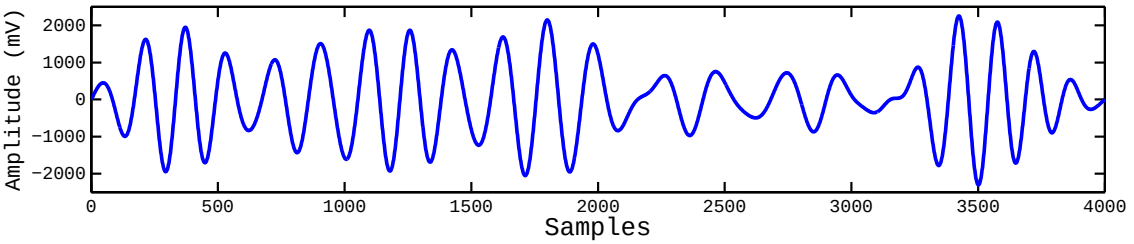

(b) Time response Signal

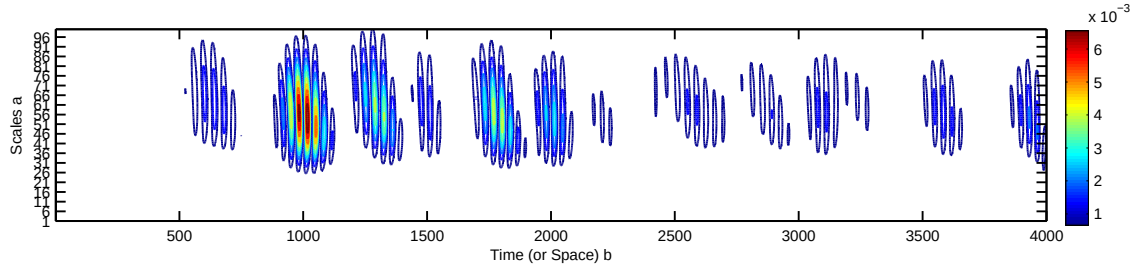

(c) Time-frequency response

Figure 3.6.: Lamb wave response in different domain

3.3.2. Frequency domain

There are some singularities induced by structural damage that are not clearly visible in the signal time domain, therefore some frequency domain transformation such as Fourier Transform (FT) is used to deal with this issue [148]. Some parameters based on this transformation could be used in SHM such as power spectrum $s_{xx}(f)$, which is the squared modulus of the FT, it gives an indication about the frequency content of the analyzed data.

It should also be noted that the use of the FT and FFT (Fast Fourier Transform) to transform a wave signal from the time to frequency domain comes at the cost of loss of temporal information of the signal [28].

3.3.3. Joint Time-Frequency domain analysis

In some cases, when the spectral content of the signal is changing in time, non-stationary signal, neither the time nor the frequency-domain is sufficient to accurately describe the signal properties. It is beneficial to combine both time and frequency domain to skip any potential loss of information carried by a Lamb wave signal. Some method such as short-time Fourier transform, Gabor transform, Wigner distribution and wavelet transform are the main approaches in this area [145]. In this work, Wavelet Transform is used in different cases. For sake of simplicity readers are recommended to the basic reference of wavelet in [71].

3.4. Statistical pattern recognition

Damage detection in structures can be regarded as a problem of pattern recognition. Patterns extracted from data represent different conditions and indicate whether the analyzed structure is undamaged or damaged. The severity of damage can also be established. Recent advancements in pattern recognition include applications of Artificial Neural Networks, and methods of novelty detection [70]. Novelty detection establishes a description of normality using features representing undamaged conditions and then tests for abnormality or novelty. However, the success or failure of the novelty detection is depending on the accuracy of the description of the normal condition. In reality, the normal condition of the system may experience a wide range of variation due to operational and environmental changes of the system [126]. The statistical pattern recognition paradigm can be described as a four-part process [33]:

(i) operational evaluation,

(ii) data acquisition,

(iii) feature extraction, and

(iv) statistical model development.

Operational evaluation decide to set the limitations on what will be monitored and how the monitoring will be accomplished. The main questions that should be answered in this part are some parameters such as environmental condition, damage definition, economic justification, limitations on acquiring data and life-safety etc.

The data acquisition portion of the Structural Health Monitoring process is the part that decide about the excitation methods, the sensor types, number and locations, and the data acquisition, storage and transmittal hardware.

A damage-sensitive feature is some quantity extracted from the measured system response data that indicates the presence of damage in a structure. Fundamentally, the feature extraction process is based on fitting some model, either physics-based or data-based, to the measured system response data. The parameters of these models or the predictive errors associated with these models then become the damage-sensitive features.

Statistical model development is concerned with the implementation of the algorithms that operate on the extracted features from the gathered data to quantify the damage state of the structure.

The algorithms used in statistical model development could be classified into two categories [33]:

(i) When data are available from both the undamaged and damaged structure, the statistical pattern recognition algorithms are referred as supervised learning. For instance, group classification and regression analysis are categories of supervised learning algorithms.

(ii) Unsupervised learning refers to algorithms that are applied to data that do not contain examples from the damaged structure. Outlier or novelty detection is the primary class of algorithms applied in unsupervised learning applications. All of the algorithms analyze statistical distributions of the measured or derived features to enhance the damage detection process.

3.5. Principal Component Analysis background

Dealing with high dimensional data, the first step in the data analysis is a dimensionality reduction. There are different reasons for that; for instance, the multidimensional data sets are difficult to interpret, and their structure cannot be visualized directly. In addition, the redundant variables create empty space and computational problems. PCA is probably the most useful tool to solve these problems [49]. Classical PCA is a linear transformation that maps the data into a lower dimensional space by preserving as much data variance as possible. In other words, it transforms n-dimensional data to new coordinate system such that when the data is projected

on these coordinates the greatest variance occurs across the first coordinate the second highest along the second and by proceeding similarly the lowest variance occurs along the nth coordinate. If the data compression is sufficient, the large number of variables is substituted by a small number of uncorrelated latent factors which can explain sufficiently the data variance.

The theory of Principal Component Analysis (PCA) has been considered in [49, 149, 150] completely. A brief description and mathematical definition in this section is presented.

To have a better point of view on what PCA is doing, let us imagine that we want to take a photo from a teapot having the most visual information (see Figure 3.7). The way to find such a position is as follows: first rotate the teapot around its center to find an axis so that the teapot has the largest extend in average along them, then continue rotating around the first axes to find another axis that is perpendicular to the first one and, moreover, the teapot has the largest extend along this new axis. By doing this, we have used principal component to find the angle that has most visual data (or in other words the highest variance). The two axes are the first and second principal component; the extend in average along the axes are the eigenvalues and the direction are the eigenvectors [151].

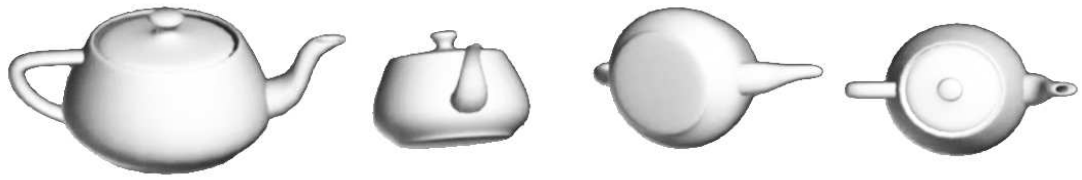

(a) appropriate angle [151] **(b)** wrong angles [151]

Figure 3.7.: Selecting the best angle to take a photo using PCA

Mathematically speaking, we can imagine the original data in a matrix form of $\mathbf{X_{n\times m}}$ containing information from n experimental trials and m sensors. It should be emphasized that the first step before applying PCA is the normalization of the data. Since physical variables have different magnitudes and scales, each data-point is standardized using the mean of all measurements of the sensor at the same time and the standard deviation of all measurements of the sensor. This procedure removes the differences between the variables' range and gives them the same importance in the data analysis. It also should be mentioned that there are some situations where scaling may be ill-advised. For instance, the data may have a channel with an abnormally low signal to noise ratio. If this channel would normally be weighted out by its low variance, standardization would clearly have an undesirable effect [53]. Once the variables are standardized, the covariance matrix $\mathbf{C}_X$ is calculated

as follows:

$$\mathbf{C}_X = \frac{1}{n-1}\mathbf{X}^T\mathbf{X}. \tag{3.23}$$

$\mathbf{C}_X$ is a square symmetric matrix $(m \times m)$ that measures the degree of linear relationship within the data set between all possible pairs of variables (sensors). The subspaces in PCA are defined by the eigenvectors and eigenvalues of the covariance matrix as follows:

$$\mathbf{C}_X\tilde{\mathbf{P}} = \tilde{\mathbf{P}}\mathbf{\Lambda}, \tag{3.24}$$

where the eigenvectors of $\mathbf{C}_X$ are the columns of $\tilde{\mathbf{P}}$ and the eigenvalues are the elements of the diagonal matrix $\mathbf{\Lambda}$ (the off-diagonal terms are zero). Columns of matrix $\tilde{\mathbf{P}}$ are sorted according to the eigenvalues by descending order and they are called the Principal Components of the data set (PCs). This matrix is also called *loading matrix* or *transformation matrix*. Eigenvalues show the active energy of the associated principal components somehow the eigenvector with the highest eigenvalue represents the most important pattern in the data with the largest variance. Usually information is measured by entropy. Information depends solely on the underlying probability distribution whereas variance both on probability distribution and the actual values of random variable (data). Choosing only a reduced number $r \ll m$ of principal components, those corresponding to the first eigenvalues, the reduced transformation matrix could be imagined as a statistical model for the structure. In this way, the new matrix $\mathbf{P}$ (sorted and reduced) can be called as PCA model. Geometrically, the PCA transforms the data in the input bands from the input multivariate attribute space to a new multivariate attribute space whose axes are rotated with respect to the original space. The axes (attributes) in the new space are uncorrelated. The transformed data matrix $\mathbf{T}$ (score matrix) is the projection of the original data over the direction of the selected principal components $\mathbf{P}_{\mathbf{m\times r}}$ as

$$\mathbf{T}_{\mathbf{n\times r}} = \mathbf{X}_{\mathbf{n\times m}}\mathbf{P}_{\mathbf{m\times r}}. \tag{3.25}$$

In the full dimension case using $\tilde{\mathbf{P}}$, this projection is unitary (since $\tilde{\mathbf{P}}\tilde{\mathbf{P}}^{\mathbf{T}} = \mathbf{I}$) and the original data can be recovered as $\mathbf{X} = \mathbf{T}\tilde{\mathbf{P}}^{\mathbf{T}}$. In the reduced case (using $\mathbf{P}$) with the given $\mathbf{T}$, it is not possible to fully recover $\mathbf{X}$, but $\mathbf{T}$ can be projected back onto the original m-dimensional space and obtain another data matrix as follows:

$$\hat{\mathbf{X}} = \mathbf{T}\mathbf{P}^{\mathbf{T}} = (\mathbf{X}\mathbf{P})\mathbf{P}^{\mathbf{T}}. \tag{3.26}$$

Considering $\hat{\mathbf{X}}$ as the projection of the data matrix $\mathbf{X}$ onto the selected r principal components and $\tilde{\mathbf{X}}$ as the projection onto the residual left components, the following decomposition can be performed:

$$\mathbf{X} = \hat{\mathbf{X}} + \tilde{\mathbf{X}}, \tag{3.27}$$

$$\hat{\mathbf{X}} = \mathbf{X}(\mathbf{P}\mathbf{P}^{\mathbf{T}}), \tag{3.28}$$

$$\tilde{\mathbf{X}} = \mathbf{X}(\mathbf{I} - \mathbf{P}\mathbf{P}^{\mathbf{T}}). \tag{3.29}$$

Therefore, the residual data matrix (the error for not using all the principal components) can be defined as the difference between the original data and the projected back:

$$\mathbf{E} = \mathbf{X} - \hat{\mathbf{X}} = \mathbf{X}(\mathbf{I} - \mathbf{P}\mathbf{P}^{\mathbf{T}}). \tag{3.30}$$

Selecting the correct number of components, r, is an important issue. Basically, there are different popular criteria which indicate the terminating condition for gathering the PCs [152]. In this thesis we use the criteria as follows:

Proportion of variance: it means the cumulative percentage of total variation in several PCs. The required number of PCs is determined to be the smallest value for which a chosen variance percentage is exceeded as

$$\frac{\sum_{j=1}^{r} l_j}{\sum_{i=1}^{m} l_i} \approx 90\%, \tag{3.31}$$

where l_i are eigenvalues and $m = rank(\mathbf{C}_X)$. However, there is no definite rule to decide exactly how much the percentage should be chosen. Jolliffe [49] suggested a value between 70% and 90%.

3.6. Outliers

The definition of an outlier usually depends on hidden assumptions regarding the data structure and the applied detection method. However, there are some general definitions that can cope with various types of data and methods. Hawkins [153]

defines an outlier as "*an observation that deviates so much from other observations as to arouse suspicion that it was generated by a different mechanism*". Barnet and Lewis [154] indicate that *"an outlying observation, or outlier, is one that appears to deviate markedly from other members of the sample in which it occurs"*. Similarly, Johnson [155] defines an outlier as *"an observation in a data set which appears to be inconsistent with the remainder of that set of data"* .

The presence of outliers in the data can be due to two main reasons. One of them is an experimental error such as instrument error, human error, error in data transmission or transcription, etc. This type of outlier frequently appears in any experiment. The other reason is the unique character of a few objects or a certain unusual environmental event that took place. For instance, the average height for a person is $180cm$ but there may exist some persons that are taller than $2m$ or shorter than $1.5m$.

Both types of outliers are important to be identified; however, the reason for their identification is twofold, either, to remove them from the data in order to obtain correct results of the analysis or to find the explanation for their outlyingness to understand better the studied process [156].

There are two main categories of approaches for outlier detection. As the first category, statistical approaches try to substitute sensitive statistical parameters such as mean and covariance with the robust ones using some estimators such as minimum covariance determinant (MCD) and minimum volume ellipsoid (MVE) respectively [157, 158]. Another approaches are related to data mining methods such as distance-based method, clustering technique, etc. The first one, distance-based method, is based on local distance measures and it is capable of handling large databases; and in the second one, clusters of small sizes are considered as clustered outliers [159].

Regardless of their source and depending on their position, outlying observations may or may not have a large effect on the results of the analysis. In PCA study, for instance, outliers could change the direction of principal components and result to non-realistic outcomes (see Figure 3.8). Figure 3.8-a shows the correct direction of first two PCs while Figure 3.8-b shows changing the direction of PCs towards the outliers.

To measure the outlyingness of observations, two measurements are defined: the robust score distance (Equation 3.32) and the orthogonal distance (Equation 3.33) of each i_{th} observation:

$$SD_i = \sqrt{\sum_{j=1}^{k} \frac{t_{ij}^2}{l_j}}, \tag{3.32}$$

$$OD_i = \|x_i - \hat{\mu} - P_{m\times k} t_i^T\|. \tag{3.33}$$

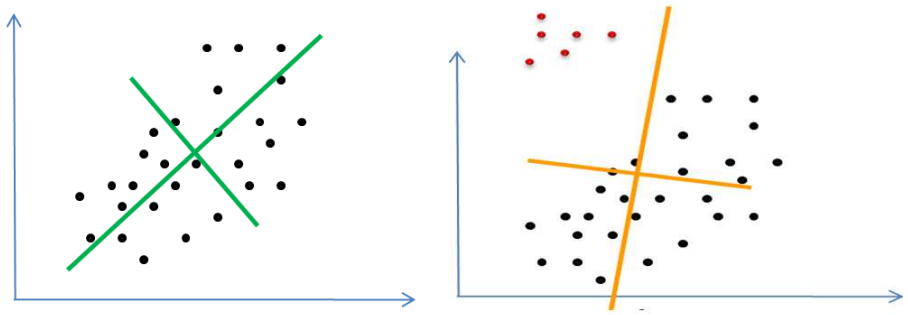

(a) PCs directions without outliers **(b)** PCs direction with outliers

Figure 3.8.: Influence of outliers on PCA components

Where, t_{ij} represents the score associated to i_{th} observation and j_{th} dimension and l_j represents the j_{th} eigenvalue from the k selected robust eigenvalues/eigenvectors. Moreover, $\hat{\mu}$ and $P_{m\times k}$ are mean and loading matrix for original data respectively. Objects whose SD and OD exceed the cutoff value (threshold) $\sqrt{\chi^2_{k,0.975}}$ are defined as outliers in the principal component space. The notation $\chi^2_{k,0.975}$ corresponds to the chi-square distribution for k significant PCs and 97.5 % level of confidence. Using the above definitions, outliers can be classified in 3 types. According to Figure 3.9, the first group is a data set which lies close to the PCA space but far from the regular observations (observation 1 and 2) where OD is less than threshold and SD is out of the limit, and this type is called *good leverage points*. Next group is called *orthogonal outliers* whose orthogonal distance to the PCA space is large but which we cannot see when we only look at their projection (observation 3). And finally, *bad leverage points*, observation 4, are data that have a large orthogonal distance and whose projection on the PCA subspace is remote from the typical projections which are out of threshold for both distances [160]. Table 3.1 summarizes the mentioned types of outliers.

Table 3.1.: Different Types of outliers

good leverage points	OD $\leq$ threshold	SD $\geq$ threshold
orthogonal outliers	OD $\geq$ threshold	SD $\leq$ threshold
bad leverage	OD $\geq$ threshold	SD $\geq$ threshold

It is highly desirable to adapt the analyze to remove or alleviate the effect of outliers. This makes the analyze robust. The term "robust" indicates that the learning from the contaminated training data will still lead to acceptable estimates of the normal behavior.

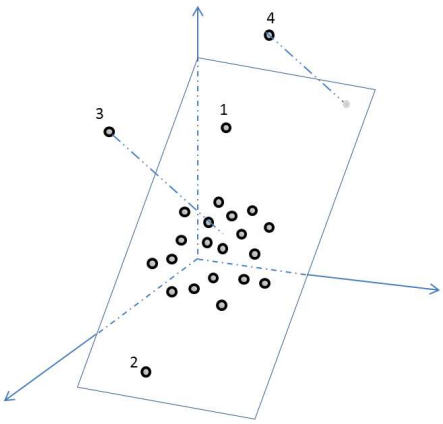

Figure 3.9.: Different types of outliers

3.7. Robust Principal Components

As it is mentioned, PCA is the most useful tool in dimensional reduction with various properties such as dimension reduction, feature selection, etc. However, despite of these features, it is known to possess some shortcomings. One of them is that both the classical variance (which is being maximized) and the classical covariance matrix (which is being decomposed) are very sensitive to anomalous observations. Consequently, the first components are often attracted towards outlying points, and may not capture the variation of the regular observations. Therefore, data reduction and modeling based on classical PCA (CPCA) becomes unreliable if outliers are present in the data. A way to deal with this problem is to remove the outlying objects observed on the score plots and to repeat the PCA analysis again. Another, more efficient way is to apply a robust, i.e. not sensitive to outliers, variant of PCA. Outliers and appropriate algorithms to deal with them are presented as follows.

3.7.1. General description of robust PCA

Robust PCA aims to obtain principal components that are not much influenced by outliers. Statistical robust PCA methods are generally based on three different approaches:

1. Taking the eigenvectors of robust covariance or correlation estimator,
2. Projection Pursuit (PP), and
3. Combination of both.

Replacement of classical covariance or correlation matrix by a robust estimator is perhaps the simplest way to have a robust PCA. For every choice of the robust covariance matrix estimator, a specific robust PCA method is obtained. Minimum covariance determinant (MCD) [161] and its fast version [162] , S-estimators [157] and Minimum Volume Ellipsoid (MVE) are some of the most well-known estimators.

For instance, MCD estimator searches for the subset of size h whose classical covariance matrix has minimal determinant. Then the location and scatter MCD estimated are given by the average and covariance matrix computed over this optimal subset. The breakdown point of this estimator is 0.5. The breakdown point of an estimator measures the maximal percentage of the data point that may be contaminated before the estimate becomes completely corrupted; it is very often used as a measure of robustness. The result of robust methods based on mentioned estimators are more robust rather than classical approach but limited to small or moderate dimensions where the number of variables (m) may never be larger than the number of observations (n).

A second approach to robust PCA uses Projection Pursuit. In [163, 164] a method has been proposed that belongs to this approach. While classical PCA searches for direction with maximal variance, Projection Pursuit (PP) intends to replace this variance by a robust criterion. PP tries to construct all possible directions in the space spanned by the data variables and then numerically evaluate a criterion for each of these vectors. The vector having the maximal value for the criterion is the first principal component.

As it is mentioned before, the first step in the classical PCA is to center the data around the *mean*. Therefore the first step to robustify the algorithm is to substitute the mean, since is not also robust itself, with a robust estimator. The L_1-median estimator is used to achieve this goal. It is defined as a point which minimizes the sum of Euclidean distances to all points in the data. For a data set $\mathbf{X} = \{\mathbf{x_1}, \ldots, \mathbf{x_n}\}$ with each $x_i \in \mathbb{R}^{\mathbb{P}}$, the L_1-median $\hat{\mu}$ is defined as

$$\hat{\mu}(X) = \underset{\mu}{argmin} \sum_{i=1}^{n} \parallel x_i - \mu \parallel, \tag{3.34}$$

where $\parallel . \parallel$ denotes the Euclidean distance [165].

Afterward it is necessary to find the directions in the data space, which are not influenced by outliers. This goal is achieved by using a robust criterion. As a robust criterion, Li *et al.* [166] suggest to use M estimator, but this estimator does not have a high breakdown point. Croux *et al.* [163] suggest to use Q_m estimator with breakdown point of 50%.

3.7.2. Algorithm of Croux and Ruiz-Gazen

For each projection, the pairwise differences between two data points are calculated which lead to a diagonal matrix. After unfolding the upper and the lower matrix diagonal to a vector, its elements are sorted and the value which corresponds to the first quartile is then taken to compute Q_m as follows:

$$Q_m = 2.2219 \times c_m \times \{\mid X_i - X_j \mid; i < j\}_{(k)}, \tag{3.35}$$

where $k = \begin{pmatrix} h \\ 2 \end{pmatrix} \approx \begin{pmatrix} n \\ 2 \end{pmatrix} /4$, $h = [n/2] + 1$ and c_m is a correction factor, which tends to 1 when the number of observations increases. The algorithm can be summarized as follows [167]:

In the data matrix $X_{n\times m}$,

1. Center $\mathbf{X}$ around L_1-median. It leads to the new centered data matrix $\mathbf{X_c}$.
2. For $i = 1$ to f_m, where f_m is the number of robust principal components to be extracted, construct a data matrix containing normalized rows of X_c (all possible eigenvectors).
3. Project all observations onto the eigenvectors.
4. Calculate the projection index of all eigenvectors.
5. Select the eigenvector with maximal value of the projection index.
6. Update the $\mathbf{X}_c$ by its orthogonal complement.
7. Go to step 2 until f_m robust PCs are found. Project all observations onto the founded eigenvectors.

3.7.3. ROBPCA

Hubert *et al* [160, 168] have proposed a method that belongs to the third approach. We briefly mention the algorithm. It is recommended to refer to [160] for more details. This algorithm uses both robust estimation and projection pursuit. Projection pursuit part is used for the initial dimension reduction and then MCD estimator is applied to this lower-dimensional data. This combination yields more accurate estimates rather than raw PP at non-contaminated data and more robust at contaminated data. In addition, this method can handle high dimensional data.

For a data matrix $\mathbf{X}_{n\times m}$, the first step would be to reduce the dimension of data to at most $n - 1$. This is specially useful when $m \geq n$. To do this, a singular value decomposition [169] of mean centered data can be used as follows:

$$\mathbf{X}_{n\times m} - \mathbf{1}_{n\times 1}\hat{\mu_0}^T_{1\times m} = \mathbf{U}_{n\times r_0}\mathbf{D}_{r_0\times r_0}\mathbf{V}^T_{r_0\times m}, \tag{3.36}$$

where $\hat{\boldsymbol{\mu_0}}$ is the classical mean vector of variables, $r_0 = rank(\mathbf{X}_{n\times m} - 1_{n\times 1}\hat{\mu_0}^T{}_{1\times m})$, $\mathbf{D}$ is a $r_0 \times r_0$ diagonal matrix, and $\mathbf{U}^T\mathbf{U} = I_{r_0} = \mathbf{V}^T\mathbf{V}$ where $\mathbf{I}_{r_0}$ is the $r_0 \times r_0$ identity matrix. Without losing any information, we now work in the subspace spanned by the r_0 columns of $\mathbf{V}$. That is, $\mathbf{X}_{n\times r_0} = \mathbf{UD}$ becomes our new data matrix. It should be emphasized that this decomposition is just used as an affine transformation and not used to retain the first eigenvectors of matrix $\mathbf{X}_{n\times m}$ as it is not robust yet. In the next stage, the h observation with the minimum outlying behaviour is found

$(h < n)$. To achieve this, for each observation $\mathbf{x_i}$, its orthogonally outlyingness is computed as

$$outl_O(\mathrm{x}_i) = \max_{\mathbf{v}\in B} \frac{\mid \mathbf{x}_i^T\mathbf{v} - t_{MCD}(\mathbf{x}_j^T\mathbf{v}) \mid}{s_{MCD}(\mathbf{x}_j^T\mathbf{v})}, \tag{3.37}$$

where B represents all directions through two data points, $t_{MCD}(\mathbf{x}_j^T\mathbf{v})$ and $s_{MCD}(\mathbf{x}_j^T\mathbf{v})$ are the MCD location and scale estimator respectively, and $j = 1, \ldots, n$ [161]. The formulation above means that for each direction $\mathbf{v} \in B$, each n observation of $\mathbf{x}_i$ is projected on $\mathbf{v}$ and its outlyingness is calculated and then the h observations with smallest outlyingness are stored in the set H_0. If we consider $\hat{\mu_1}$ and S_0 as the mean an covariance matrix of the h observations in H_0, the first $k_0 \leq r$ principal components can be retained. This can be done by decomposition of S_0 as

$$S_0 = P_0 L_0 P_0^T, \tag{3.38}$$

with $L = diag\left(\tilde{l_1}, \ldots, \tilde{l_r}\right)$, $r \leq r_1$, and then selecting appropriate k_0 eigenvectors. After that, the data points are projected on the subspace spanned by the first k_0 eigenvectors of S_0 as

$$X^{\star}_{n\times k_0} = \left(X_{n\times r_1} - \mathbf{1}_n \hat{\mu_1^T}\right) P_{r_1\times k_0}, \tag{3.39}$$

where $\mathbf{P_{r_1\times k_0}}$ consists of the first k_0 columns of P_0 in Equation (3.38). In the third stage, the robust scatter matrix of the observations in $X^{\star}_{n\times k_0}$ is estimated using MCD estimator. To do this we need to find the specific h data points whose covariance matrix has minimal determinant. This may be achieved by applying Fast-MCD algorithm described in [162], which leads to robust center and covariance matrix and finally, robust scatter matrix as

$$T_{n\times k} = \left(X_{n\times p} - 1_n \hat{\mu^T}\right) P_{m\times k}, \tag{3.40}$$

where $\hat{\mu}$ is called robust center and $P_{m\times k}$ are robust principal components by decomposing the robust covariance matrix S of rank k given by

$$S = P_{m\times k} L_{k\times k} P^T_{m\times k}, \tag{3.41}$$

where $L_{k,k}$ is diagonal matrix with the eigenvalues $[l_1, \ldots, l_k]$.

3.7.4. Robust Fuzzy principal component

Another illuminating robust approach is to use robust fuzzy principal component analysis (RFPCA). It has been proved that RFPCA method achieves better result than classical PCA mainly because it is more compressible. In this method the first fuzzy principal components account for significantly more of the variance than their classical counterparts. Therefore, by carrying more information in primary PCs, it

can provide more information for any damage detection approach based on it and as a result, distinguishing much better between the healthy and damaged structures [170, 171].

Considering a data set with n observations like $X = \{x_1, \ldots, x_n\}$ the optimization function E subject to $u_i \in \{0, 1\}$ is defined by:

$$E\left(U, w\right) = \sum_{i=1}^{n} u_i e\left(x_i\right) + \eta \sum_{i=1}^{n} \left(1 - u_i\right), \tag{3.42}$$

$e\left(x_i\right)$ measures the error between x_i and the class center as follows:

$$e(x_i) = \| \; x_i - w^T x_i w \; \| \tag{3.43}$$

The goal is to minimize E with respect to U and w, where $U = \{u_i, i = 1, \ldots, n\}$ is the membership sets and η is the threshold. Since u_i is the binary variable and w is the continuous variable, the optimization with gradient descent approach is hard to solve. Therefore, a new objective function is proposed by [171] as follows:

$$E = \sum_{i=1}^{n} u_i^{m_1} e\left(x_i\right) + \eta \sum_{i=1}^{n} \left(1 - u_i\right)^{m_1}. \tag{3.44}$$

subject to $u_i \in [0, 1]$ and $m_1 \in [1, \infty)$. Now u_i being the membership of x_i belonging to data cluster and $(1 - u_i)$ is the membership of x_i belonging to noise cluster. m_1 is the so-called fuzziness variable. This idea is similar to the C-means algorithm [170].

Since now u_i is a continuous variable, the difficulty of mixture of discrete and continuous optimization can be avoided and a gradient descent approach can be used. Firstly, the gradient of Equation (3.44) is computed respect to u_i and equaled to zero, therefore:

$$u_i = \frac{1}{1 + \left(e\left(x_i\right)/\eta\right)^{1/(m_1 - 1)}} \tag{3.45}$$

By substituting this membership in (3.44) the following equation is obtained:

$$RE = \sum_{i=1}^{n} \left(\frac{1}{1 + \left(e\left(x_i\right)/\eta\right)^{1/(m_1 - 1)}} \right)^{m_1 - 1} e\left(x_i\right). \tag{3.46}$$

On the other hand, the gradient respect to w is

$$\frac{\partial E}{\partial w} = \beta\left(x_i\right)\left(\frac{\partial e\left(x_i\right)}{\partial w}\right), \tag{3.47}$$

where

$$\beta\left(x_i\right) = \left(\frac{1}{1+\left(e\left(x_i\right)/\eta\right)^{\frac{1}{m_1-1}}}\right)^{m_1}, \tag{3.48}$$

and m_1 is the fuzziness variable. If $m_1 = 1$, the fuzzy membership reduces to the hard membership and can be determined by the following rule:

$$u_i = \left\{ \begin{array}{cc} 1 & if(e\left(x_i\right)) < \eta \\ 0 & otherwise \end{array} \right\}. \tag{3.49}$$

Now η is a hard threshold in this situation. There is no general rule for the setting of m_1, but most papers set $m_1 = 2$. In [171], authors derived the following algorithm for the optimization procedure:

1. Initially set the iteration count $t = 1$, the iteration bound T, learning coefficient $\alpha_0 \in (0, 1]$, soft threshold η to a small positive value and randomly initialize the weight w.
2. While t is less than T, do steps $3 \rightarrow 9$.
3. Compute $\alpha_t = \alpha_0(1 - \frac{t}{T})$, set $i = 1$ and $\sigma = 0$
4. For the number of observations, do steps $5 \rightarrow 8$
5. Compute y=$w^T x_i, u = yw$ and $v = w^T u$
6. Update the weight as: $w^{new} = w^{old} + \alpha_t \beta\left(x_i\right)\left[y\left(x_i - u\right] + (y - v)x_i\right]$
7. Update the temporary count $\delta = \delta + e_1\left(x_i\right)$
8. Add 1 to i.
9. Compute $\eta = (\delta/n)$ and add 1 to t.

The weight w in the updating rules converges to the principal component vector almost surely [172, 173].

3.8. Andrew plots

Graphical representation of multivariate data has been an important issue in exploratory data analysis. Most data that are collected are multivariate in nature, and much of them can be regarded as continuous. In the initial stages of analysis, graphic displays can be used to explore the data, but for multivariate data, traditional histograms or two or three-dimensional scatter plots may miss complex relationships that exist in the data set. A number of methods for graphically displaying multivariate data have been suggested. One of the most appealing methods is of Andrews Plots [174]. Andrews Plots provide a means for the simultaneous display method of several continuous variables. For a multivariate observation $y = (y_1, y_2, \cdots, y_p)^T$ Andrew suggests a representation of this multivariate point by a curve in argument t $(-\pi \leq t \leq \pi)$

$$f_y(t) = \frac{y_1}{\sqrt{2}} + y_2 \sin(t) + y_3 \cos(t) + y_4 \sin(2t) + y_5 \cos(2t) + \cdots \tag{3.50}$$

in a two-dimensional space. The coefficient of $y_1, y_2, \ldots$ are nothing but the terms in the Fourier series. By storing the coefficients $y_1, y_2, \ldots$ in a column vector

$$a(t) = \left(\frac{1}{\sqrt{2}}, \sin(t), \cos(t), \cdots \right)^T \tag{3.51}$$

Equation (3.50) can be expressed as $f_y(t) = a(t)y$, thereby identifying $f_y(t)$ as a particular linear combination y for a fixed t. Thus for a given t_0, $(t_0, f_y(t_0))$ represents a point on the curve, and by varying t between $-\pi$ and π an Andrews curve is obtained as a collection of all such points. Corresponding to n different multivariate observations, there will be n different Andrews curves. A plot consisting of such curves is called an Andrews plot.

3.8.1. Classifying cases with Andrew Plots

Andrews plots can be used as a technique for classifying observations into groups. Where unknown grouping of cases exists within a data set, an Andrews Plot can be used to discover this effect. Cases within one group will have similar patterns of values for the variables used in the Andrews Plot, and similar curves will be produced for these cases. Cases in a second group will have a different profile of values for the variables from those in the first group, and thus the curves produced for this second group will show a different pattern from those for the first group.

Andrews plots can also be used to allocate a case to one of a number of groups that are known to exist in the data set. Curves for cases whose grouping is known are

created and then the curve for the unknown case superimposed. The unknown case is allocated to the group whose set of curves its own curve most closely matches [175].

3.8.2. Andrew Plots and its properties

Andrews pointed out certain useful properties of $f_y(t)$ as follows:

- If the vector y represents the mean of n multivariate observations, $y_1, y_2, \ldots, y_n$, then $f_{\overline{y}}(t) = \overline{f}_y(t) = n^{-1} \sum_{i=1}^{n} f_{y_i}(t)$. Thus, the function $f_y(t)$ preserves the mean and as a result, in the Andrews plots the average of the data will be represented by the average of the corresponding Andrews curves in the plot.

- Apart from a constant, the L_2 distance between two curves $f_x(t)$ and $f_y(t)$, $\int_{-\pi}^{\pi}(f_x(t) - f_y(t))^2 dt = \pi \sum_{i=1}^{\pi}(x_i - y_i)^2$ Thus, the points which are closer to each other are represented as curves which are nearer to each other and vice versa. This distance preserving property follows from the Parseval relation and will, in fact, hold for any orthonormal basis set.

- Consider a fed $t = t_0$, The value of $f_y(t_0)$ represents apart from a constant, the length of the projection of y on the vector $a(t_0)$. Such projections may reveal patterns, groupings or outliers in the data, which may belong to this particular one-dimensional subspace.

- Apart from a constant, the curves also (almost) preserve the variances, provided the data are uncorrelated, with a common variance σ^2. In particular, $Var(f_y(t)) = \sigma^2(\frac{1}{2} + \sin^2 t + \cos^2 t + \sin^2 2t + \cos^2 2t)$. If the number of components in y is odd, then the variance of $f_y(t)$ is $\sigma^2(p/2)$. In case of even number of components, say $p = 2r$, it can be shown that $\sigma^2(r - \frac{1}{2}) \leq f_y(t) \leq \sigma^2(r + \frac{1}{2})$ and hence for large p, the $Var(f_y(t))$ is practically stable for all t between $-\pi$ and π.

These are the properties which result in less subjectivity and/or ambiguity compared to other graphical displays for multivariate data, when they are being gauged by human eyes. Distance related issues such as clustering or outlier identification are dealt with in a more concrete fashion due to the distance preserving property. Outliers or influential observations away from the center of the data can also be detected by locating the curves away from the average curve due to the average preserving property. Any peculiar patterns can often be identified due to the constant variance property. In general, the constant variance property is less useful since most multivariate data are either correlated and/or have unequal variances across the variables.

3.8.3. Andrews plots and Principal Components

One of the major shortcoming of Andrews plots is that, while they are able to preserve the distance and the average, they are not order preserving. In other words, the technique places greater weight on those variables listed first (e.g., y_1, y_2) and less weight on variables listed later (y_{n-1}, y_n). It is thus recommended that principal components of the original data be produced and used in the order reflecting their importance, unless there is a natural ordering that can be used. Consequently, their shapes, patterns, clustering, etc., may be affected by interchanging the coefficients of the terms in the Fourier series. Mathematically, if $y^\bigstar$ is a permutation of y, then $f_y^\bigstar(t) = a(t)y^\bigstar$ and $f_y(t) = a(t)y$ will represent different curves and their shapes and/or specific patterns may be drastically altered or get hidden. As noted by [174], since low frequencies (large periods) are more readily caught by human eyes than the high frequencies, it is useful to associate the most important variables with high periods and thus arrange the variables in a multivariate vector y by the decreasing order of their importance.

To achieve this goal and as it is mentioned in Equation (3.24), the columns of matrix $\tilde{P}$ are sorted according to the eigenvalues by descending order. The eigenvector with the highest eigenvalue represents the most important pattern in the data with the largest quantity of information. therefore, Andrew plot can be created based on the ordered data as $f_y(t) = a(t)T$. This is the technique that it is used in this thesis.

3.8.4. Alternatives for Andrew plots

Several authors, including Andrews himself, have suggested variations to the vector of functions used in Andrews plots. In this work three different alternative for Andrew plots are used as below. Equation (3.52) is original Andrew plot [174] and Equation (3.53), Equation (3.54) and Equation (3.55) are some alternatives for original counterpart [176].

$$f_y^{(1)}(t) = \frac{y_1}{\sqrt{2}} + y_2\sin(t) + y_3\cos(t) + y_4\sin(2t) + y_5\cos(2t) + \ldots - \pi \leq t \leq \pi \quad (3.52)$$

$$f_y^{(2)}(t) = y_1\cos(t) + y_2\cos(\sqrt{2t}) + y_3\cos(\sqrt{3t}) + y_4\cos(\sqrt{4t}) + \ldots - \pi \leq t \leq \pi \quad (3.53)$$

$$f_y^{(3)}(t) = y_1\sin(t) + y_2\cos(t) + y_3\sin(2t) + y_4\cos(2t) + \ldots - \pi \leq t \leq \pi \quad (3.54)$$

$$f_y^{(4)}(t) = \frac{1}{\sqrt{2}} \{y_1 + y_2(\sin(t) + \cos(t)) + y_3(\sin(t) - \cos(t)) + y_4(\sin(2t) + \cos(2t)) + \ldots\} \tag{3.55}$$

In this thesis the different alternatives are tested in the terms of damage detection.

3.9. Fuzzy similarity classifier based on Łukasiewicz-Structure

The concept of similarity is of fundamental importance in different fields and it can be considered as a many valued generalization of the classical notation of equivalence. For instance, similarity plays an essential role in taxonomy, recognition, case-based reasoning and many other fields. Fuzzy similarity is an equivalence relation that can be used to classify multivalued objects. To define the Fuzzy similarity we previously need to consider some definitions.

Definition **1** *A lattice L is a set in which for any $x, y \in L$, $x \wedge y$ and $x \vee y$ exist in L. $x \wedge y$ is called conjunction (meet, infimum) $x \vee y$ is called disjunction (join, supremum) of x and y.*

Definition **2** *A lattice is called residuated if it contains the greatest element* 1*, and binary operations $\odot$ (called multiplication) and $\rightarrow$ (called residuum) such that following conditions hold*

1. *$\odot$ is associative, commutative and isotone*
2. *$a \odot 1 = a$ for all elements $a \in L$ and*
3. *for all elements $a, b, c \in L$, $a \odot b \leq b$ if and only if $a \leq b \rightarrow c$.*

Definition **3** *Let L be a residuated lattice and X is a non-empty set. L– valued binary relation S defined in X is a fuzzy similarity if it fulfills the following conditions [177]:*

1. *Reflexivity: $\forall x \in X : S\langle x, x\rangle = 1$*
2. *Symmetricity: $\forall x, y \in X : S\langle x, y\rangle = S\langle y, x\rangle$*
3. *Transitivity: $\forall x, y, z \in X : S\langle x, y\rangle \odot S\langle y, z\rangle \leq S\langle x, z\rangle$.*

Definition **4** *Łukasiewicz structure:*

$a \odot b = max\{a + b - 1, 0\}$, $a \rightarrow b = min\{1, 1 - a + b\}$, $a \leftrightarrow b = 1 - |a - b|$

DEFINITION **5** *In generalized Łukasiewicz structure, the equivalence relation can be defined as*

$a \leftrightarrow b = 1 - |a^p - b^p|^{1/p}$

Here p is an arbitrary fixed natural number.

If the value for the magnitude of each different feature of one object can be expressed between $[0, 1]$ we can use fuzzy similarity for finding similar pairs. Let $X_{n\times m}$ be a set of n objects each of which having m features (variable). If we know the similarity value of the features $f_1, \ldots, f_m$ between the objects, it is possible to choose the objects that have the highest similarity value. The problem lies in finding, for object x_i, a similar object x_j, where $1 \leq i, j \leq n$ and $i \neq j$. By choosing the Łukasiewicz structure for the features of the objects we obtain m fuzzy similarities, one for each feature, on comparing two objects (x_1, x_2) [178]:

$$S_{fi}\langle x_1, x_2\rangle = x_1(f_i) \leftrightarrow x_2(f_i), \tag{3.56}$$

where $x_1, x_2 \in X$ and $i \in 1, \ldots, m$. As the Łukasiewicz structure is chosen for the feature of objects, we can define the fuzzy similarity as follows [170]:

$$S\langle x_1, x_2\rangle = \frac{1}{m}\sum_{i=1}^{m}(x_1(f_i) \leftrightarrow x_2(f_i)). \tag{3.57}$$

It is very important to realize that this is true only in the Łukasiewicz structure. Readers are recommended to read [179] for more information about Łukasiewicz structure. Moreover, in the Łukasiewicz structure we can assign different non-zero weights $(W_1, \ldots, W_m)$ to the different features and obtain the following equation, which again meets the definition of the fuzzy similarity:

$$S\langle x_1, x_2\rangle = \frac{\sum_{i=1}^{m} W_i(x_1(f_i) \leftrightarrow x_2(f_i))}{\sum_{i=1}^{m} W_i}. \tag{3.58}$$

A weighted similarity measure in the generalized Łukasiewicz structure can be defined as follows:

$$S\langle x_1, x_2\rangle = \frac{1}{m}\sum_{i=1}^{m} W_i \sqrt[p]{(1- \mid (x_1(f_i))^p - (x_2(f_i))^p \mid}. \tag{3.59}$$

This formula uses an arithmetic mean but it is clear that other means can also be used. This can be implemented into the similarity measure based on the Łukasiewicz

structure. The formula of the similarity based on the generalized mean and the generalized Łukasiewicz structure attains the following form [180]:

$$S\langle x_1, x_2\rangle = \left[\frac{1}{m}\sum_{i=1}^{m} W_i \left(\sqrt[p]{(1- \mid (x_1(f_i))^p - (x_2(f_i))^p \mid}\right)^m\right]^{1/m} \tag{3.60}$$

This formulation above is used as a new damage detector index to compute the similarity between features from any observation captured from current status of structure (probably damaged) and the pristine structure (Baseline). The features are selected using PCA and are fed to the formulation above.

3.10. Wavelet Ridges

The novel concept of continuous *wavelet transform* was first presented by Morlet in 1984 [181]. An overview of wavelet can be found in [182]. For completeness, a brief description of wavelet is given here. A wavelet is a waveform of limited duration that has an average value of zero as

$$\int_{-\infty}^{\infty} \psi(t)dt = 0, \tag{3.61}$$

this signal is called *mother wavelet*. This waveform plays the role of the window in short-time Fourier transform, but it can scale up or down its size without changing its shape. There is an infinite number of possible choices for the mother wavelets that could be chosen depending on the usage such as Daubechies, Gaussian, Haar, Morlet etc. For instance, Gaussian family, obtained as derivatives of the Gaussian function, are efficient in detecting sharp signal transitions and irregularities. Although Ovanesova *et al.* [183] mention that it is important to consider the ability of the chosen wavelet to perform the discrete wavelet transform (DWT) or the fast wavelet transform (FWT), due to their capability of handling discrete digital signals which is necessary for practical SHM applications, different examples in literature shows that there is no unique mother wavelet that can be used satisfactorily in SHM [184]. A basic criterion to improve the efficiency of the transform could be that the waveform of a selected wavelet function should be as similar as possible to the waveforms of major components of the e signal to be transformed [3]. Due to this fact and according to the excitation signal used in this work (see Figure 3.10) either the Morlet or the 4^{th} level of Daubechies function family (db4) could be an appropriate choice.

The Wavelet transform (WT) is a signal processing technique based on a windowing approach of dilated 'scaled' and shifted wavelets. The wavelet transform unfolds

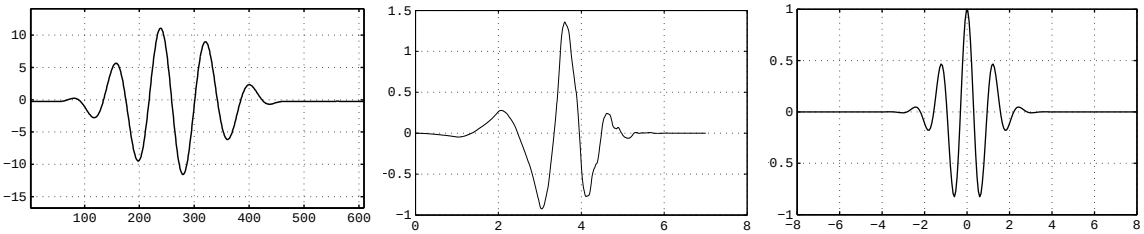

(a) Actuating signal **(b)** Daubechies wavelet **(c)** Morlet wavelet

Figure 3.10.: Similarity of wavelet mother to the actuating signal

a time function into a two-dimensional function of scale parameter s and dilating parameter u. Scale parameter scales a function by compression or stretching it and u translates the signal along the time axis. Stretching or compressing a function is collectively referred to as dilation or scaling and corresponds to the physical notion of scale. The wavelet function which is dilated by the scale parameter s, and translated by u is defined as

$$\psi_{u,s}(t) = \frac{1}{\sqrt{s}}\psi\left(\frac{t-u}{s}\right), \tag{3.62}$$

where $s \in \mathbb{R}^+ - \{0\}$ and $u \in \mathbb{R}$. Like the Fourier transform, the wavelet transform uses inner products to measure the similarity between the segment of the signal of interest and the wavelet. The wavelet transform (CWT) of $x(t)$ at the scale s and the position u is computed by correlating x with the wavelet function:

$$CWT(s,u) = \int_{-\infty}^{\infty} x(t)\frac{1}{\sqrt{s}}\psi\left(\frac{t-u}{s}\right)dt. \tag{3.63}$$

The normalization constant $s^{-1/2}$ is chosen such that every daughter wavelet (scaled wavelet) has identical energy. Dilation of the wavelet signal results in smaller time windows for higher frequencies and the opposite for lower frequencies, which is a more natural procedure for decomposition of a transient signal since a longer observation time is necessary for analyzing slower varying components of the signal [81]. The wavelet transform can be seen as a bank of filters which are constructed by dilation/compression of the single function $\psi(t)$. The wavelet transform has a number of salient properties. The most useful ones include (a) conservation of energy property, (b) localization in time and frequency domains, (c) multi-resolution properties, (d) ability to detect abrupt changes in a signal, and (e) relationship between scale and frequency [72]. Due to mentioned properties, wavelet is being applied to a broad range of engineering applications such as signal processing, data compression, computer graphic and clustering techniques [26].

Carmona *et al* [185, 186] suggest that fundamental information about structural dynamics is contained in the *maxima lines* or *ridges* of the CWT where the modulus of the CWT is concentrated in this neighborhood. More specific, the ridge can be defined as the location where the modulus of the CWT reaches its local maximum along the scaling direction. These are essentially the points in the time-frequency plane where the natural frequency of the translated and dilated wavelet coincides with the local frequency, or one of the local frequencies, of the signal. These the author believes that ridges form the skeleton of the transform [187]. The signal may even be reconstructed accurately from these special lines. Therefore, ridges of CWT could be used as an appropriate alternative for pure signal to apply damage detection algorithms because all significant information of signal are in these curves and in addition information in ridge are less redundant rather than the wavelet transform. Moreover, real and imaginary part of wavelet coefficients extracted along the ridge, can approximate the signal and its Hilbert transform that could be used to calculate energy envelope of signal [188].

In the literature, some ridge extraction algorithms have been proposed. In some of the proposed approaches, calculating the wavelet coefficient is not necessary [189, 185]. For instance, Haase *et al.* [186] derive sets of ordinary differential equations which are directly integrated in physical space leading to ridges. Generally, in the simple case where the signal possesses a unique ridge, for each fixed value of position variable b, we can search for a value of scale, say a_b, such that,

$$Ridge = \max_{a} \mid SG(b,a) \mid . \tag{3.64}$$

This yields an estimate for the ridge, which is precise enough for most of the applications [190]. Regarding to this definition, the wavelet ridges are simply the maxima points of the normalized scalogram representing the wavelet coefficients with respect to the different time and scale values.

In this study, PCA is applied on wavelet ridge instead of original data and the efficiency of this substitution is demonstrated by implementing the proposed method on various structures. The result and more detailed study can be seen in section 5.5.

3.11. Wave cluster

The aim of data-clustering methods is to group the objects in databases into meaningful subclasses. Clustering tries to detect groups and assign labels to the objects based on the cluster that they belong to. A good clustering algorithm should be time efficient, order-insensitive and be able to identify clusters irrespective of their shapes and relative position. Clustering algorithms are categorized into four main

groups: partitioning algorithms [191], hierarchical algorithms [192], density based algorithms [193] and grid based algorithms [194, 195].

Partitioning methods relocate instances by moving them from one cluster to another, starting from an initial partitioning. To do this, some iterative control strategy is used to optimize an objective function such as Error Minimization Algorithm ($k-$means) [191], Graph-Theoretic Clustering [196], and others.

Hierarchical algorithms construct the clusters by recursively partitioning the instances. This algorithm iteratively splits the database into smaller subsets until some termination condition is satisfied. Comparing with partitioning algorithm, hierarchical algorithms do not need k as input parameter. This is an advantage but in contrary the termination condition need to be declared [197].

Density based algorithm allocate the observation with the similar probability distribution to the same cluster. The overall distribution of the data is assumed to be a mixture of several distributions. This algorithm aims to identify the cluster and its distribution parameter [193].

Grid based methods partition the space into a finite number of cells that form a grid structure on which all of the operations for clustering are performed. The main advantage of the approach is its fast processing time because it is independent of the number of objects. In this work we use a spatial data-mining method termed Wave Cluster that belongs to this category.

Wave Cluster is an efficient method with low computational complexity. The results are less affected by noise and the method is not sensitive to the order of input objects. The main idea of Wave Cluster is to transform the original feature space by applying wavelet transform and then find the dense regions in the new space. In this procedure the process of finding the connected components in the transformed space is easier than in the original feature space, because the dense regions in the feature space will be more salient [198]. Applying wavelet transform on a signal decomposes it into different frequency sub-bands. The high frequency parts of the signal are related to the regions where there is a rapid change such as boundaries of cluster, while the low frequency part corresponds to the areas that the objects are more concentrated, the cluster themselves. In another words, observations in a $2D$ feature space are considered as an image where each pixel of image corresponds to one cell in the feature space. To achieve this goal, the discrete wavelet transform (DWT) is used. Using DWT, details and approximation of signal are decomposed for different steps. Approximation or average sub-band carries information about content of cluster and details sub-bands have information about the boundaries of clusters.

The multidimensional spatial data objects can be represented in a $d-$dimensional *feature space*. For an object with d numerical attributes, the feature vector will be one point in $d-$dimensional feature space. Wave Cluster proposes to look at the feature space from signal processing perspective. It means that the high frequency parts of the signal correspond to the regions of the feature space where there is

a rapid change in the distribution of objects, that is, the boundaries of clusters. The low-frequency parts of the $d-$dimensional signal which have high amplitude correspond to the areas of the feature space where the objects are concentrated, in other words, the clusters themselves. For instance, Figure 3.11 presents a $2D$ feature space where each point of the image represents the feature values of one object in spatial dataset. Thanks to the properties of wavelet transform for detecting rapid changes in the signal, we can apply wavelet transform to find high-frequency and low-frequency parts of the $d-$dimensional signal that bring about clusters detection.

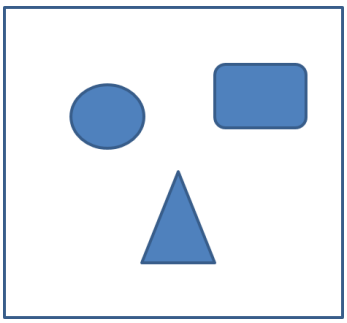

Figure 3.11.: A sample $2D$ feature space

Wavelet transform can be generalized to $d-$dimensional signal in which a $1D$ transform can be applied multiple times. The key point of Wave Cluster is to apply wavelet on feature space instead of the objects themselves to find the clusters. Wavelet decomposes the original feature space into an *approximation* which has information about the content of clusters, an *details* which have information about the boundaries of the clusters.

According to Sheikholeslami et al [195, 198], WaveCluster algorithm is implemented through the following steps:

Input: Multidimensional data objects' feature vectors

Output: clustered objects

1. Quantize feature space, and then assign objects to the cells.
2. Apply wavelet transform on the quantized feature space.
3. Find the connected components (clusters) in the sub bands of transformed feature space, at different levels.
4. Assign labels to the cells.
5. Make the look-up table.
6. Map the objects to the clusters.

To describe the algorithm in details, let $A_1 \times A_2 \times \ldots \times A_d$ be a $d-$dimensional feature space. The input dataset is a set of $d-$dimensional points $O = \{o_1, o_2, \ldots, o_N\}$, where $o_i = (o_{i1}, o_{i2}, \ldots, o_{id})$, $1 \leq i \leq N$. The first step is to quantize A_i feature

space to m_i number of intervals. For sake of simplicity, m_i could be equal for all dimensions. Each cell is defined as an intersection of one interval from each dimension. It has the form $< c_{i1}, c_{i2}, \ldots, c_{id} >$ where $c_{ij} = [l_{ij}, h_{ij})$. We say that a point $o_k =< o_{k1}, \ldots, o_{kd} >$ is contained in a cell c_i if $l_{ij} \leq o_{ki} \leq h_{ij}$ for $1 \leq j \leq d$. We count only the number of observations belong to the cells as statistic to be used.

In the next step, discrete wavelet transform will be applied on the quantized (each cell now is represented by the number of observation belong to it) feature space. Applying wavelet transform on the cells results in a new feature space and hence new units. There are many well-known algorithms for finding connected components in image and Wave Cluster uses the algorithm in [199] to find the connected components in the $2-$dimensional feature space. The founded clusters are in the transformed feature space and are based on wavelet coefficients. Thus, they cannot be directly used to define the clusters in the original feature space. Wave Cluster makes a hookup table to map the units in the transformed feature space to the units in the original feature space. Finally, Wave Cluster assigns the label of each unit in the feature space to all the objects whose feature vector is in that unit, and thus the clusters are determined [195, 198].

As all data should be at least read, the required time for this algorithm to detect the clusters is linear in terms of number of input. After reading the data, the processing time will be only a function of number of cells in the feature space. Therefore, applying PCA as a primary step to reduce the dimension of the data is a beneficial step based on the fact that Wave Cluster will be very efficient for low number of feature space dimension.

3.12. Orthogonal Distance as damage index

When data are projected on the reduced dimension PCA-subspace, they could be categorized as four types of observations. For instance, Figure 3.12 shows the different types of observations when a three dimensional data set is projected on a two-dimensional PCA-subspace. The first group are normal observations or regular observations that form one homogeneous group that is close to the PCA subspace. The second group is a data set which lies close to the PCA space but far from the regular observations (observation 1 and 2). This type of observations are called *good leverage.* Next group is called *orthogonal outliers* whose their distance to the PCA space, orthogonal distance (OD), is large but they are undetectable whether we only look at their projection (observation 3). And finally, *bad leverage points*, observation 4, are data that have a large orthogonal distance to the PCA space and whose projection on the PCA subspace, score distance (SD), is remote from the typical projections and they are out of threshold for both distances [160]. To distinguish between regular observations and the three types of abnormal observations for higher dimensional data, the two mentioned distances are defined as below. First

score distance SD_i of each observation, given by

$$SD_i = \sqrt{\sum_{j=1}^{k} \frac{t_{ij}^2}{l_j}}, \tag{3.65}$$

and the orthogonal distance

$$OD_i = \|x_i - \hat{\mu} - P_{m\times k} t_i^T\|. \tag{3.66}$$

In these equations mentioned above, t_{ij} represents the score associated to i_{th} observation and j_{th} dimension and l_j represents the j_{th} eigenvalue from the k selected robust eigenvalues/eigenvectors. Moreover, $\hat{\mu}$ and $P_{m\times k}$ are mean and loading matrix for original data respectively.

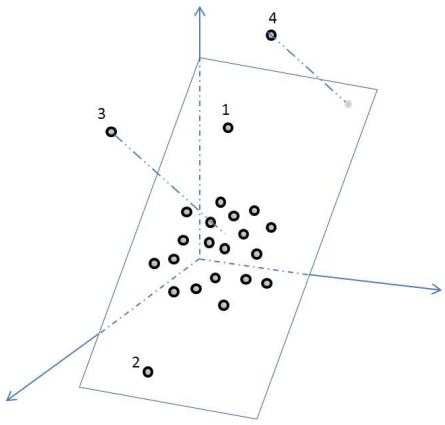

Figure 3.12.: Different types of observations when a three-dimensional data set is projected on a two-dimensional PCA-subspace

In next section, we will show that how orthogonal distance is used as a damage detection index. Indeed we use robust version of PCA (ROBPCA) too calculate the OD of observations.

3.12.1. Damage detection strategy based on PCA orthogonal distance

As was described before, the defined distances in section 3.12 could be used as a damage detector index. To achieve this goal, a methodology is proposed based on OD as a damage detection index. At the beginning, it is necessary to collect data from the healthy status of the structure (baseline). This data are used as

a reference; the new observation (one by one) from unknown status of structure (probably damaged) is added to the baseline to create the test data. As the majority of data in test data belong to the healthy status, the PCA space inherits its behavior from healthy structure. Therefore, any new data that does not belong to the pristine condition is expected to have distinct OD. In this way, the OD of the any new observations from unknown status of structure is compared with the OD from data from pristine status. This is the key-point in this algorithm that means if the new observation does not belong to the majority of data (pristine condition), then their OD is significantly different from the ODs of other observations. Besides, in this work, we use a robust variant of PCA to achieve this goal since the robust PCA is able to distinguish the contaminated observation from the healthy observation with more robust and reliable outcome. Figure 3.13 depicts the described algorithm. OD calculated in this way is used as a damage index.

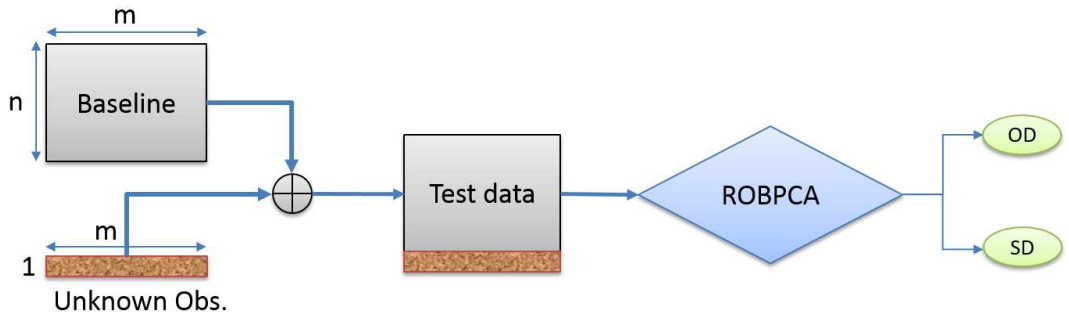

Figure 3.13.: Damage detection algorithm using ROBPCA orthogonal distance

3.13. The effect of environmental changes on damage detection

In section 3.6, the effect of outliers on data interpreting and damage detection is presented. In addition to the outliers that can affect the efficiency of any damage detection algorithm, environmental changes are another most important technical challenges in SHM approaches. Most existing approaches for activating and receiving Lamb waves were developed with the scenario that the structure to which the transducers are affixed is placed in laboratory conditions with ideal environmental temperatures (20°CC - 25°CC). The effects of environmental temperature and moisture on the activation and acquisition of wave signals as well as wave propagation characteristics have not been of concern. It has been demonstrated that there is no particular need to apply corrections to compensate for a small change in ambient temperature in normal applications. However, an engineering structure such as an aerospace vehicle may work intermittently in diverse environments with temperature fluctuations of hundreds of Celsius or more (e.g., day vs. night, high altitude

vs. ground). Therefore, it is necessary, to be able to distinguish between influences on the signal driven by environmental changes and influences driven by damage.

When the structure is under not variant environmental conditions, although many damage detection techniques are successfully applied to scale models or specimen tests in controlled laboratory environments, the performance of these techniques in field is still questionable. Therefore there is still some obstacles for deploying a SHM system for in-service structures is the environmental and operational variation of structures. In fact, these changes can often mask subtler structural changes caused by damage. Often the so-called damage-sensitive features employed in these damage detection techniques are also sensitive to changes in environmental and operational conditions of the structures.

When the environmental or operating variability is an issue, there are three different situations for dealing with the problem. First, when direct measurements of the varying environmental are available; in this case, regression and interpolation analysis can be performed to relate measurements relevant to structural damage and those associated with environmental and operation variation of the system.

On other situations that direct measurements of environmental parameters are difficult to achieve and the damage signature is *orthogonal* to environmental signature, it also may possible to distinguish this change.

Finally, there are other researchers who attempt to explicitly extract features that are mainly sensitive to damage but insensitive to operational and environmental variations.

3.13.1. Temperature compensation techniques

Due to the effect of temperature fluctuation mentioned above, a simple baseline comparison methods are unable to distinguish damage from environmental and operational effects.

Different methodologies are proposed to compensate the effect of temperature such as interpolation and extrapolation of baseline [33], baseline signal stretch (BSS) [106] or optimal baseline selection (OBS) [37, 129].

In this work, first the effect of temperature is analyzed on the performance of the damage index and then the OBS technique is used to compensate the effect of temperature on the damage damage detection index.

In OBS technique (See Figure 3.14), to discriminate the effects of damage from those of environmental changes, a "bank" of baseline signals acquired at the various temperatures $(T_1, T_2, \ldots, T_n)$ and later the response data (from unknown status) is compared with baseline database to find the closest match (T_i). The selected baseline is used as the data representing pristine structure in this temperature. Unlike BSS, that technique does not change the time-trace but simply reduces the temperature difference seen. To achieve the highest performance, the baseline database

should be formed at number of temperatures spanning the expected service range. In the next step, the best baseline signal is selected using appropriate measurement distance. Michaels [37] suggests three differential features which calculate the difference between the signal and the baseline. The first feature is the normalized squared error between the signal and baseline,

$$E_1 = \frac{\int_0^T [y(t) - x(t)]^2 \, dt}{\int_0^T x(t)^2 dt}. \tag{3.67}$$

Here $y(t)$ is the signal and $x(t)$ is the baseline and T is the time window over which the signal are compared. The second feature is the signal difference coefficient as,

$$E_2 = 1 - \frac{\int_0^T [x(t) - \mu_x] [y(t) - \mu_y]}{\sigma_x \sigma_y}, \tag{3.68}$$

where μ is the mean and σ the standard deviation.

In contrary to E_1, the second feature is affected only by change in the shape of the signals, not by amplitude variation. The third feature is based on the loss of local temporal coherence between the signal and baseline as,

$$\gamma_{xy}(\tau, t) = \frac{R_{xy}(\tau, t)}{\sqrt{R_{xx}(0, t) R_{yy}(0, t)}}, \tag{3.69}$$

where is the normalized version of the short time cross correlation as:

$$R_{xy}(\tau, t) = \frac{1}{\Delta T} \int_{t - \frac{\Delta T}{2}}^{t + \frac{\Delta T}{2}} x(s) w(s - t) y(s + \tau) w(s + \tau - t) ds, \tag{3.70}$$

where $w(t)$ is a windowing function and τ is the cross correlation lag. The loss of local coherence is how far the average of the local coherence as,

$$E_3 = 1 - \frac{1}{T} \int_0^T \underset{\tau}{max} \mid \gamma_{xy}(\tau, t) \mid dt. \tag{3.71}$$

The result and more discussion about applying this technique is presented in chapter 6.

In this chapter the theoretical background for different methodologies are presented. These techniques will be used in different case studies to detect probable damages. The details and results are presented in following chapters.

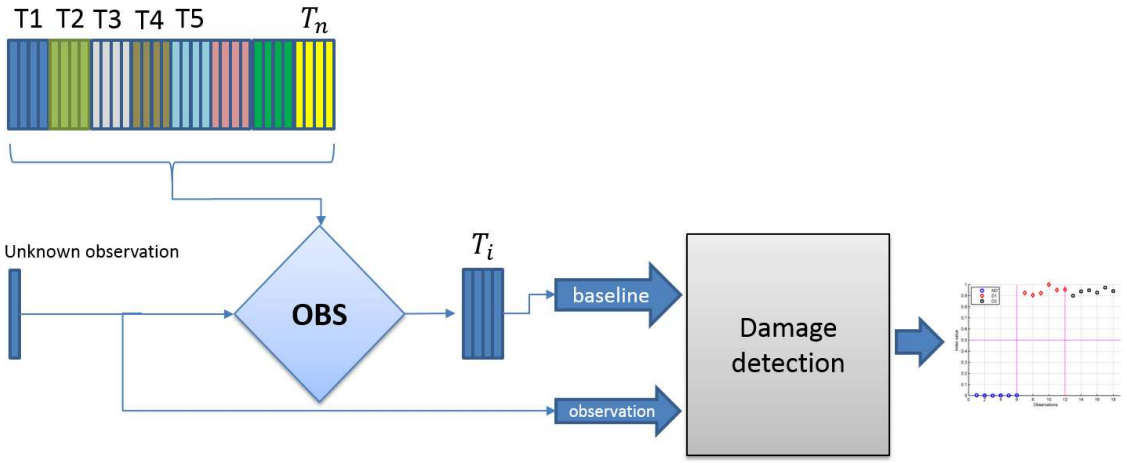

Figure 3.14.: Schematic of OBS temperature compensation technique

4. CASE STUDIES

Collecting reliable and pure data is a vital part of any scientific development. To this aim, a series of experiments is performed to capture necessary data for testing and proving the methodologies that are developed in this thesis. Experiments are performed in four laboratories.

1. CoDAlab Structural Health Monitoring laboratory, Technical University of Catalunya (UPC), Barcelona, Spain.
2. SHM laboratory in Universidad Politécnica de Madrid (UPM), Madrid, Spain.
3. Institut für Mechanik und Regelungstechnik, Siegen, Germany.
4. Structural Health Monitoring laboratory, University of California San Diego, USA.

The first laboratory is the local laboratory where the current thesis is performed. The SHM laboratory of the CoDAlab group is funded by the "Ministerio de Ciencia e Innovación" of Spain through the coordinated research project DPI2008-06564-C02-01/02 and DPI2011-28033-C03-03, and running the experiments was performed in collaboration with former Ph.D. student *Dr. Diego Tibaduiza.*

The second laboratory is located in UPM. In 2011, a short visit was made to run some experiments on a real scale structure with the supervision of Professor Alfredo Güemes.

The third laboratory is located in Institut für Mechanik und Regelungstechnik from University of Siegen, Germany. The opportunity reached thanks to a stay scholarship related to the Formación de Personal Investigador (FPI) grant of the author by the Spanish Ministry of Science and Innovation. This visit was performed for six months at the second half of 2011.

The last laboratory is located in the Department of Structural Engineering at the University of California San Diego. This opportunity also reached thanks to a stay scholarship related to the FPI Grant of the author. This visit was performed for three months at the second half of 2013. The laboratory and research group is supervised by Prof. Michael Todd. He has taught undergraduate courses in dynamics, vibrations, nondestructive testing and evaluation, solid mechanics, and mechanical system testing, correlation, and model updating.

4.1. SHM laboratory, Technical University of Catalunya, Spain

CoDAlab SHM laboratory consists of basic equipment for generating and acquisition procedure available to be implemented on different structures.

In general, CoDAlab has:

1. A portable National Instruments chassis (NI-PXI 1033): this chassis provides 5 slots; each of which can host a slot from instruments cards for different procedures.
2. A NI PXI-5114 card, it is an 8-bit Digitizer/oscilloscope of 250MS/s with 40mV to 40V input ranges.
3. A card NI PXI-5412, it is an arbitrary waveform generator with 14-bit resolution and 100 MS/s sampling rate.
4. A Cross point Matrix Switch card.
5. Wideband Power amplifier 7602M [200].
6. Computational equipment, for connecting to chassis and generating, acquisition and applying different approaches.
7. A shelf for hanging-up the test structures.

Figure 4.1 and Figure 4.2 show the mentioned equipment available in CodaLab SHM laboratory. Using the equipment and thanks to the comprehensive platform provided by Lab-View, a series of experiments are conducted mainly on an aluminum plate. The main challenge on doing this experiment was to initialize an automatic platform. In other words, it has been attempted to design and develop a platform that allows to activate and receive signals from a network of transducers automatically. This aim is achieved in collaboration with former Ph.D. student *Dr. Diego Tibaduiza.* The main abilities of this system are:

1. Create an appropriate excitation signal based on a Matlab function able to be customized according to the needs.
2. Exciting the actuator and receiving the Lamb wave signal from the sensors.
3. Supporting a network of transducers up to 32 PZTs.
4. Programmable to automatically run the whole experiment.
5. Saving and converting data to a Matlab friendly file.
6. Error handling.
7. Sending email when the experiment is done.
8. User friendly interface.

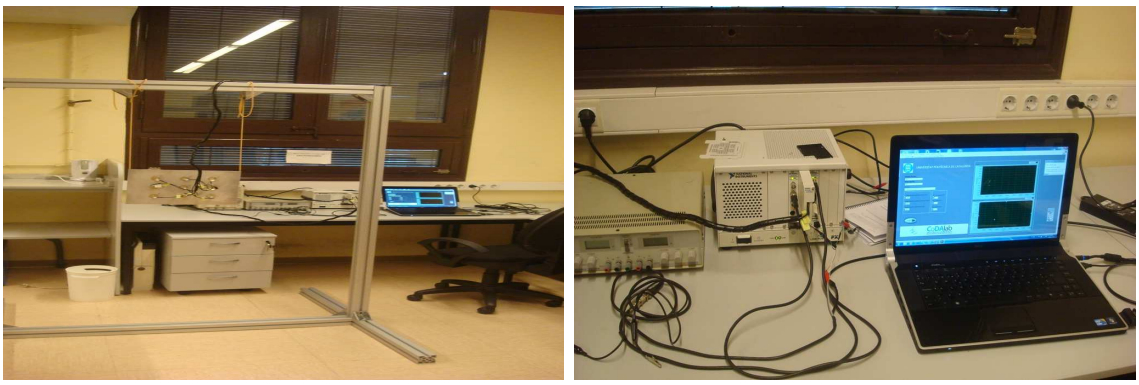

(a) Structure holding platform **(b)** Acquisition setup

Figure 4.1.: CoDAlab Laboratory, Technical University of Catalunya, Spain

(a) Wideband power amplifier [200] **(b)** National Instrument Chassis [201]

Figure 4.2.: Acquisition setup, Technical University of Catalunya, Spain

4.2. SHM laboratory, Universidad Politécnica de Madrid (UPM), Spain

The experiments performed on a skin panel of the torsion box of the wing. This structure is divided into small sections by stringers and ribs. The schematic and snapshot of this case study is shown in Figure 4.3. As an acquisition setup, the structure is equipped with piezoelectric transducers (PZT) from PI Ceramics with reference number PIC151 with $10mm$ diameter. The positions of PZT's are distributed over the surface to excite the structure and detect time varying strain response data. The transducers dimensions are $26mm$ in diameter and $0.4mm$ in thickness. A burst signal with three peaks at different frequencies are used as excitation signal. The same acquisition setup from CoDAlab laboratory is used in this case study (see Section 4.1). Before applying the signal to the structure, it is amplified to 30 V peak-to-peak using a wideband power amplifier. All data are averaged to obtain one signal for each 10 experiments in order to reduce the noise in the experiments. All data collections are done in room temperature without any temporal changes during the experiments. Due to the limitation to apply real damages on the structure, damages are simulated by placing an appropriate mass in different

locations. Adding mass to a structure cause changing acoustic impedance change of propagating wave that simulates the damage effect. The experiments are performed on both faces of the structure and they are described as follows.

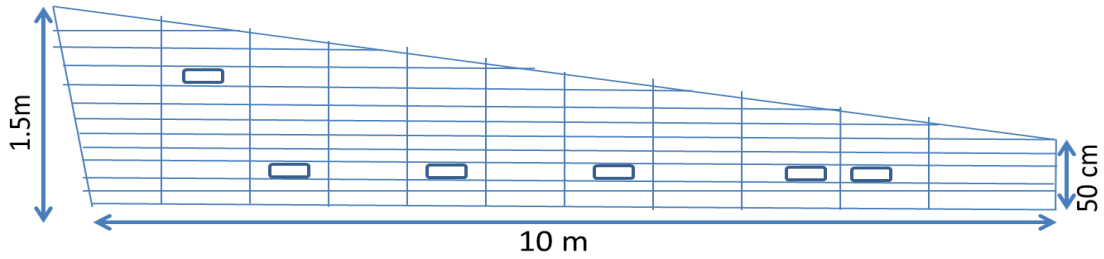

(a) Skin panel schematic

(b) Skin panel snapshot

Figure 4.3.: Aircraft skin panel located in SHM Lab., Madrid

4.2.1. Case study 1, the face without stringers and ribs

As a first case study, PZTs are mounted on the plane surface of skin panel where there are neither stringers nor ribs as obstacles. They are located at 9.5cm distance from each other in the straight line and 5cm distance from the closest edge of structure. Figure 4.4 shows the sensor location and damage position in this case study. The actuating signal is applied to the first PZT ($S1$) and the response is captured on the second PZT (S2). Damage is located on the route between S1 and S2. The structure was excited by signals of 75KHz to 370KHz with 5KHz steps. Figure 4.5 shows a few examples of the response signal at 4 different frequencies. The whole captured signal is used without performing any mode selection. All captured signals are denoised using discrete wavelet transform with Daubechies wavelets family until third level. In this case study, a number of 50 observations for any status of the structure is captured.

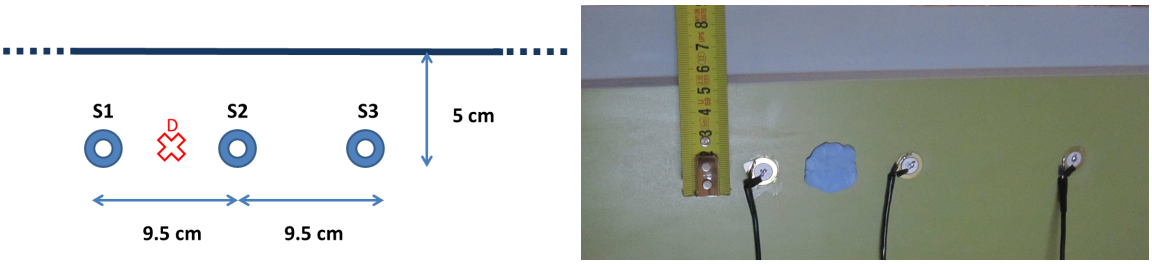

(a) Schematic **(b)** Snapshot

Figure 4.4.: Sensor location and damage position, case study 1, schematic and snapshot, SHM Lab., Madrid

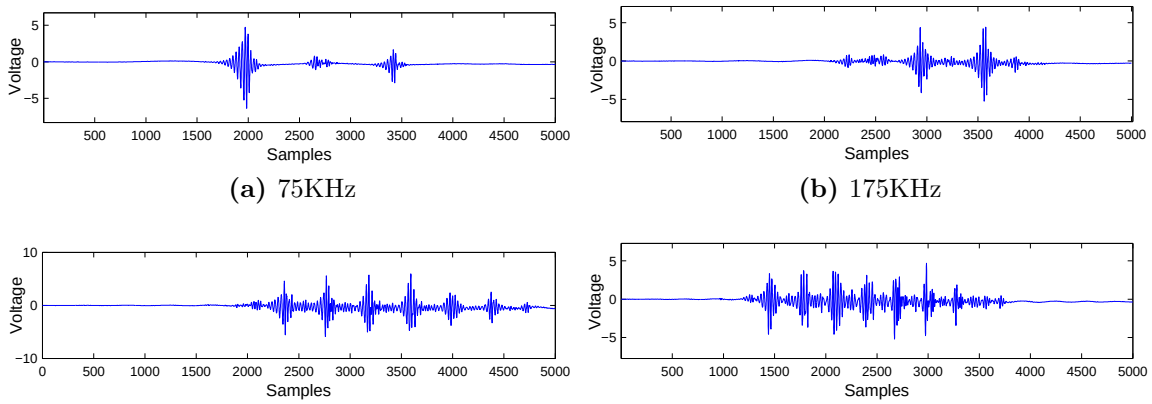

(a) 75KHz **(b)** 175KHz

(c) 275KHz **(d)** 365KHz

Figure 4.5.: Response signal, case study 1, captured by sensor 2, SHM Lab., Madrid

4.2.2. Case study 2, the face with stringers and ribs

The second case study is performed on the second face of the structure. This side is divided into many sections by stringers (vertical lines) and ribs (horizontal lines). Sensors are located somehow that each pair of PZT (S1 and S2) and (S3 and S4) are located in the same section. Figure 4.6-a shows a scheme of sensor location and damage positions. Two damages are simulated by adding mass as shown in Figure 4.6-b and Figure 4.6-c. Excitation is performed on different frequencies from 125KHz to 365KHz with 10KHz steps. In this case study a number of 30 observations are captured for each status of the structure.

4.2.3. Turbine blade

The specimen used in this case study is a turbine blade of a commercial aircraft. The blade is manufactured by a homogenous material with a similar density to that

(a) Sensor location and damage position schematic **(b)** Damage 1 **(c)** Damage 2

Figure 4.6.: Sensor location and damage position, case study 2, SHM Lab., Madrid

of titanium ($3.57g/ml$). The blade is suspended by two elastic ropes. Seven PZT sensors are distributed over the surface to detect time varying strain response data. Three of the sensors are located on one face and four on the other face as can be seen in Figure 4.7-a. To alleviate the influence of environmental conditions and isolate the experiments from environmental conditions the blade is suspended by elastic ropes.

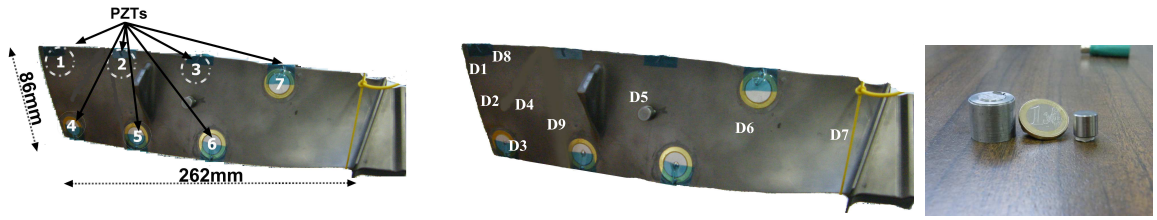

(a) PZT's location **(b)** damage location **(c)** simulated damage

Figure 4.7.: Turbine blade, SHM Lab. Madrid

Damages were simulated adding masses at several locations as shown in Figure 4.7-b and Figure 4.7-c. Data are captured and arranged in two parts. First, baseline signal from non-damaged structure are gathered and used as training data to build the statistical model using PCA. In next step, damages are simulated and related data are captured for each damage. 80% of data captured from pristine structure is used to create the model. The rest of training data and all data from different structure's status are used for testing. Totally 140 experiments are performed and recorded, 50 for undamaged structure and 10 per each damage.

4.3. Institut für Mechanik und Regelungstechnik, Siegen, Germany

The Department of Engineering Mechanics is concerned with oscillatory processes in solid mechanics. A series of tests were executed during 6 months staying in this department. Mainly it has been tried to concentrate on testing related to environmental changes beside other tests such as fuselage and impact classifications. All experiments were executed using a HandyScope acquisition system [202] that is running under Matlab platform. Structures were excited with signals with different frequencies. A brief description of the performed experiment are presented.

4.3.1. Aluminum Plate

A variety of aluminum plates in small scale were used to capture the information in presence of seeded damages that could happen in real scale structures. To do this, a small size aluminum plate ($200 \times 40 \times 2mm$) was produced in the laboratory. Different damages with different severity were applied and the appropriate data were captured. The schematic and a snapshot of the mentioned experiment can be seen in Figure 4.8. The damages were done by making a hole with different dimensions (see Figure 4.9). In this specimen, sensors are placed of $41mm$ far from each other. Totally 7 damages are introduced with increasing the size and depth. The beam is equipped with temperature sensors to make sure that there is no significant temperature fluctuation during the experiment.

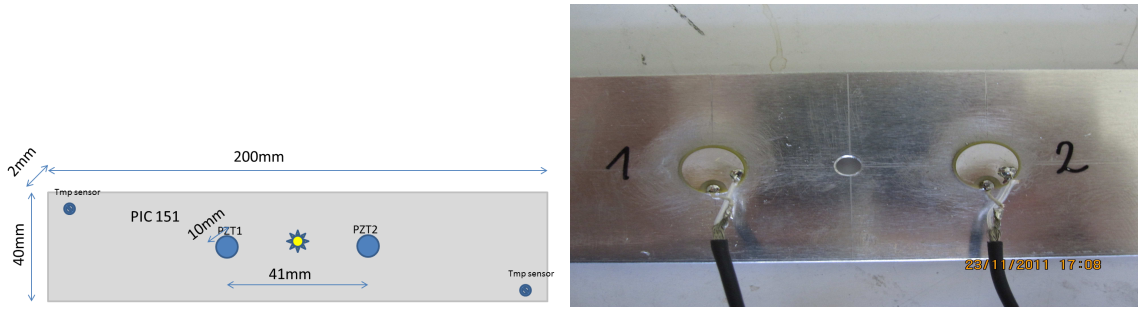

(a) Schematic **(b)** Snapshot

Figure 4.8.: Small scale aluminum plate with seeded damages, SHM Lab. Germany

4.3.2. Composite plate

Composites are widely used in aerospace structures because of special properties they offer. Due to complexity of wave propagation in composites, any kind of damage detection and localization seems to be more sophisticated. In this case study a

(a) Damage 1 **(b)** Damage 2

Figure 4.9.: Damages with different dimensions in small scale aluminum plate, SHM Lab. Germany

composite plate is used as the specimen (see Figure 4.10-b). The plate is made of 4 equal layers and stacking of [0/90/0/90] with dimensions: $200mm \times 250mm$ and a thickness of approximately $1.7mm$ (see Figure 4.10-a). Nominal material parameters of the unidirectional (UD) layers are $E1 = 122GPa$, $E2 = 10GPa$, $v_{12} = 0.33$, $v_{13} = 0.3$, $v_{23} = 0.34$, $G_{12} = G_{13} = 7.4GPa$ and $G_{23} = 5.4GPa$. The density is about $1700kg/m^3$.

Nine PZT transducers PIC-151 from PI Ceramics were attached to the surface of the structure with equidistant spacing. The piezo transducers have a diameter of $10mm$ and a thickness of $0.5mm$. The excitation signal to the actuators was generated using the arbitrary signal generation capability of a HandyScope HS3.

Damages are simulated by adding appropriate mass powered by magnet to hold them and apply enough pressure on the plate (see Figure 4.10-c).

A 10 V Hann-windowed tone-burst signal is used as an actuating signal with different carrier frequencies (30, 50, 60 KHz) with 3 cycles.

For sake of simplicity and according to the symmetry of the structure, transducers number 4, 5, 7 and 8 are used for this experiment (the rest of transducers was allocated because of other experiments in the local laboratory). The four transducers are used as actuator and 13 observations are recorded per sensor. Actuating the structure is performed for any status of structure including pristine and structure with different simulated damages. Signals are de-noised and decimated using Matlab® software. Observations are used in two different ways. Primary, damage detection is performed per each route. A route is defined as the path between one transducer as an actuator and another as a sensor; hence there are 3 different routes for each actuator. Secondly, data from each actuator to all other sensors are folded in a unique matrix and the same procedure is repeated for damages in the area surrounded by 4 transducers.

4.3.3. Fuselage

Laboratory benchmarks are usually used to test and make rudimentary proofs for algorithms. But applying any algorithm on a real scale structure is critical in this field. The structure which is described in this section is a fuselage of a commercial aircraft. This structure includes a curved plate, four vertical stringers and seven

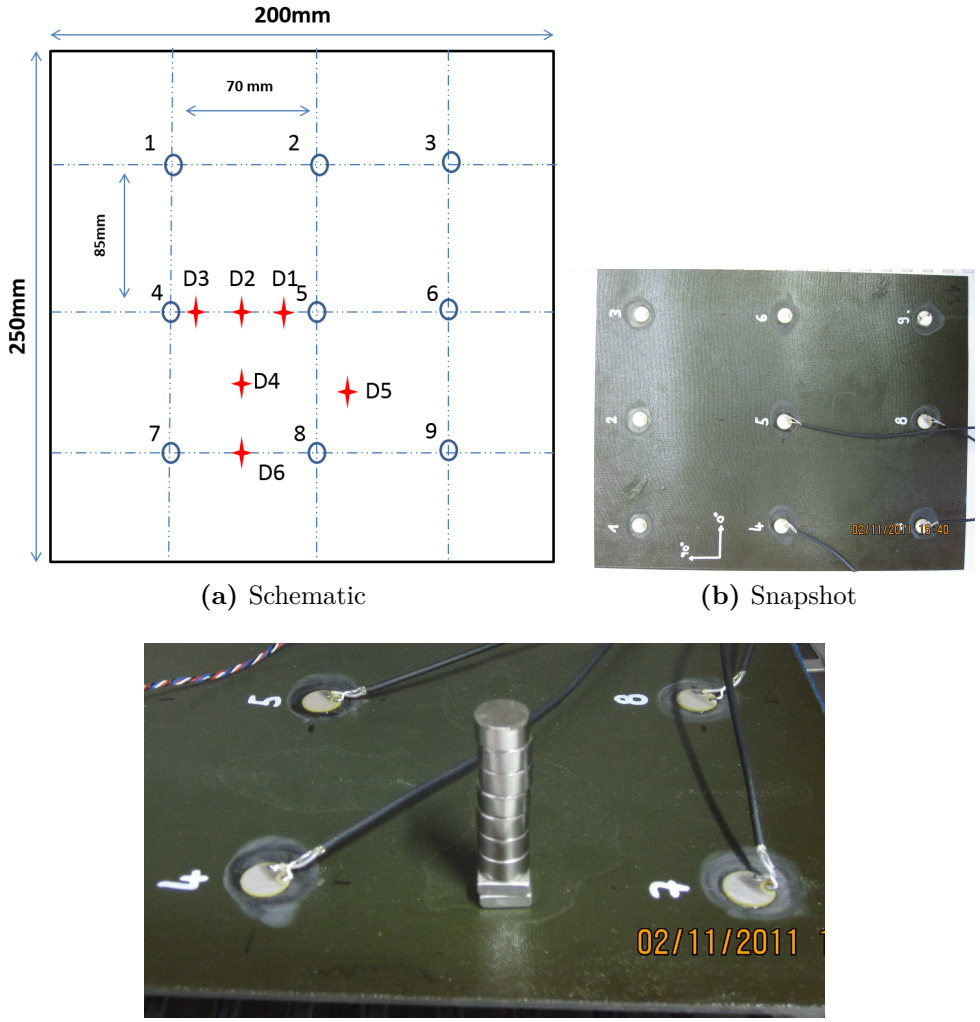

(a) Schematic

(b) Snapshot

(c) Snapshot of damage

Figure 4.10.: Composite plate for damage detection, schematic and snapshot, SHM Lab. Germany

horizontal ribs. The fuselage was instrumented with nine broadband piezoceramic PIC-255 from PI Ceramics bonded on the curved plate surface with the purpose of transmitting and receiving ultrasonic guided waveforms. The transducers dimensions were diameter $10mm$ and thickness $0.25mm$. The transducers configuration is illustrated in Figure 4.11-a. The area surrounded by 4 transducers are selected to run the experiment. The length, width and thickness of the fuselage are $2000mm$, $1250mm$ and $2mm$, respectively. In a network of PZTs consists of 4 PZT, any PZT is excited with an appropriate signal and the dynamic response is recorded by the other PZTs. This procedure is repeated for all PZTs.

In this structure, due to limitation to apply real damages, damages are simulated using adding mass (see Figure 4.11-e) on the surface of the structure in different

places in the measurement area (see Figure 4.11-b). Totally 12 routes exist each route connecting an actuator and a sensor. First and second damages are simulated by locating appropriate mass on routes between first and second transducer and the next 2 damages are located on the route between transducer 1 and 3. Figure 4.11-c and 4.11-d illustrate the structure from different views.

4.3.4. Environmental effects, temperature and humidity

To test the effect of temperature fluctuation, various experiments performed using an industrial chamber and a commercial fridge. Mentioned experiments performed in a range of +25°C to +70°C (using chamber) and also +25°C to −30°C (using fridge) that cover the majority of working conditions. Composite plate and the aluminum plate described in Section 4.3.2 and 4.3.1 respectively, are used in this experiment. Figure 4.12 shows the different part of this experiment such as chamber snapshot, chamber control panel and different specimen hanged in the chamber.

4.3.5. Tube benchmark

One of the most important fields of non-destructive testing (NDT) and SHM is the monitoring of pipework in gas and oil industries, suspension bridge cables, nuclear fuel cladding tubes etc. Thanks to the available tube benchmark, several experiments were executed on a pipe such as crack and corrosion in presence of liquid or without liquid. The excitation was done using the same acquisition system used before in this laboratory. Figure 4.13 shows the test bench snapshot, tube snapshot, corrosion and cracks as simulated damages. The dimension of tube is $40mm$ and $37.5mm$ for outer and inner diameter respectively. As the tube was removable, all the screws are fasten with the handy machine with $50N$ to be sure they have the same power.

Waves are generated by actuating the 4 PZTs on the left side of the pipe using a 180KHz tone burst signal with the amplitude of 10 volts and these are captured by each of the 4 PZTs on the right side. The PZTs are numbered in order of up, rear, down and front in both sides starting from actuators (i.e. PZT 1 correspond to left side and upper position and so on). Therefore, 16 routes exist each route connecting an actuator on the left side and a sensor on the right side. Each experiment is repeated 20 times for each route to reduce noise and a mean signal is saved to obtain one observation. Finally, 30 observations are captured for each route in each state (different damages and pristine structure).

Damages are presented by adding measured cuts with different depths in order to simulate damages with different severity ($0.75mm$ crack depth, $2mm$ crack depth and $16mm$ width, $2mm$ crack depth and $30mm$ wide, complete hole). Figure 4.13-f shows an example of mentioned damages. Damages are placed in a line between actuator 2 and sensor 6.

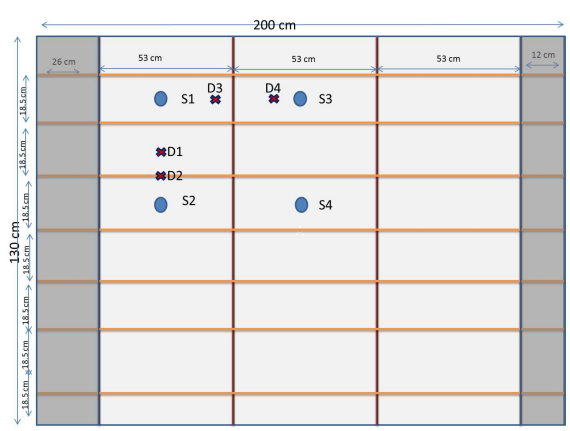

(a) Schematic

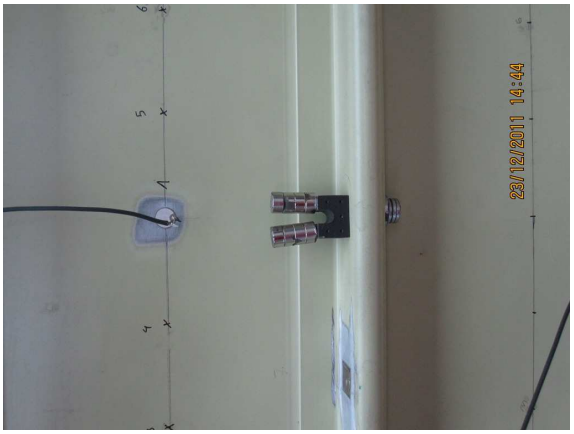

(b) Sensor

(c) Snapshot

(d) Snapshot

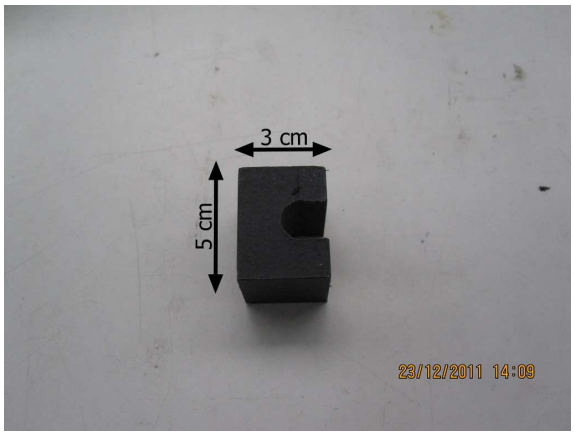

(e) Damage

Figure 4.11.: Fuselage structure, SHM Lab. Germany

(a) Chamber

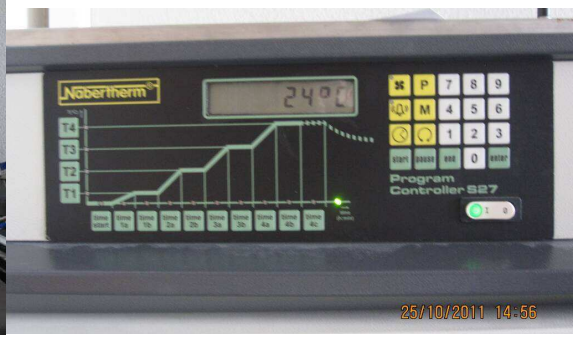

(b) Panel Control

(c) Composite plate hanging

(d) Aluminum plate hanging

(e) Composite plate

(f) Aluminum plate hanging

Figure 4.12.: Experimental setup for temperature tests, SHM Lab., Germany

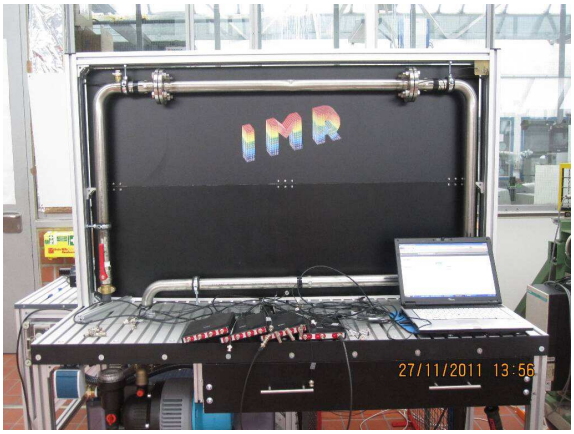

(a) Whole system snapshot

(b) Snapshot

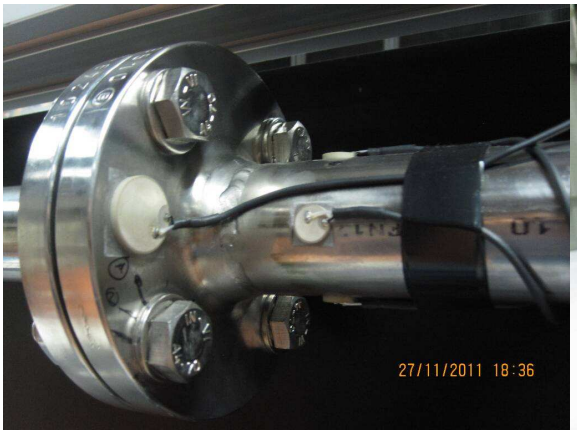

(c) Sensor position

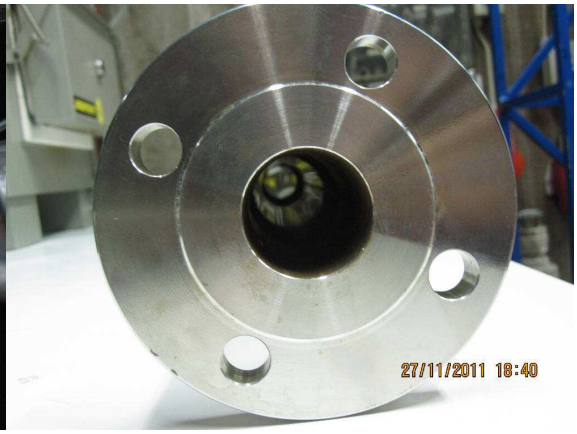

(d) Tube snapshot

(e) Different types of damage

(f) Crack

Figure 4.13.: Tube benchmark experimental setup, SHM Lab., Germany

4.4. SHM laboratory, University of California San Diego (UCSD), USA

UCSD SHM group is primarily involved in developing novel SHM solutions and SHM-enabling technologies (such as energy harvesting) for different "smart structures" applications (mechanical, aerospace, and civil). Moreover, UCSD SHM group is involved in various projects such as Wind Turbine Embedded SHM, Ultrasonic Guided Waves SHM, Uncertainty in System Identification, Automated Development of SHM Algorithms, Embedded FBG Monitoring, Energy Harvesting and others. As SHM is a very multi-disciplinary field, any SHM strategy inevitably must include elements of data acquisition/sensing, data mining and feature extraction from acquired data, and statistical modeling and classification of features weighed by costs in a way that facilitates risk-informed decision-making. As such, SHM research involves structural engineering, mechanical engineering, electrical engineering, computer science, statistical science, and even economics and policy. Their laboratory is equipped by data acquisition devices, computational facilities, etc. In addition, ttheir collaboration with industry enables to run a vast type of experiments in different SHM fields.

During the three months stay in UCSD SHM laboratory, several experiment were performed. The main focus was on temperature effects on signal propagation and damage detection in different specimens. Moreover, different tests were executed on a complex specimen as airplane skin panel, to confirm the ability of algorithms in more realistic specimens. This aim was achieved thanks to the temperature chamber available in the NDT laboratory supervised by Professor Francesco Lanza. The author wants to give special thanks to Professor Lanza group, specially their visiting student *Piotr Kijanka* from Department of Robotics and Mechatronics AGH University of Science and Technology of Poland for their collaboration during the temperature tests.

4.4.1. A large-scale, complex composite structure representative of a component from an aerospace application

The specimen that is used in this case study is a representative of a component from an aerospace application. Although details of the structure are restricted to be published, the experimental setup and the type of signal that was captured are described as follows. For sake of ease this experiment is called "UCSD, first case study".

The acquisition system consists of a National Instrument chassis (NI PXIe 1073), containing Simultaneous-Sampling DAQ (NI TB-2708), a switch card, a digitizer and a signal generator. Moreover, the signal is amplified with a high bandwidth amplifier. Figure 4.14 shows the acquisition system. It should be mentioned that

data for all case studies in this Lab is performed using the mentioned acquisition setup.

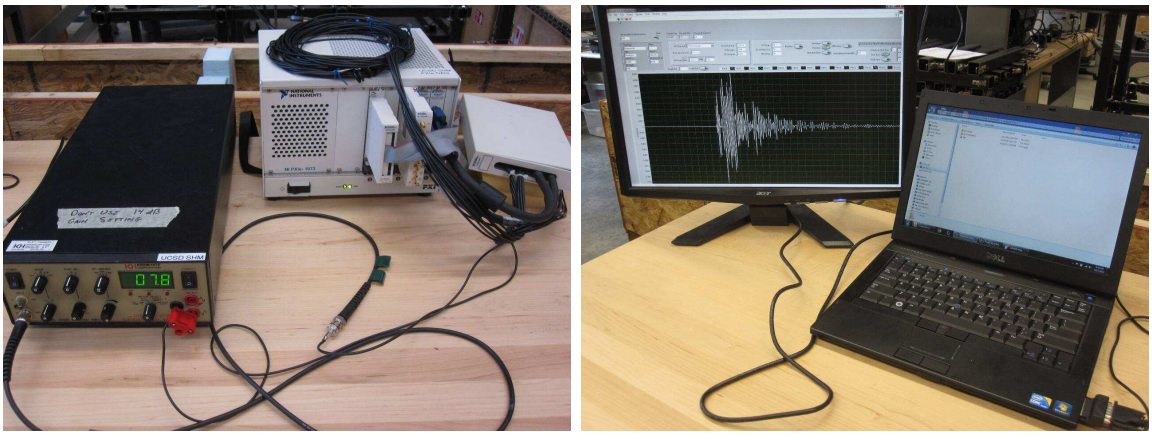

(a) NI chassis and amplifier, UCSD SHM Laboratory

(b) Computational system

Figure 4.14.: Acquisition system, UCSD SHM Lab. USA

Circular PZTs from PI ceramics are used as actuator and sensors with $1cm$ diameter, and Permatex epoxy is used to attach them to the surface of the structure. Besides, damages are simulated by adding appropriate mass on the surface of the structure. Figure 4.15 show the PZT transducers and the simulated damages.

(a) PZT transducers

(b) Simulated damages

Figure 4.15.: PZT and simulated damage, first case study, UCSD SHM Lab. USA

A number of 3 PZTs are located in a line with a $310mm$ distance. 4 types of damage are simulated on the route between PZTs as Figure 4.16 demonstrates. $D1$ and $D2$ are simulated by the same amount of magnets and for damages $D3, 4, 5$ more amount of magnets are added.

Figure 4.16.: PZT and damage location, first case study, UCSD SHM Lab. USA

Actuating signal is generated in different frequencies such as (200,300,400 and 450) KHz using hamming window with 3 cycles. Switching is performed to capture all routes. The route here refers to each path between two transducers. Figure 4.17 shows an example of captured signal on different routes.

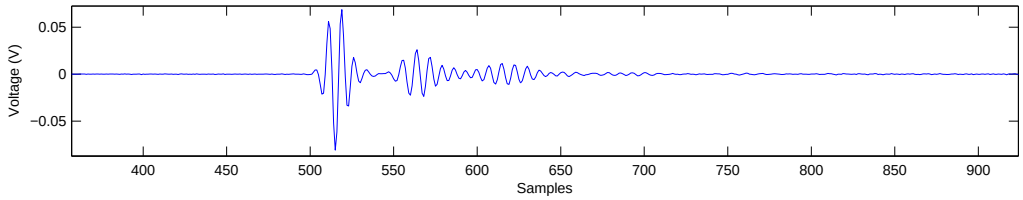

(a) Actuator 1 to sensor 2 (route 1-2)

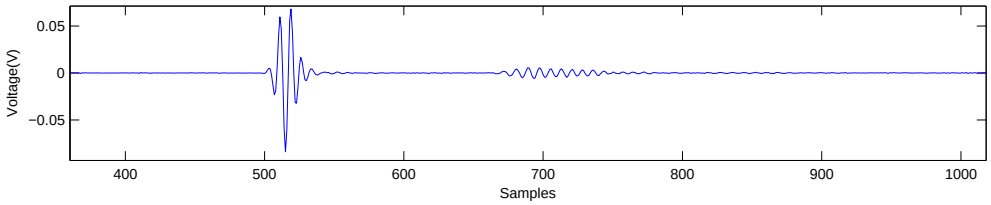

(b) Actuator 1 to sensor 3 (route 2-3)

Figure 4.17.: Recorded signal, first case study, UCSD SHM Lab. USA

4.4.2. Composite plate equipped with Macro-Fiber Composite

This experiment is performed on a composite plate with the dimension of $305 \times 305 \times 2mm$, which is equipped with Macro-Fiber Composite (MFC) piezo designed by NASA. MFC transducers are composed of PZT fibers that are uni-directionally aligned, embedded into an epoxy matrix, and sandwich between two sets of interdigitated electrode patterns. Because of their polymer-based composite design, MFC transducers are more flexible and durable than monolithic PZT transducers. Figure 4.18 shows the schematic of plate and sensor location in addition to the MFC piezo transducers. The MFC consist of polyimid films with interdigital electrodes that are glued on the top and the bottom of rectangular piezoceramic fibers. The interdigitated electrodes deliver the electric field required to activate the piezoelectric effect in the fibers and allows to invoke the stronger longitudinal piezoelectric effect along the length of the fibers. When this actuator embedded in a surface or attached to

flexible structures, the MFC actuator provides distributed solid-state deflection and vibration control. The major advantages of the piezoelectric fiber composite actuators are their high performance, flexibility, and durability when compared with the traditional piezoceramic, PZT, actuators. In addition, the ability of MFC devices to couple the electrical and mechanical fields is larger than in monolithic PZT [203].

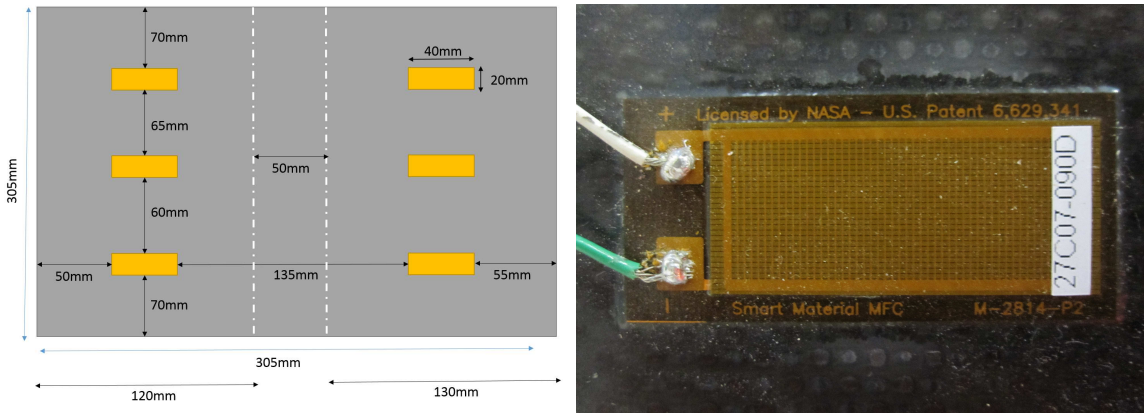

(a) Plate dimension and sensor location **(b)** MFC transducers

Figure 4.18.: Composite plate equipped with MFC transducers, UCSD SHM Lab.

Signals are actuated on 4 different frequencies $(100, 200, 300, 250)$ KHz with 16 times averaging per each observation. The sample frequency is set on 2.5MHz. There is $50ms$ delay between each observation. Totally 5 damages are simulated in different locations as Figure 4.19 shows.

Switching is done to capture signal on all available routes between transducers. Figure 4.20 shows a sample of signal captured by MFC transducers.

4.4.3. Composite plate equipped with PZT

This case study is performed on a composite plate with the dimension of $305 \times 305 \times 2mm$, which is equipped with PZT ceramics. PZTs are located in $20cm$ distance from each other and $5cm$ from each edge of the structure. Figure 4.21 shows the schematic, sensor location and a snapshot of the specimen.

Damages are simulated on 4 different locations by adding appropriate mass (magnets). Figure 4.21-a and 4.21-b shows the schematic and a snapshot of damages on the specimen surface.

Signals are recorded in different frequencies such as $150, 200, 300, 350$ and 400KHz. Switching makes it possible to scan all routes between transducers. Figure 4.23 shows the two samples of recorded signals in this case study.

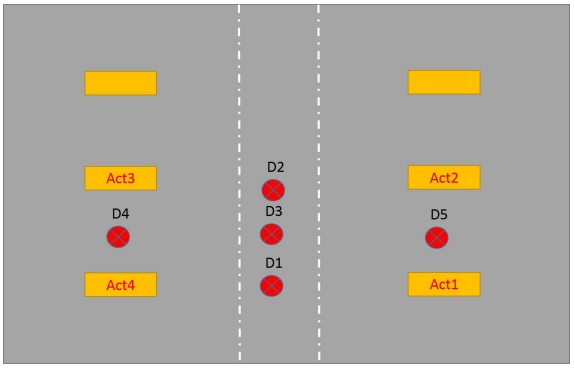

(a) Damage location

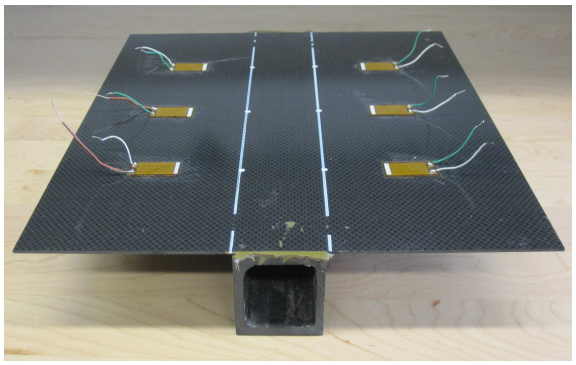

(b) Snapshot

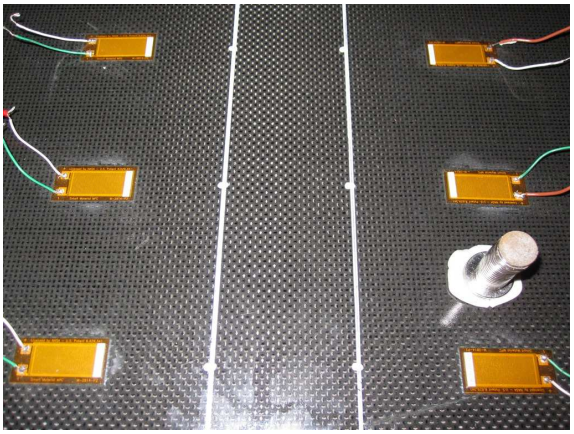

(c) Damage 5

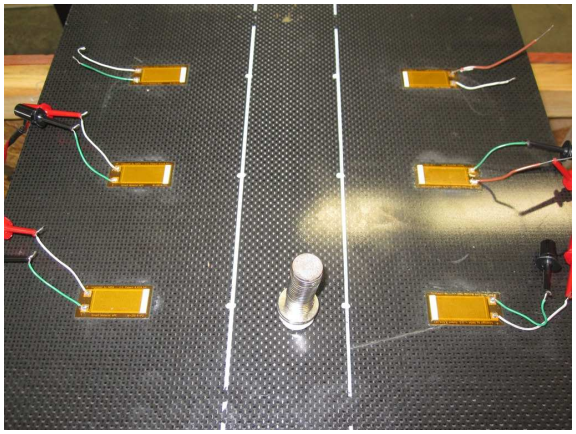

(d) Damage 1

Figure 4.19.: Damage location and a snapshot of composite plate, UCSD SHM Lab. USA

4.4.4. Temperature effect on composite plate

Heating/cooling chamber is used to change the environmental temperature and observe the effect of temperature change on wave propagating and damage detecting techniques. Using this chamber the temperature is changed from +25°C to +60°C (heating) and then decreased until -20°C (cooling) with 5°C resolution. Figure 4.22 shows the chamber and the composite plate inside.

This case study is done on both composite plates equipped with PZT and MFC transducers detailed in Sections 4.4.2 and 4.4.3. Damages are simulated by adding appropriate mass and the same temperature sweeping is repeated on the structure when there is damage on the surface of the structure. Figure 4.22 shows a snapshot of simulated damages.

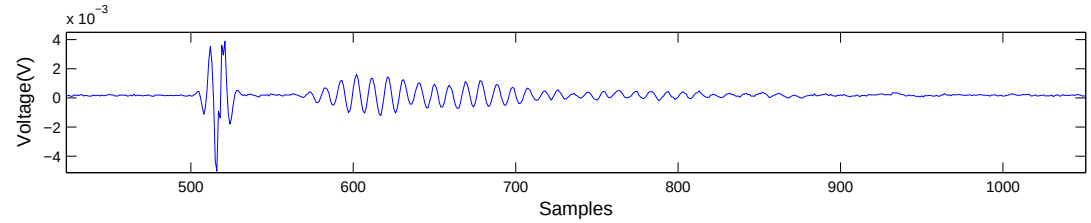

(a) Captured signal on route $1 \rightarrow 2$

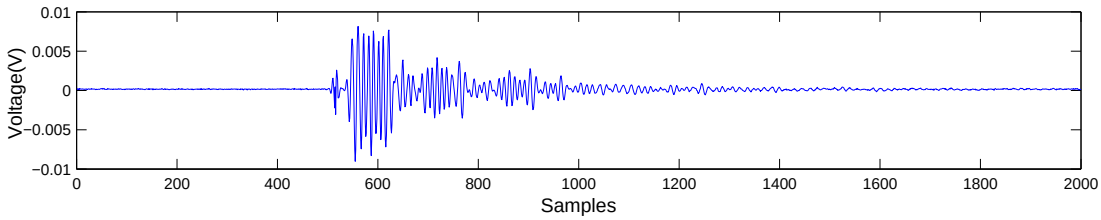

(b) Captured signal on route $1 \rightarrow 3$

Figure 4.20.: Recorded signal, composite plate, UCSD SHM Lab. USA

4.4.5. Temperature effect on the UCSD first case study

A vast study is performed on the effect of changing temperature on the UCSD first case study. Due to the size of specimen, it was not possible to use the chamber to sweep the temperature. Therefore, a heating lamp is used to increase the temperature. As this temperature is not completely controllable unlike the heating chamber, we just run the experiment in specific temperatures such as 24°C,40°C,46°C,55°C,62°C. The case study is repeated different period of day and in different days to enhance the data reliability. A laser thermometer is used record the surface temperature of the specimen. Figure 4.24 shows the laser thermometer and the heating lamp that is used in this experiment.

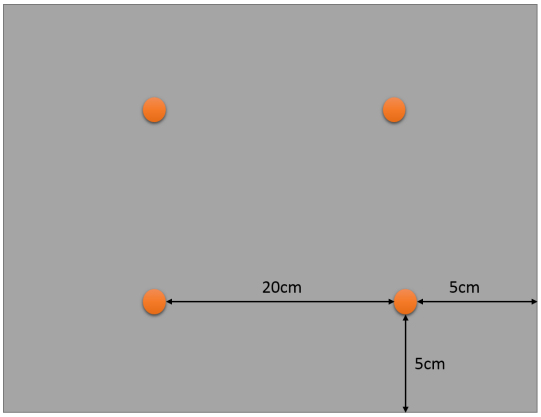

(a) Schematic

(b) Specimen and chamber snapshot

(c) Damage location schematic

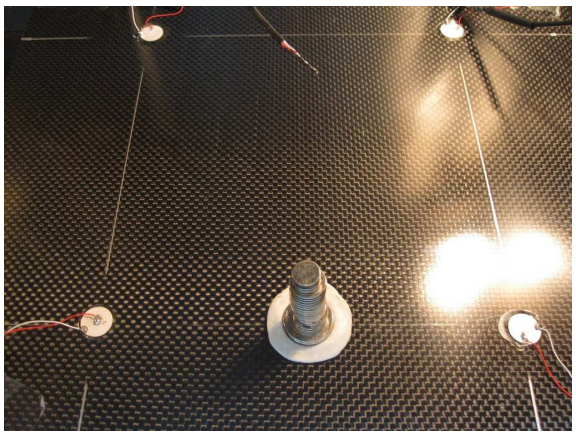

(d) Damage 1 Snapshot

Figure 4.21.: Composite plate with PZT, UCSD SHM Lab. USA

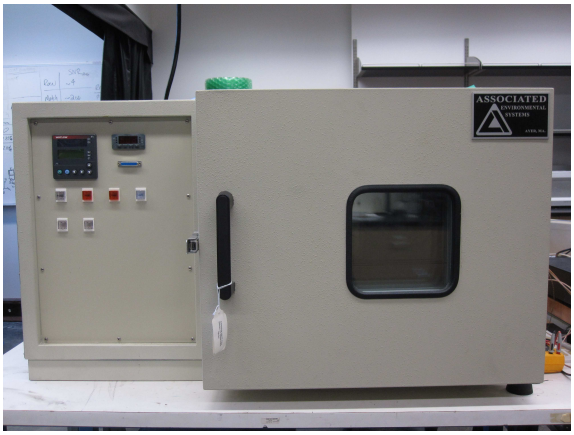

(a) The chamber

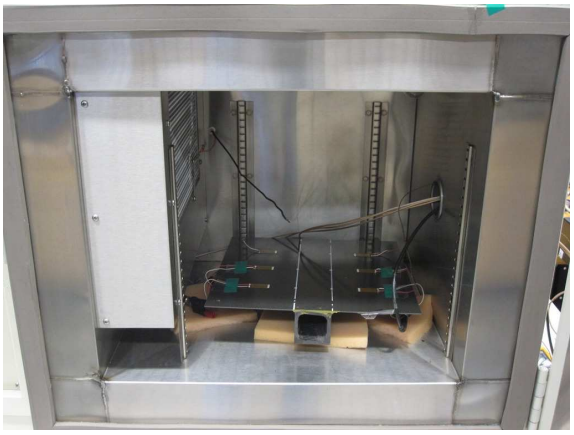

(b) Specimen inside the chamber, MFC

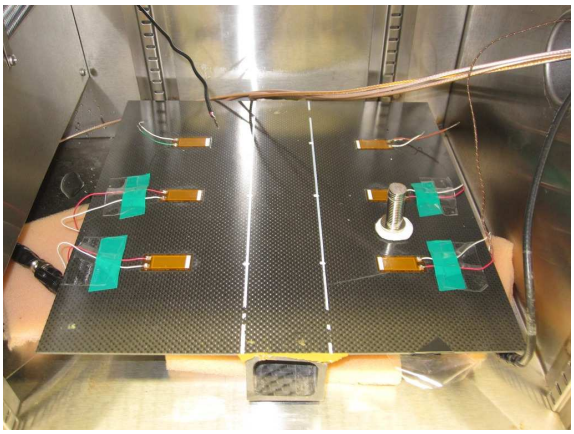

(c) Damage 1 snapshot, MFC plate

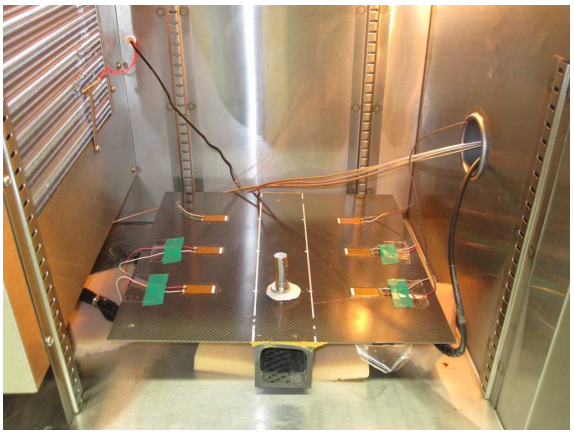

(d) Damage 2 snapshot, MFC plate

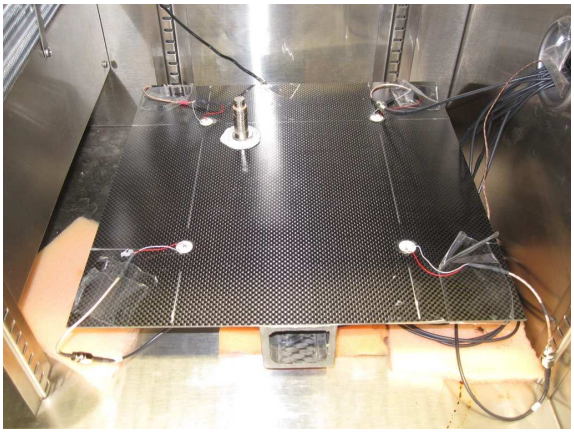

(e) Damage 4 snapshot, PZT plate

(f) Specimen snapshot in chamber, PZT plate

Figure 4.22.: Temperature study, composite plate with PZT and MFC, UCSD SHM Lab., USA

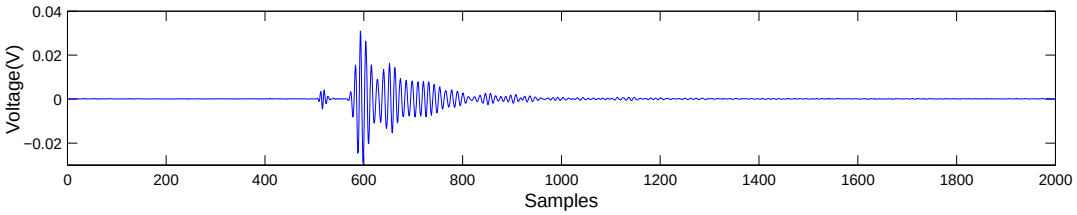

(a) Signal from route 4 → 1, 25°C

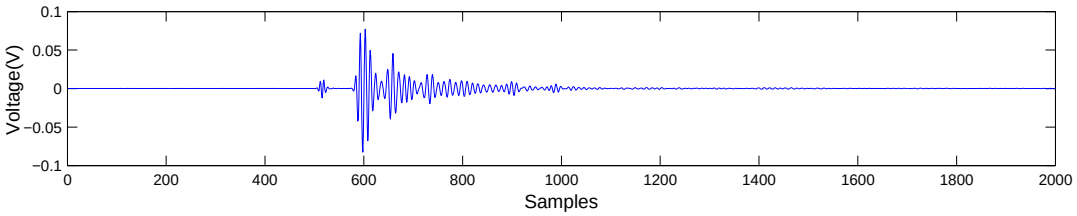

(b) Signal from route 4 → 3, 25°C

Figure 4.23.: Recorded signal under temperature change, composite plate with PZT, UCSD SHM Lab. USA

(a) Laser thermometer

(b) Heating lamp

Figure 4.24.: Laser thermometer and heating lamp, UCSD SHM Lab., USA

5. DAMAGE DETECTION METHODOLOGY AND RESULTS

In current chapter and the next one, the main achievements and contributions of this thesis are presented. At the beginning, we describe the general methodology that are developed in the CoDAlab research group. After that, we briefly present the drawbacks of this methodology and the solutions that are presented in this thesis to improve that. Then, the main contributions of the thesis are briefly described. In next subsections of this chapter, the result from different novel approaches are scrutinized.

5.1. General methodology

As mentioned before, PCA is widely used in SHM in different ways. In addition to dimension reduction that is the simplest way of using PCA, it could be directly applied on time or frequency domain, as a feature extraction tool, such as the works in [56, 52]; or applied on extracted feature matrix from time or frequency data [63, 53] and searching for the novelty that represents the existence of damage in the structure. Another recent way of PCA application, presented by the research group, is to generate *a statistical data-driven model* of the structure in pristine conditions using PCA and to use this model for detecting damages in current status [64]. To achieve this, the first part is to pre-process the signal that is captured from sensors in healthy status. This could be done using methods such as denosing, averaging, removing mean, etc. Then, PCA is applied on the pre-processed data. The loading matrix of data (matrix $\tilde{\mathbf{P}}$) generated from healthy structure is calculated using equations (3.24). Then, the reduced number of principal components, P, those corresponding to the first eigenvalues are kept (based on the criterion mentioned in Section 3.5). The reduced transformation matrix can be viewed as a statistical model for the structure. By Equation (3.25), pre-processed test data from current status of the structure are projected over the directions of the principal components. Then, scatter plots of scores matrix, $\mathbf{T}$, or any other derivative damage index such as $\mathbf{Q}$ and $\mathbf{T^2}$ statistics could be used to interpret the existence and detection of probable discordancy in the structure. Figure 5.1 gives a scheme for the implementation of

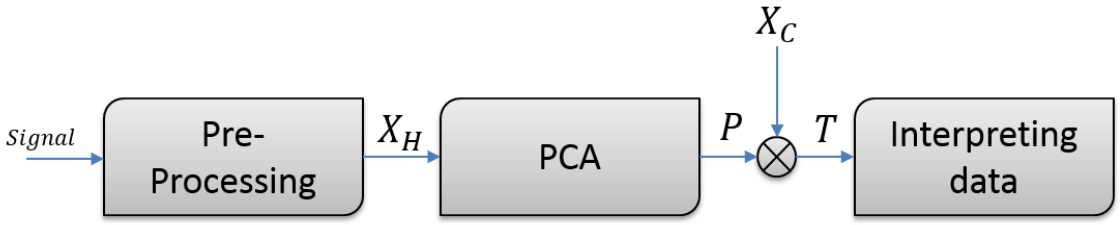

(a) Schematic of using PCA in damage detection

Figure 5.1.: General damage detection methodology based on PCA

the described method in SHM. In this figure $\mathbf{X}_H$ and $\mathbf{X}_C$ stand for healthy and current status of the structure, respectively.

In this thesis, PCA is used in two ways. The first one is simply dimension reduction tool to decrease the captured high dimensional signal to the low dimensional data and the second approach is as a tool to generate the statistical model as described above.

5.2. Main thesis contribution in damage detection

As it was mentioned in Section 3.6, outliers have significant effect on any damage detection based on PCA. Therefore, as one of the main contribution, this work proposes to use robust counterpart as a more reliable variant of PCA. To do this, this work presents the damage detection methodology using robust PCA methods. To achieve this, different robust PCA are applied in this thesis such as ROBPCA (see Section 3.7.3), Croux (see Section 3.7.2) and RFPCA (see Section 3.7.4). As it may be seen in Figure 5.2, classical PCA is substituted by a different robust version. This may increase the reliablity of the detection in case there would be high possibility of outlier presence.

To decide about the presence of damage in the structure, detail interpretation of

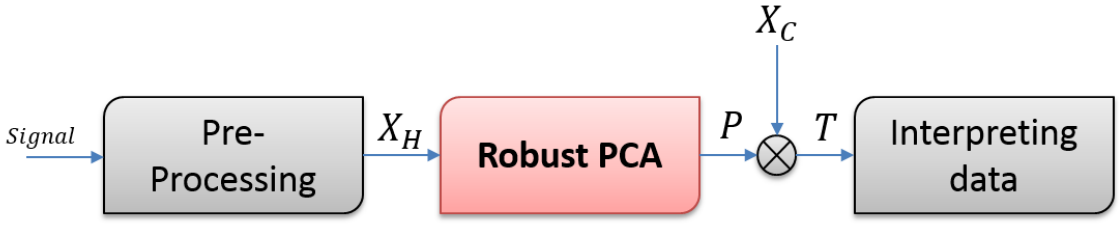

(a) Schematic of using PCA in damage detection

Figure 5.2.: Substituting classical PCA with Robust counter part for damage detection

(a) Schematic of using PCA in damage detection

Figure 5.3.: Proposing new indices for data interpretation

data are necessary. Damage indices are features that are extracted from the signal, which are sensitive to the damage and could be used to show if there is damage in the structure. As it was mentioned, the scatter plots of scores matrix obtained by projecting data from current status of structure could be used as damage index. To improve this part, in this thesis, different indices such as Andrew plots (see Section 3.8), Fuzzy similarity classifier (see Section 3.9), wavelet clustering (see Section 3.11) and orthogonal distance (see Section 3.12) are suggested. Results show that the presented indices are able to detect damages in different structures. This part of contribution focuses on the interpreting data as Figure 5.3 shows.

Another contribution of this thesis is to present a novel method to pre-process signals captured from the sensors. This method is based on Wavelet Ridge (see Section 3.10). In this method, Wavelet ridges are used instead of the original signal and results show that this could improve the damage detection performance.

5.3. Damage detection using robust PCA as pattern recognition

5.3.1. ROBPCA implementation and results

To prove the efficiency of the mentioned methodology, the robust methododology explained in Section 3.7 (ROBPCA) is applied to the specimen described in Section 4.2.3 (Aircraft turbine blade).

As PZT's can be used alternately as sensors and actuators, in excitation phase, one PZT is working as actuator and the others as sensors. The actuator is excited by a burst signal of three peaks and 350KHz of frequency. An actuating signal (before amplifying) and a measured signal in one of the sensors are shown in Figure 5.4.

Damages are simulated by adding masses at several locations as shown in Figure 4.7-b and Figure 4.7-c. Data are captured and arranged in two parts. First, baseline signal from non-damaged structure are gathered. In next step, damages are simulated and related data are captured for each damage. 80% of data captured from

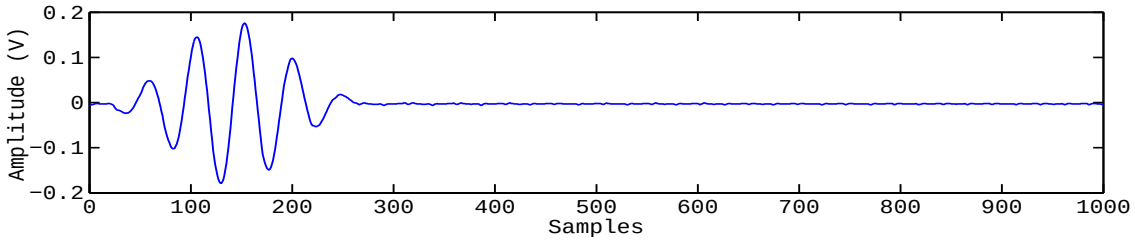

(a) Excitation signal

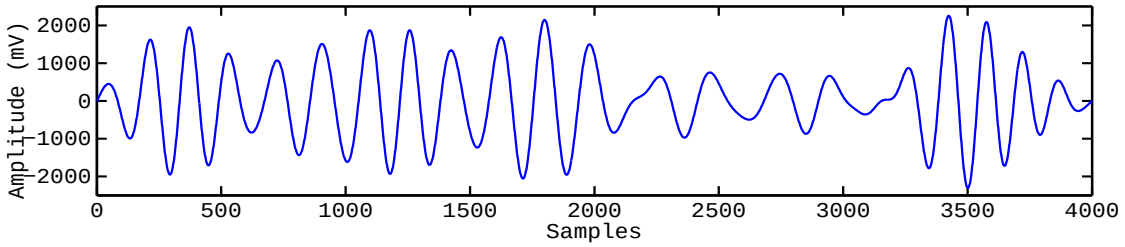

(b) Dynamical response

Figure 5.4.: Excitation signal and dynamical response, turbine blade, Madrid

pristine structure (training data) is used to create the statistical model. The rest of this data set and all data from different structure's status are used for testing. Totally 140 experiments are performed and recorded, 50 for undamaged structure and 10 per each damage. The recorded data are organized in such a way that the response data over a whole time period captured from all sensors are folded in a $2D$ matrix where rows show the observation and columns consist of the package of data from each sensor laid beside each other. This method highlights the correlations in time for each signal and the correlations between sensors. Therefore, 6 packages of data from each sensor containing 4000 recorded samples are arranged (folded). To do this, in each excitation step a single PZT is used as actuator, and the others are sensors that receive the wave propagated across the structure at different points. For each experiment, the time histories recorded by each sensor at each sampling time are stored by the data acquisition system into a matrix with dimensions $n \times m$, where n represents the number of experiments and m the number of samples [204]. Denoting J as the number of PZT sensors at each experiment, there is a number J of such matrices. Therefore, the whole set of the data collected in each excitation phase can be organized in a $3D$ matrix $(n \times m \times J)$ or in a $2D$ matrix $(n \times Jm)$ where data from each sensor are located sequentially as illustrated in Figure 5.5. The folded data for any specific actuator are supplied to the methodology for damage detection that is described in Section 5.1.

To compare the performance of ROBPCA with classical PCA, both methods are applied on training data and the first two principal components are used as a model. This selection is based on the proportion method mentioned before using Equation 3.31. As it is shown in Figure 5.6, first two classical PCs convey 74% of variance

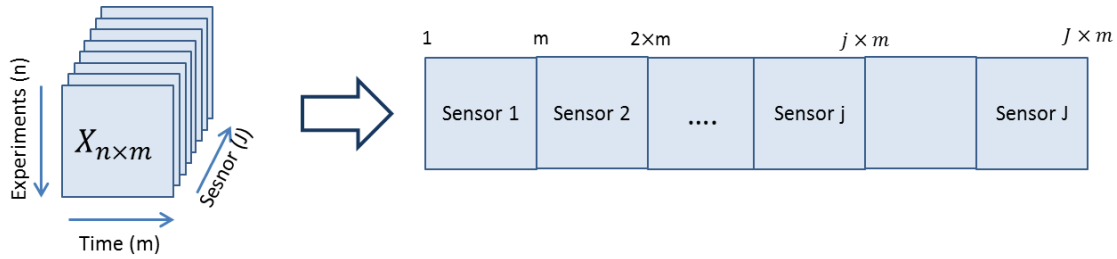

(a) [64]

Figure 5.5.: Arranging the collected data in 3D to bi-dimensional matrix

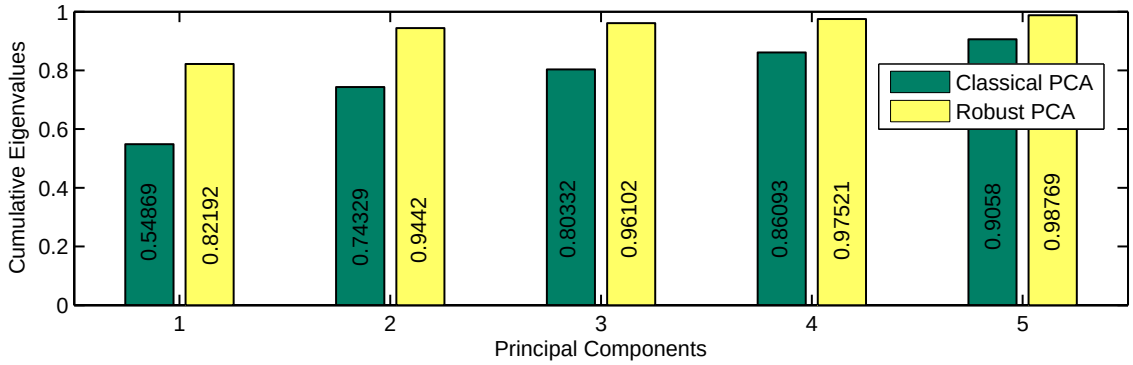

Figure 5.6.: Cumulative Covariance by principal component, classical PCA vs. ROBPCA

of data meanwhile the two first components on robust PCA carry more percentage of variance, about 94%. It means that the robust method holds more information using the same quantity of principal components, comparing with classical method.

In the next step, scatter plot of score and orthogonal distances are shown for the training data. This plot is used to distinguish between regular observations and three types of outliers. In this plot the horizontal and vertical axis represent the robust score distance (Equation 3.32) and orthogonal distance (Equation 3.33) respectively. According to Figure 5.7, classical PCA does not show any observation as an outlier that means its orthogonal and score distance cross the threshold at the same time but, in the diagnostic plots based on robust PCA, two observations are selected as outliers as their both score distance and orthogonal distance are higher than the selected criteria demonstrated by horizontal and vertical lines. These lines indicate the orthogonal and score distance limitation (threshold) respectively.

To see the outlyingness behaviour of the mentioned observation (effect over PCA model), the scatter plot of the first two scores is depicted by each observation (see Figure 5.8). In this figure all status of the structure, including pristine condition, depicted in green, and all damages are plotted. Pattern 1, belonging to damage 1, is removed due to its long distance from other patterns. As it can be seen in Figure 5.8, an outlier observation in classical PCA is obviously separated from the group

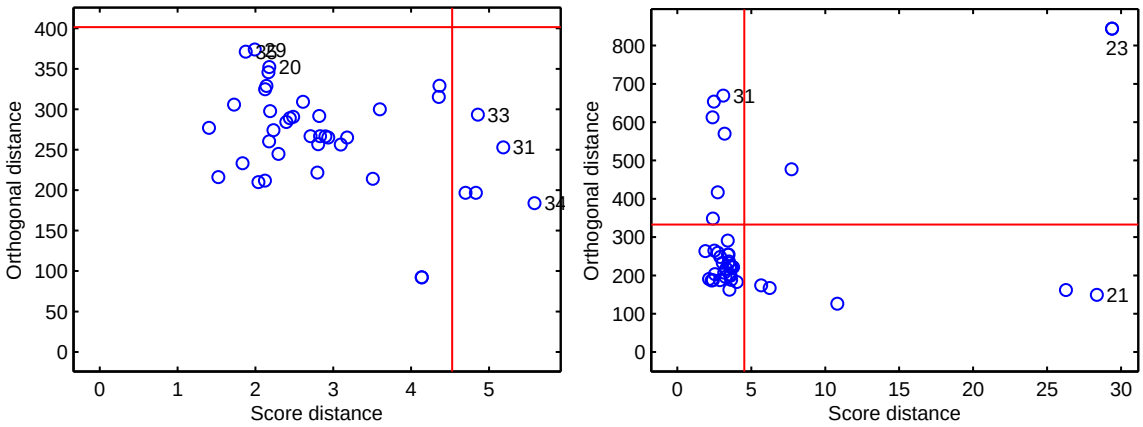

(a) classical PCA **(b)** ROBPCA

Figure 5.7.: Scatter plots of score and orthogonal distances for training data, classical PCA vs. ROBPCA

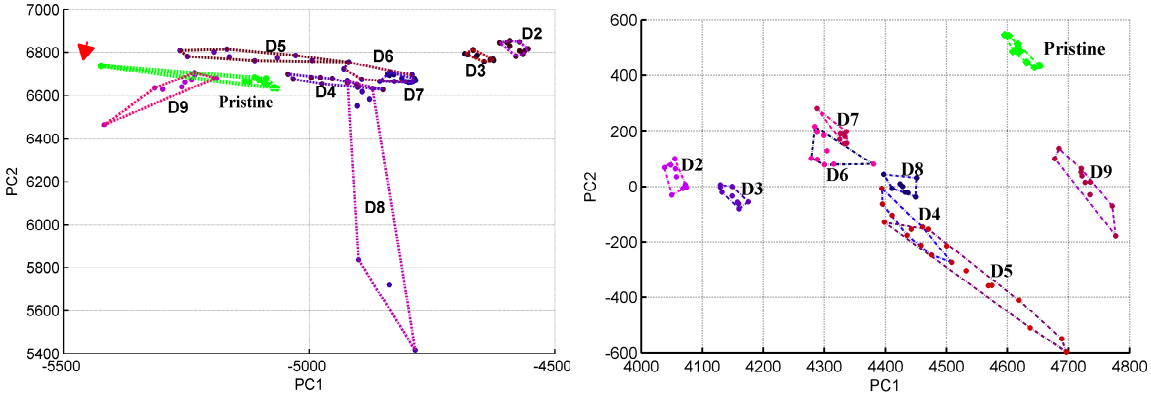

(a) Classical PCA **(b)** ROBPCA

Figure 5.8.: Scatter plots of scores for testing data, Classical PCA vs. ROBPCA

of observation in the pattern (pointed out by the arrow) whereas this observation is recognized and removed by robust method that leads to more united pattern. As it can be seen, although in both methods the healthy pattern is separated from other patterns, the robust method (ROBPCA) can distinguish different patterns much more clear and recognizable.

To perform a deeper validation of the proposed methodology, a controlled portion of outlying observations are added to the training data. The ability of the ROBPCA to discern and mitigate outliers is tested, and, its aptitude for detecting and classifying different damages in presence of outliers is analyzed. To achieve this goal, 20% of data, (8 observations) randomly selected from damages data are added to the baseline. It should be mentioned that, as these observations are selected from the data from damaged structure, they are considered as outliers. Then classical and

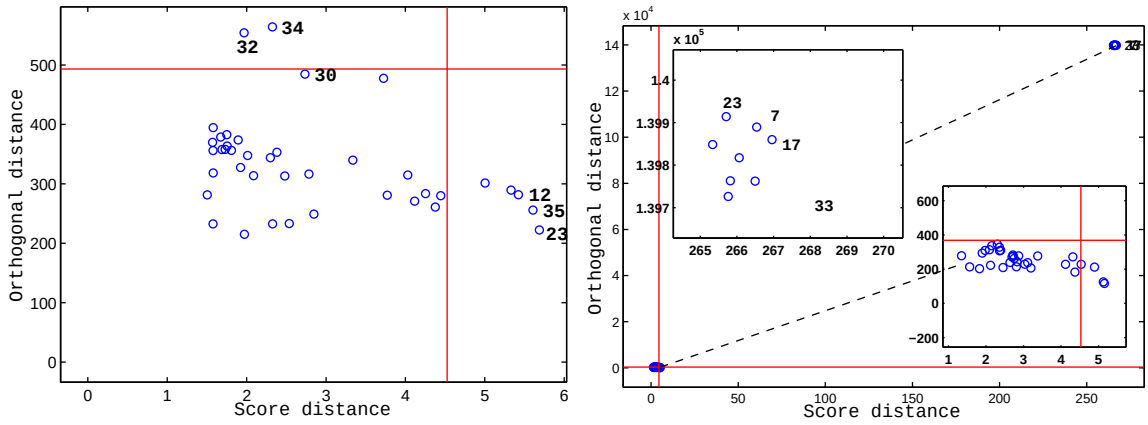

(a) classical PCA **(b)** ROBPCA

Figure 5.9.: Detecting outliers by diagnostic plot, classical PCA vs. ROBPCA

ROBPCA are applied into the general methodology to establish the model. Using diagnostic plot as is shown in Figure 5.9, robust PCA is capable of distinguishing artificially added outliers from the original data, while on the contrary, classical PCA is impotent. Although some outliers are detected by orthogonal distance and others by score distance in classical PCA, there are many false alarms (detecting outliers when they are not outliers). Therefore, the model generated using classical PCA is affected by outliers but the robust approach produces a robust model.

Due to the mentioned reason, damage identification would not be satisfied using ill-posed model generated by classical PCA. Figure 5.10 confirms this claim. As it is clear in this figure, classical PCA cannot distinguish between pristine pattern and damage patterns whereas ROBPCA makes a clear difference between all of them.

To set up a more quantitative and qualitative comparison, a Hausdorff distance [205] is used to measure the distance of different patterns in the scatter plots of scores. Hausdorff distance is the greatest of all the distances from a point in one set to the closest point in the other set and it is defined as follows:

$$h(A, B) = max_{a \in A}\{min_{b \in B}\{d(a, b)\}\} \tag{5.1}$$

Figure 5.11 shows a comparison of the distance between different patterns from healthy pattern in both classical and robust method. As it is observed, in almost all cases, patterns in the robust method keep more distance from the healthy pattern, which means better separation and detection.

In addition, using ROBPCA leads to have more united patterns comparing to the classical one. In another words, the members of a significant pattern in ROBPCA keep closer distance to each other, which means more united patterns. Figure 5.12

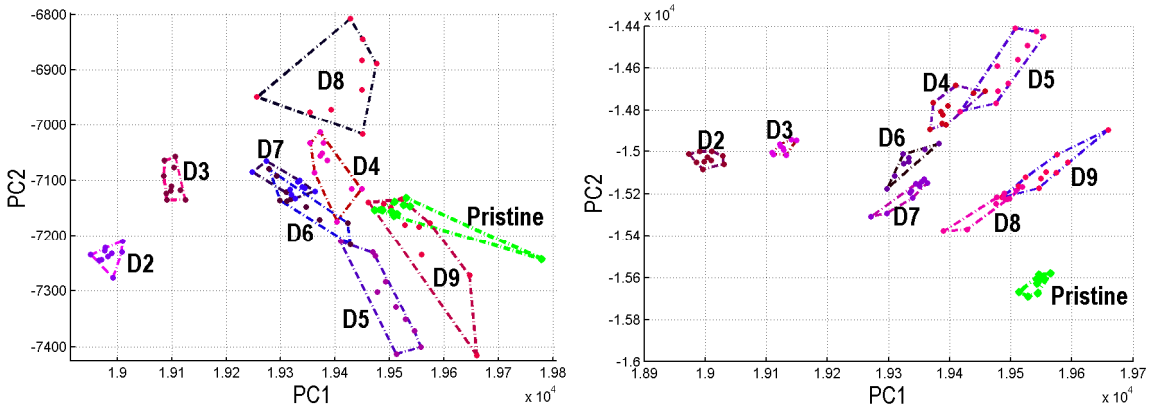

(a) classical PCA **(b)** ROBPCA

Figure 5.10.: Damage detection in presence of outliers, classical PCA vs. Robust PCA

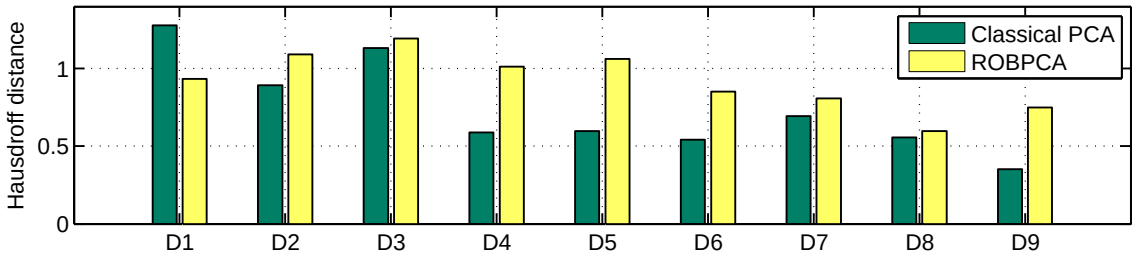

Figure 5.11.: Hausdorff distance between pristine pattern and damages patterns

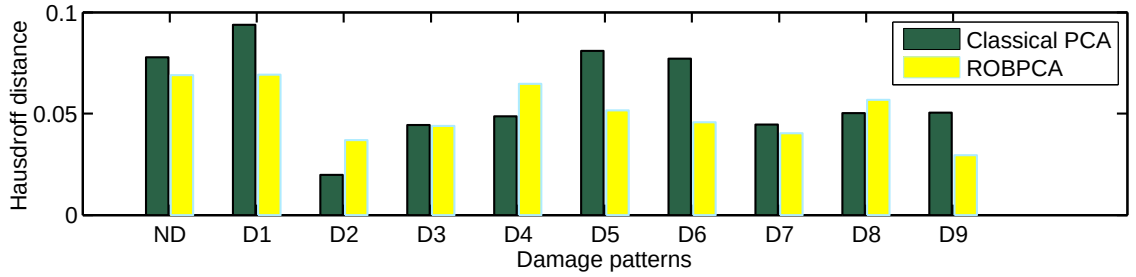

Figure 5.12.: Hausdorff distance between members of a pattern, Classic PCA vs. ROBPCA (the less the better)

shows the comparison between unity of patterns in ROBPCA and classical counterpart using auto hausdroff distance. The lesser distance, the more concentrated pattern.

Although ROBPCA performs better in identifying damages in presence of outliers, it is inherently slower. For instance, in a desktop computer with 3GHz CPU and $4GB$ RAM, processing ROBPCA takes 0.6 seconds whilst the classical method just takes 0.24 seconds that is about two and half times faster than the robust one. Therefore in online damage detection application, this issue should be considered to establish a tradeoff between the performance of system and the speed.

In this Section the idea of using robust principal component analysis is introduced as a comprehensive alternative for its classical version as a reliable method to deal with outliers and contaminated data. It is a fact that outliers are widely existent in experimental data due to different reasons; therefore using robust PCA can avoid many false-positive detection. Among different types of robust PCAs, ROBPCA is an method that can handle high dimension of data. Results show that ROBPCA is able to compress data more than its counterpart, which leads to carrying more information in primary principal components. This benefit supports any damage identification method based on Principal Component to have more accurate result. As it has been shown, robust PCA can detect and classify different damages in some cases where classical method is not capable of that.

Another ROBPCA method that is used in this work is so called Croux method. Due to the similarity of this method to ROBPCA, we do present the result of applying Croux method in Section 5.3.3 where all robust PCAs are compared with each other to show their performance.

5.3.2. RFPCA implementation and results

In this section another robust PCA is used as a damage detection tool. The new technique is so called Robust Fuzzy Principal Component Analysis (RFPCA). The theoretical backgaround of RFPCA is described in Section 3.7.4. This technique is appied on the tube benchmark case study, which detailed in Section 4.3.5. The captured data from pipe benchmark consist of damages (cuts) with different severities. Figure 5.13 shows a sample of the received waves after a decimating by 10 and de-noising procedure for different routes for the same excitation signal (burst with 3 peaks).

The same damage detection strategy described in Section 5.1 is used, while RFPCA plays the feature extraction role here.

To perform a comparison between classical PCA and the RFPCA, the scores in two dimensions are compared with each other. For instance, Figure 5.14 shows the score depicted in the first-second and second-third PCs space both in PCA and RFPCA for route $1 \rightarrow 5$.

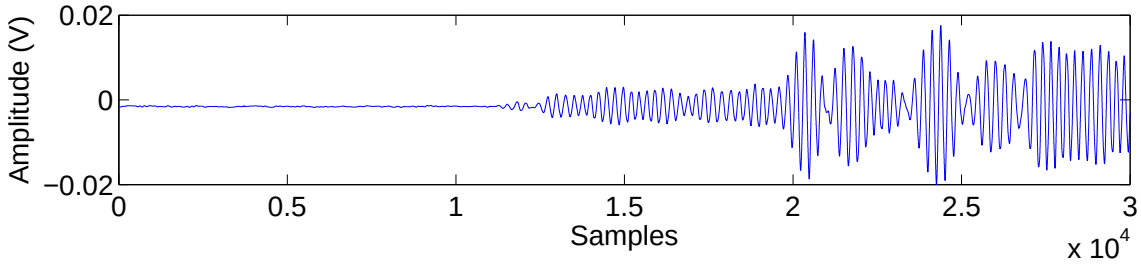

(a) route 1→6

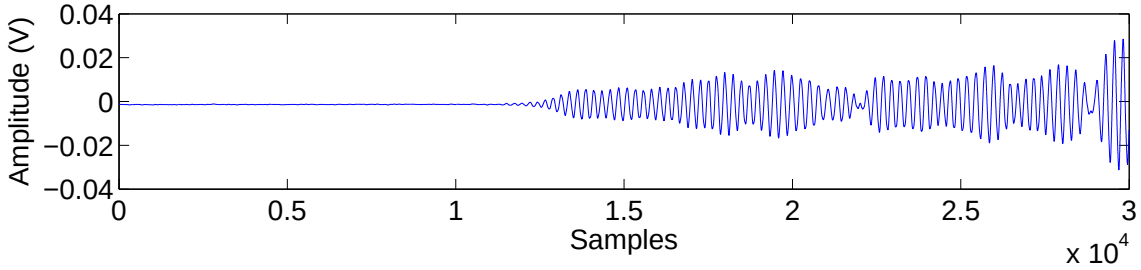

(b) route 2→8

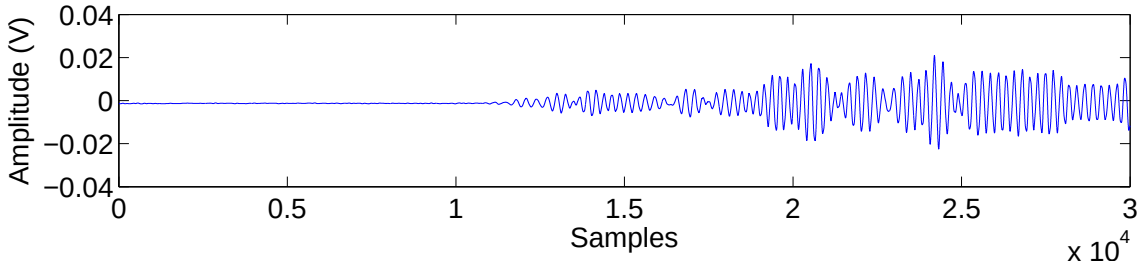

(c) route 3→7

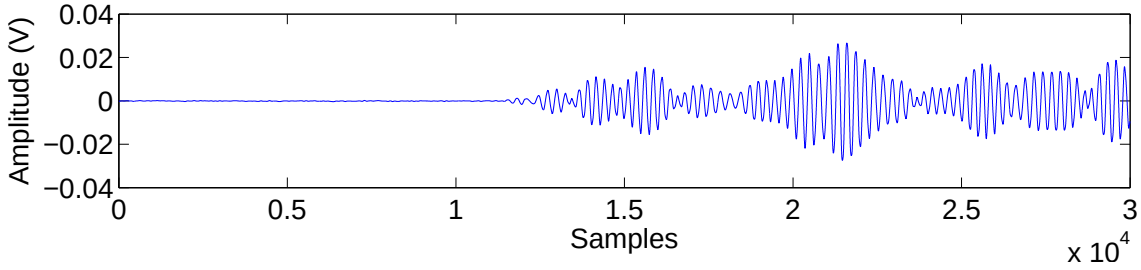

(d) route 4→8

Figure 5.13.: Received wavestone in tube benchmark

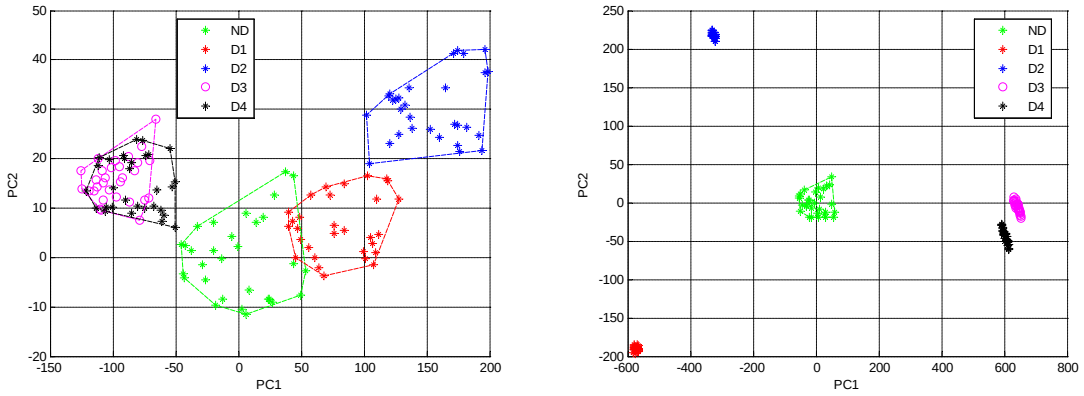

(a) scores on first and second PCs using PCA **(b)** scores on first and second PCs using RFPCA

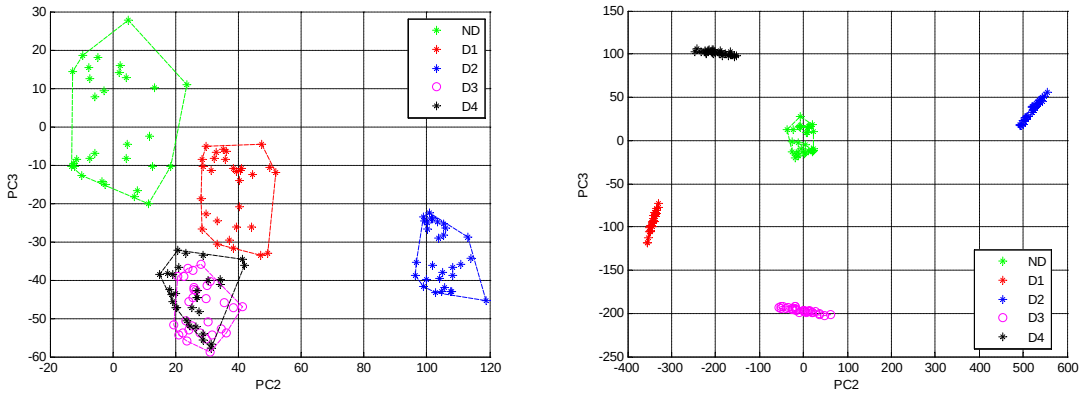

(c) second and third PCs using PCA **(d)** second and third PCs using RFPCA

Figure 5.14.: Classical PCA vs RFPCA on route 1→5

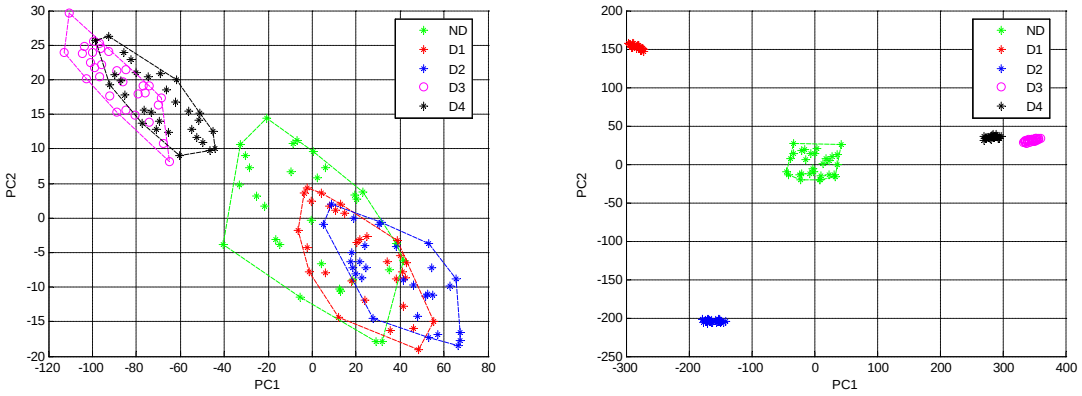

(a) classical PCA **(b)** RFPCA

Figure 5.15.: Route 1 → 6 from actuator 1 to sensor 6 for classical PCA and RFPCA

Using the route from the actuator 1 to sensor 5, it can be seen from Figure 5.14 that classical PCA can distinguish between damaged and healthy structure but it is unable to distinguish all damages from each other (i.e. damage 3 and 4 have overlap), whereas RFPCA provides much better separation between all the patterns related to any state of the structure. It should be mentioned that in some routes, e.g. route 1 → 6, classical PCA even is not able to separate the healthy and damaged structure with minimum damage severity state, while RFPCA can achieve this goal as depicted in Figure 5.15. Analyzing the rest of the routes, the same results can be observed, much better separation between patterns are obtained by means of RFPCA.

The main reason for achieving better results by RFPCA is that it can compress information much better than classical PCA, i.e. the primary principal components count for significantly more of the variance than their classical counterparts hence; they convey more information from the structure, and thereupon better result is achieved. Hence not only RFPCA can distinguish the healthy structure from the damaged structure and discern between different damages much sharper than the traditional counterparts but also in some cases traditional PCA is incapable of discerning the pristine from damaged structure.

5.3.3. Comparison of all robust PCAs techniques

Finally in this section a brief comparison between the mentioned three robust PCA methods (ROBPCA, Croux, FRPCA) is presented. The mentioned robust methods are applied on the turbine blade specimen that is described in Section 4.2.3. To achieve this, data from second actuator is used with 40% added outliers. The results show (see Figure 5.16) that ROBPCA can achieve the best result between all robust

PCA techniques for damage detection purposes. However all of them still show a superior competence over the classical counterpart. It can be clearly seen that Classical PCA can not distinguish the pattern belonging to the healthy status of the structure from other patterns. In other words, classical PCA is not able to detect damages whereas robust PCAs are. It should be also mentioned that, among different robust PCAs studied in this thesis, the ROBPCA algorithm shows the better results as not only the pattern from healthy structure is clearly separable from the other but also all patterns are clearly separated. This separation is particularly relevant since it leads to damage classification.

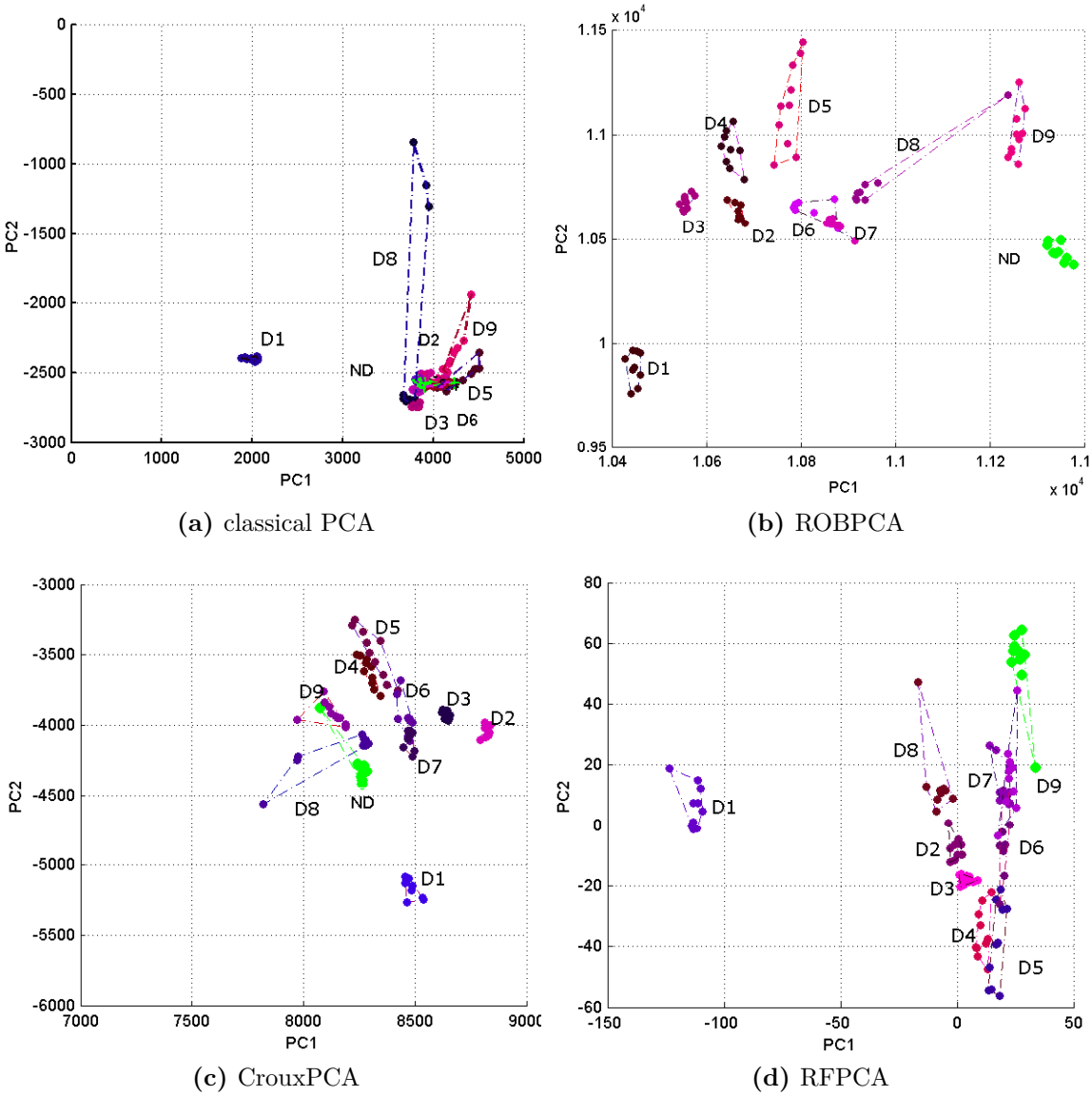

(a) classical PCA **(b)** ROBPCA

(c) CrouxPCA **(d)** RFPCA

Figure 5.16.: Comparison of all PCA approaches

5.4. New indices

In this section, we propose some novel indices that are used for damage detection. These indices are considered as new solution for the last part of the general methodology, that is data interpretation. Proposed indices are tested and their performance are approved using various case studies described in Chapter 4. Although in this work robust PCA is proposed as a better alternative for PCA, the classical counterpart is used as dimension reduction to prove the efficiency of the new indices. This is done in this way because the author considers that if new indices are able to perform efficiently using classical PCA, they definitely can have a good result using robust PCA.

5.4.1. Damage detection using Wave Cluster

Although PCA and its robust counterpart show a successful role in damage detection, they still need a complimentary step for automatic damage classification. It means that a human effort still is required to classify different existing clusters. In previous works in the research group, self-organizing map (SOM) [206] was proposed as a classifier method. In this thesis another classifier method based on wavelet is proposed that posses several merits. This section is dedicated to use this classifier concentrating on automatic classification of damages with different severity. To do this, PCA is used as a tool for dimensionality reduction and then a wavelet classifier (see Section 3.11) is applied on the result to classify different patterns in the structure each of them associated to significant states of the structure. This work involves experiments with a composite plate powered by piezoelectric transducers as sensors and actuators that is described in Section 4.3.2.

To start detection and classification procedure, route between transducer 5 and 4 is chosen as a primary route to be analyzed. To do this, signals from actuator 5 to sensor 4 are collected in 4 different states of structure including pristine, damage 1, 2 and 3 (see Figure 4.10). Above all, PCA is applied on collected data associated to this route contain of 4 packages (1 by status) each one consist of 13 observations. As a result the dimension of data is reduced to the first two principal components $X_{52\times 2}$.

In the second step, Wave Cluster is applied on the data with reduced dimension to classify the clusters. As a result, Wave Cluster algorithm indicates 4 different clusters in data set. In figure 5.17, all observations are depicted based on the Wave Cluster labeling. As it can be seen in this figure, observations belong to different clusters including pristine (connected circle) and three different damages (dashed circles) are clearly distinguished and classified clearly. It should be highlighted that Wave Cluster releases the need for visually exploring the groups depicted on the new dimension space (PC1-PC2) by automatically labeling the observations belonging to the same group.

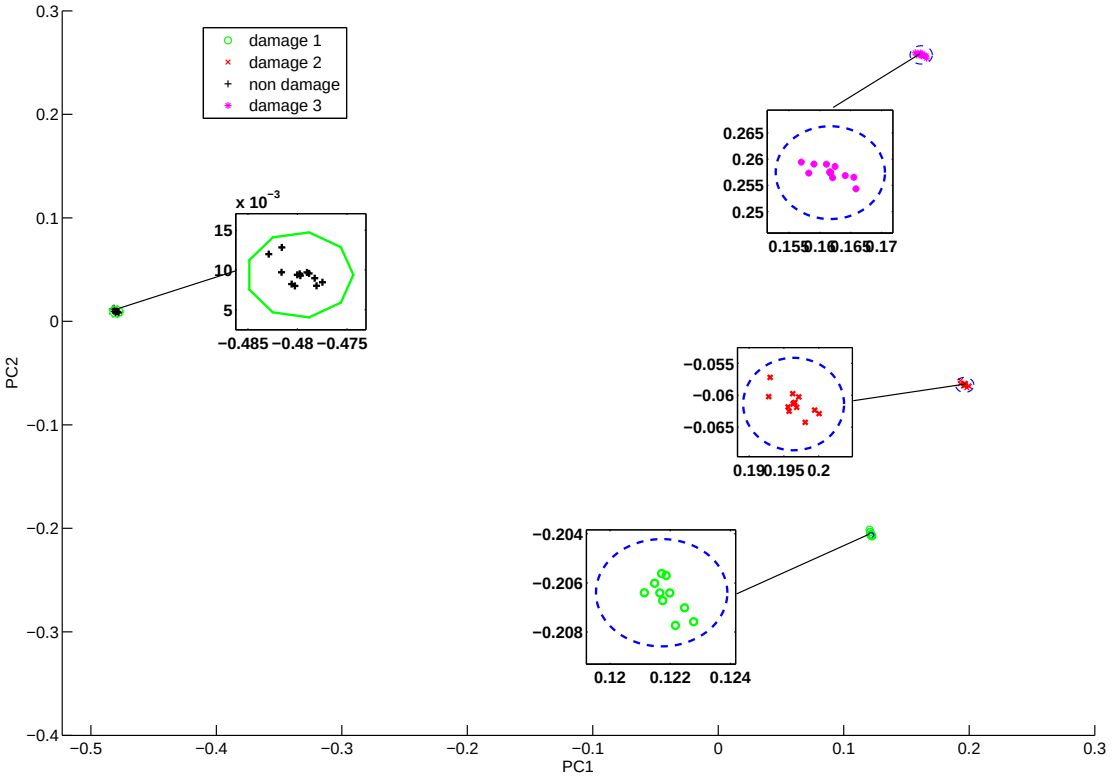

Figure 5.17.: Damage Classification in route 5 → 4

For more comprehensive test, the collected data from all sensors associated with a significant actuator are folded in a single observation. As we mentioned before in Section 5.3.1, Mujica et al [64] suggest a method to organize recorded data somehow that response over a whole time period excited by an actuator and captured from all sensors are folded in a 2×D matrix where rows show the observation and columns are consists of package of data from each sensor laid beside each other. This method highlights the correlations in time for each signal and the correlations between sensors. Therefore, for the first actuator, 3 packages of data from each sensor containing 3000 recorded samples per observation are used. Figure 5.18 shows the result of clustering applied on actuator-based data. As it can be seen from the figure, all clusters related to different condition of structure are distinctly separated and automatically categorized.

Beside all benefits exhibited by Wave Cluser algorithm, it is not accurate in some cases. For example, in some cases where few specific clusters, probably similar, are located far away from the majority of other clusters, Wave Cluster algorithm considers these clusters as unique clusters. For example, as Figure 5.19 shows, two damages (Damage 1 and 3) that are highly located similarly are clustered as alike damage.

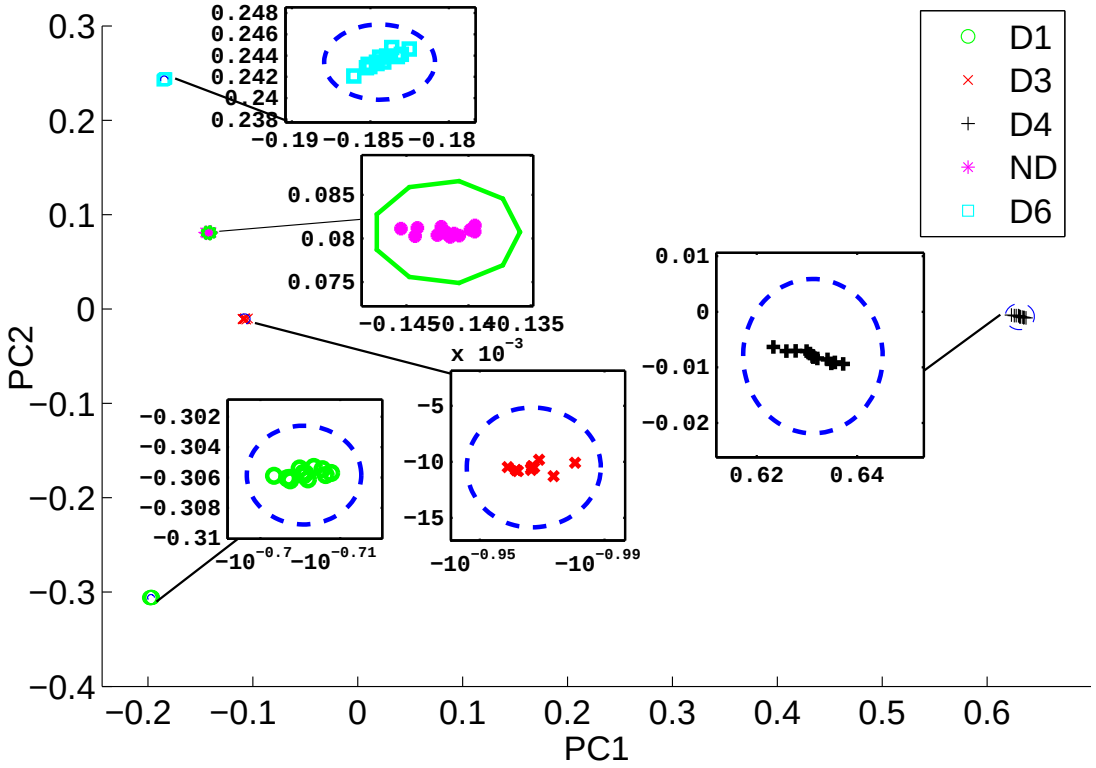

Figure 5.18.: Clustering using Wave Cluster applied on folded data belonging to one actuator

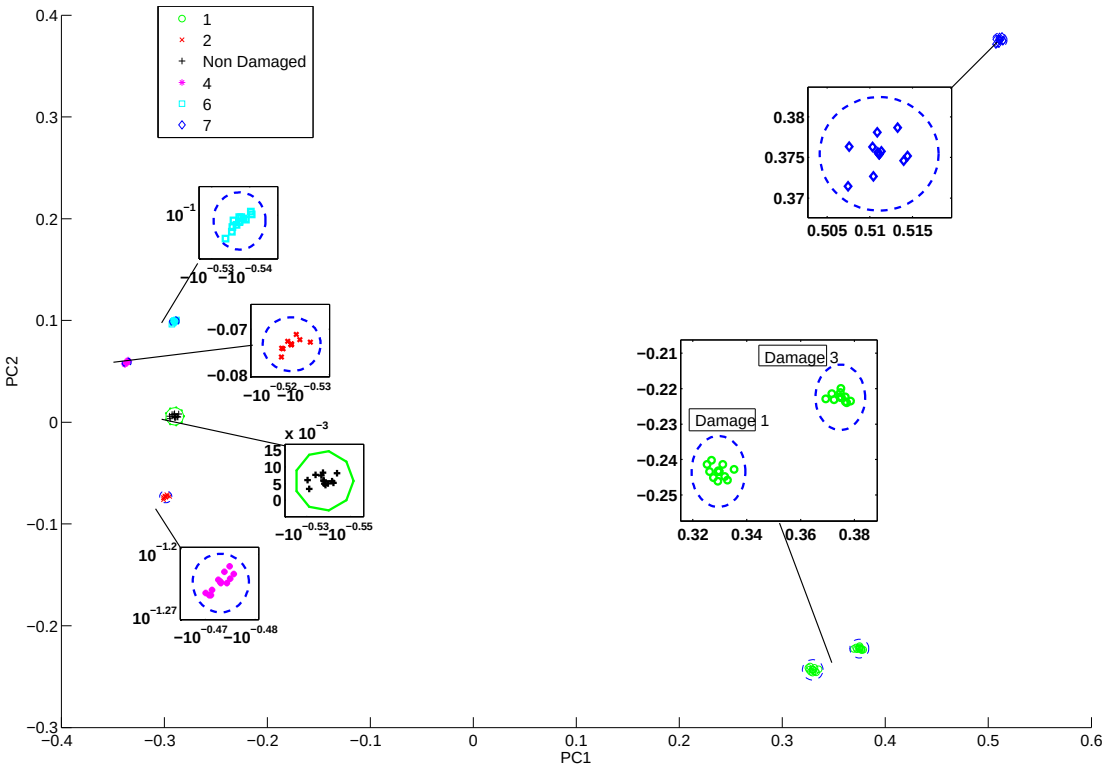

Figure 5.19.: Clustering failure using Wave Cluster

5.4.2. Damage detection using Andrew plots

Although PCA and its robust variant are useful tools for damage detection, the representation of the result is limited to two or three dimensions. This problem also happens for other exploratory data analysis. Therefore, in the initial stages of analysis, graphic displays can be used to explore the data, but for multivariate data, traditional histograms or two or three-dimensional scatter plots may miss complex relationships that exist in the data set. As it is mentioned in Section 3.8, in this thesis Andrew plots are applied to represent the results of analysis using PCA. To achieve this goal, the turbine blade specimen described in Section 4.2.3 is used in this section.

The ability of Andrew plots to classify observations into groups and detect observations that do not belong to a specific structure could be used as a method to detect observations that are from the healthy structure. On the other hand it has been mentioned that because of Andrew plots properties, it would be necessary to associate the most important variables with high periods and thus arrange the variables in a multivariate vector by the decreasing order of their importance. To this aim, the obtained data from PZT sensors are reduced in dimension and ordered using PCA. In other words, PCA is used as a dimensional reduction tool to provide the Andrew plot with the ordered coefficients. To do this, primary PCs are used as coefficients of Andrew plots. Andrew curves are calculated for each observation and

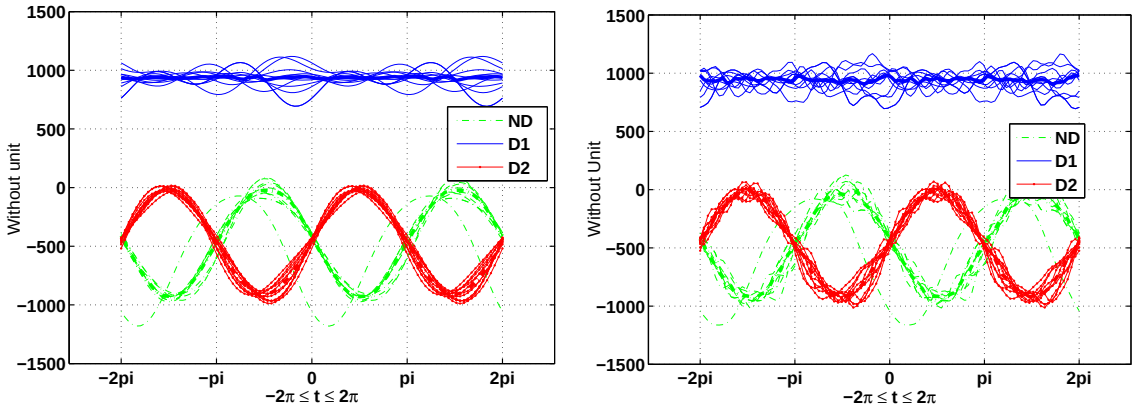

(a) for first 5^{th} PCs **(b)** for first 7^{th} PCs

Figure 5.20.: Andrew plots damage detection

finally all curves are depicted in the same plot to display the result. It could be seen that using less number of PCs generates smoother function and more proper figure to distinguish the damages from non damaged structure. In this work, to have a better view, curves were evaluated for values of time (t) from -2π to 2π. Equation 3.50 is re-written using PCs as below

$$f_y^{(1)}(t) = \frac{pc1}{\sqrt{2}} + pc_2 \times \sin(t) + pc_3 \times \cos(t) + pc_4 \times \sin(2t) + \cdots \tag{5.2}$$

Figure 5.20 shows the result of Andrew plots for 2 different data from damages ($D1$ and $D2$) and non-damage in the structure using the first five Principal Components. As it is shown, there are three different patterns. The pattern depicted in green (dashed line) comes from non-damaged structure, while other two patterns, depicted in red (dash-dot line) and blue (solid line), are related to damage 1 and damage 2 respectively. According to the figure, different patterns are distinguished clearly from each other. This property not only can be used to detect probable damages in the structure but also could classify any type of damages. To do this, enough amount of experiments should be conducted to create a baseline from the healthy structure using Andrew plots and PCA. After collecting enough data from the non-damaged structure, available pattern could be used as baseline to show that whether the next observation belongs to the healthy structure pattern or there is a probable damage in the structure.

It is obvious that if, instead of the first five PCs, the first seven PCs are chosen, the figures will be less smooth since the higher frequencies are included. Figure 5.20-b confirms this idea. Another alternatives for original Andrew plots are also used to see if they are able to distinguish the patterns of damaged structure from non-damaged. Figure 5.21-a shows the result of Equation 3.53 (Gnanadesikan).

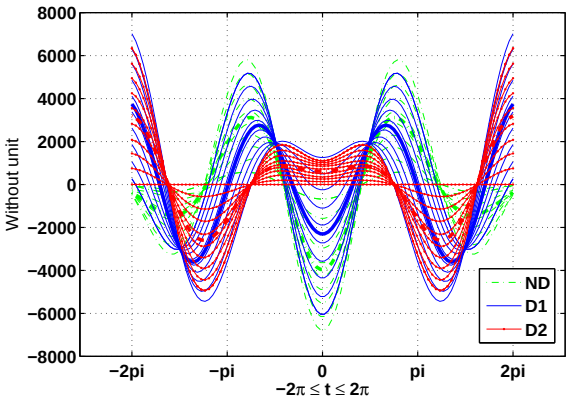

(a) Gnanadesikan plot, first 5^{th} PCs

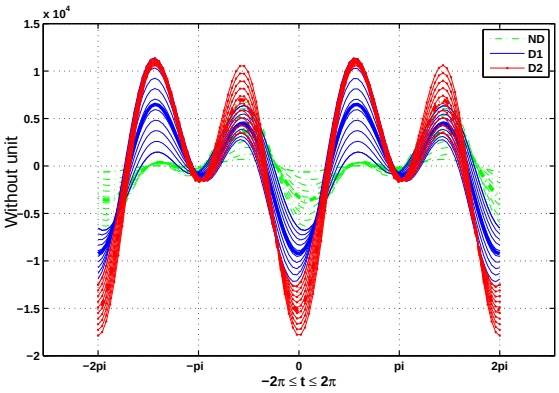

(b) Paranjape plot, first 5^{th} PCs

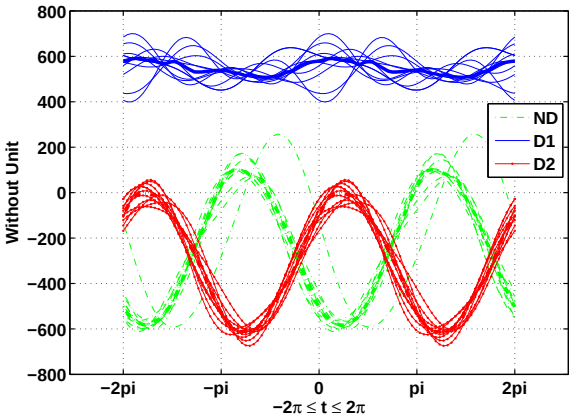

(c) Ravindra plot, first 5^{th} PCs

Figure 5.21.: Andrew plot alternatives

According to the figure, although patterns are not clearly seperated, all functions belong to a certain group intersect each other in the certain point. In other words, using this unique property, any new data could be categorized as non-damaged, known damaged pattern or new type of damage. Therefore, both damage detection and classification are satisfied in this method.

Figure 5.21-b belongs to Equation 3.54 (Paranjape): the same behavior is seen where functions belonging to the equal pattern meet each other in the same point.

The last one (see Figure 5.21-c) is depicted using Equation 3.55 (Ravindra). The behavior of this function is very close to the original Andrew plot.

As a brief conclusion, Andrew plots, as graphical representation of multivariate data, could be used as an index to identify any probable damage in the structure when 2 or 3 dimensional data are not sufficient to depict the behaviour of the data. As the order of coefficients of terms is very important in Andrew plot equation, these coefficients should be rearranged depending on their importance. PCA or its robust counterparts can be used in this manner for both ordering and reducing the

dimensionality. Obtained curves clearly seperate observation from different groups. Therefore, using depicted figures, any damage can be separated from healthy observation in which not only detect the damage but also clarify the type of damage. Results from the experiments confirm this idea where two different simulated damages are detected and classified.

5.4.3. Damage detection based on Fuzzy Similarity

In this section, a novel index is presented that is based on Fuzzy Similarity. The result that are presented here show that the proposed index is able to successfully distinguish between different status of the structure. The new index is applied on data captured from the laboratory wing case studies that is described in Section 4.2.1 and 4.2.2.

5.4.3.1. The methodology

The proposed damage detection methodology based on Fuzzy similarity to interpretate result can be described as follows. Mathematical background of Fuzzy similarity is scrutinized in Section 3.9. In this method PCA is utilized as dimension reduction and feature selection tool and similarity classifier based on Łukasiewicz-Structure is used as similarity measurement tool.

At the first step the time respone signal captured from sensors are pre-processed to remove noise. Then PCA is applied on the denoised data to reduce dimension and extract the features. Appropriate number of features (scores) are selected based on the criterion mentioned in Equation 3.31. After selecting the adequate number of features, all selected features from pristine structure and also from current status of structure are scaled between $[0-1]$ to fulfill the requirement of the methodology as mentioned in the theoretical background. Data from pristine structure are used to calculate the representative of the structure called *ideal vector* in healthy condition. This could be done by calculating the mean of learning data in pristine condition or any other statistic representative such as median, etc. Data feature from current status of the structure is compared with ideal vector using similarity classifier measurement (see Equation 3.60). The quantity of similarity for any observation is calculated. This quantity is used as a indicator to distinguish observations that may be affected due to damage. This means that the similarity value between ideal vector and any observation belonging to the healthy status of structure is suppose to be different from the similarity value between ideal vector and any other observation that may be affected by existence of damage in the structure. The described algorithm is briefly depicted in Figure 5.22.

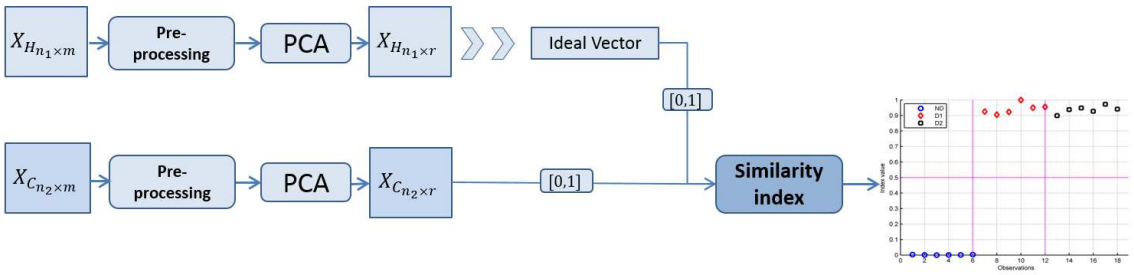

Figure 5.22.: Damage detection algorithm using Similarity Classfier

5.4.3.2. Organizing data

To validate the proposed methodology, an extensive study is performed. Initially, the similarity index is used to demonstrate its ability to distinguish the different status of the structure between healthy and damaged. This is performed for different exciting frequencies. In the next step, the algorithm is tested on actuator-based data (described in Section 5.3.1) captured from the set of transducers attached on the surface of the structure. Then, the threshold value is studied to find a criterion able to certify the existence of damage. After that, influence of the parameter p is analyzed. This parameter is relevant in tuning the index in Equation 3.60. In the next step, the proposed index is compared with the Euclidean distance and finally the algorithm proposed in this work is compared with the general damage detection methodology based on classical PCA that is described in Section 5.1.

The captured data from the laboratory wing case studies are organized as follows. For both case studies, 80% of data from healthy structure is used as training set and 20% as testing set. Therefore, for the first case study, 40 observations captured from the pristine status are used as a training data set and 10 as a testing dataset, which are captured from both pristine and different status of the structure. For the second case study, the same approach is followed that leads to 24 observations for training and 6 observations for testing.

Figure 5.23 shows this result of the methodology for the first case study for $p = 0.5$ and $p = 0.6$ in 145KHz. As it can be seen in this figure, similarity index for the first 10 observations that belong to the healthy structure are in the same range, whereas similarity index for the next 10 observations that belong to the damaged status are clearly separated as they stand in a different range. It should be mentioned that the similarity values are reduced from 1 ($\mid 1 - SV \mid$) and then are normalized between $[0, 1]$ for sake of simplicity for comparison purposes considering the maximum value as 1 that means more distance from the healthy condition. The results show a clear distinguishing and separation between the similarity values for observation from healthy and damaged structure.

The test continues by proving the efficiency of the method at different frequencies and a constant p. As it can be seen in Figure 5.24, a clear detection is achieved for all performed frequencies. This shows the flexibility of the algorithm to achieve

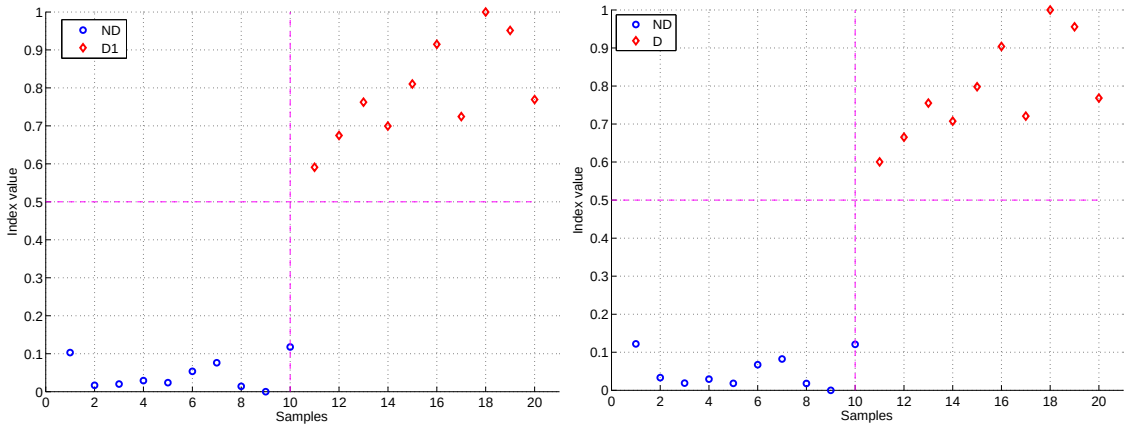

(a) p=0.5 **(b)** p=0.6

Figure 5.23.: Damage detection using Fuzzy similarity, exciting S1 at 145KHz and capturing from S2 (∘-Undamaged , ◇−Damaged)

acceptable results in different frequencies.

To have a comprehensive validation, the methodology, is performed for the second case study (Section 4.2.2). As it is mentioned before, data in this case study are collected (folded) for any individual actuator. Therefore, the test can be performed for any actuator separately. This is done to prove the efficiency of the algorithm for this type of data folding, which is widely used [204, 68, 207]. Figure 5.25 shows the result. It may clearly be seen that all damages are well distinguished from the healthy structure.

In next step, the methodology is repeated for the first actuator for constant p ($p = 0.5$) for different exciting frequencies. The results re-confirm the efficiency of the algorithm for different frequencies when folded data are used (see Figure 5.26).

5.4.3.3. Assigning threshold

Assigning an appropriate threshold level for novelty detection is an important issue in order to efficiently discriminate between undamaged and damage states. Some approaches such as Monte Carlo are proposed [126]. In this work, the critical value is assessed as follows:

1. Ideal vector is calculated from 80% of the data gathered from the healthy structure.
2. The quantity of the rest of observations from healthy structure is increased by adding white noise with signal to noise ratio of 90%. For instance, 500 more observations are genereated using this method.
3. The Fuzzy similarity index for all new generated observations are calculated (separately for each p).

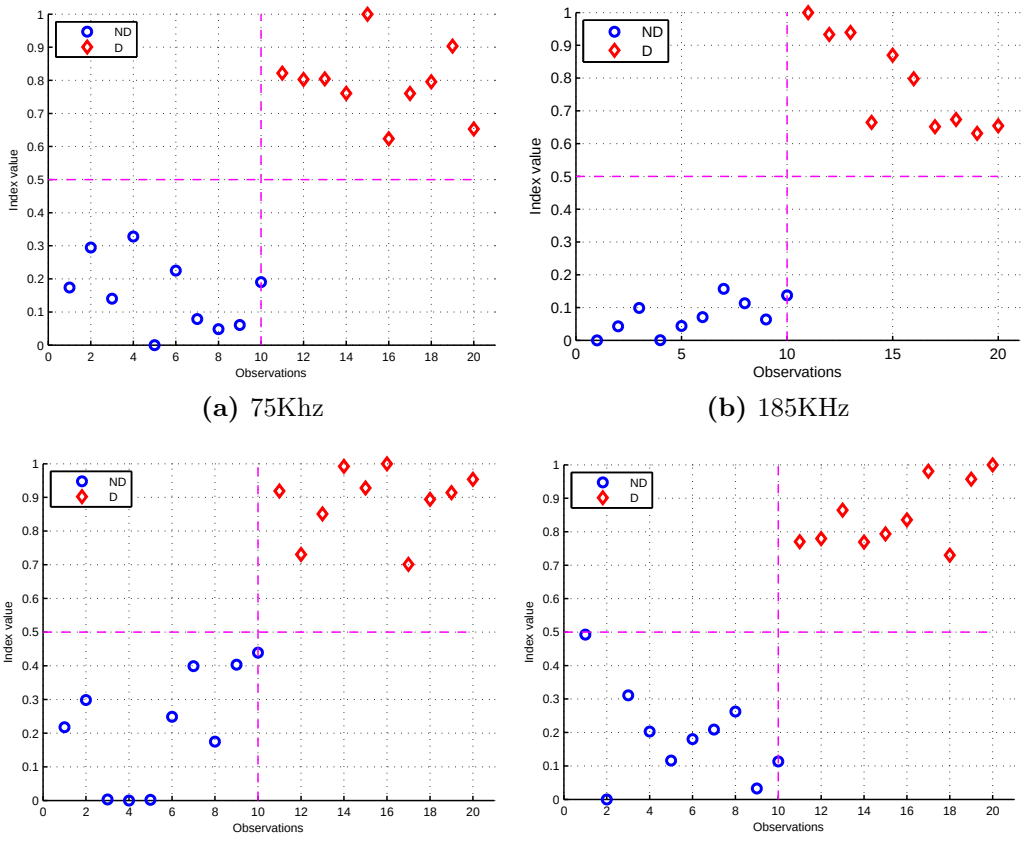

(a) 75Khz **(b)** 185KHz

(c) 300KHz **(d)** 360KHz

Figure 5.24.: Damage detection using Fuzzy similarity at different frequencies with $p = 0.6$ ($\circ$-Undamaged , $\diamond-$Damaged)

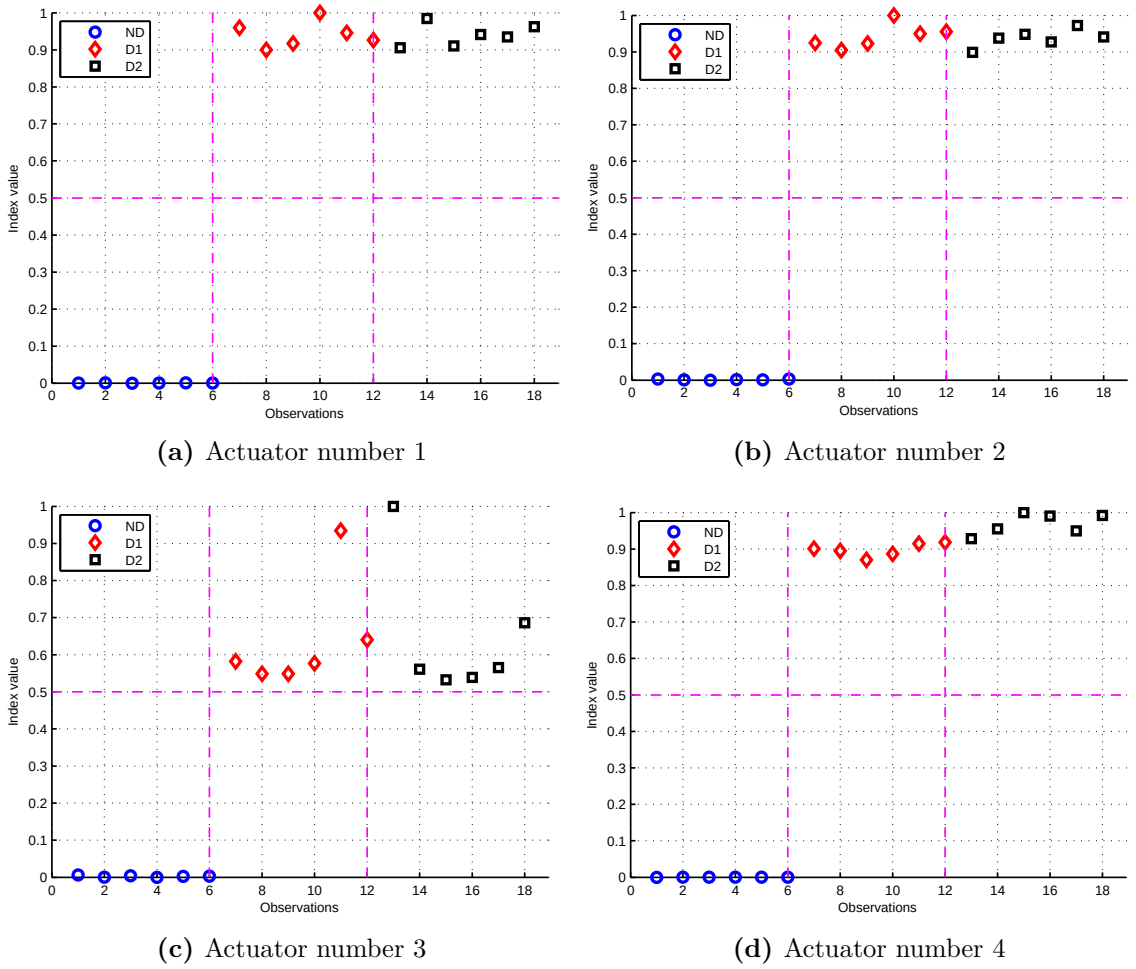

(a) Actuator number 1

(b) Actuator number 2

(c) Actuator number 3

(d) Actuator number 4

Figure 5.25.: Damage detection using Fuzzy similarity applied on folded data, at 125KHz and $p = 0.6$

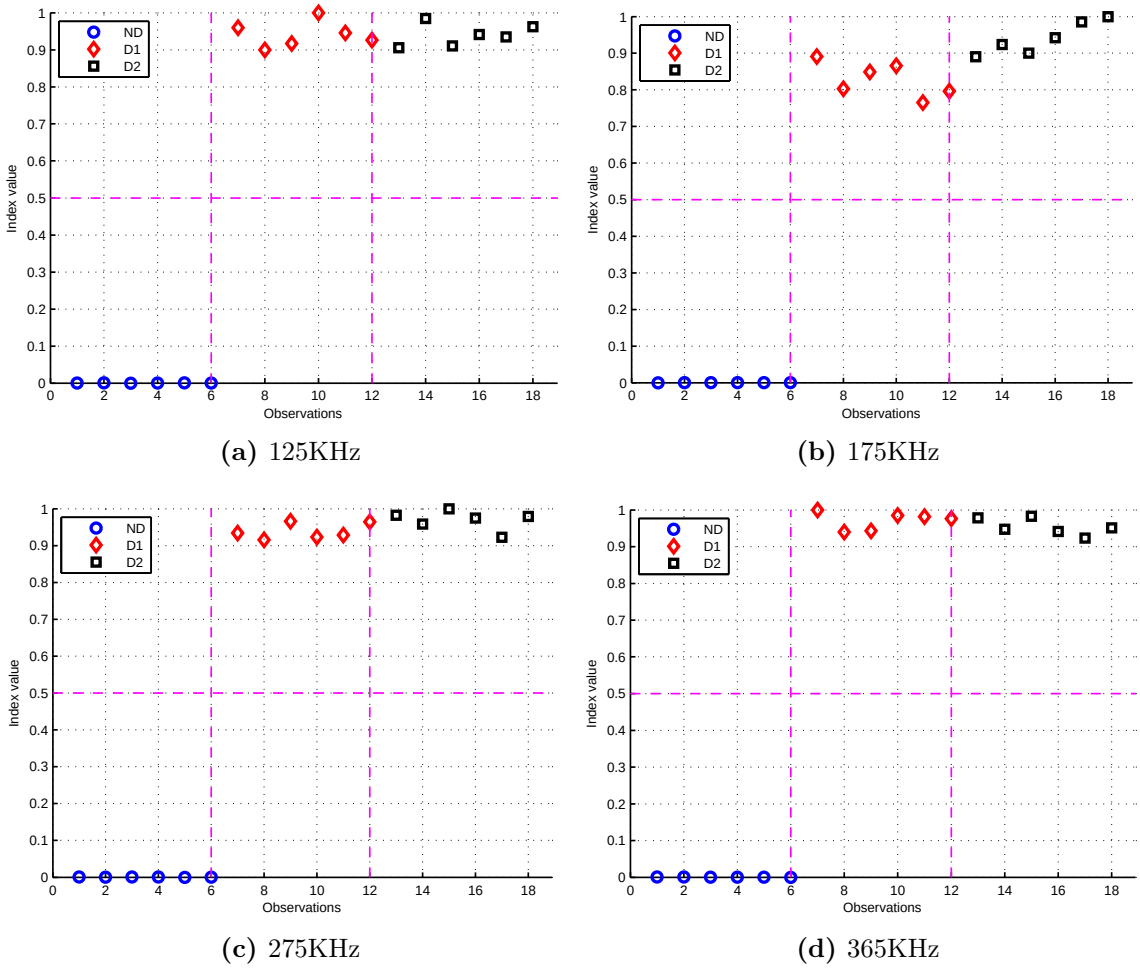

(a) 125KHz **(b)** 175KHz

(c) 275KHz **(d)** 365KHz

Figure 5.26.: Damage detection using Fuzzy similarity conducted on the second case study for transducer 1 and $p = 0.5$ at different frequencies

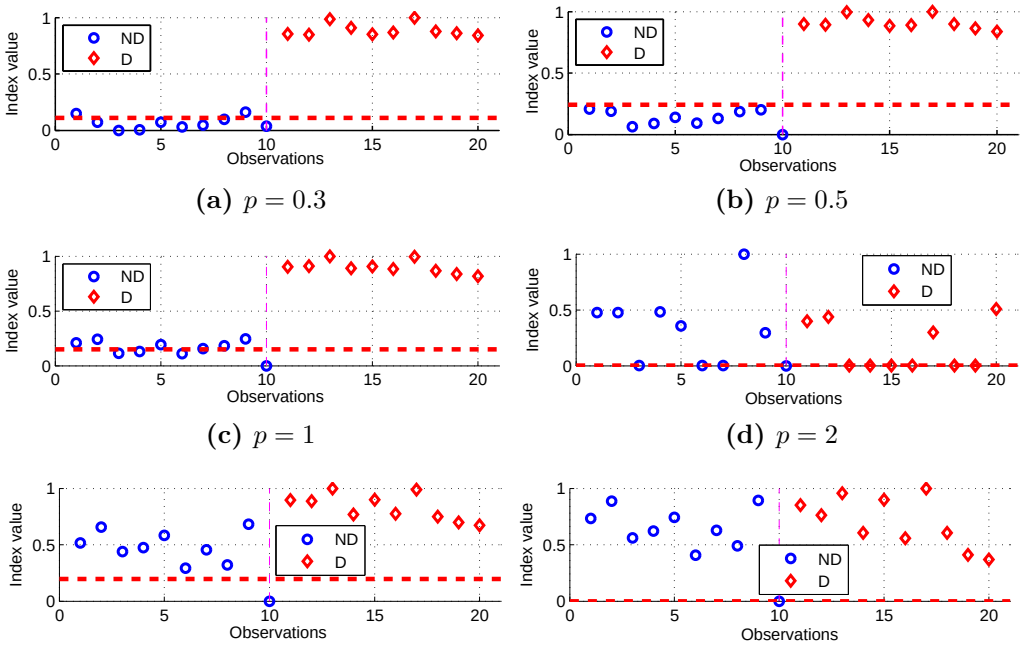

(a) $p = 0.3$ **(b)** $p = 0.5$

(c) $p = 1$ **(d)** $p = 2$

(e) $p = 5$ **(f)** $p = 10$

Figure 5.27.: Damage detection with different values of p conducted on the first case study, UPM SHM Lab.

4. The largest value among all calculated indices is designated as a threshold.

Figure 5.27 shows that considering $p = 0.5$, the selected threshold is able to separate each observation from healthy and damaged structure appropriately.

5.4.3.4. Selecting the appropriate value for p

As it was described in Section 3.9, the similarity is a function of the parameter p. Although p is an arbitrary value, the results show that the best value for p is around $p = 0.5$. Increasing the value of p, decreases the accuracy of the detection, somehow that the damage index is not capable of separate data from damaged structure and non-damage structure that causes *false-positive* detection. Figure 5.27 confirms the claim. As it may be seen from the figure, for $p \geq 5$, damage detection is failed. The horizontal line in each figure depicts the calculated threshold level.

To assess the effect of changing p in the sensitivity and accuracy of the damage detection method, the receiver operating characteristic (ROC) curve is plotted regarding to change of p. The ROC is a graphical plot which illustrates the performance of a binary classifier system as its discrimination threshold is varied. It is created by plotting the fraction of true positives out of the actual total positive vs. the fraction of false positives out of total actual negatives at various threshold settings. The closer the curve follows the left-hand border and then the top border of the ROC

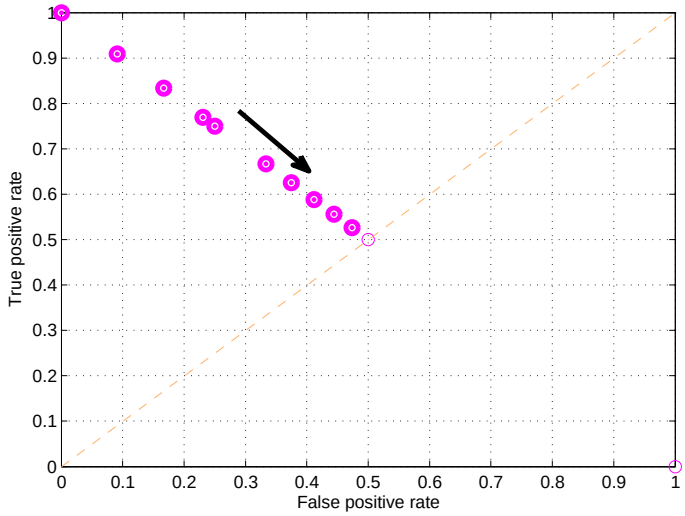

Figure 5.28.: ROC for Fuzzy similarity classifier by changing p

space, the more accurate the test is. On the other hand, the closer the curve comes to the 45−degree diagonal of the ROC space, the less accurate the test is. The ROC test is performed when p is changing. As it can be seen in Figure 5.28, increasing p causes decreasing in sensitivity of the algorithm.

5.4.3.5. Comparing with Euclidean distance novelty index

Euclidean distance is the most similar novelty index to the index that is presented in this work. The Euclidean metric is the "ordinary" distance between two points x and y. It is the length of the line segment connecting them defined as follows:

$$d(x, y) = \sqrt{\sum_{i=1}^{n} (x_i - y_i)^2} \tag{5.3}$$

The competency of the new damage index is compared with classical Euclidean distance at different frequencies. The same damage detection methodology is used. It means, after dimension reduction and obtaining the ideal vector, Euclidean distance is used to calculate the similarity of observations with the ideal vector. Figure 5.29 shows the result of using Euclidean distance in the first case study. As it may be seen in this figure, for the majority of applied frequencies (except in 185KHz), the Euclidean distance results in false-positive or false-negative decision for some observations as it can be seen from the figure. For instance, in Figure 5.29-a the majority of observation belonging to the damaged status are not detected (false-negative) or in Figure 5.29-d, some observation that belong to the healthy status are detected as damaged (false-positive).

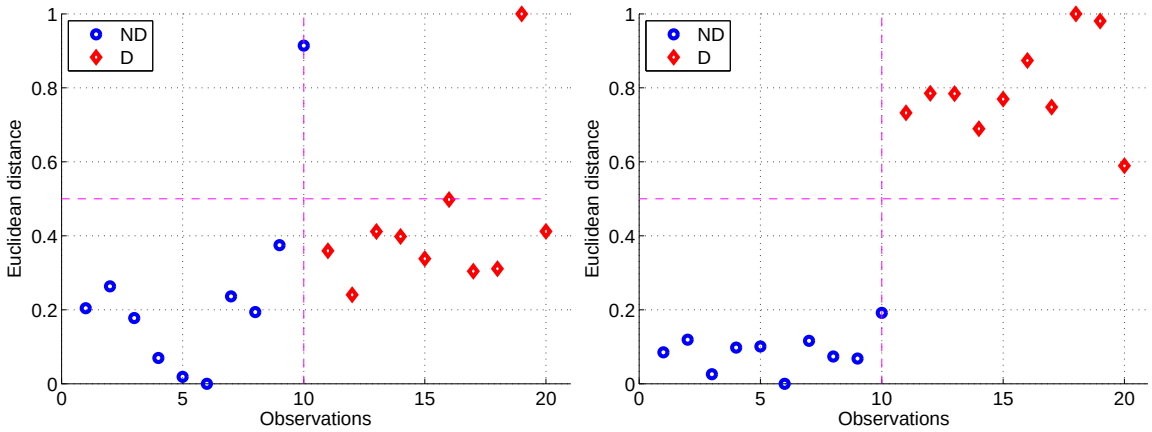

(a) 75 KHz **(b)** 185 KHz

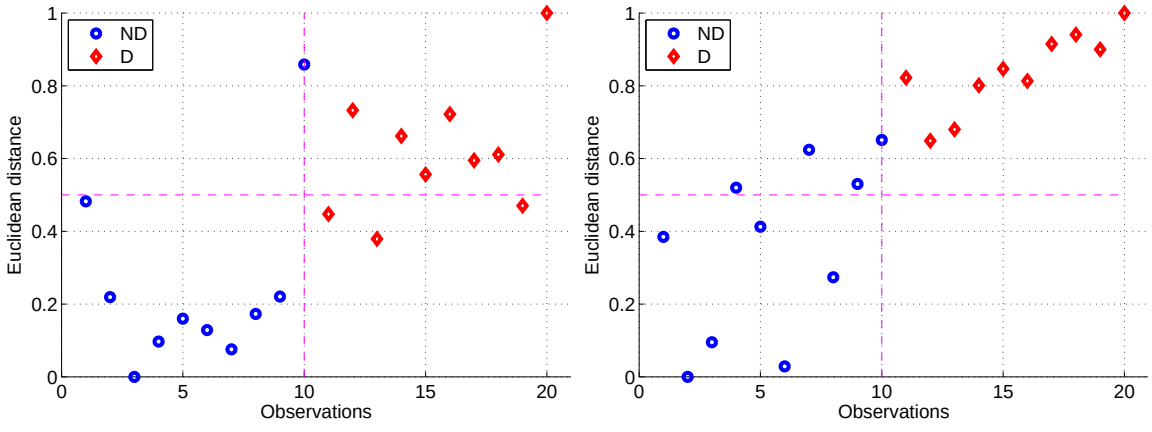

(c) 300 KHz **(d)** 360 KHz

Figure 5.29.: Euclidean distance, first case study, different frequencies, UPM SHM Lab.

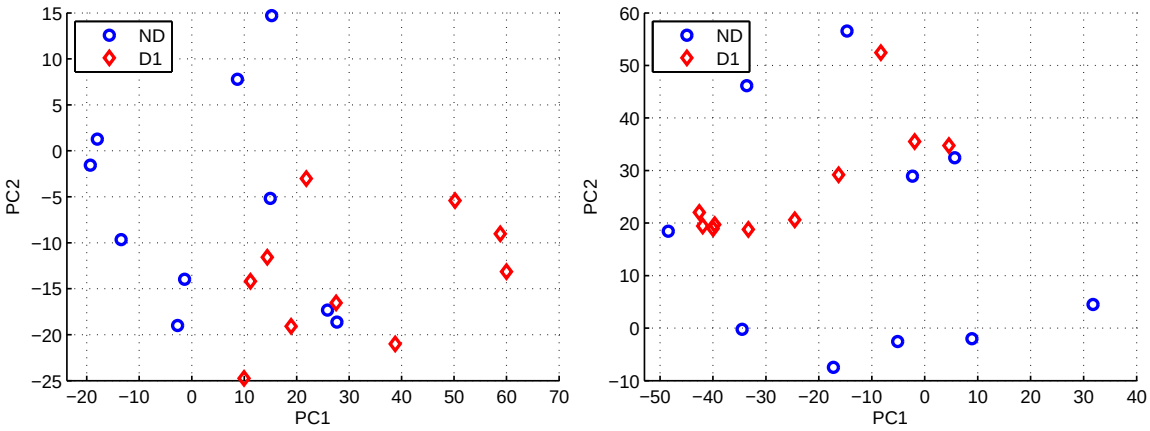

(a) 145KHz **(b)** 185KHz

Figure 5.30.: Damage detection based on PCA scores conducted on the first case study, UPM SHM Lab.

To further evaluate the proposed methodology, it is compared with the general damage detection strategy based on PCA as both dimension reduction and data interpreting tool. This method is previously described in Section 5.1. The result for the first case study shows that this method is not able to distinguish the different status of the structure. As it may be seen in Figure 5.30, there is no clear separation between observation captured from pristine structure and damaged condition.

The analogous result is achieved when the described methodology is applied on the second case study. For instance, as it may be seen in Figure 5.31, damage detection is not obtained using the data that are folded for actuator 1 or 3. Results show that observations are not separated from each other, which means failure in damage detection.

In this section, Fuzzy similarity is introduced as a new damage index. Its performance is evaluated and confirmed using different case studies. To provide more comprehensive study on this index, it is compared with two other common damage detetion methodologies such as Euclidean distance. In addition, the optimal value for p parameter is evaluated and is has been demonstrated that, according to the ROC curves increasing the value of p causes decreasing the sensitivity of the index.

5.4.4. Damage detection using robust PCA Orthogonal Distance

5.4.4.1. OD distribution

The probability distribution function (PDF) of OD is not known exactly. As first analysis, the PDF of OD is estimated. The analysis is performed on data from pristine condition in 25°C. To achieve this, Lilliefors test [208] is applied. Lilliefors

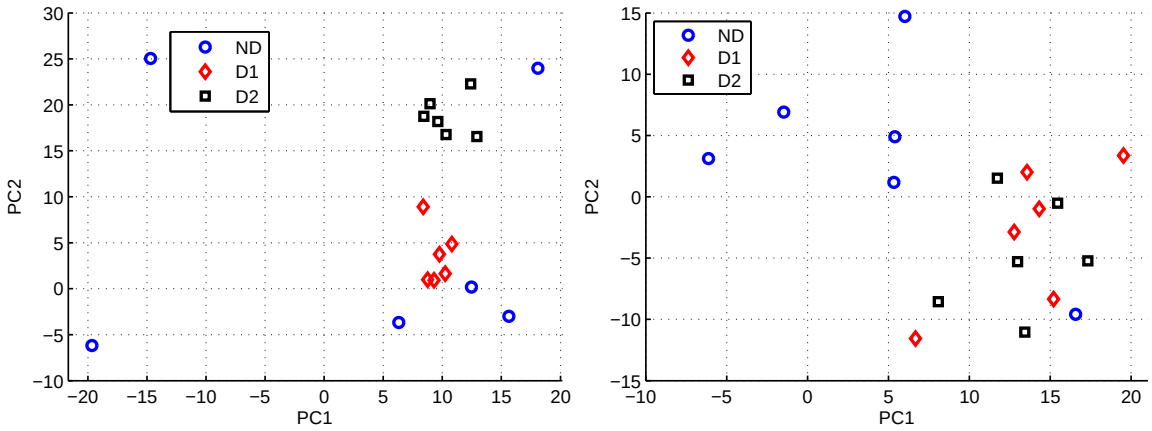

(a) Actuator 1 **(b)** Actuator 3

Figure 5.31.: Damage detection based on PCA scores, second case study, 125 KHz using two actuators, UPM SHM Lab.

Table 5.1.: Result of Lilliefors test on case study 1, different routes and status

	$1 \rightarrow 2$ (ND)	$1 \rightarrow 2$ (D5)	$1 \rightarrow 3$ (ND)	$1 \rightarrow 3$ (D3)
normal	rejected	rejected	rejected	rejected
extreme	accepted	rejected	accepted	accepted

	$1 \rightarrow 4$ (ND)	$1 \rightarrow 4$ (D1)
normal	accepted	accepted
extreme	rejected	rejected

test is an alternative for Kolmogorov-Smirnov test to check the null hypothesis that the sample in vector OD comes from a specific distribution or not. In contrast to the Kolmogorov-Smirnov, in Lilliefors test it is not necessary that the distribution should be known. The test is done with 5% significance level. Moreover, the test is applied on different routes from different status of the structure (damaged and undamaged). This is due the fact that as the specimen is not isotropic, different routes may fit different PDF. As Table 5.1 shows null hypothesis that the OD comes from normal distribution is rejected for routes $1 \rightarrow 2$ and $1 \rightarrow 3$ but it is accepted for route $1 \rightarrow 4$.

Figure 5.32 shows the visual probability density of OD in all routes when they are healthy and when they are provided with simulated damage. Moreover, OD moments show (see Table 5.2), extreme value distribution might be a better choice comparing with other distribution such as normal or Weibull. Moreover, Table 5.2 demonstrate the moments of OD for different routes. For instance, having Kurtosis different from 3, non-equality of mean and median and also negative Skewness could be enough reason to cancel the hypothesis of allocating normal distribution to the OD for the first two routes.

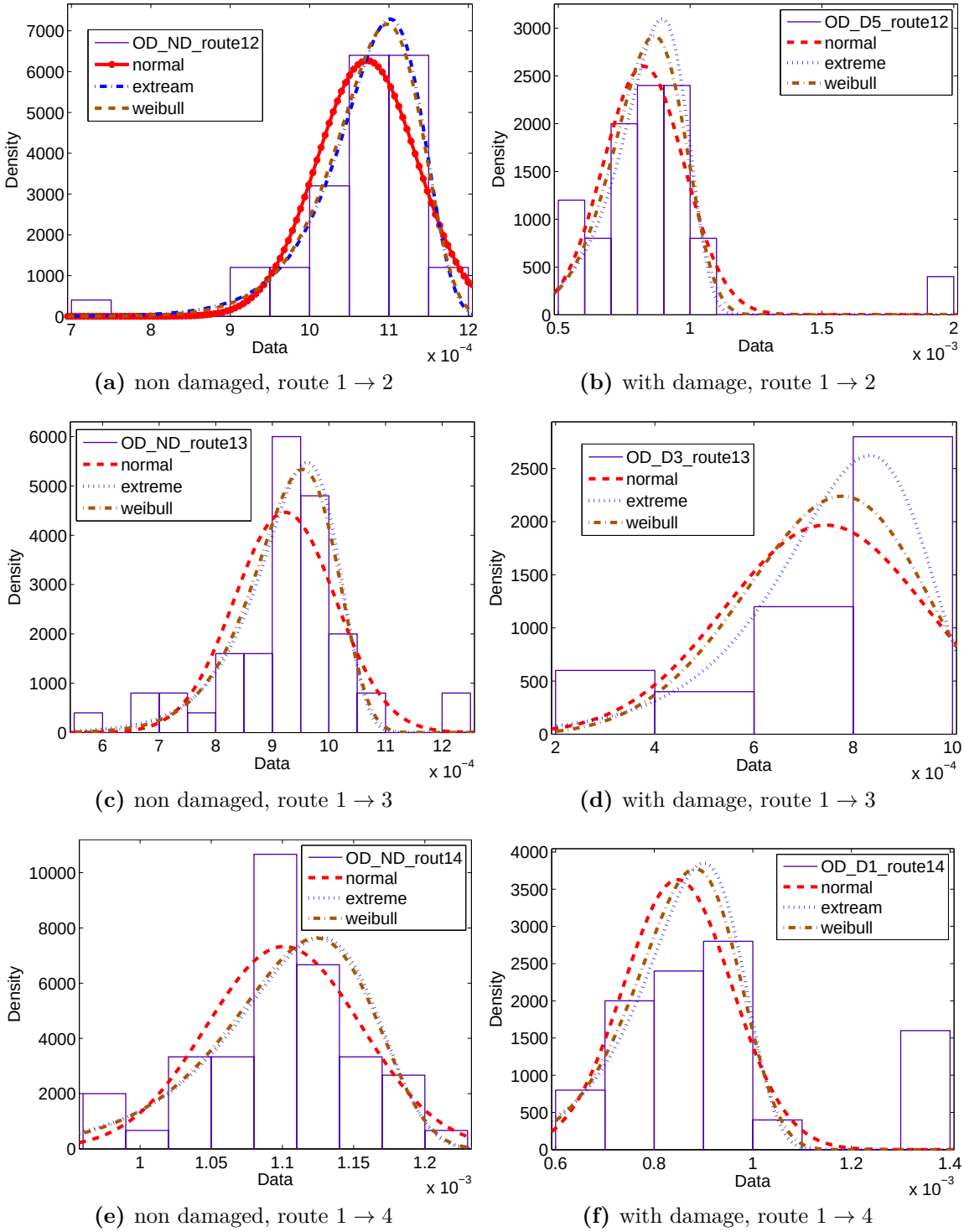

(a) non damaged, route $1 \rightarrow 2$ **(b)** with damage, route $1 \rightarrow 2$

(c) non damaged, route $1 \rightarrow 3$ **(d)** with damage, route $1 \rightarrow 3$

(e) non damaged, route $1 \rightarrow 4$ **(f)** with damage, route $1 \rightarrow 4$

Figure 5.32.: Orthogonal distance distribution, case study 1, different routes

Table 5.2.: OD moments

	$1 \rightarrow 2$, ND	$1 \rightarrow 2$, D5	$1 \rightarrow 3$, ND	$1 \rightarrow 3$, D3
Mean	0.0011	0.00082	0.00092	0.00074
Median	0.0011	0.00087	0.00094	0.00081
Skewness	-1.73	-0.67	-0.53	-0.96
Kurtosis	7.71	2.57	5	2.85

	$1 \rightarrow 4$, ND	$1 \rightarrow 4$, D1
Mean	0.0011	0.00091
Median	0.0011	0.00089
Skewness	-0.43	-0.16
Kurtosis	3.05	2.10

5.4.4.2. Damage detection using OD

Based on the method mentioned in Section 3.12.1, the OD is used as a damage index. Figure 5.33 shows the result in second case study. As it is evident, OD is able to clearly distinguish between observation from healthy status and the observation from damaged status. As it can be seen, different damages ($D1$,$D2$,$D3$,$D4$) are visibly separated from non-damage (ND) status on different routes. A route is defined as a path between transducer pairs such as exciting actuator 1 and capturing signal in transducer 2. As this separation is compliantly evident, no threshold is applied here. It should be mentioned that the temperature is constant at room temperature ($\backsim 25°C$) in this study. Moreover, the same idea can be applied on different routes. For instance, Figure 5.34 show the result of damage detection on route $2 \rightarrow 1$ and $3 \rightarrow 1$. As it could be seen, the OD shows the significant difference for observation related to the damaged status that is located on the mentioned route. As an example, OD is clearly distinguished for the $D2$ on route $2 \rightarrow 1$.

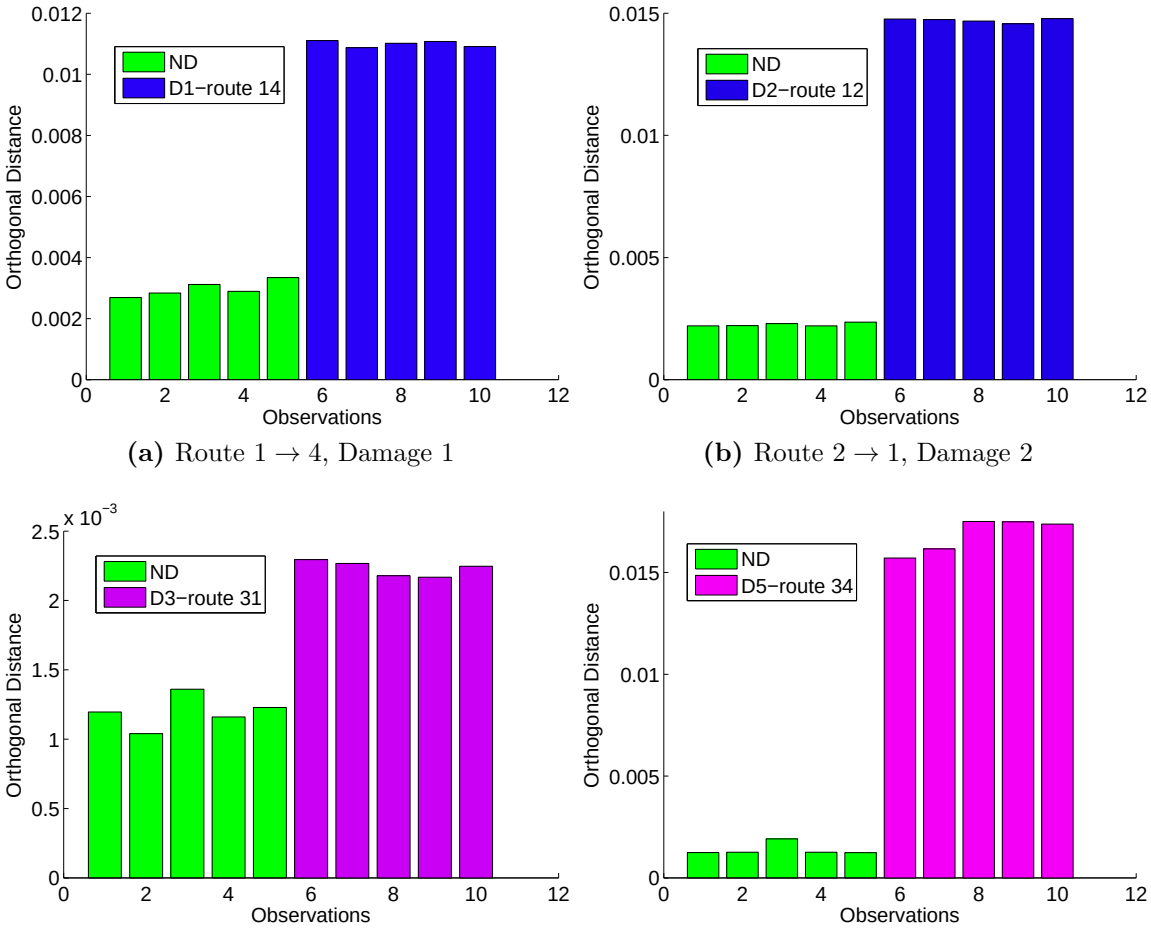

(a) Route $1 \rightarrow 4$, Damage 1

(b) Route $2 \rightarrow 1$, Damage 2

(c) Route $3 \rightarrow 1$, Damage 3

(d) Route $3 \rightarrow 4$, Damage 5

Figure 5.33.: Damage detection using OD, case study 2, $400KHz$

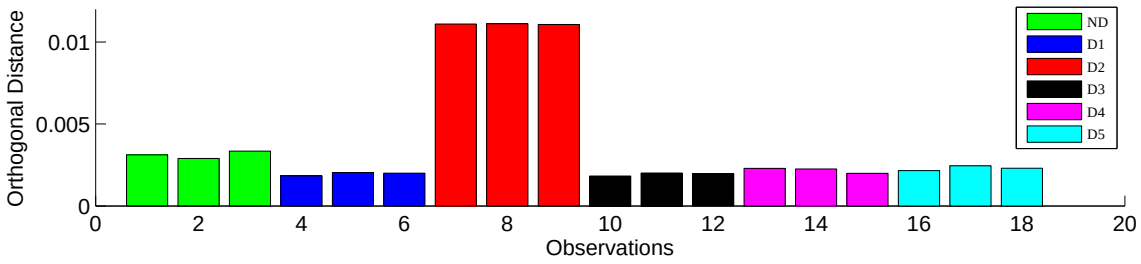

(a) Route $2 \rightarrow 1$

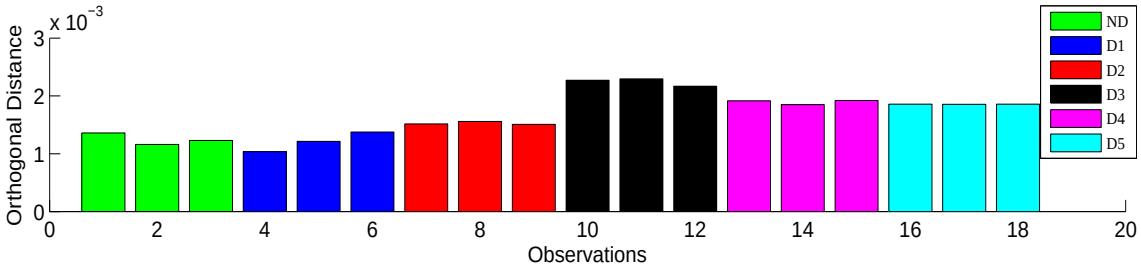

(b) Route $3 \rightarrow 1$

Figure 5.34.: Damage detection using OD for routes, case study 2, $400KHz$

5.5. Wavelet ridge as data pre-processing technique

In Section 5.1, two different general methodologies for damage are discussed that are based on PCA. The first one is when PCA plays a dimension reduction tool and the second one is when PCA is used to generate a statistical model. In both techniques, it is necessary to process data before subjecting captured signal to the PCA. It was mentioned that some mandatory pre-processing techniques such as denoising or averaging are vital to be applied. In this section, we present a new pre-processing technique. To prove the efficiency of the proposed methodology, it is applied on three different structures with distinct complexity. The brief description of this technique alongside PCA is described as follows. At the beginning it is applied on a simple aluminum beam and the results are demonstrated (see Section 4.3.1). In the next step, the efficiency of the method is challenged by applying on two more complex structure such as a commercial A320 airbus fuselage (see Section 4.3.3) and a pipe benchmark consist of damages (cuts) with different severity (see Section 4.3.5).

This technique is a combination of Wavelet and PCA methods to gain the maximum properties of each of them together for damage detection in different types of the structures. The new strategy concentrates on using PCA as dimensional reduction and damage detection tool based on a specific feature that is obtained by WT. These features are obtained by calculating Ridge of WT. After that, PCA is applied on ridge of WT instead of applying on original data captured from the structure. This application is performed on pristine status of the structure and is compared with the unknonwn (probably damaged) status of the structure to detect any probable

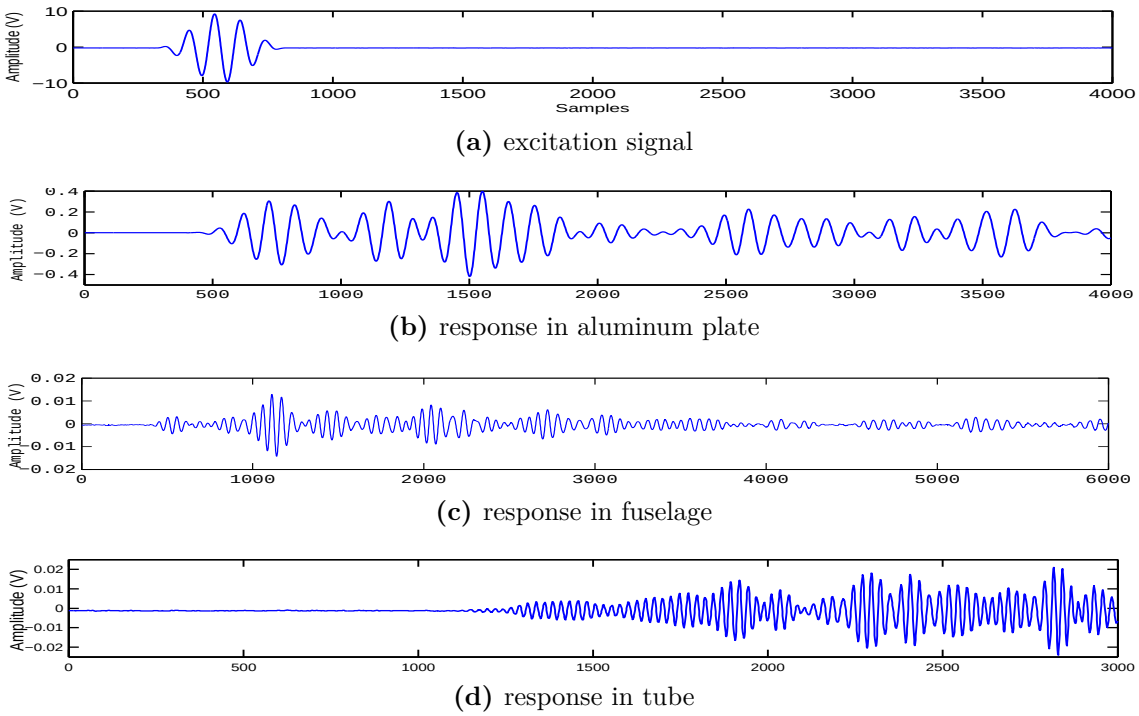

(a) excitation signal

(b) response in aluminum plate

(c) response in fuselage

(d) response in tube

Figure 5.35.: Excitation signal and responses in different case studies , Siegen SHM Lab.

discordancy that may be as a result of damage.

As an acquisition setup, all structures are equipped by piezoelectric transducers (PZT) from PI Ceramics with reference number PIC151 with 10mm diameter. The PZT's are distributed over the surface to excite the structure and detect time varying strain response data. A 10 V Hann-windowed signal is used as an actuating signal with different carrier frequencies with 3 cycles. Figure 5.35 shows the actuating signal and receiving signal for all mentioned structures. Received signals are de-noised before further process. Due to the obstacles such as stringers, and instinct properties of commercial A320 airbus fuselage material, propagating signal is highly attenuated (see Figure 5.35-d) but still is sufficient for signal processing. For any status of the structure 25 observations are collected. 40.000, 60.000 and 30.000 data samples are collected for the beam, fuselage and tube respectively. All data collections are done in room temperature without any environmental changes during the experiments.

As mentioned before, collected data from structures are organized in a form of $X_{n\times m}$ matrix. Continues wavelet transform is applied on each observation using the Daubechies 4 mother wavelet function family to construct the scalogram. Then ridge of constructed scalogram is calculated by finding maximum value through scale on each sample. For instance, Figure 5.36 shows the process of finding ridge of WT on data captured from aluminum beam by transducer located on the right side.

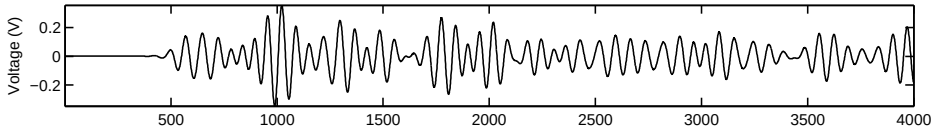

(a) A sample dynamic response - aluminum beam

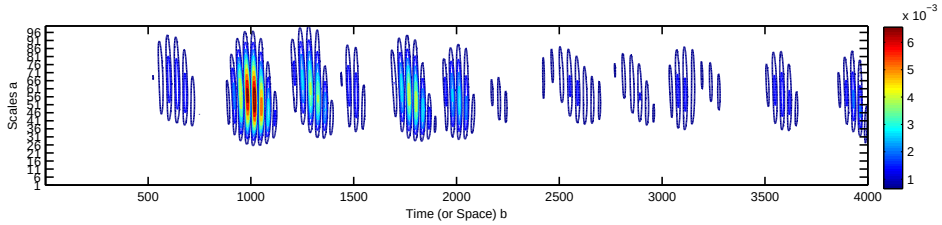

(b) Wavelet Scalogram

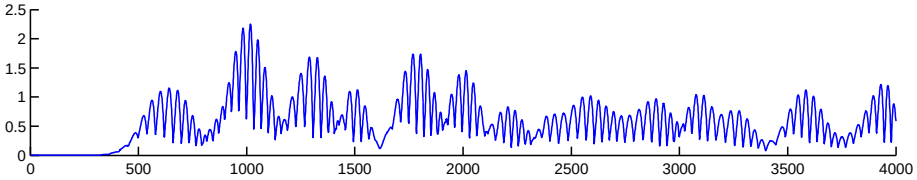

(c) Wavelet Ridge

Figure 5.36.: Calculating the wavelet ridge of a signal, aluminum beam

Calculated ridges sequences can be collected together to form a new matrix with the same dimension of the original matrix ($R_{n\times m}$). In this method, Ridge matrix is used instead of the original data as all significant information of signal are in this curves and more over information in ridge are less redundant. Therefore PCA is applied on Ridge matrix and the result of this application is compared with the situation when PCA is directly applied on original data.

Figure 5.37 shows the result of this methodology on the aluminum beam. As it may be seen, in a simple structure, PCA application on both original and ridge data can distinguish the pattern clearly. In order to have a better comparison, it is possible to measure and compare the distance between different patterns with pristine pattern in both conditions. This comparison indicates which method can distinguish patterns better. To achieve this goal, the Hausdorff distance [205] is used.

As it is shown in Figure 5.38, patterns generated by applying PCA on ridge data keep longer distances from the original pattern (healthy conditions), which leads to better distinguishing different status of structure.

To obtain a deeper validation, the same methodology is applied on fuselage structure. As it was mentioned before, the test area on the fuselage structure is surrounded by 4 traducers as it is shown in Figure 4.3.3-b. Each of these transducers can act as sensor and actuator. Damages are simulated by adding mass on the routes between transducers (see Figure 4.3.3-b). Each route is defined as the path between two

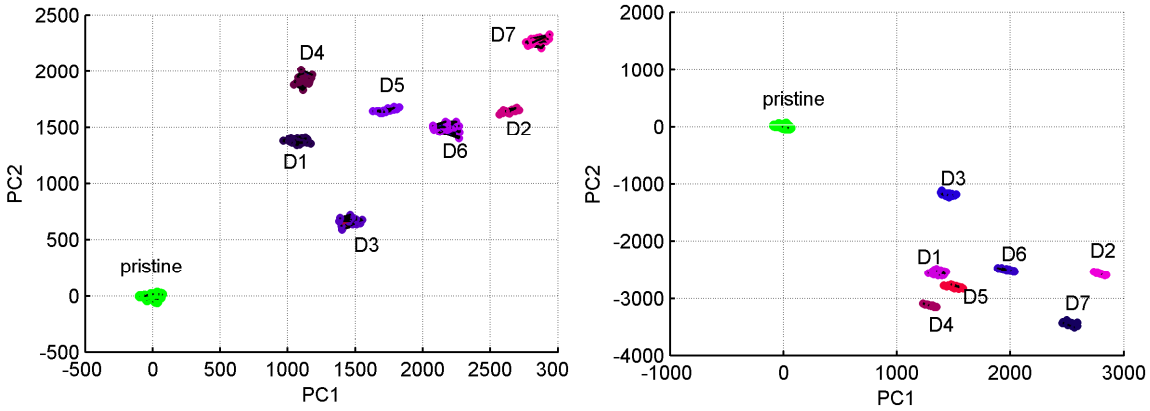

(a) on original data **(b)** on wavelet ridge

Figure 5.37.: Damage detection on aluminum beam: original data vs. wavelet ridge

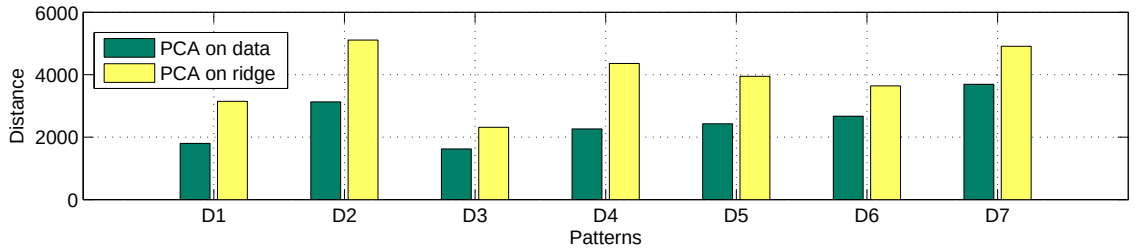

Figure 5.38.: Distance (between pristine and other patterns) applied PCA: direct data vs. Ridge

transducers from actuator to sensor.

The mentioned methodology is applied on data collected from each route. For instance, the route between transducers 1 and 2 passes through damages 1 and 2. Therefore, it is expected that applying damage detection on this route lead to detecting damages 1 and 2 and the same is expected to happen on another route that passes through damages 3 and 4.

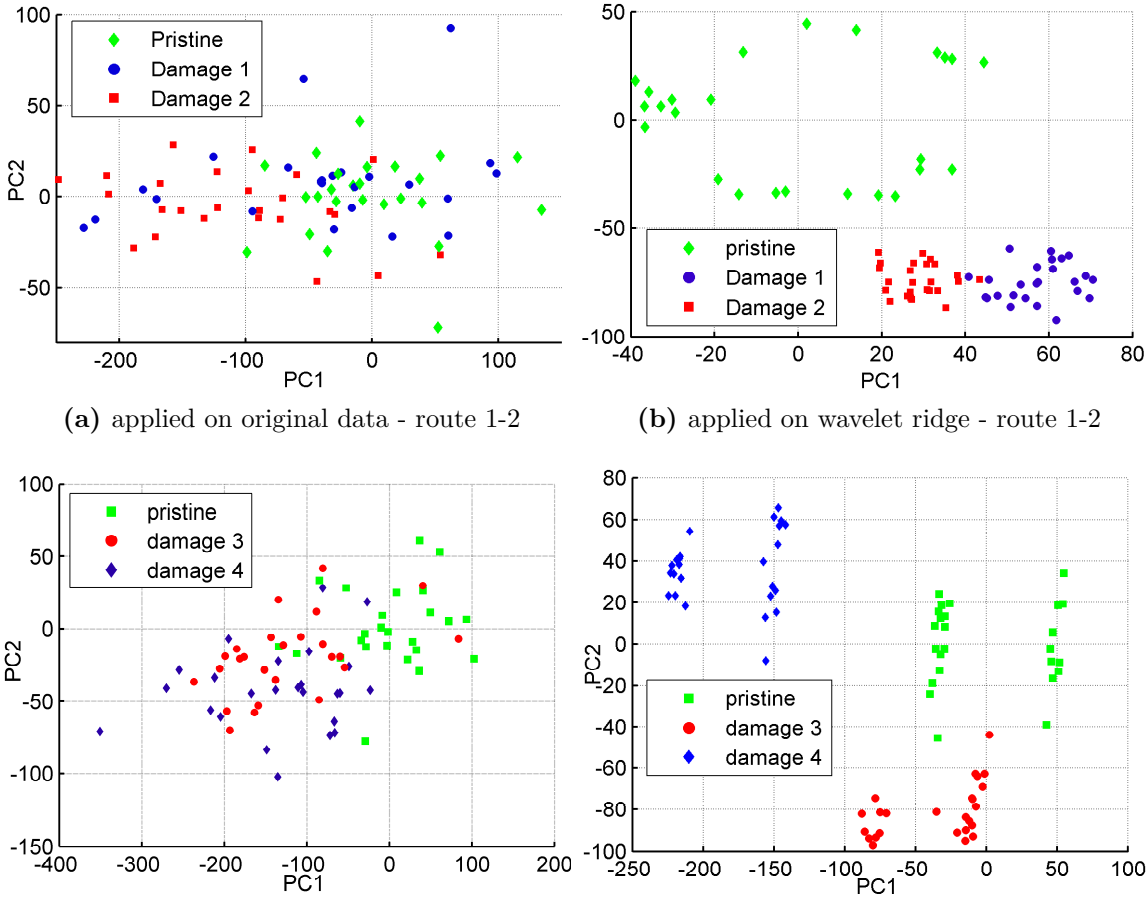

(a) applied on original data - route 1-2

(b) applied on wavelet ridge - route 1-2

(c) applied on original data - route 3-4

(d) applied on wavelet ridge - route 3-4

Figure 5.39.: Damage detection on fuselage using Wavelet Ridge

Figure 5.39 summarizes the result of this application. As it can be seen in Figure 5.39-a, applying PCA on direct data captured from route between transducer 1 and 2 can not distinguish between different type of patterns. This means that the damage detection is failed (false negative). On the other side, Figure 5.39-b demonstrates the application of PCA on ridge data. As it is obvious in this figure, an acceptable separation is obtained. Although the separation is not excellent, it is enough to infer the existence of other pattern rather than the healthy one and this could be enough reasonable in a complex structure like a commercial aircraft fuselage to lead to more analyze to confirm the presence of damage. Figure 5.39-c and Figure 5.39-d

also confirm the same inference on another route passing through another damages. For example, figure 5.39-c confirms the inability of PCA to detect damage 3 and 4 based on original data obtained in this route while Figure 5.39-d depicts the better result obtained from applying PCA on wavelet ridge of data.

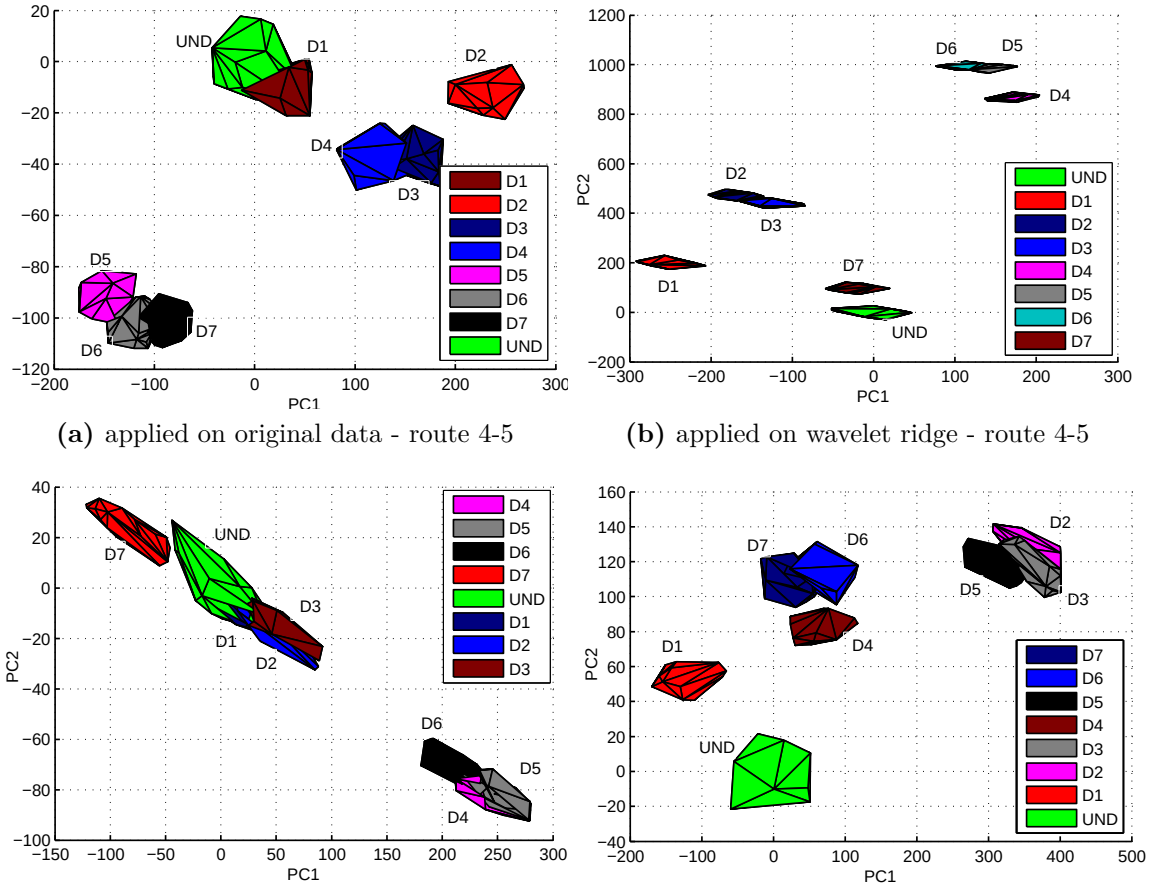

(a) applied on original data - route 4-5

(b) applied on wavelet ridge - route 4-5

(c) applied on original data - route 4-6

(d) applied on wavelet ridge - route 4-6

Figure 5.40.: Damage detection on tube benchmark, applying PCA on original data vs. on wavelet ridge, different routes

And the last test to evaluate the method, it is performed on the tube benchmark to detect damages. Obtained results re-confirms the advantage of applying PCA on wavelet ridge rather than original data. For instance, Figure 5.40 shows the result of applying PCA on original data and wavelet ridge in different routes. To have a better visualization results are plotted in a mesh form. The similar definition is used here as any specific route is the path between a specific actuator and a sensors. As it could be seen on Figure 5.40-a, undamaged pattern overlay on a pattern from damaged status when PCA is applied on original data, whereas pristine pattern is clearly separated from others when PCA is applied on wavelet ridge. Moreover, the same application on another route provides similar result as it could be seen on

figure 5.40-c and 5.40-d.

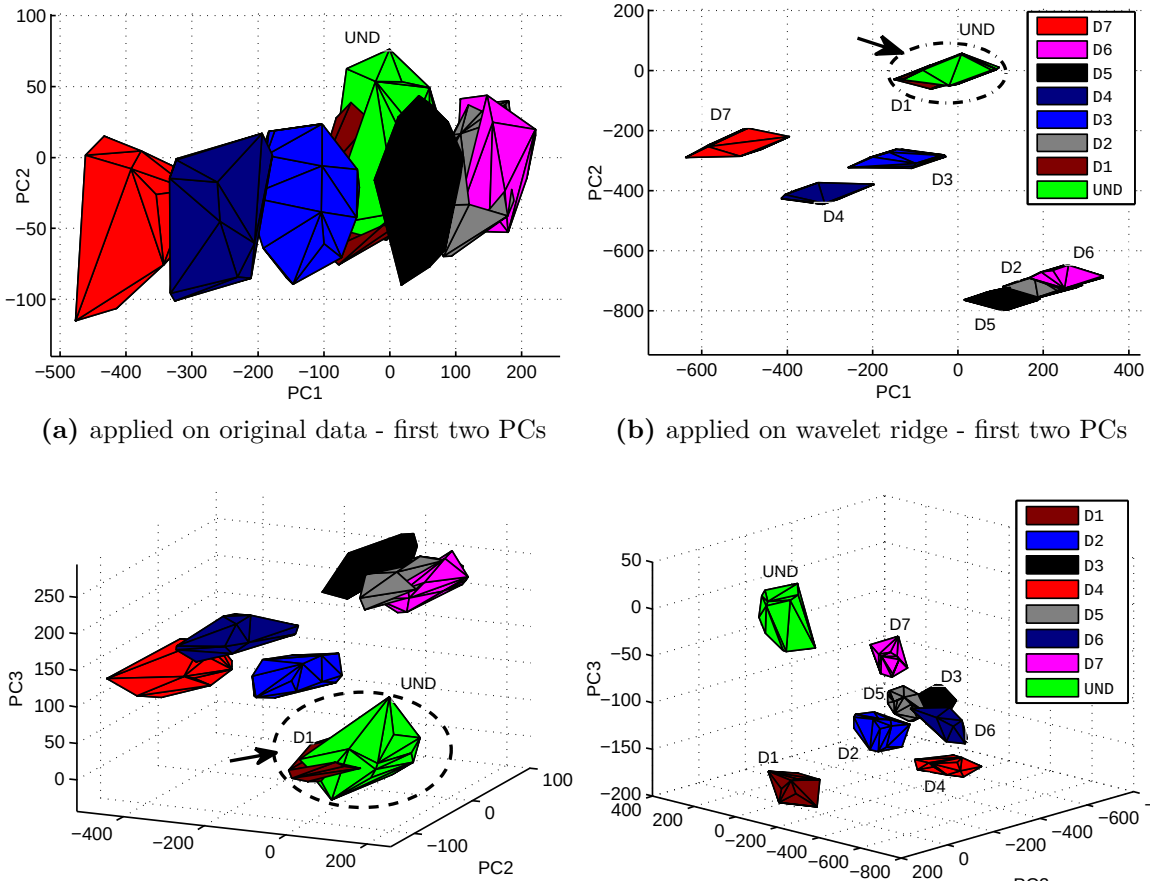

(a) applied on original data - first two PCs

(b) applied on wavelet ridge - first two PCs

(c) applied on original data - first three PCs

(d) applied on wavelet ridge - first three PCs

Figure 5.41.: Damage detection using Wavelet Ridge on tube benchmark, first two and three PCs

It should be emphasized that, although in the majority of cases, first two PCs are sufficient to achieve a favorable result, some times it is necessary to use more than two PCs. This probably happens when first two PCs are not carrying enough variance quantity that make it necessary to use more than two PCs. The criteria for selecting appropriate number of PCs are mentioned clearly in [152]. In spite of the mentioned fact, still applying PCA on wavelet ridge leads to more profitable result. As a case in point, applying PCA on both original data and wavelet ridge does not lead to a clear pattern separation (although wavelet ridge looks much better) when first two PCs are used. Therefore it is necessary to enlist more PCs. Nevertheless, it still is not sufficient using three PCs when PCA is applied on original data. As it Figure 5.41-c illustrates, pattern of healthy structure still overlaps with other patterns. On the contrary, a clear pattern separation is achieved using wavelet ridge (see Figure 5.41-d).

In this section, a new combination of two well-known methodologies, PCA and WT, is presented. This new look attempts to jointly benefit from the advantages of both methodologies in damage detection. It is shown that the new combination is able to provide a more accurate and reliable damage detection strategy. Experimental results show that in a variety of structures with different complexity, using both approaches together is recommended. Although this combination implies more computational costs, it may avoid failure of damage detection such as false negative. Indeed, it is shown that in not complicated structures such as aluminum beam the new combination can improve the results in terms of more separated patterns of different status. Such a result was obtained from the first experiment. Besides, using the new combination avoid wrong recognition of patterns where using PCA alone lead to not clear seperation of patterns dedicated to damaged status from the healthy status as it was described in the last two experiments.

6. TEMPERATURE EFFECT COMPENSATION

In this section, the effect of temperature fluctuation on all presented methodologies in this thesis is studied. First, the effect of temperature change on wave propagation is analyzed. To achieve this, the performance and efficiency of all presented methods are reviewed when temperature is changed. Results show that the temperature variation has a significant on the ability of mentioned damage detection techniques. Therefore, it is necessary to mitigate the temperature effect. To achieve this, a temperature compensation method is applied on each of presented methods to make sure that the presented methods are able to successfully perform damage detection even in a varying environmental conditions.

6.1. Environmental effect on SHM

Environmental variation is the one of the main obstacles for developing SHM solutions. In fact, these changes can often mask the structural changes caused by damage [105]. Among various environmental conditions, temperature changes are of particular interest because temperature is a global environmental condition and its variations substantially alter the recorded waveform [106].

As many structures exhibit daily and seasonal temperature variations and SHM systems will need to operate across a variety of environmental conditions, understanding and considering the effect of temperature on SHM methodologies is critical. In another words, SHM systems will not be accepted in practical applications unless robust techniques are developed to explicitly account for environmental and operational constraints/conditions of the systems to be monitored [105].

Several investigation were performed to find out the effect of temperature in SHM methodologies and various researchers acknowledged potential adverse effects of varying operational and environmental conditions on vibration-based damage detection [109, 106, 110].

The main reason to such effects are categorized as follows:

- Change in the properties of piezoelectric transducer (majority) such as piezoelectric constants [111, 112].

- Alternation in properties of adhesive used to bond transducers to the host structures.
- Thermal expansion such as change in plate thickness, piezo dimensions and distances traveled by the guided wave in the structure [112].
- Change in elastic properties including density and Young module that causes changes in wave velocity [3].

When environmental or operational conditions change, the propagating medium and guided wave behavior also change. Therefore, simple baseline comparison methods are unable to distinguish damage from environmental and operational effects [128].

6.2. Temperature effect on wave propagation

As it is mentioned in the Theoretical Background (see Section 3.13.1), temperature fluctuation has different effect on wave propagation and therefore on any damage detection methodology. In this section, the effect of temperature fluctuation is studied on different aspects of wave propagation. Amplitude variation is probably the first effect that could be seen directly when temperature changes. To demonstrate the temperature effect on signal propagation, a series of tests are performed using the structures described in Section 4.4.4 and Section 4.4.5. In this section we refer them as Case Study 1 and 2 respectively. Figure 6.1 shows the peaks of receiving signal at different temperature. The figure clearly depicts the magnitude reduction when the temperature is increasing. As it can be seen in this figure, both case studies confirms this effect.

In addition to the amplitude reduction, this figure clearly shows the velocity decrement (increase time of arrival). According to this figure, signals propagated at higher temperatures seems to arrive later than signals propagated at lower temperatures due to decreasing group velocities of the propagating wave components as well as slightly increasing the distances that the guided wave should travel in the structure.

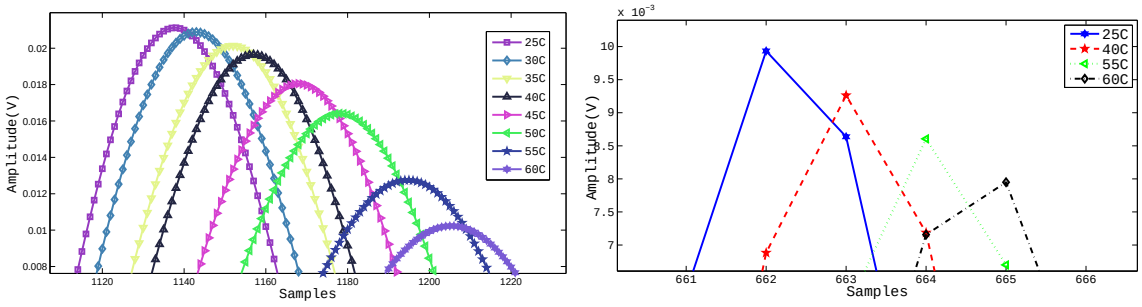

(a) Case study 1 **(b)** Case study 2

Figure 6.1.: Temperature effect on magnitude and velocity of propagated wave

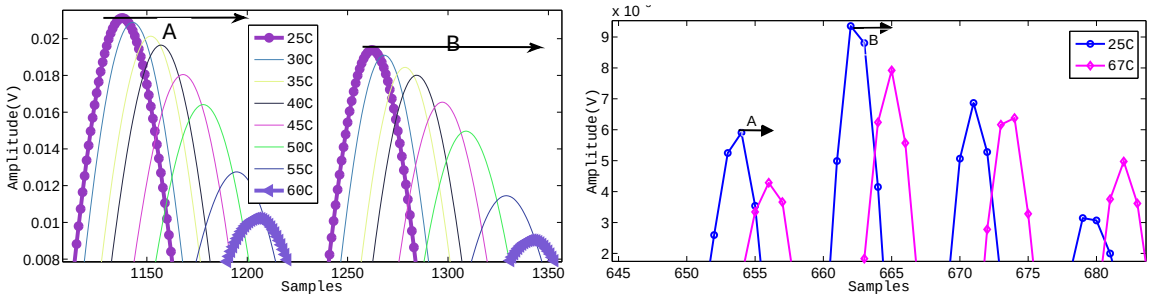

(a) Case study 1 **(b)** Case study 2

Figure 6.2.: Time-dependent time shift due to temperature fluctuation

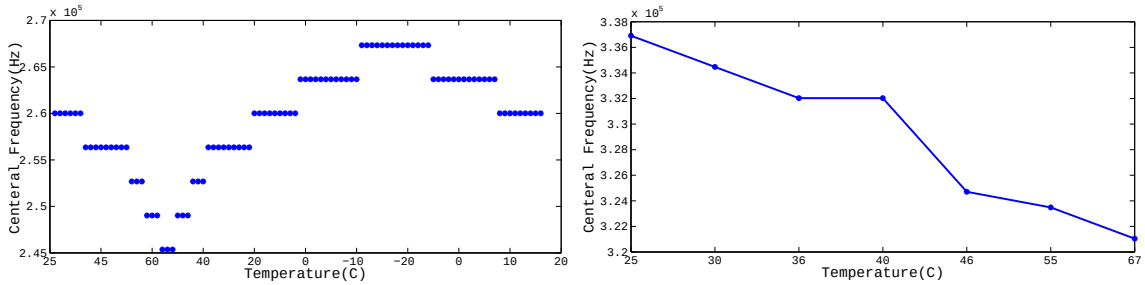

(a) Case study 1 **(b)** Case study 2

Figure 6.3.: Central frequency shift due to temperature fluctuation

Besides, in Figure 6.2 the time-dependent time shift is clearly evident. As it can be seen, the time shift is increasing by the time. This figure shows that in the first case study (Figure 6.2-a), the time shift between signal in 25°CC and 60°CC is increasing by time ($B > A$) where B and A are the differences between the peak of signals in the lowest (25°CC) and highest temperature (60°CC). The same phenomenon happens in the second case study (see Figure 6.2-b).

Changing the central frequency is another phenomenon that happens when temperature is changed. Figure 6.3 shows the central frequency change of the received waves regarding to the constant excitation frequency. As it could be seen in both case studies, central frequency decreases when temperature increases but the opposite trend happens when the temperature reduces that means central frequency increases (see Figure 6.3-a).

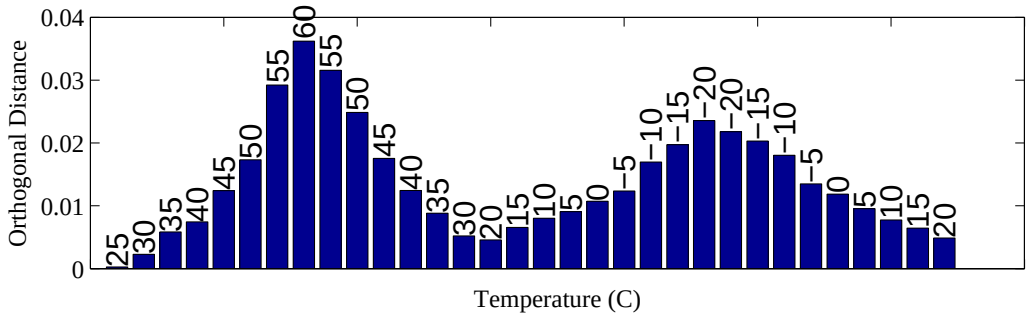

Figure 6.4.: Effect of temperature on OD, case study 1, route $1 \rightarrow 2$

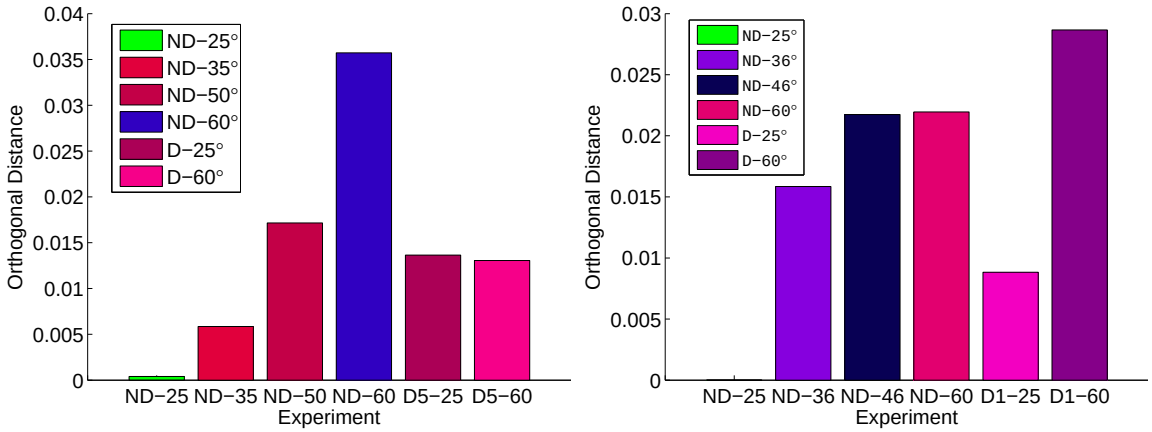

(a) Case study 1, route $1 \rightarrow 2$ **(b)** Case study 2, route $1 \rightarrow 4$

Figure 6.5.: Temperature effect on damage detection using OD

6.3. Temperature effect and compensation: Robust orthogonal distance

In Section 6.2 the temperature effect on wave propagation is demonstrated. In this section this effect on Orthogonal Distance (OD) is analyzed. Results show that OD is highly affected by temperature fluctuation. As it can be seen in Figure 6.4, OD is changing relatively and proportionally by the temperature change. Temperature change has a direct effect on OD as increasing the temperature cause OD incrementation and vice-versa. This causes a false positive alarm when OD is applied as damage detection index. Figure 6.5, clearly shows that OD from non-damaged (ND) structure in higher temperature is even more than calculated OD for the damaged structure. Both case studies confirm the same effect. Results on both case studies affirm that damage detection goal is not achieved when there is a possibility of temperature change in the system. Therefore, temperature compensation should be applied to relieve the adverse effect of temperature on wave propagation.

To improve the damage detection reliability, temperature compensation is applied

using Optimal Baseline Selection (OBS) methodology. To do this, a bank of baseline is recorded on different temperatures in both case studies. For the first case study, a collection of 96 observations (in healthy status of structure) is used as a baseline bank for temperature range $-20°C$ to $+60°C$. For the second case study, 70 observations cover the temperature range $+25°C$ to $65°C$. According to OBS, when a new observation from unknown status and unknown temperature is recorded, it should be compared with the baseline bank to find out the best matched signal using equations (3.67), (3.68) or (3.71). For instance, for a observation recorded in a healthy status at $60°C$ differential feature are calculated to find the closest observation in data bank. As it could be seen in Figure 6.6-a, in this case all the differential features $(E1, E2, E3)$ reach the same minimum. As another example, for an observation at $35°C$ from structure when damage D2 is simulated, the observation number 13 is selected (see Figure 6.6-b). According to the both figures, although $E1$, $E2$ or $E3$ may have different values along the bank of observations, they select the same observation.

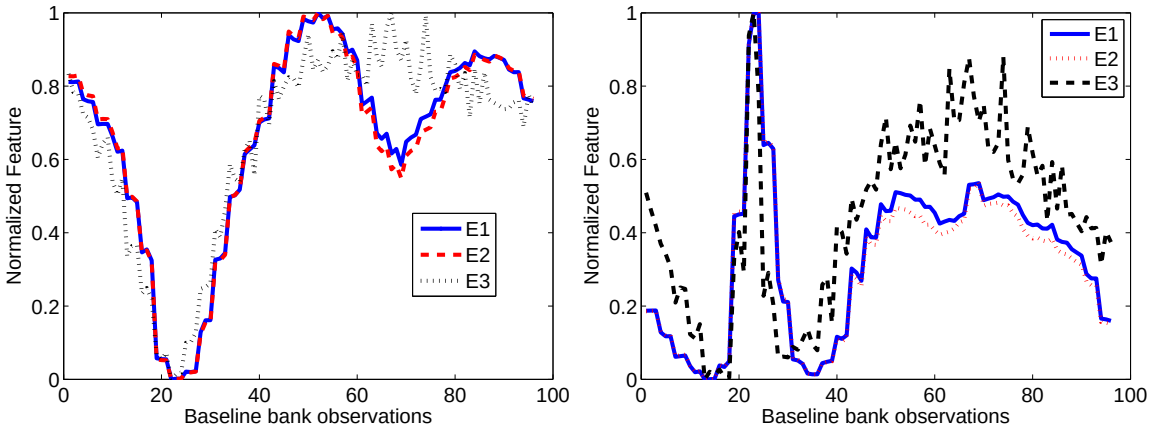

(a) ND $60°C$ **(b)** D2 at $35°C$

Figure 6.6.: Differential features comparison

The selected single baseline is statistically enhanced to form a baseline package that the new observation could be added to. To do this, 50 observations are generated with the signal/noise ratio of 95 percentages from the selected single baseline. After that, the observation from unknown status of the structure is added to this collection and the same damage detection methodology is applied.

Figure 6.7 shows the result of this methodology applied on both case studies. As it could be seen clearly, observation from healthy status are not considered as a damage anymore; instead, damage detection is clearly achieved without any false positive alarm.

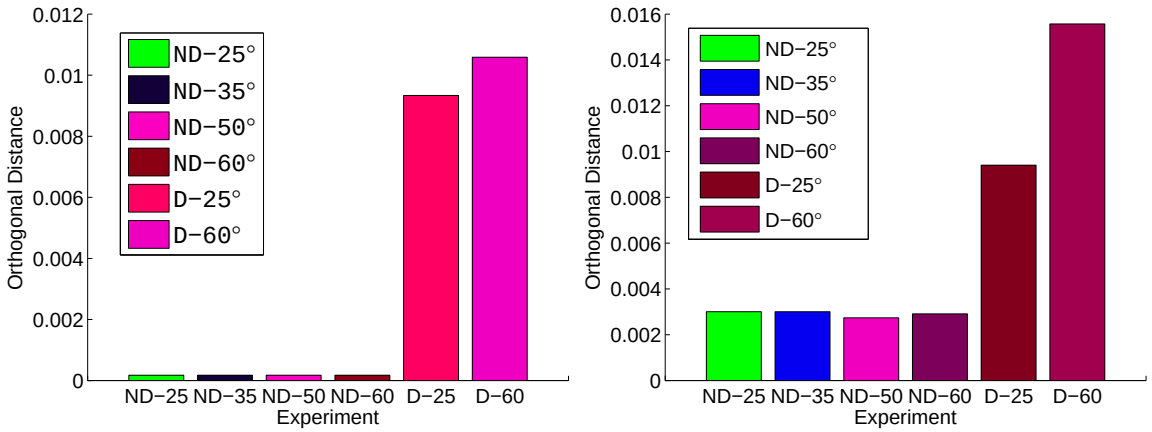

(a) Case study 1, route $1 \rightarrow 2$ **(b)** Case study 2, route $1 \rightarrow 4$

Figure 6.7.: Damage detection using temperature compensation

6.4. Temperature effect and compensation: PCAs

In this section, the effect of temperature on PCA scores is considered. The case study consist of a composite plate equipped with PZTs that is described in Section 4.4.3. It is used to analyze this effect and then the temperature compensation methodology is applied.

As a first step, data from intact structure in room temperature is considered as a principal baseline (X_H). To show the effect of temperature on PCA scores, data from healthy structure but in different temperatures are considered as unknown observation (X_c) and the PCA general damage detection strategy described in Section 5.1 is applied using different PCA including robust and classic counterparts. The data are approximately collected at $T1 = 30°C$, $T2 = 35°C$, $T3 = 40°C$, $T4 = 45°C$, $T5 = 50°C$, $T6 = 55°C$, $T7 = 60°C$. Then PC scores are pictured for those temperatures for all PCA variants. This is done for different routes and the result for route $1 \rightarrow 2$ is pictured in Figure 6.8. As figures clearly show, PC scores are significantly changing with temperature change. For instance, Figure 6.8-a,c,e show a decreasing trend on first PCA score and an increasing trend for the second PCA score when temperature is increasing for all types of PCAs. On the other side, Figure 6.8-a shows a decreasing trend for the third PC when applying classical PCA while it shows increasing trend when ROBPCA and RFPCA are applied. Although it seems that this behavior could be generalized for the changing behavior of PC scores, the behavior of PC scores on the other routes cancels this interpretation. For instance, first PC score calculated based on data from route $3 \rightarrow 4$ shows the contrary behavior as it decreases for classical PCA. (see Figure 6.9-a). Moreover, the second PC that increases for all PCA variants on the route $1 \rightarrow 2$, shows the contrary trend on route $3 \rightarrow 4$. It is important to mention that, as the types of sensors and the

distance are almost the same for all routes therefore this variable change could not be due to the sensor behavior. Finally, it is not possible to realize a specific trend for scores for PC scores but it is defiantly possible to conduct a significant change on scores when temperature is changing.

To investigate if the effect of temperature masks the effect of damage or not, PCA scores are pictured for the undamaged structure as well as the damaged structure (Dx). To do this, the data from route $3 \rightarrow 4$ are chosen. As it is described in Section 4.4.3, damage is simulated by placing an appropriate mass on this route. After applying PCA and plotting the scores for first-second PCs, it seems that the increasing temperature can have more significant effect on PCA scores. As Figure 6.10 shows, patterns from the healthy structure (ND) when temperature is more than $T1 = 30°\text{C}$ such as patterns $T1, T2, \ldots, T7$, clearly have more distance from healthy pattern (ND) comparing to the pattern belonging to the structure when damage is applied on the route $D2{-}T1$. The dashed-circle around ND demonstrates this reality better. This interpretation is valid for all PCAs as it can be seen in Figures 6.10-b and *c*. This shows that PC scores are not robust when temperature is changing.

To achieve a more quantitative comparison, Hausdorff distance is used to calculate the distance between patterns in different status such as ND in different temperature and $D2$. The definition of Hausdorff distance is described previously in Equation (5.1). This distance is calculated between all patterns ($ND - T1, ND - T2, \ldots, ND - T7$) belonging to the healthy structure in different temperatures and $D2 - T1$ belonging to the structure when $D2$ is applied in $T1$ temperature (plotted in red color) and the baseline (ND) in around room temperature. As seen in Figure (6.11), Hausdorff distance for patterns from structure in situation above room temperature is significantly more than this distance for pattern when the structure is affected by simulated damage. This confirms that the temperature effect can obviously mask the effect of damage that cause false positive decision. This phenomenon is repeated for all types of PCAs (ROBPCA, Croux, RFPCA) as it can be seen in Figure (6.11)-b,c,d respectively.

According to the result gained up to now, classical PCA and its variation are significantly affected by temperature that makes any damage detection based on PCA not reliable if there is a high possibility of ambient fluctuation. Therefore, it is vital to compensate temperature. To do this, Optimal Baseline Selection (OBS) is used which is described in section (3.13.1). Applying OBS leads to promising result as is depicted in Figure (6.12). According to the result, applying OBS alleviates the effect of temperature. As (6.12)-a shows, in 200KHz on route $3 \rightarrow 4$, the Hausdorff distance to healthy patterns (selected using OBS) for observation captured in pristine status is much less than the distance from damaged structure. This is valid for all PCA variants that shows OBS decrease the possibility of false positive decision. The same is valid for another frequency, for instance Figure (6.12)-b, confirms the same behavior for 350KHz on the same route.

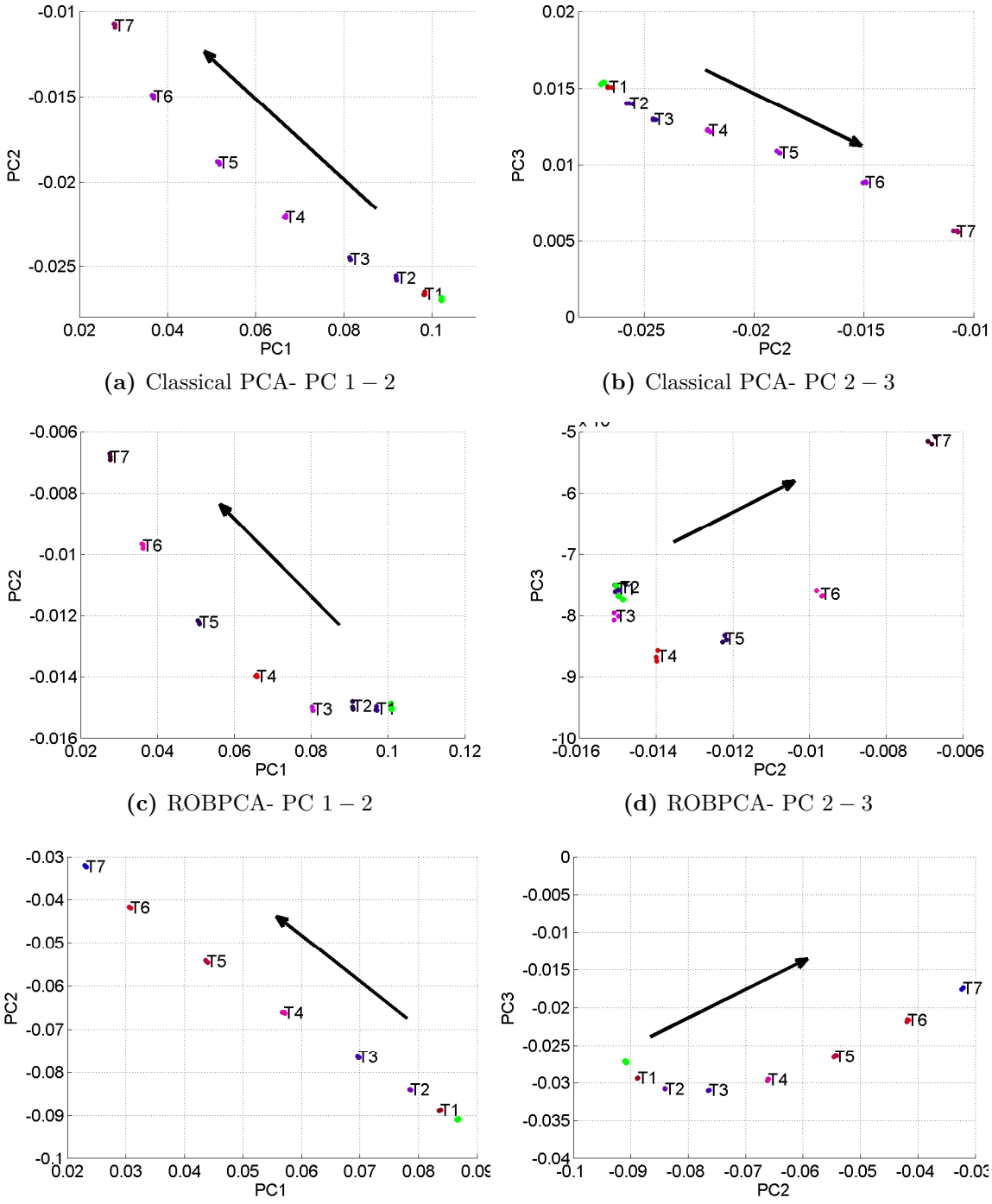

(a) Classical PCA- PC $1-2$ **(b)** Classical PCA- PC $2-3$

(c) ROBPCA- PC $1-2$ **(d)** ROBPCA- PC $2-3$

(e) FRPCA- PC $1-2$ **(f)** FRPCA- PC $2-3$

Figure 6.8.: Effect of temperature change on PCA variants on route $1 \rightarrow 2$

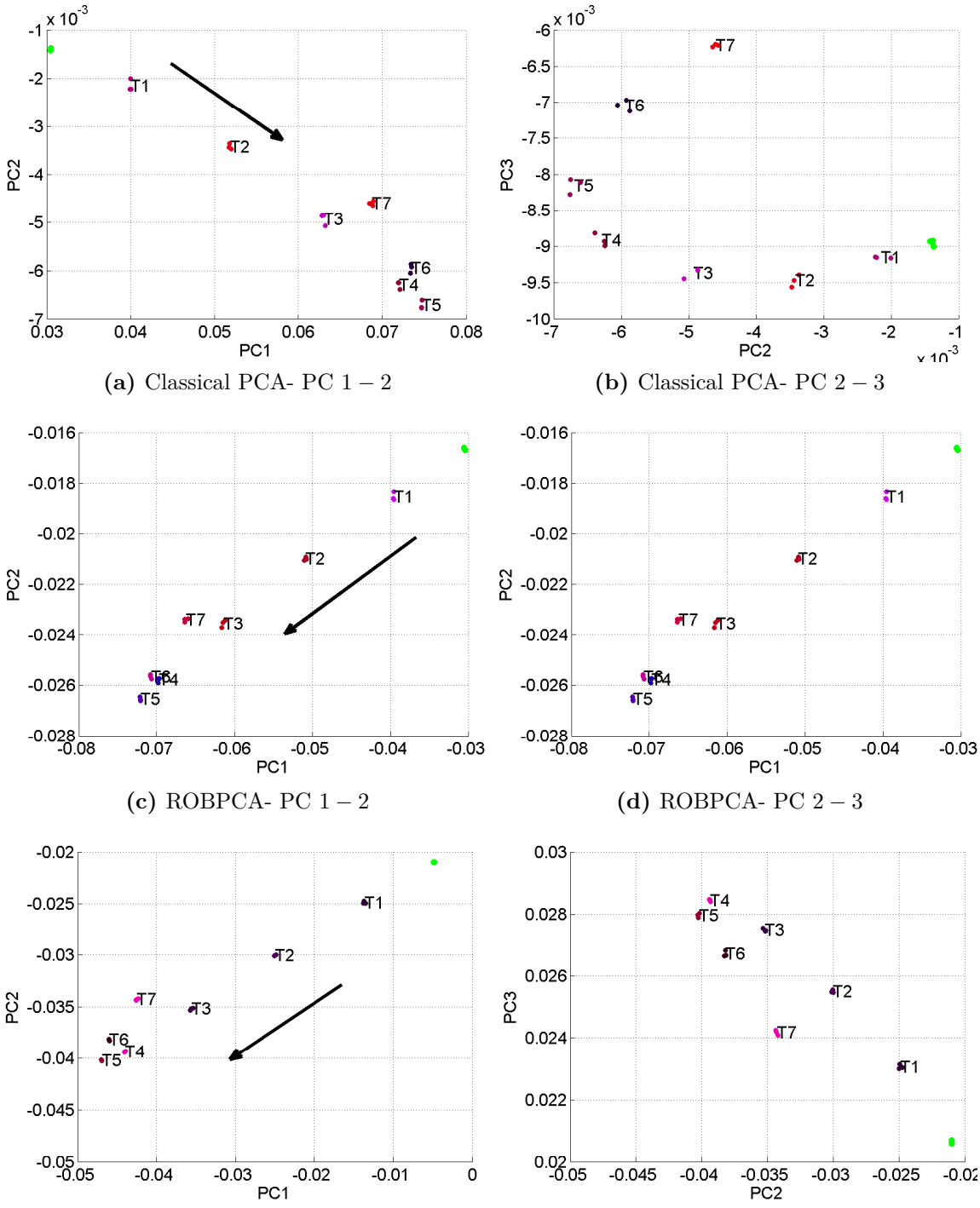

(a) Classical PCA- PC 1 – 2

(b) Classical PCA- PC 2 – 3

(c) ROBPCA- PC 1 – 2

(d) ROBPCA- PC 2 – 3

(e) NFRPCA- PC 1 – 2

(f) NFRPCA- PC 2 – 3

Figure 6.9.: Effect of temperature change on PCA variants on route 3 → 4

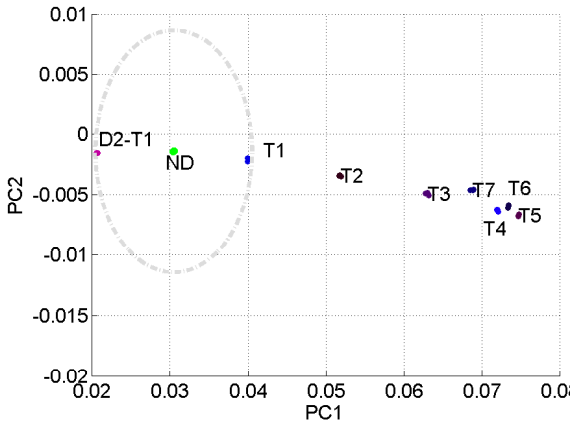

(a) Classical PCA- PC 1 – 2

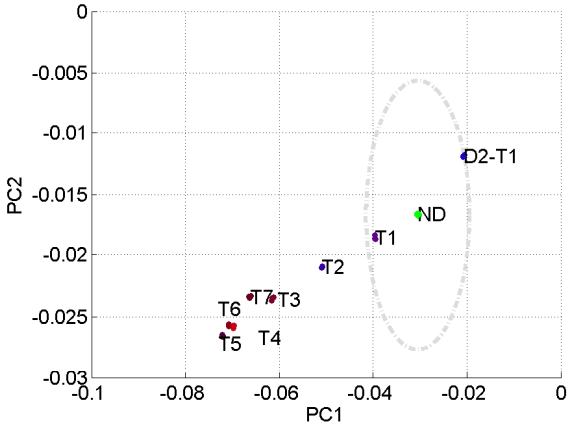

(b) ROBPCA PCA- PC 2 – 3

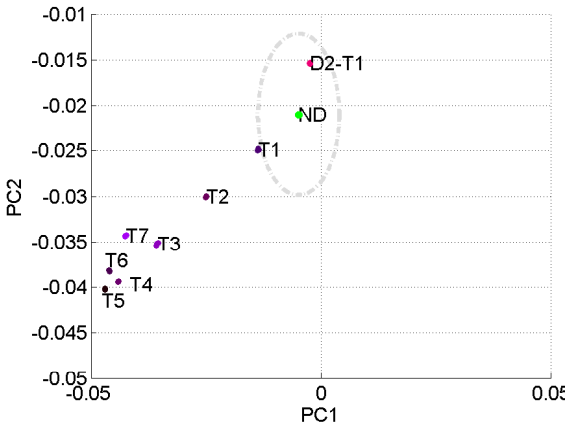

(c) RFPCA PCA- PC 2 – 3

Figure 6.10.: Comparing the effect of damage and temperature on PCA

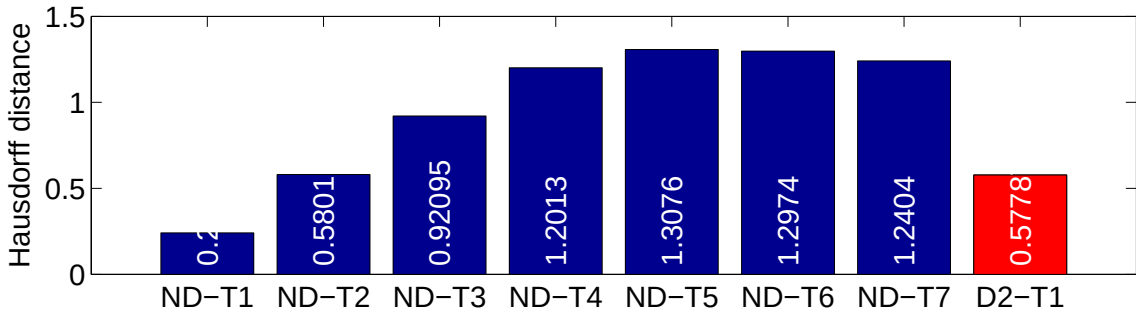

(a) Classical PCA

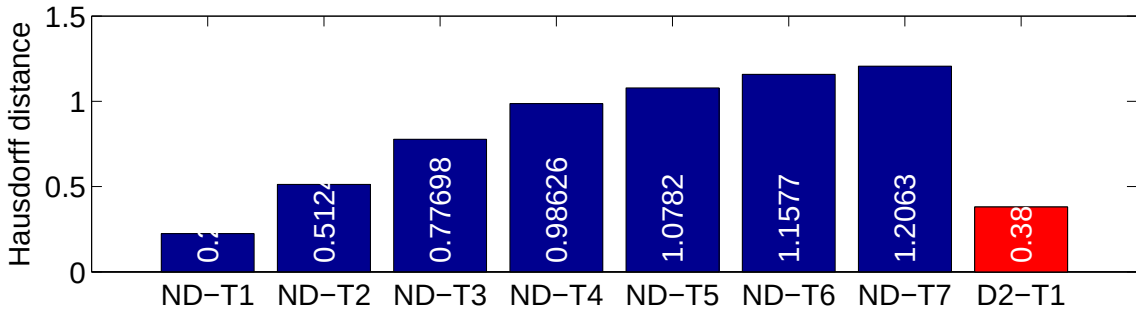

(b) ROBPCA

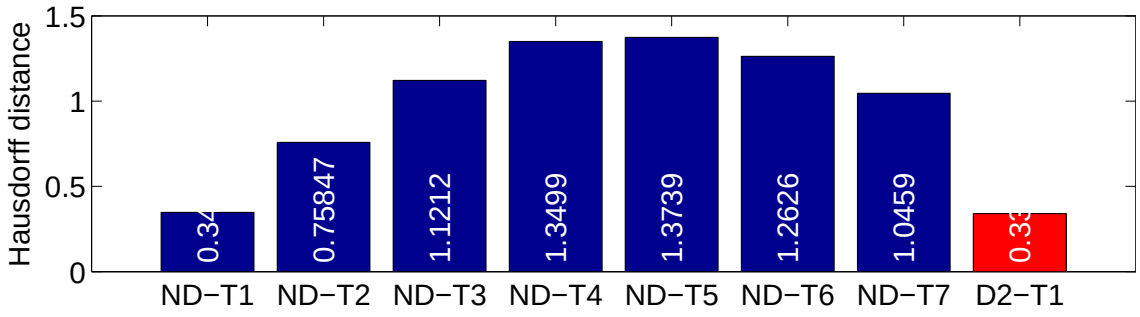

(c) Croux PCA

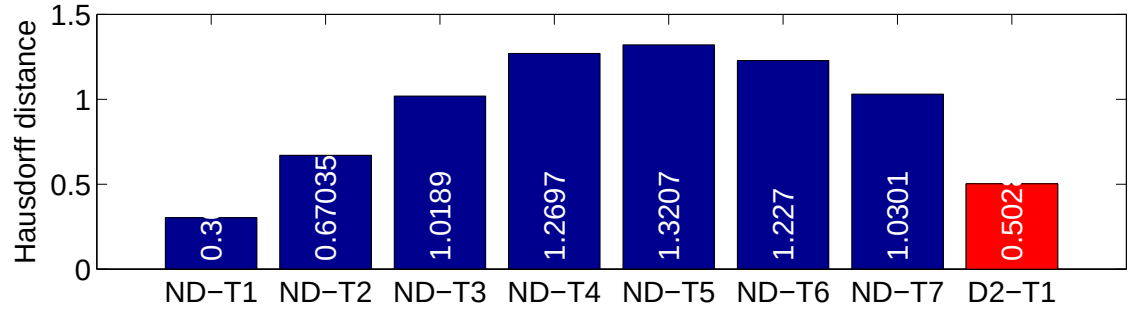

(d) RFPCA

Figure 6.11.: Hausdorff distance between different patterns and pattern from healthy structure in room temperature, all PCA variants, route $3 \rightarrow 4$, PC $1-2$, $350KHz$

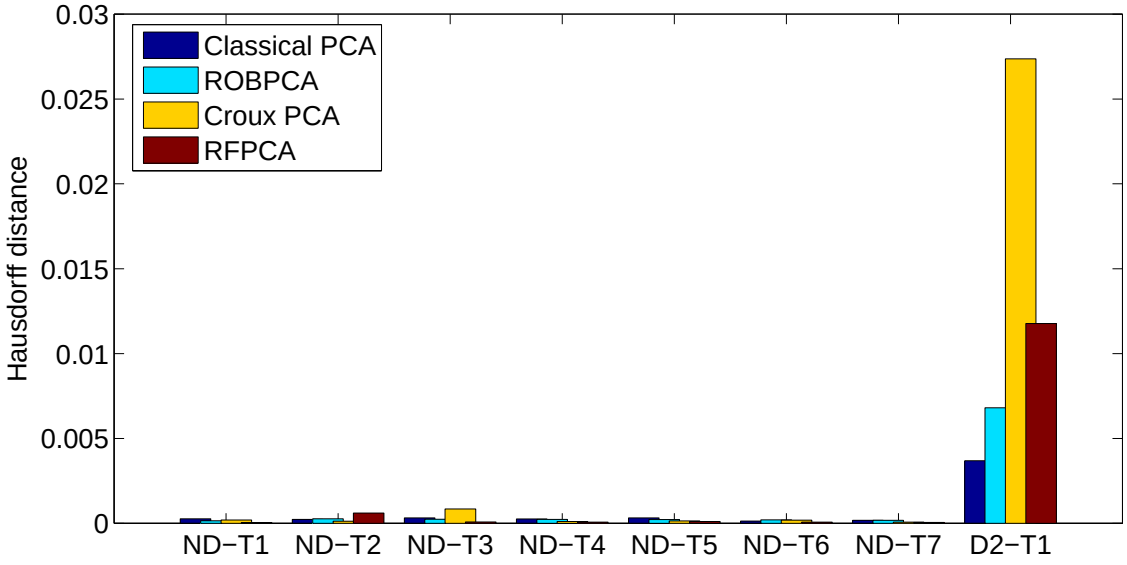

(a) 200KHz

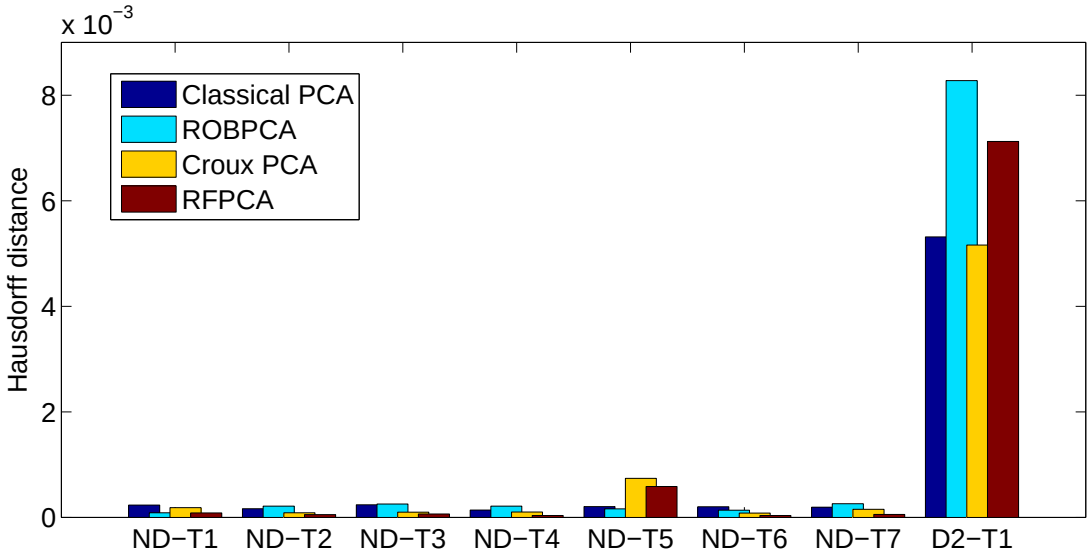

(b) 350KHz

Figure 6.12.: Temperature compensation PCA, Route 3 → 4,

6.5. Temperature effect and compensation: Andrew plots method

In Section 5.4.2, it is described how Andrew plot can be used as a damage detection technique to demonstrate indexes that have more than 3 dimensions. In this section, the effect of temperature change is demonstrated when Andrew plot is used based on different principal component variants. To perform the analysis, the composite plate equipped with PZT sensors that is described in section 4.4.3 is used. In this case study, the technique is performed on the data captured in 350KHz on the route $3 \rightarrow 4$. The first three PC scores are used to calculate the Andrew plots using Equation (3.50). As it was mentioned before, the data are approximately collected at $T1 = 30°C$, $T2 = 35°C$, $T3 = 40°C$, $T4 = 45°C$, $T5 = 50°C$, $T6 = 55°C$, $T7 = 60°C$. Figure 6.13 shows the result. As it can be seen from this figure, temperature clearly changes the result of the analysis. For instance, for Andrew plot calculated using PC scores of classical version, non-damaged status in different temperatures are even more separable from the Andrew plot when specimen is simulated with damage $D2$. The same phenomenon is seen when Andrew plot is applied using other PCA variants such as ROBPCA (Figure 6.13-b), Croux PCA (Figure 6.13-c) and RFPCA (Figure 6.13-d). In this figure $ND, D2$ stands for pristine structure and structure when $D2$ is applied around the room temperature respectively. To avoid overlapping of different patterns, just two temperatures are shown ($T7$ and $T4$).

To mitigate the effect of temperature, the temperature compensation technique (OBS) described in Section 3.13.1 is applied on Andrew plot. The promising results show that using temperature compensation may reduce the effect of temperature fluctuation as it can be seen in Figure 6.14. In this figure, Andrew plot index for healthy status of structure in two different temperatures (25°C and 60°C) are very close to each other whereas the Andrew plot index calculated when structure is subjected to $D2$ is clearly separated. This effect is valid for all results obtained from other PCA variants. In this analysis, the same case study is used with the same setting (route $3 \rightarrow 4$, first 3 PCs, 350KHz).

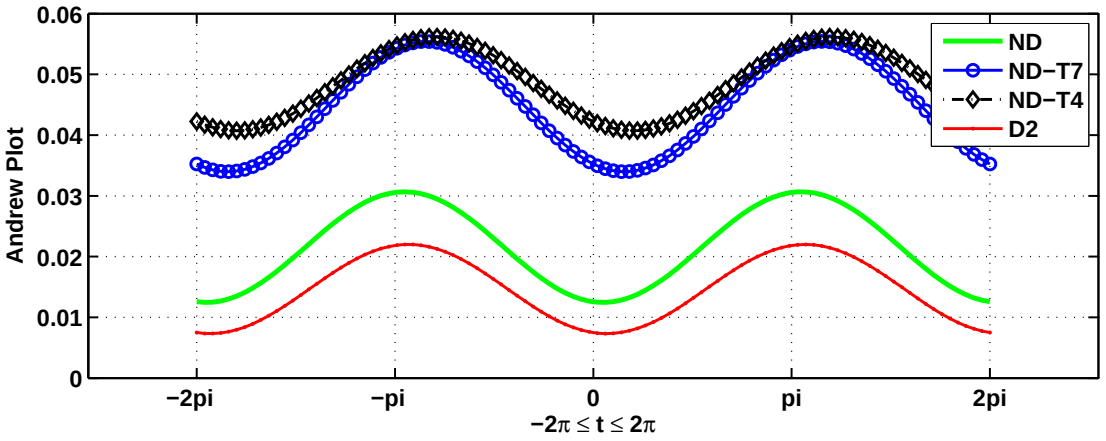

(a) Classical PCA

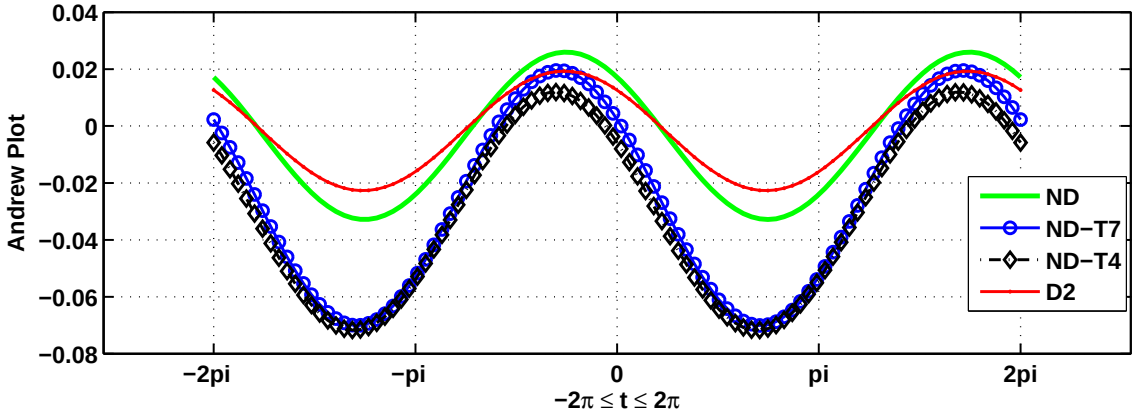

(b) ROBPCA

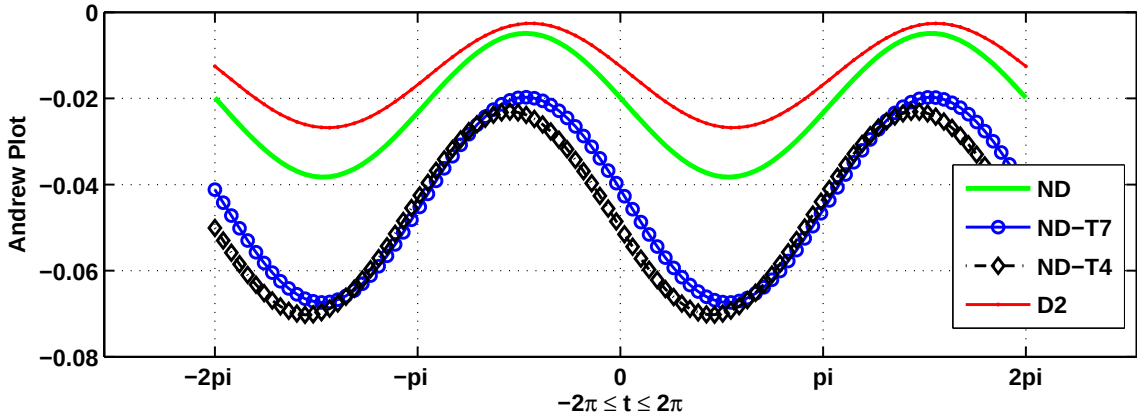

(c) Croux PCA

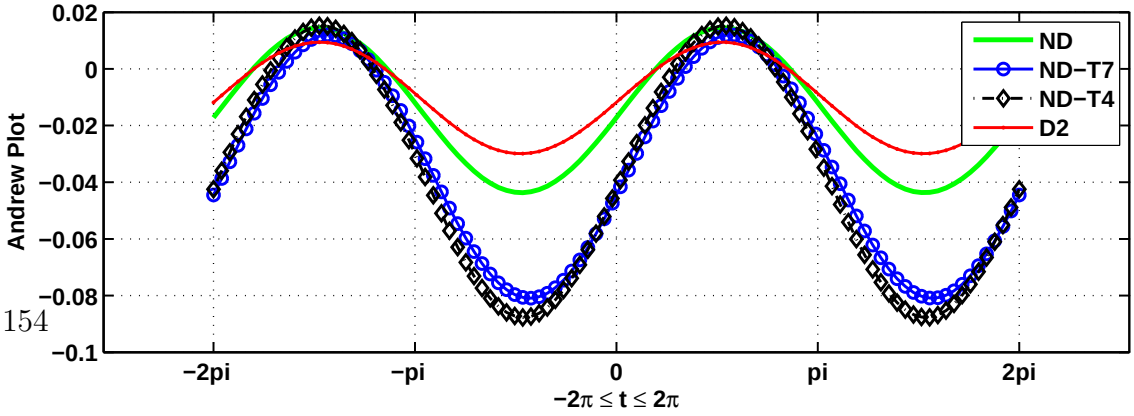

(d) RFPCA

Figure 6.13.: Temperature effect on Andrew plots technique calculated based on PCA variants

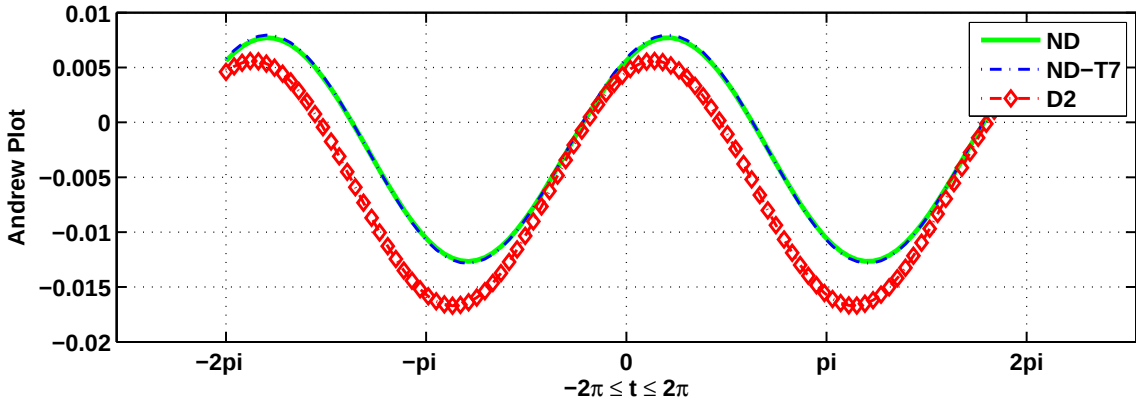

(a) Classical PCA

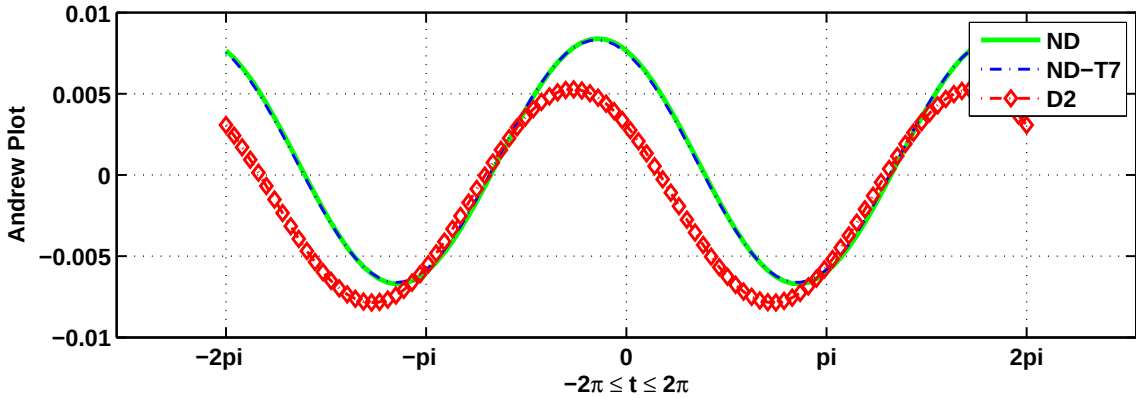

(b) ROBPCA

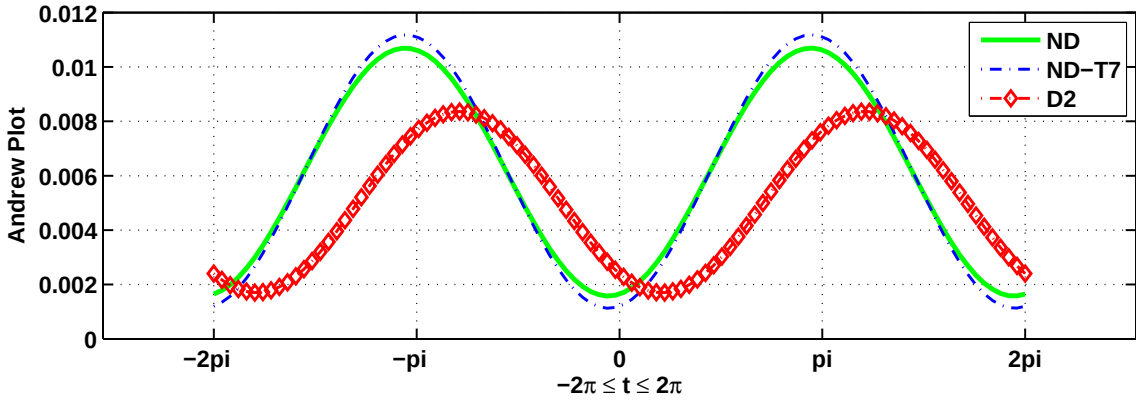

(c) Croux PCA

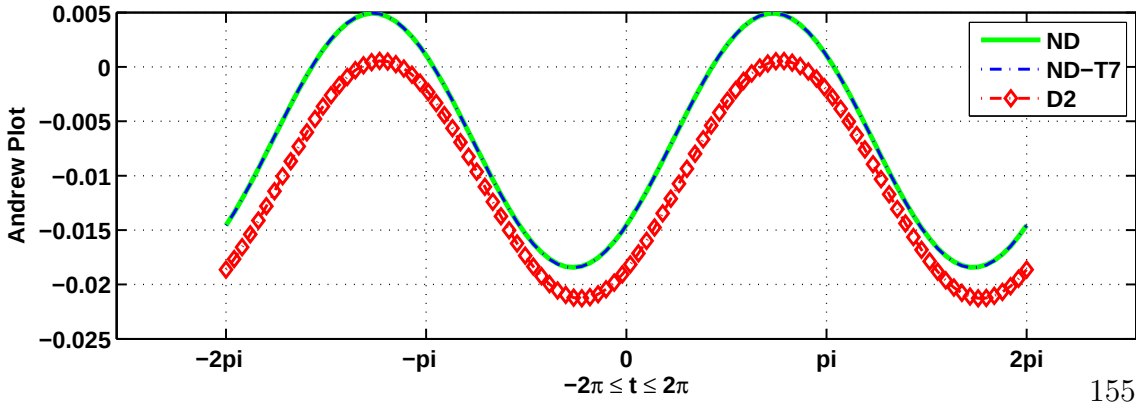

(d) RFPCA

Figure 6.14.: Temperature compensation for Andrew plots calculated based on PCA variants

6.6. Temperature effect and compensation: Similarity classifier method

In this section, the effect of temperature on similarity classifier method is considered. Basically, as this method is applied on the original data and it was previously showed that signal is affected by the temperature, therefore the same phenomenon is expected for this method. To check the claim above, the similarity classifier is applied on the composite plate equipped with PZTs mentioned in Section 4.4.3. The analysis is performed on 350KHz for the route 3 $\rightarrow$ 4 where the damage 2 is simulated. As it could be seen in Figure 6.15, temperature has a clear effect on the index but it does not mask the effect of damage. In other words, the damage is still distinguishable from the other status.

To achieve better analysis, data captured from the structure are analyzed for all temperatures when damage 2 is simulated for different frequencies. Figure 6.16 shows the result of this analysis. As it is depicted, the same result is achieved for other frequencies. For instance, for 400KHz the damage effect dominate the effect of temperature. The same result is achieved for 300KHz, 350KHz and 400KHz.

The same method is applied on the structure when damage 3 is simulated. As it is described in Section 4.4.3, this damage is located on route between the first and third transducer. The analysis is performed on different frequencies. The result is presented in Figure 6.17. The same outcome is obtained in this analysis as could be seen, the damage effect is still distinguishable from the temperature effect but not so clearly.

Although similarity classifier shows a better resistance against the temperature effect, at least in this case study, it is still favorable to apply temperature compen-

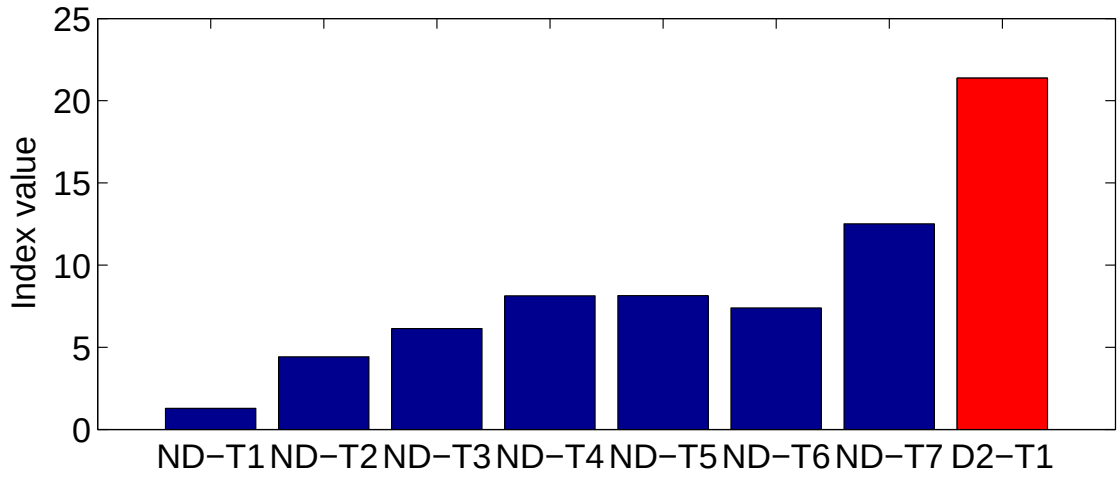

(a) case study in 4.4.3, route 3 $\rightarrow$ 4, $350KHz$

Figure 6.15.: Temperature effect on similarity classifier

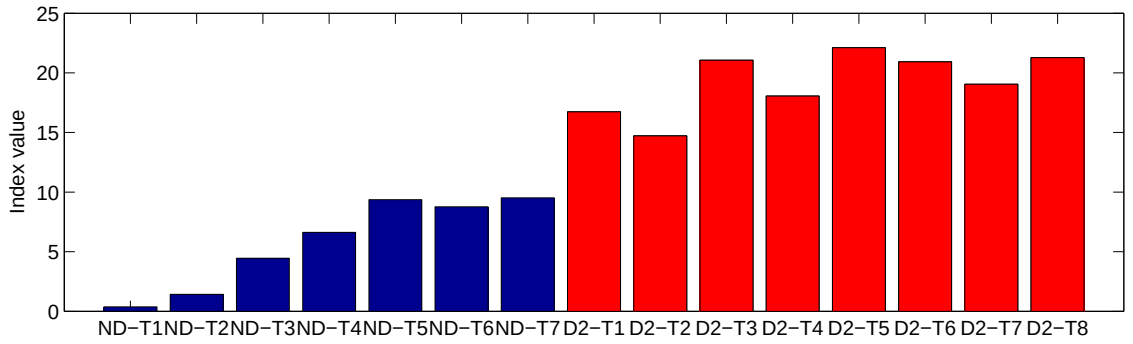

(a) $300KHz$

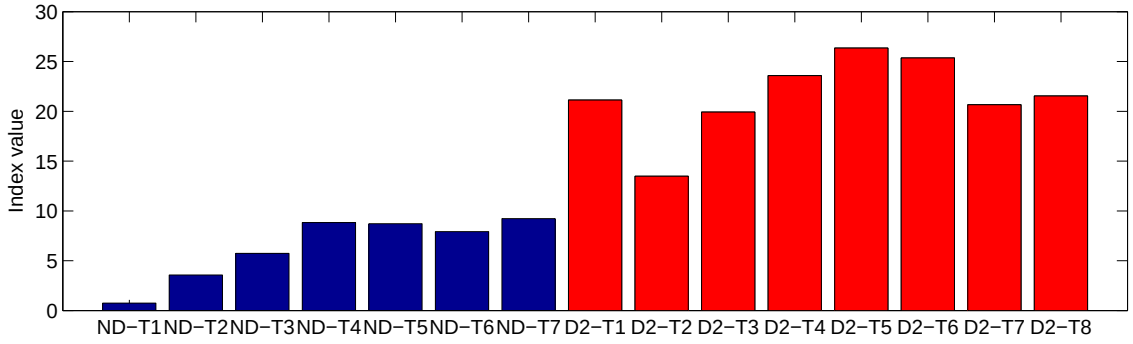

(b) $350KHz$

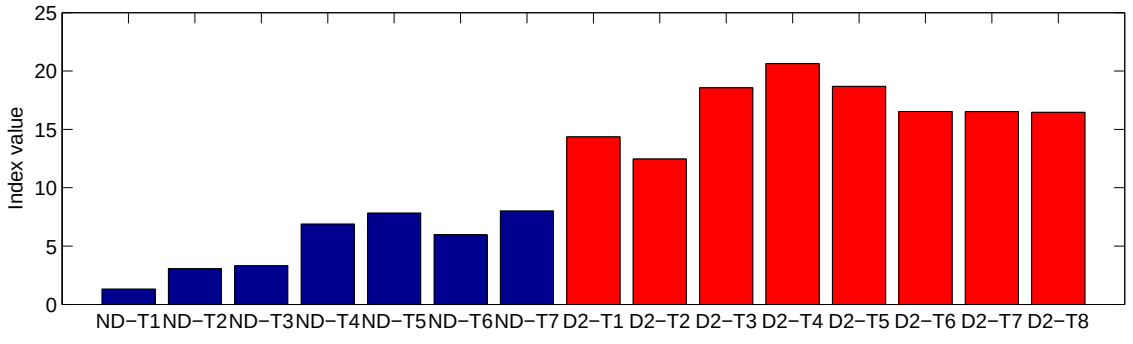

(c) $400KHz$

Figure 6.16.: Temperature effect on similarity classifier, route $3 \rightarrow 4$, with $D2$, different frequencies

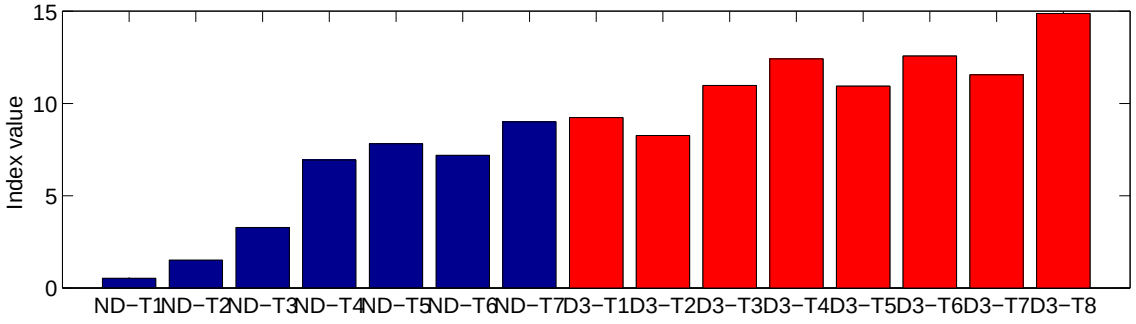

(a) $300KHz$

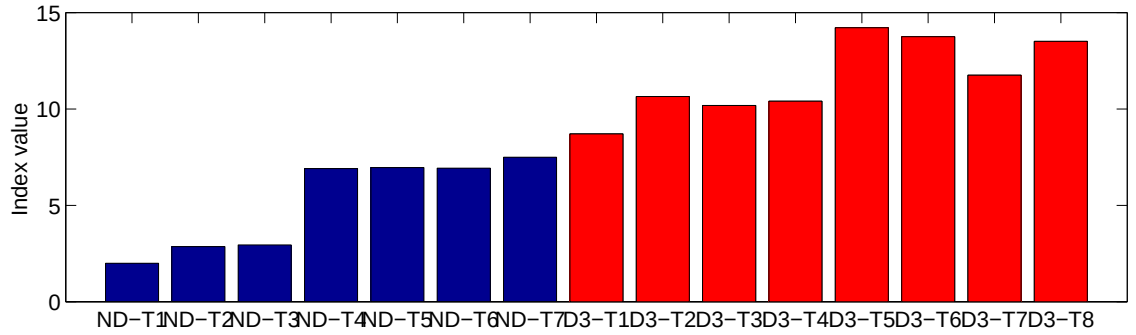

(b) $350KHz$

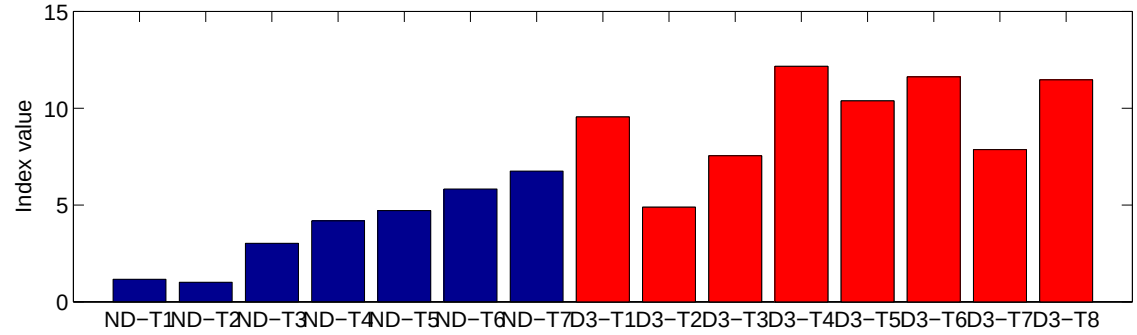

(c) $400KHz$

Figure 6.17.: Temperature effect on similarity classifier, route $1 \rightarrow 3$, with $D3$, different frequencies

sation on the methodology. The result of applying OBS technique is demonstrated for different frequencies (300KHz, 350KHz and 400KHz) in Figure 6.18. This figure shows the analysis applied on the same case study (see Section 4.4.3) on the route $3 \rightarrow 4$. As it can be seen from the figure, applying OBS leads to relieve the effect of temperature and makes the damage effect more separable.

The same analysis is applied on route $1 \rightarrow 3$ where damage 3 is applied. Results are shown in Figure 6.19. The same description is valid for this result.

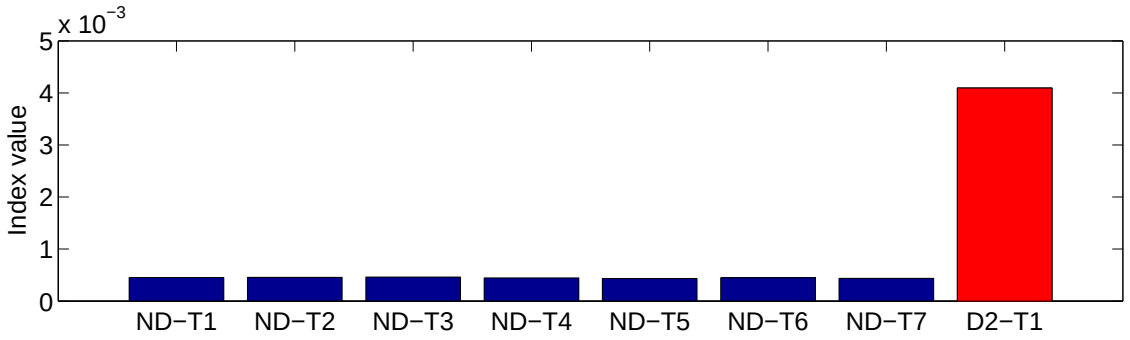

(a) $300KHz$

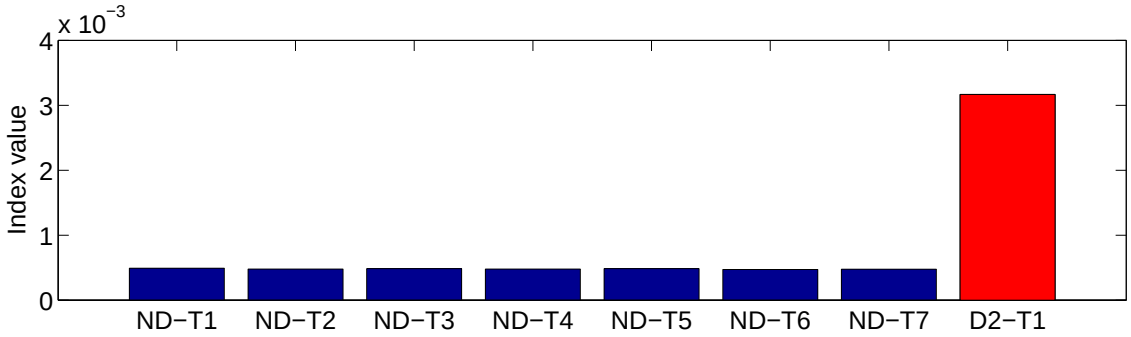

(b) $350KHz$

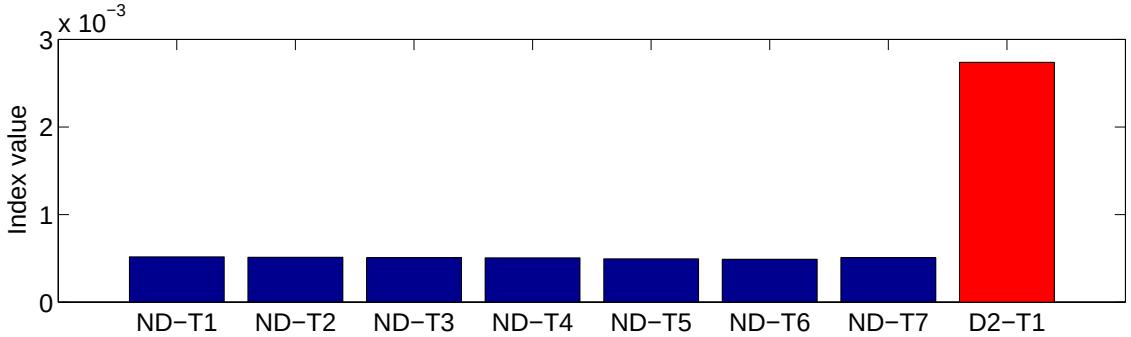

(c) $400KHz$

Figure 6.18.: Temperature compensation: similarity classifier, route $3 \rightarrow 4$, with $D2$, different frequencies

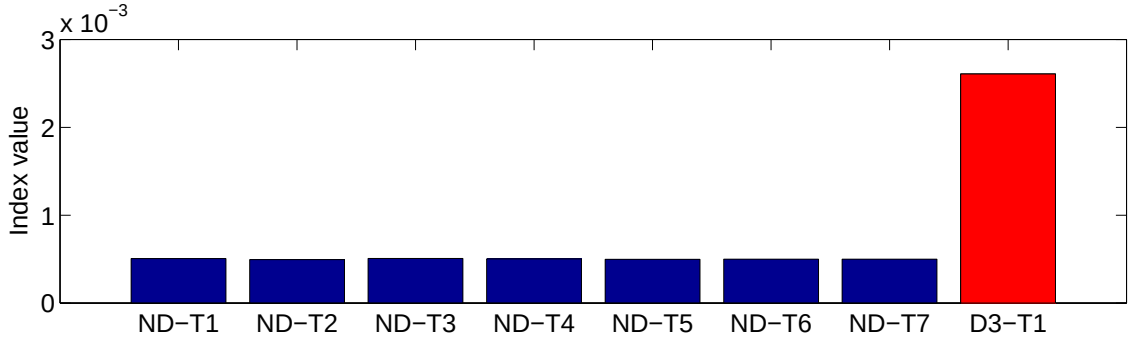

(a) $300KHz$

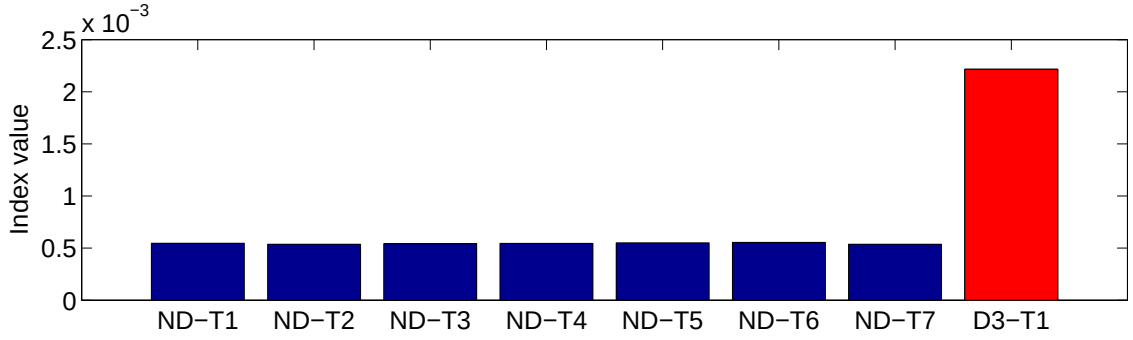

(b) $350KHz$

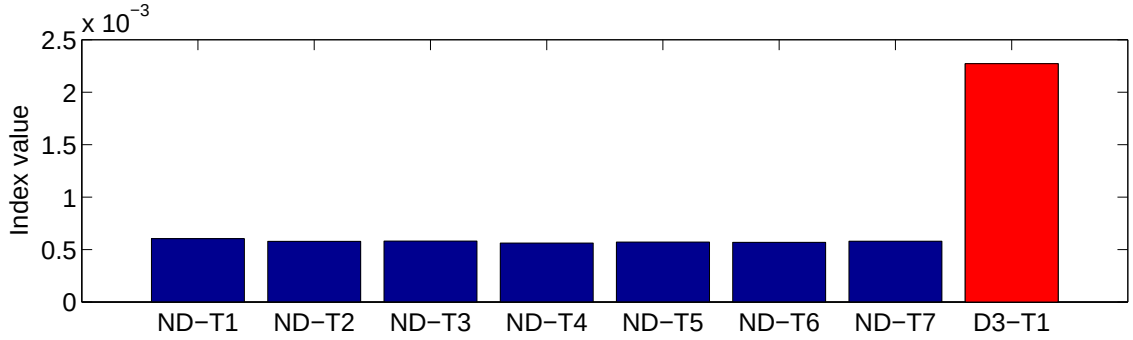

(c) $400KHz$

Figure 6.19.: Temperature compensation: similarity classifier, route $1 \rightarrow 3$, with $D3$, different frequencies

6.7. Temperature effect and compensation: Wavelet ridge

In this section, temperature effect is considered on wavelet ridge. Wavelet ridge background is described in Section 3.10 and its application on damage detection is described in Section 5.5. As it is presented in Section 5.5, applying PCA on wavelet ridge has benefit over applying directly on original signal. In this part, the stability of wavelet ridge is tested when temperature is fluctuated. To do this, case study described in Section 4.4.2 is chosen to perform the analysis.

As the first part of the analysis, the effect of temperature fluctuation on wavelet ridge is demonstrated. This is done in two different trends. First, when temperature is increasing from room temperature 25°C to 60°C, and in the second step, the effect is considered when temperature is decreased from 25°C to −20°C. Figures 6.20-a and 6.20-b show this effect respectively for the pristine structure (ND). As it can be seen from the results, for the first trend a slight decrease in amplitude of wavelet coefficients and a delay is clear when temperature is increasing, while the opposite trend is obvious when temperature is reducing. It should be mentioned that this result is equal to the temperature effect on captured signal in time domain.

In the second step, similarity classifier is applied on wavelet ridge and the effect of temperature fluctuation is considered. As Figure 6.21-a shows, the index value when it is applied on wavelet ridge is increasing when the temperature is increasing from 25°C to 60°C, and then decreasing when the temperature returns to the room

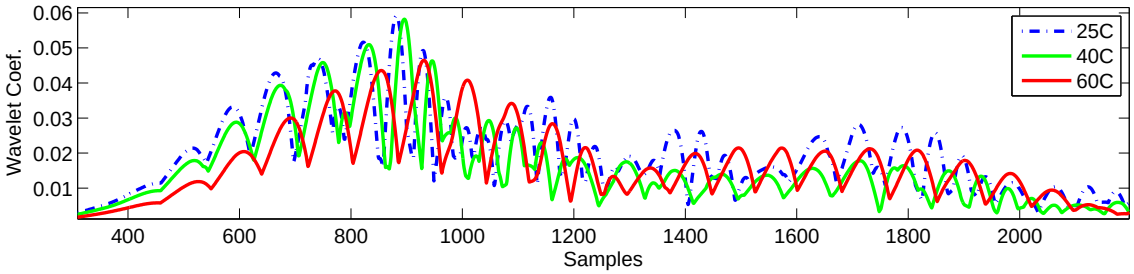

(a) 25°C to 60°C

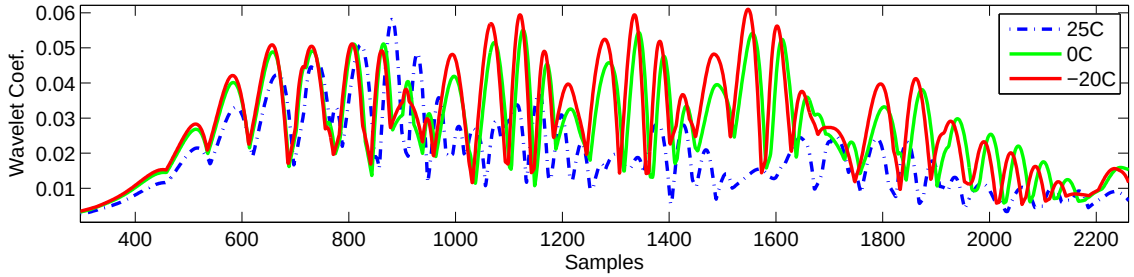

(b) 25°C to −20°C

Figure 6.20.: Temperature effect on Wavelet Ridge, pristine structure, route 1 → 2

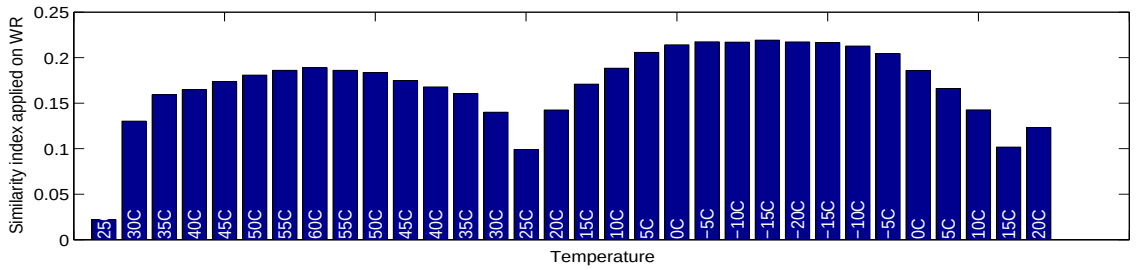

(a) Result of similarity classifier applied on Wavelet ridge when temperature is changing, route $1 \rightarrow 2$, $350KHz$

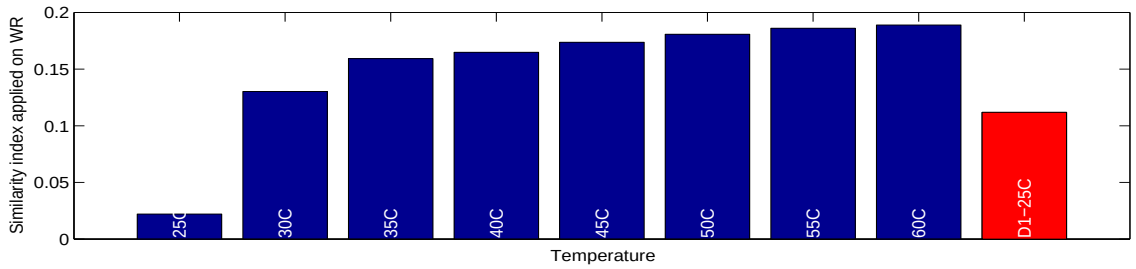

(b) Temperature may mask the effect of simulated damage, route $1 \rightarrow 2$, $350KHz$

Figure 6.21.: Temperature effect on Wavelet Ridge when similarity classifier is applied

temperature. The same trend can be seen when temperature is decreasing from room temperature to $-20°C$ and returns to the room temperature. Moreover, Figure 6.21-b, shows that the temperature masks the effect of damage as the index value for healthy status of the structure is greater than when damage is simulated (depicted in red color) in the structure. This analysis is performed on data captured on $350KHz$ from route $1 \rightarrow 2$ where damage 1 is simulated.

To compensate the effects of temperature, OBS (see Section 3.13.1) is applied. According to the result depicted in Figure 6.22, temperature effect is relieved when temperature compensation is applied. Mentioned figure shows that, when OBS is applied, damage is easy distinguishable from other healthy status of structure even when there is a huge fluctuation on the temperature.

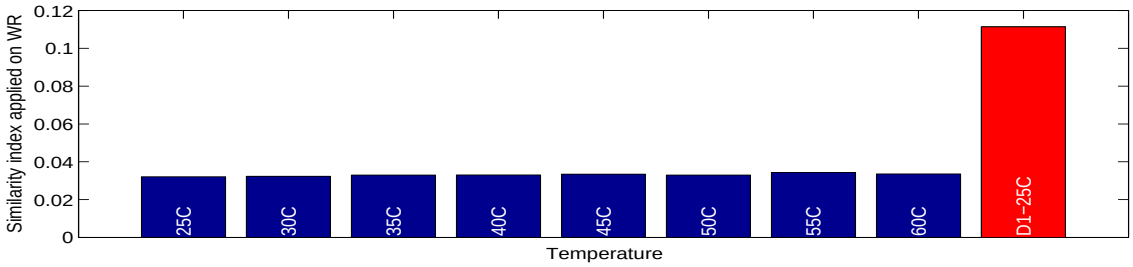

Figure 6.22.: Temperature compensation applied on Wavelet Ridge and similarity classifier

7. CONCLUSION AND FUTURE WORK

This thesis is dedicated to the development of new techniques for structural health monitoring. This development is focused on presenting novel methodologies for damage detection in different types of structures. Different signal processing and pattern recognition methods are used to achieve this goal. These techniques applied on following structure such as aluminum and composite plates, fuselage, commercial aircraft wing, tube, etc. Moreover, the effect of temperature change on presented methods is analyzed. It has been shown in this work that temperature has an adverse effect on presented techniques, therefore it is necessary to implement an appropriate temperature compensation method to assure that the presented techniques are reliable even when temperature is changing. From the application of these methods, several advantages are obtained as shown by the results throughout this manuscript. In this section, a brief conclusion on the described methods is presented and after that, some future work is suggested for further investigation.

7.1. Instrumentation and data acquisition

PZT transducers are used in all case studies that are performed in this work. Different types of PZTs are used in this work. Results show that PZTs are a wise choice to be a part of data acquisition system because of few benefits that they have, for instance:

1. Reasonable price
2. The necessary data acquisition system that is necessary to work with PZTs are cheaper comparing with other transducers such as fiber optics
3. They are relatively easy to be implemented in the structure
4. They can be used as both sensor and actuator without any change

In addition to the PZTs them self, the adhesive that is used to attach them to the structure plays an important role. As a first impact of adhesive, they could cause change in captured signal when temperature changes. Therefore, it is necessary to use an adequate adhesive that is robust in the temperature range that the specimen is subjected to.

7.2. Data pre-processing and organizing

As it is mentioned, data pre-processing is an important step before applying any damage detection techniques. For instance, averaging may help to remove the ambient noise when data are recorded. In addition, denoising could be applied mathematically using DWT or by applying appropriate filter during data recording. In addition, since data from different sensors have different magnitudes and scales, normalizing data is an vital step that should be performed.

In addition, it has been shown in this work that the presented methods that are able to work on data that are organized based on a specific route or based on actuator. Different studies presented in this work confirms this claim.

Moreover, in this work a novel data pre-processing technique is presented that is based on Wavelet ridge. This technique suggests that, wavelet ridge can be used instead of the original data captured from the structure. To test this technique, it is combined with PCA. This new look attempts to jointly benefit from the advantages of both methodologies in damage detection. It is shown that the new combination is able to provide a more accurate and reliable damage detection strategy. Experimental results show that in a variety of structures with different complexity, using both approaches together is recommended. Although this combination implies more computational costs, it may avoid failure of damage detection such as false negative. Indeed, it is shown that in not complicated structures such as aluminum beam, the new combination can improve the results in terms of more separated patterns of different status. Such a result was obtained from the first experiment. Besides, using the new combination avoid wrong recognition of patterns where using PCA alone lead to not clear separation of patterns dedicated to damaged status from the healthy status as it was described in the last two experiments.

7.3. Damage detection

Damage detection is probably the most important step in structural health monitoring field. In this work, different new techniques are presented that achieve this goal. The efficiency of these techniques are tested on various structures with different complexity.

This thesis shows that PCA as one of widely used technique in SHM, could be impotent if there is a probability of outlier existence in the captured data. It is mentioned that this could happen due to different reasons such as experimental or human errors. Therefore, this issue is necessary to be considered. To achieve this, the idea of using robust principal component analysis is introduced as a comprehensive alternative for its classical version as a reliable method to deal with outliers and contaminated data. It is a fact that outliers are widely existent in experimental

data due to different reasons; therefore using robust PCA can avoid many false-positive detection. Among different types of robust PCAs, three most important methods are used in this work. Results show that robust PCA is able to compress data more than its classical counterpart, which leads to carrying more information in primary principal components. This benefit supports any damage identification method based on Principal Component to have more accurate result. As it has been shown, robust PCA can detect and classify different damages in some cases where classical method is not capable of that. Beside mentioned benefits, robust method shows slower behavior rather than the classical one, which should be considered in online algorithms. It can be clearly seen from the results that in some studies, classical PCA can not distinguish the pattern belonging to the healthy status of the structure from other patterns. In other words, classical PCA is not able to detect damages whereas robust PCAs are. It should be also mentioned that, among different robust PCAs studied in this thesis, the ROBPCA algorithm shows the better results as not only the pattern from healthy structure is clearly separable from the other but also all patterns are clearly separated. This separation is particularly relevant since it leads to damage classification.

Another issue that exists in damage detection is to present graphical representation of multivariate data. This thesis shows that, Andrew plots, as graphical representation of multivariate data, could be used as an index to identify any probable damage in the structure when 2 or 3 dimensional data are not sufficient to depict the behavior and feature of the data. This problem also happens for other exploratory data analysis. Therefore, in the initial stages of analysis, graphic displays can be used to explore the data, but for multivariate data, traditional histograms or two or three-dimensional scatter plots may miss complex relationships that exist in the data set. Moreover, it is shown that as the order of coefficients of terms is very important in Andrew plot equation, these coefficients should be rearranged depending on their importance. This thesis shows that PCA or its robust counterparts can be used in this manner for both ordering and reducing the dimensionality. Obtained curves clearly separates observation from different groups. Therefore, using depicted figures, any damage can be separated from healthy observation in which not only detect the damage but also clarify the type of damage. Results from the experiments confirm this idea where two different simulated damages are detected and classified.

Another technique that is presented in this thesis is based on Fuzzy classifier. It is shown that using the Fuzzy similarity classifier, the similarity between structure's main features in healthy condition is compared with their counterparts captured from unknown status of the structure. Feature selection and dimension reduction is performed thanks to PCA. The combination of these two algorithms leads to an accurate methodology for damage detection. The proposed index is evaluated using data captured from a skin panel of the torsion box of the wing. Moreover, it is shown than the proposed methodology for damage detection can clearly discriminate between healthy states and the existence of damage in real scale structures where traditional damage detection method based on PCA is not able to do by itself. Be-

sides, the new damage index is compared with the classical Euclidean damage index and the competency of the new index is proved. Results show that the Euclidean distance is not able to obtain appropriate result in all frequencies. In addition, the optimal value for p parameter is evaluated and is has been demonstrated that, according to the ROC curves increasing the value of p causes decreasing the sensitivity of the index.

Wave Cluster is a technique that is presented in this work for automatic damage classification. It is shown in this work that although some techniques such as PCA or its robust counterpart show a successful role in damage detection, they still need a complimentary step for automatic damage classification. It means that a human effort still is required to classify different available clusters. Wave cluster is an alternative technique for other methods such as self-organizing map (SOM). Wave cluster is based on wavelet is proposed that posses several merits.

In this thesis, the ability of using orthogonal distance (OD) of observations from robust PCA subspace as a damage feature is shown. It is presented that the new feature is capable of distinguishing the observation from damaged structure from the healthy status. To achieve this, we present a damage detection strategy based on OD. Moreover, the probability distribution function of OD is estimated and it is shown that extreme value distribution could be an acceptable choice.

7.4. Temperature effect and compensation

Temperature fluctuation has adverse effect on wave propagation and therefore, any damage detection methodology can be affected by temperature change. In this thesis, the effect of temperature fluctuation is studied on different aspects of wave propagation. Moreover, the stability and the performance of all presented damage detection techniques are studies when there is a significant change in ambient temperature. According to the result obtained, in almost all of the presented methods, temperature has a significant adverse affect that can not be neglected. Therefore, a simple baseline can not be used to provide with efficient damage detection technique. To mitigate the effect of temperature, different techniques are reviewed in this work and finally, optimal baseline selection (OBS) is used as a reliable technique to remove the adverse effect of temperature. This technique is applied on all the presented damage detection method and result show that applying OBS assure that the presented damage detection techniques can achieve more reliable result even when there is a possibility of temperature change.

7.5. Proposed future research

SHM is a relatively new field that many issues still remain open. Hereby some major fields that can be studied as future works for this thesis are presented here.

It is mentioned in the case studies performed in this thesis that due to the limitation for seeding real damages to the structure, the majority of damages are simulated by adding mass on the surface of the specimen. Although added mass can approximately simulate the effect of real damages on wave propagation such as leaking the propagation energy, they still can not be an ideal representative of the real damages. Therefore, future investigation using real damages could be interesting.

Moreover, it is necessary to investigate on the efficiency of presented methods to detect and classify different types of damages such as cracks, corrosion, fiber mission, etc.

It is mentioned that temperature fluctuation is an important issue that needs to be considered but it is not the only one. Other ambient alternation could affect the investigation. Therefore, another interesting would be to analyze the effect of other environmental changes such as humidity, dust, etc. Although, some experiments are performed during this study (result are not presented in this thesis), analyzing other environmental changes are in great demand.

The selection of case studies for a specific damage detection in this work is based on the availability of data from the experiment during the mathematically and computationally development of the technique. Therefore, it also could be interesting to run a comprehensive study to test all detection technique on all the case studies that are presented here. Generally speaking, in SHM field there is not a unique method that can cover all the investigation area, but testing a method on different case studies can increase the reliability of the mentioned method to be implemented in a real industrial specimen.

In this work, temperature compensation is successfully performed when the obtained data belonging to the unknown status of the structure is considered to be in the temperature range that the bank of baseline is recorded. Therefore, it could be useful to test a new observation that does not belong to the temperature range of the the baseline bank.

During this study, transducers are distributed through the structure based on a basic and simple scheme. To improve the efficiency and performance of the methods, it could be useful to apply some optimization on sensor distribution. This is vital as in real structure the number and the position of senors play a vital role as increasing the number of sensors cause a tangible increase in total mass of a structures such as an airplane.

Although some complex structures such as fuselage, skin panel, etc. are tested in this study and the performance of the damage detection on these structure is analyzed, still there is a need to validate the proposed methodologies in more complex studies such as bridge.

The last but not the least is about the energy consumption of the whole system as data acquisition and signal processing. The good point about the PZT transducers is that they could be used as a convertor to harvest the ambient energy for further

use. In another words, investigation on energy harvesting on a such a system is an open and promising field that could bring many benefits to a online system for those kind of usage that the energy consumption is a vital issue.

A. Publications

Status of the publications mentioned below are updated until April 2014.

Book chapters

1. Gharibnezhad, Fahit, Luis Eduardo Mujica, and José Rodellar. 2011. "Damage Detection Using Robust Principle Component Analysis." In Advances in Dynamics, Control, Monitoring and Applications, 8–17. Universitat Politecnica de Catalunya.
2. Gharibnezhad, Fahit, Luis Eduardo Mujica, and José Rodellar. 2014. "Features for Damage Detection and Temperature Stability." In Emerging Design Solutions in Structural Health Monitoring Systems, [Accepted]. IGI Global.

Journal papers

1. Gharibnezhad, Fahit, Luis Eduardo Mujica, José Rodellar, and Claus Fritzen Peter. 2013. "Damage Detection Using Principal Component Analysis Based on Wavelet Ridges." Key Engineering Materials 569 - 570: 916–923.
2. Gharibnezhad, Fahit, Luis Eduardo Mujica, and Jose Rodellar. 2011. "Comparison of Two Robust PCA Methods for Damage Detection in Presence of Outliers." Journal of Physics: Conference Series 305 (1): 12009.
3. Gharibnezhad, Fahit, Luis Eduardo Mujica, and José Rodellar. "Applying Robust Variant of Principal Component Analysis as a Damage Detector in Presence of Outliers." Mechanical Systems and Signal Processing. [Accepted]
4. Gharibnezhad, Fahit, Luis Eduardo Mujica, José Rodellar, and Alfredo Guemes. "Introducing a New Index for Damage Detection Based on Lukasiewicz-Structure." Structural Control and Health Monitoring. [Submitted]
5. Gharibnezhad, Fahit, Luis Eduardo Mujica, José Rodellar, and Michael Todd. "Considering Temperature Effect on Robust PCA Orthogonal Distanceas a Damage Detector." Structural Control and Health Monitoring. [Submitted]

Conference papers

1. Gharibnezhad, Fahit, Luis Eduardo Mujica, José Rodellar, and Michael Todd. 2014. “Fuzzy Similarity Classifier as Damage Index: Temperature Effect and Compensation.” In 7th European Workshop on Structural Health Monitoring. Nantes, France.
2. Gharibnezhad, Fahit, Luis Eduardo Mujica, José Rodellar, and Michael Todd. 2014. “Wavelet Ridge as Damage Index: Temperature Effect and Compensation.” In 6WCSCM. Barcelona, Spain.
3. Gharibnezhad, Fahit, Luis E Mujica, José Rodellar, and Claus-Peter Fritzen. 2013. “Automatic Damage Classification Using Wavelet Dlassifier Based on Principal Component Analysis.” In The 9th International Workshop on Structural Health Monitoring. Stanford University, Stanford, CA.
4. Gharibnezhad, Fahit, Luis Eduardo Mujica, José Rodellar, and Claus Peter Fritzen. 2013. “Damage Detection Using Robust Fuzzy Principal Component Analysis.” In 6th European Workshop on Structural Health Monitoring, 1–6. Dresden, Germany.
5. Gharibnezhad, Fahit, Luis Eduardo Mujica, and José Rodellar. 2011. “Damage Detection in the Presence of Outliers Based on Robust PCA.” In 8th International Conference on Structural Dynamics. Leuven, Belgium.
6. Gharibnezhad, Fahit, Luis Eduardo Mujica, and José Rodellar. 2011. “Damage Detection Using Andrew Plots.” In 8th International Workshop on Structural Health Monitoring. Stanford University, Stanford, CA.

Bibliography

[1] B. Glisic and D. Inaudi. *Fibre optic methods for structural health monitoring*. Wiley-Interscience, 2007.

[2] S. Gopalakrishnan and M. Ruzzene. *Computational Techniques for Structural Health Monitoring*. Springer, 2011.

[3] Z. Su and L. Ye. *Identification of Damage Using Lamb Waves: From Fundamentals to Applications*. Springer-Verlag Berlin Heidelberg 2009, 48 edition, 2009.

[4] G. S. Campbell and R. Lahey. A survey of serious aircraft accidents involving fatigue fracture. *International Journal of Fatigue*, 6(1):25–30, 1984.

[5] List of accidents and incidents involving commercial aircraft (Wikipedia).

[6] http://en.wikipedia.org/wiki/Bridge_collapse.

[7] http://diversitytomorrow.com/thread/384/0/.

[8] S. Anton. *Baseline-Free and Self-Powered Structural Health Monitoring*. Master thesis, Virginia Polytechnic Institute and State University, 2008.

[9] E. Cross. *On Structural Health Monitoring in Changing Environmental and Operational Conditions*. PhD thesis, The University of Sheffield, 2012.

[10] F. Lili. *Structural health monitoring based on principal components analysis implemented on a distributed and open system*. Master of philosophy, City University of Hong Kong, 2006.

[11] A. Croxford, P. Wilcox, B. Drinkwater, and G. Konstantinidis. Strategies for guided-wave structural health monitoring. *Proceedings of the Royal Society A: Mathematical, Physical and Engineering Sciences*, 463(2087):2961–2981, November 2007.

[12] D. Adams. *Health monitoring of structural materials and components*. 2007.

[13] C. Boller, F. Chang, and Y. Fujino. *Encyclopedia of Structural Health Monitoring*. Wiley, 2009.

[14] S. Doebling, C. Farrar, and M. Prime. Damage identification and health monitoring of structural and mechanical systems from changes in their vibration characteristics a literature review. Technical report, 1996.

[15] M. B. Doebling, S. W., Farrar, C. R., & Prime. A Summary Review of Vibration-Based Damage Identification Methods. *The Shock and Vibration Digest*, 30(2):91–105, 1998.

[16] J. J. Farrar, C. R., Hemez, F. M., Shunk, D. D., Stinemates, D. W., Nadler, B. R., & Czarnecki. A review of structural health monitoring literature: 1996-2001. Technical report, Los Alamos, New Mexico: Los Alamos National Laboratory., 2001.

[17] C. R. C. Farrar, S. W. Doebling, and D. a. Nix. Vibration based structural damage identification. *Philosophical Transactions of the Royal Society of London. Series A: Mathematical, Physical and Engineering Sciences*, 359(1778):131–149, January 2001.

[18] C. R. Farrar and K. Worden. An introduction to structural health monitoring. *Philosophical Transactions. Series A, Mathematical, Physical, and Engineering Sciences*, 365(1851):303–15, February 2007.

[19] E. P. Carden. Vibration based condition monitoring: A review. *Structural Health Monitoring*, 3(4):355–377, December 2004.

[20] K. Worden and G. Manson. The application of machine learning to structural health monitoring. *Philosophical transactions. Series A, Mathematical, physical, and engineering sciences*, 365(1851):515–37, February 2007.

[21] C. Study. Vibration-based Damage Identification Methods: A Review and Comparative Study. *Structural Health Monitoring*, 10(1):83–111, April 2010.

[22] P. C. Chang, A. Flatau, and S. C. Liu. Review paper: health monitoring of civil infrastructure. *Structural health monitoring*, 2(3):257–267, 2003.

[23] D. Barke and W. K. Chiu. Structural health monitoring in the railway industry: a review. *Structural Health Monitoring*, 4(1):81–93, 2005.

[24] P. Pawar and R. Ganguli. *Structural Health Monitoring Using Genetic Fuzzy Systems*. Springer, 2011.

[25] T. Clarke and F. Simonetti. *Guided wave health monitoring of complex structures by sparse array systems*. PhD thesis, 2010.

[26] M. M. R. Taha. Wavelet Transform for Structural Health Monitoring: A Compendium of Uses and Features. *Structural Health Monitoring*, 5(3):267–295, September 2006.

[27] A. Larder. Helicopter HUM/FDR: benefits and developments. *ANNUAL FORUM PROCEEDINGS-AMERICAN HELICOPTER SOCIETY*, 55(May):25–27, 1999.

[28] W. Staszewski, G. Tomlinson, and C. Boller. *Health Monitoring of Aerospace Structures Smart Sensor Technologies and Signal Processing*. Wiley Online Library, 2004.

[29] K. Worden and J. M. Dulieu-Barton. An Overview of Intelligent Fault Detection in Systems and Structures. *Structural Health Monitoring*, 3(1):85–98, March 2004.

[30] B. Culshaw. Smart structures and materials. *Boston, MA: Artech House, 1996.*, (November):27–41, 1996.

[31] http://arc-p-shift.blogspot.com.es/.

[32] http://woodstone-corp.com/.

[33] D. Inman, Charles R. Farrar, V. L. Junior, and V. S. Junio. *Damage Prognosis: for Aerospace, Civil and Mechanical systems.* John Wiley & Sons Inc, 2005.

[34] P. Capoluongo, C. Ambrosino, S. Campopiano, A. Cutolo, M. Giordano, I. Bovio, L. Lecce, and A. Cusano. Modal analysis and damage detection by Fiber Bragg grating sensors. *Sensors and Actuators A: Physical*, 133(2):415–424, 2007.

[35] http://grafeno.com/tag/corrosion/.

[36] C. Lee, J. Scholey, and P. Wilcox. Guided wave acoustic emission from fatigue crack growth in aluminium plate. *Advanced Materials*, 14:23–28, 2006.

[37] J. E. Michaels. Detection, localization and characterization of damage in plates with an in situ array of spatially distributed ultrasonic sensors. *Smart Materials and Structures*, 17(3):35035, 2008.

[38] P. Cawley. The detection of delaminations using flexural waves. *NDT International*, 23(4):207–213, August 1990.

[39] A. Rytter. *Vibration based inspection of civil engineering structures.* PhD thesis, University of Aalborg, Denmark, 1993.

[40] D. Balageas, C.-P. Fritzen, and A. Güemes. *Structural Health Monitoring*, volume 7. ISTE Ltd, London, March 2006.

[41] C. P. Fritzen. Vibration-Based Techniques for Structural Health Monitoring. In D. Balageas, C.-P. Fritzen, and A. Güemes, editors, *Structural Health Monitoring*, chapter 2, pages 45–225. ISTE Ltd, 2006, London, 2006.

[42] D. Balageas, C.-P. Fritzen, and A. Güemes. Structural Health Monitoring. In *Structural Health Monitoring*, chapter Vibration-, pages 45–224. 2006.

[43] Z. Su, L. Ye, and Y. Lu. Guided Lamb waves for identification of damage in composite structures: A review. *Journal of sound and vibration*, 295(3-5):753–780, 2006.

[44] A. Raghavan. *Review of guided-wave structural health monitoring.* PhD thesis, 2007.

[45] D. E. Chimenti. Guided Waves in Plates and Their Use in Materials Characterization. *Applied Mechanics Reviews*, 50(5):247, 1997.

[46] K. Pearson. On lines and planes of closest fit to systems of points in space. *Philosophical Magazine*, 2(6):559–572, 1901.

[47] H. Hotelling. Analysis of a complex of statistical variables into principal components. *Educational Psychology*, 24(6):417–441, 1933.

[48] J. Lumley. *Stochastic Tools In Turbulence*. Academic Press, New York, 1970.

[49] I. Jolliffe. *Principal Component Analysis*, volume 2. John Wiley & Sons, Ltd, 2002.

[50] C. Ding and X. He. K-means clustering via principal component analysis. In *Proceedings of the twenty-first international conference on Machine learning*, page 29, 2004.

[51] A. Ben-Hur and I. Guyon. Detecting stable clusters using principal component analysis. *Methods and Protocols*, 224(1):159–182, 2003.

[52] M. Johnson. Waveform based clustering and classification of AE transients in composite laminates using principal component analysis. *NDT and E International*, 35(6):367–376, 2002.

[53] G. Manson, K. Worden, K. Holford, and R. Pullin. Visualisation and Dimension Reduction of Acoustic Emission Data for Damage Detection. *Journal of Intelligent Materials Systems and Structures*, 12(8):529–536, August 2001.

[54] W. Li, T. Shi, G. Liao, and S. Yang. Feature extraction and classification of gear faults using principal component analysis. *Journal of Quality in Maintenance Engineering*, 9(2):132–143, 2003.

[55] F. Tong, S. Tso, and M. Hung. Impact-acoustics-based health monitoring of tile-wall bonding integrity using principal component analysis. *J. Sound and Vibration*, 294(1-2):329–340, June 2006.

[56] F. Mustapha, G. Manson, S. G. Pierce, and K. Worden. Structural Health Monitoring of an Annular Component using a Statistical Approach. *Strain*, 41(3):117–127, August 2005.

[57] F. Mustapha, K. Worden, and S. Pierce. Damage detection using stress waves and multivariate statistics, an experimental case study of an aircraft component. *Strain*, 43(1):47–53, 2007.

[58] M. Cammarata, P. Rizzo, D. Dutta, and H. Sohn. Application of principal component analysis and wavelet transform to fatigue crack detection in waveguides. *Smart Structures and Systems*, 6(4):349–362, 2010.

[59] G. K. J.-C. Golinval, P. De Boe, A.-M. Yan. Structural damage detection based on PCA of vibration measurements. In *58th Meeting of the Soc. for Mach. Failure Prevention Tech*, Virginia Beach,USA, 2004.

[60] P. De Boe and J.-C. Golinval. Principal Component Analysis of a Piezosensor Array for Damage Localization. *Structural Health Monitoring*, 2(2):137–144, June 2003.

[61] M. Pirra, E. Gandino, A. Torri, L. Garibaldi, and J. M. Machorro-Lopez. PCA algorithm for detection, localisation and evolution of damages in gearbox bearings. *Journal of Physics: Conference Series*, 305(1):012019, July 2011.

[62] R. Zimroz and A. Bartkowiak. Investigation on Spectral Structure of Gearbox Vibration Signals by Principal Component Analysis for Condition Monitoring Purposes. *Journal of Physics: Conference Series*, 305(1):012075, July 2011.

[63] Q. He, R. Yan, F. Kong, and R. Du. Machine condition monitoring using principal component representations. *Mechanical Systems and Signal Processing*, 23(2):446–466, February 2009.

[64] L. Mujica, J. Rodellar, A. Fernandez, and A. Guemes. Q-statistic and T2-statistic PCA-based measures for damage assessment in structures. *Structural Health Monitoring*, 10(5):539–553, November 2010.

[65] N. Baydar, Q. Chen, A. Ball, and U. Kruger. Detection of Incipient Tooth Defect in Helical Gears Using Multivariate Statistics. *Mechanical Systems and Signal Processing*, 15(2):303–321, March 2001.

[66] L. E. Mujica, W. Staszewski, J. Rodellar, J. Vehi, and K. Worden. Extended PCA visualisation of system damage features under environmental and operational variations. *Proc. SPIE 7286, Modeling, Signal Processing, and Control for Smart Structures*, 44(0), 2009.

[67] G. Tondreau, D. Arnaud, and P. Evangelos. Experimental damage detection using modal filters on an aircraft wing. In *Proceedings of the 8th International Conference on Structural Dynamics, EURODYN 2011*, Leuven, Belgium, 4-6 July 2011, 2011.

[68] D. A. Tibaduiza, L. E. Mujica, and J. Rodellar. Damage classification in structural health monitoring using principal component analysis and self-organizing maps. *Structural Control and Health Monitoring*, 2012.

[69] Z. Peng. Application of the wavelet transform in machine condition monitoring and fault diagnostics: a review with bibliography. *Mechanical Systems and Signal Processing*, 18(2):199–221, March 2004.

[70] L. Cohen. Time-frequency distributions-a review. *Proceedings of the IEEE*, 77(7):941 – 981, 1989.

[71] S. Mallat. *A Wavelet Tour of Signal Processing*. Academic Press, San Diego, 1999.

[72] X. Deng and Q. Wang. Structural health monitoring using active sensors and wavelet transforms. In *In 1999 Symposium on Smart Structures and Materials*, number March, pages 1–5, 1999.

[73] M. Piombo, B. A. D., Fasana, A., Marchesiello, S., & Ruzzene. Modelling and Identification of the Dynamic Response of a Supported Bridge. *Mechanical Systems and Signal Processing*, 14(1):75–89, January 2000.

[74] W. J. Staszewski. Identification of non-linear systems using multi-scale ridges and skeletons of the wavelet transform. *Journal of Sound and Vibration*, 214(4):639–658, July 1998.

[75] J. H. Suh, S. R. T. Kumara, and S. P. Mysore. Machinery Fault Diagnosis and Prognosis: Application of Advanced Signal Processing Techniques. *CIRP Annals - Manufacturing Technology*, 48(1):317–320, 1999.

[76] H. Sohn, G. Park, J. R. Wait, N. P. Limback, and C. R. Farrar. Wavelet-based active sensing for delamination detection in composite structures. *Smart Materials and Structures*, 13(1):153–160, February 2004.

[77] T. Dawood, M. Sahin, R. Shenoi, and T. Newson. Real-time damage detection of a composite cantilever beam using wavelet transforms. In *First European Workshop on Structural Health Monitoring*, Paris, France, 2002.

[78] Z. Hou, M. Noori, and R. Amand. Wavelet-based approach for structural damage detection. *Journal of Engineering Mechanics*, 126(7):677–683, 2000.

[79] W. J. Staszewski and G. R. Tomlinson. Application of the wavelet transform to fault detection in a spur gear. *Mechanical Systems and Signal Processing*, 8(3):289–307, 1994.

[80] S. Masuda, A., Nakaoka, A., Sone, A., and Yamamoto. Health monitoring system of structures based on orthonormal wavelet transform. *Seismic Engrg.*, 312:161–167, 1995.

[81] A. Abbate, J. Koay, J. Frankel, S. C. Schroeder, and P. Das. Signal detection and noise suppression using a wavelet transform signal processor: application to ultrasonic flaw detection. *Ultrasonics, Ferroelectrics and Frequency Control, IEEE Transactions on*, 44(1):14–26, January 1997.

[82] S. Legendre and D. Massicotte. Wavelet-transform-based method of analysis for Lamb-wave ultrasonic NDE signals. *Instrumentation and Measurement, IEEE Transactions on*, 49(3):524–530, 2000.

[83] C. Sung, H. Tai, and C. Chen. Locating defects of a gear system by the technique of wavelet transform. *Mechanism and Machine Theory*, 35(8):1169–1182, August 2000.

[84] Y. Yan and L. Yam. Online detection of crack damage in composite plates using embedded piezoelectric actuators/sensors and wavelet analysis. *Composite Structures*, 58(1):29–38, October 2002.

[85] M. Browne, S. Shiry, M. Dorn, and R. Ouellette. Visual feature extraction via PCA-based parameterization of wavelet density functions. In *International Symposium on Robots and Automation, Toluca, Mexico*, volume 648, pages 1–5. Citeseer, 2002.

[86] C. Ogaja, J. Wang, and C. Rizos. Principal component analysis of wavelet transformed GPS data for deformation monitoring. In *Proceedings of IAG Scientific Meeting*, volume 2, 2001.

[87] K. N. Kesavan and A. S. Kiremidjian. A wavelet-based damage diagnosis algorithm using principal component analysis. *Structural Control and Health Monitoring*, 19(8):672–685, 2011.

[88] A. Tjirkallis, A. Kyprianou, and G. Vessiaris. Structural Health Monitoring under Varying Environmental Conditions Using Wavelets. *Key Engineering Materials*, 569 - 570:1218–1225, 2013.

[89] M. Soorgee and A. Yousefi-Koma. Crack Diagnosis in Plates Using Propagated Waves and Hilbert Huang Transformation. In *4th international conference on NDT*, page 6, Chania, Crete-Greece, 2007.

[90] H. Sohn, H. Park, K. Law, and C. Farrar. Damage detection in composite plates by using an enhanced time reversal method. *Journal of Aerospace Engineering*, 20(3):141–151, 2004.

[91] B. Poddar, C. R. Bijudas, M. Mitra, and P. M. Mujumdar. Damage detection in a woven-fabric composite laminate using time-reversed Lamb wave. *Structural Health Monitoring*, 11(5):602–612, July 2012.

[92] J. E. Michaels and T. E. Michaels. An integrated strategy for detection and imaging of damage using a spatially distributed array of piezoelectric sensors. *Smart Materials and Structures*, 17(3):035035, 2008.

[93] Y. Lu, X. Wang, J. Tang, and Y. Ding. Damage detection using piezoelectric transducers and the Lamb wave approach: II. Robust and quantitative decision making. *Smart Materials and Structures*, 17(2):025034, April 2008.

[94] X. Wang, Y. Lu, and J. Tang. Damage detection using piezoelectric transducers and the Lamb wave approach: I. System analysis. *Smart Materials and Structures*, 17(2):025033, April 2008.

[95] V. Meruane and W. Heylen. Damage Detection with Parallel Genetic Algorithms and Operational Modes. *Structural Health Monitoring*, 9(6):481–496, March 2010.

[96] Q. Zhou, Y. Ning, L. Luo, and J. Lei. Structural damage detection method based on random forests and data fusion. *Structural Health Monitoring*, 12(1):48–58, November 2012.

[97] C. Haynes, M. D. Todd, E. Flynn, and a. Croxford. Statistically-based damage detection in geometrically-complex structures using ultrasonic interrogation. *Structural Health Monitoring*, 12(2):141–152, December 2012.

[98] S. Casciati. Statistical approach to a SHM benchmark problem. *Smart Struct. Syst*, 6(1):17–27, 2010.

[99] E. Figueiredo, C. Farrar, and M. Todd. Autoregressive Modeling with State-Space Embedding Vectors for Damage Detection under Operational and Environmental Variability. In *The Fifth European Workshop on Structural Health Monitoring*, Sorrento, Italy, 2010.

[100] T. R. Fasel and M. D. Todd. An adhesive bond state classification method for a composite skin-to-spar joint using chaotic insonification. *Journal of Sound and Vibration*, 329(15):3218–3232, July 2010.

[101] Y. J. Yan, L. Cheng, Z. Y. Wu, and L. H. Yam. Development in vibration-based structural damage detection technique. *Mechanical Systems and Signal Processing*, 21(5):2198–2211, 2007.

[102] T. R. Fasel, S. W. Gregg, T. J. Johnson, C. R. Farrar, and H. Sohn. Experimental modal analysis and damage detection in a simulated three story building. In *Proceedings of IMAC XX: A Conference on Structural Dynamics*, 2002.

[103] H. Sohn and C. R. Farrar. Damage diagnosis using time series analysis of vibration signals. *Smart materials and structures*, 10(3):446, 2001.

[104] H. Sohn, C. Farrar, and N. Hunter. Structural health monitoring using statistical pattern recognition techniques. *Journal of Dynamic Systems*, 123(4):706, 2001.

[105] H. Sohn. Effects of environmental and operational variability on structural health monitoring. *Philosophical Transactions. Series A, Mathematical, Physical, and Engineering Sciences*, 365(1851):539–60, February 2007.

[106] Y. Lu and J. E. Michaels. A methodology for structural health monitoring with diffuse ultrasonic waves in the presence of temperature variations. *Ultrasonics*, 43(9):717–31, October 2005.

[107] C. Farrar, W. Baker, T. Bell, and K. Cone. Dynamic characterization and damage detection in the I-40 bridge over the Rio Grande. Technical report, 1994.

[108] M. G. Wood. *Damage Analysis of Bridge Structures Using Vibrational Techniques*. PhD thesis, University of Aston,Birmingham, UK, 1992.

[109] E. J. Blaise and F.-K. Chang. Built-in damage detection system for sandwich structures under cryogenic temperatures. In *Third International Workshop on Structural Health Monitoring*, pages 154–163, July 2001.

[110] G. Konstantinidis, P. D. P. P. D. Wilcox, and B. B. W. Drinkwater. An investigation into the temperature stability of a guided wave structural health monitoring system using permanently attached sensors. *Sensors Journal, IEEE*, 7(5):905–912, 2007.

[111] R. B. Williams, D. J. Inman, and W. K. Wilkie. Temperature-dependent thermoelastic properties for macro fiber composite actuators. *Journal of Thermal Stresses*, 27(10):903–915, 2004.

[112] a. Raghavan and C. E. Cesnik. Effects of Elevated Temperature on Guided-wave Structural Health Monitoring. *Journal of Intelligent Material Systems and Structures*, 19(12):1383–1398, May 2008.

[113] M. Schulz and M. Sundaresan. Piezoelectric materials at elevated temperature. *Journal of Intelligent Material Systems and Structures*, 14(11):693–705, 2003.

[114] R. G. Rohrmann, M. Baessler, S. Said, W. Schmid, and W. F. Ruecker. Structural causes of temperature affected modal data of civil structures obtained by long time monitoring. In *Proceedings of IMAC-XVIII: A Conference on Structural Dynamics*, volume 4062, pages 1–7. Society of Photo-Optical Instrumentation Engineers, 2000.

[115] Y. Xia, H. Hao, G. Zanardo, and A. Deeks. Long term vibration monitoring of an RC slab: temperature and humidity effect. *Engineering Structures*, 28(3):441–452, 2006.

[116] B. Peeters and G. De Roeck. One-year monitoring of the Z 24-Bridge: environmental effects versus damage events. *Earthquake engineering & structural dynamics*, 30(2):149–171, 2001.

[117] S. Alampalli. Influence of in-service environment on modal parameters. In *PROCEEDINGS-SPIE THE INTERNATIONAL SOCIETY FOR OPTICAL ENGINEERING*, volume 1, pages 111–116. SPIE INTERNATIONAL SOCIETY FOR OPTICAL, 1998.

[118] E. J. Cross, G. Manson, K. Worden, and S. G. Pierce. Features for damage detection with insensitivity to environmental and operational variations. *Proceedings of the Royal Society A: Mathematical, Physical and Engineering Sciences*, 468(2148):4098–4122, October 2012.

[119] G. Manson. Identifying damage sensitive,environmental insensitive featuresfor damage detection. In *In Proceedings of the IES conference*, University of Wales Swansea, UK, 2002.

[120] A.-M. Yan, G. Kerschen, P. Deboe, J.-C. Golinval, and P. De Boe. Structural damage diagnosis under varying environmental conditions part II: local PCA for non-linear cases. *Mechanical Systems and Signal Processing*, 19(4):865–880, July 2005.

[121] A. Bellino, A. Fasana, L. Garibaldi, and S. Marchesiello. PCA-based detection of damage in time-varying systems. *Mechanical Systems and Signal Processing*, 24(7):2250–2260, October 2010.

[122] B. Lee, G. Manson, and W. Staszewski. Environmental Effects on Lamb Wave Responses from Piezoceramic Sensors. *Materials Science Forum*, 440-441:195–202, 2003.

[123] J. T. Chambers, B. L. Wardle, and S. S. Kessler. Durability assessment of Lamb wave-based structural health monitoring nodes. In *Proceedings of the 47th AIAA/ASME/ASCE/AHS/ASC Structures, Structural Dynamics, and Materials Conference*, pages 1–12, 2006.

[124] H. Sohn, K. Worden, and C. R. Farrar. Statistical Damage Classification Under Changing Environmental and Operational Conditions. *Journal of Intelligent Material Systems and Structures*, 13(9):561–574, September 2002.

[125] F. di Scalea and S. Salamone. Temperature effects in ultrasonic Lamb wave structural health monitoring systems. *The Journal of the Acoustical Society of America*, 124(July):161, 2008.

[126] K. Worden. Novelty Detection in a Changing Environment: Regression and Interpolation Approaches. *Journal of Sound and Vibration*, 258(4):741–761, December 2002.

[127] J. P. Andrews, a. N. Palazotto, M. P. DeSimio, and S. E. Olson. Lamb Wave Propagation in Varying Isothermal Environments. *Structural Health Monitoring*, 7(3):265–270, July 2008.

[128] J. Harley and J. Moura. Scale transform signal processing for optimal ultrasonic temperature compensation. *Ultrasonics, Ferroelectrics and Frequency Control, IEEE Transactions on*, 59(10):2226–36, October 2012.

[129] G. Konstantinidis and B. Drinkwater. The temperature stability of guided wave structural health monitoring systems. *Smart Materials and Structures*, 15(4):967, 2006.

[130] A. J. Croxford, J. Moll, P. D. Wilcox, and J. E. Michaels. Efficient temperature compensation strategies for guided wave structural health monitoring. *Ultrasonics*, 50(4-5):517–28, April 2010.

[131] B. C. Lee and W. J. Staszewski. Modelling of Lamb waves for damage detection in metallic structures: Part II. Wave interactions with damage. *Smart Materials and Structures*, 12(5):815, 2003.

[132] D N Alleyne, B. Pavlakovic, M. J. S. Lowe, and P. Cawley. Rapid, Long Range Inspection of Chemical Plant Pipework Using Guided Waves. *Key Engineering Materials*, 270-273(2001):180–187, August 2001.

[133] M. L. P Wilcox, M Evans, B Pavlakovic, David N Alleyne, K Vine, P Cawley. Guided wave testing of rail. *Insight*, 45(6):413–420, 2003.

[134] S. Grondel, C. Paget, C. Delebarre, J. Assaad, and K. Levin. Design of optimal configuration for generating A0 Lamb mode in a composite plate using piezoceramic transducers. *The Journal of the Acoustical Society of America*, 112(1):84–90, July 2002.

[135] E. V. Glushkov, N. V. Glushkova, O. V. Kvasha, and R. Lammering. Selective Lamb mode excitation by piezoelectric coaxial ring actuators. *Smart Materials and Structures*, 19(3):35018, 2010.

[136] L. Rayleigh. On waves propagated along the plane surface of an elastic solid. *Proceedings of the London Mathematical*, iv(42), 1885.

[137] H. Lamb. On waves in an elastic plate. *Proceedings of the Royal Society, A: Mathematical, Physical and Engineering Sciences*, 93(648):114–128, 1917.

[138] J. Rose. *Ultrasonic Waves in Solid Media*. Cambridge University Press, August 1999.

[139] J. L. Rose, J. J. Ditri, A. Pilarski, K. Rajana, and F. Carr. A guided wave inspection technique for nuclear steam generator tubing. *NDT & E International*, 27(6):307–310, December 1994.

[140] J. Achenbach. *Wave Propagation in Elastic Solids*. North-Holland Pub. Co./American Elsevier Pub. Co., New York, USA, 1973.

[141] N. Gandhi. *Determination of dispersion curves for acoustoelastic lamb wave propagation*. PhD thesis, 2010.

[142] Piezo-University, 2013.

[143] S. Kessler and S. Spearing. In-situ damage detection of composites structures using Lamb wave methods. In *Proceedings of the First European Workshop on Structural Health Monitoring*, pages 10–12, 2002.

[144] C. Wang. Diagnosis of impact damage in composite structures with built-in piezoelectrics network. In *SPIE's 7th Annual International Symposium on Smart Structures and Materials*, pages 13–19, 2000.

[145] S. V. Dangeti. *Denoising Techniques-A Comparison (Ph.D. Thesis)*. Master's thesis, Louisiana State University, 2003.

[146] A. Antoniadis. Wavelets in statistics: A review. *Journal of the Italian Statistical Society*, 6(2):97–130, 1997.

[147] Mathworks. Automatic 1-D de-noising, 2012.

[148] C. Boller. Ways and options for aircraft structural health management. *Smart Materials and Structures*, 10(3):432–440, June 2001.

[149] J. Shlens. A tutorial on Principal Component Analysis. *Systems Neurobiology Laboratory, University of California at San Diego*, page 12, 2005.

[150] L. I. Smith. A tutorial on Principal Components Analysis. Technical report, Cornell University, USA, 2002.

[151] Visumap. A Layman's Introduction,, 2011.

[152] C. Wan and A. Mita. Early warning of hazard for pipelines by acoustic recognition using principal component analysis and one-class support vector machines. *Smart Structures and Systems*, 6(4):1–17, 2010.

[153] D. M. Hawkins. *Identification of Outliers*. Monographs on Applied Probability and Statistics. Taylor & Francis, 1980.

[154] V. Barnett and T. Lewis. *Outliers in statistical data*. Wiley series in probability and mathematical statistics: Applied probability and statistics. Wiley & Sons, 3, illustr edition, 1994.

[155] R. A. Johnson and D. W. Wichern. *Applied Multivariate Statistical Analysis*. Pearson Prentice Hall, 6, illustr edition, 2007.

[156] M. Daszykowski, K. Kaczmarek, Y. Vander Heyden, B. Walczak, and Y. Vanderheyden. Robust statistics in data analysis - A review Basic concepts. *Chemometrics and Intelligent Laboratory Systems*, 85(2):203–219, February 2007.

[157] P. J. Rousseeuw and A. M. Leroy. *Robust Regression and Outlier Detection*. Wiley Series in Probability and Statistics. Wiley, 2003.

[158] E. Acuna and C. Rodriguez. A meta analysis study of outlier detection methods in classification. Technical report, Department of Mathematics, University of Puerto Rico at Mayaguez, Venice, 2004.

[159] I. Ben-gal. Outlier Detection. In *Data Mining and Knowledge Discovery Handbook*, pages 131–146. Springer US., 2005.

[160] M. Hubert, P. J. Rousseeuw, and K. V. Branden. ROBPCA a new approach to robust principal component analysis. *Technometrics*, 47(1):64–79, 2005.

[161] P. J. Rousseeuw. Least Median of Squares Regression. *Journal of the American Statistical Association*, 79(388):871–880, December 1984.

[162] P. J. Rousseeuw and K. Van Driessen. A fast algorithm for the minimum covariance determinant estimator. *Technometrics*, 41(3):212–223, 1999.

[163] C. Croux and A. Ruiz-Gazen. High breakdown estimators for principal components: the projection-pursuit approach revisited. *Journal of Multivariate Analysis*, 95(1):206–226, July 2005.

[164] M. Hubert. A fast method for robust principal components with applications to chemometrics. *Chemometrics and Intelligent Laboratory Systems*, 60(1-2):101–111, January 2002.

[165] C. Croux, P. Filzmoser, and H. Fritz. A Comparison of Algorithms for the Multivariate L1-Median. *CentER Discussion Paper Serie*, 2010-106, 2010.

[166] G. Li and Z. Chen. Projection-Pursuit Approach to Robust Dispersion Matrices and Principal Components: Primary Theory and Monte Carlo. *Journal of the American Statistical Association*, 80(391):759–766, September 1985.

[167] I. Stanimirova. A comparison between two robust PCA algorithms. *Chemometrics and Intelligent Laboratory Systems*, 71(1):83–95, April 2004.

[168] S. Engelen, M. Hubert, K. V. Branden, and K. U. Leuven. A Comparison of Three Procedures for Robust PCA in High Dimensions. *Analysis*, 34(2):117–126, 2005.

[169] S. Vanlanduit, E. Parloo, B. Cauberghe, P. Guillaume, and P. Verboven. A robust singular value decomposition for damage detection under changing operating conditions and structural uncertainties. *Journal of Sound and Vibration*, 284(3-5):1033–1050, June 2005.

[170] P. Luukka. Classification based on fuzzy robust PCA algorithms and similarity classifier. *Expert Systems with Applications*, 36(4):7463–7468, May 2009.

[171] T.-N. Yang and S.-D. Wang. Robust algorithms for principal component analysis. *Pattern Recognition Letters*, 20(9):927–933, September 1999.

[172] E. Oja. A simplified neuron model as a principal component analyzer. *Journal of mathematical biology*, 15(3):267–73, January 1982.

[173] E. Oja and J. Karhunen. On stochastic approximation of the eigenvectors and eigenvalues of the expectation of a random matrix. *Journal of mathematical analysis and applications*, 106(1):69–84, 1985.

[174] D. Andrews. Plots of high-dimensional data. *Biometrics*, 28(1):125–136, 1972.

[175] N. Spencer. Investigating data with Andrews plots. *Social science computer review*, 21(2):244, 2003.

[176] R. Khattree. Andrews plots for multivariate data: some new suggestions and applications. *Journal of Statistical Planning and Inference*, 100(2):411–425, February 2002.

[177] L. A. Zadeh. Similarity relations and fuzzy orderings. *Inf. Sci.*, 3(2):177–200, April 1971.

[178] P. Luukka, K. Saastamoinen, and V. Kononen. A classifier based on the maximal fuzzy similarity in the generalized Lukasiewicz-structure. In *Fuzzy Systems, 2001. The 10th IEEE International Conference on. IEEE*, volume 1, pages 195–198. Ieee, 2001.

[179] J. Lukasiewicz. *Selected Works*. Cambridge University Press, Cambridge, 1970.

[180] P. Luukka and T. Leppälampi. Similarity classifier with generalized mean applied to medical data. *Computers in Biology and Medicine*, 36(9):1026–40, September 2006.

[181] A. Grossmann and J. Morlet. Decomposition of Hardy functions into square integrable wavelets of constant shape. *SIAM journal on mathematical analysis*, 15(4):723–736, 1984.

[182] a. Graps. An introduction to wavelets. *IEEE Computational Science and Engineering*, 47(2):50–61, 1995.

[183] A. V. Ovanesova and L. E. Suárez. Applications of wavelet transforms to damage detection in frame structures. *Engineering Structures*, 26(1):39–49, January 2004.

[184] A. Tjirkallis. *Real time structural health monitoring under varying environmental and operational conditions using wavelet transform modulus maxima decay lines similarity*. PhD thesis, University of Cyprus, 2013.

[185] R. Carmona, W. Hwang, and B. Torresani. Characterization of signals by the ridges of their wavelet transforms. *IEEE Transactions on Signal Processing*, 45(10):2586–2590, 1997.

[186] M. Haase and J. Widjajakusuma. Damage identification based on ridges and maxima lines of the wavelet transform. *International Journal of Engineering Science*, 41(13):1423–1443, 2003.

[187] B. B. Hubbard. *World According To Wavelests: The Story Of A Mathematical Technique In Making.* Ak Peters Series. Universities Press, 1996.

[188] T. Kijewski and A. Kareem. Wavelet transforms for system identification and associated processing concerns. In *Proceedings of ASCE Engineering Mechanics Conference*, pages 1–8, Columbia University, New York, NY, 2002.

[189] A. Z. Abid, M. a. Gdeisat, D. R. Burton, and M. J. Lalor. Ridge extraction algorithms for one-dimensional continuous wavelet transform: a comparison. *Journal of Physics: Conference Series*, 76:012045, July 2007.

[190] R. Carmona, W. L. Hwang, B. Torresani, and Rene Carmona Wen L. Hwang Bruno Torresani. *Practical Time-Frequency Analysis: Gabor and Wavelet Transforms, with an Implementation in S.* Wavelet Analysis and Its Applications. Elsevier Science, 1998.

[191] L. Kaufman and P. J. Rousseeuw. *Finding groups in data: an introduction to cluster analysis.* Wiley series in probability and mathematical statistics. Applied probability and statistics. Wiley. com, 2005.

[192] T. Zhang, R. Ramakrishnan, and M. Livny. An Efficient Data Clustering Method for Very Large Databases, 1996.

[193] M. Ester, H. Kriegel, J. Sander, and X. Xu. A density-based algorithm for discovering clusters in large spatial databases with noise. *Proceedings of the 2nd International on KDD*, 96:226–231, 1996.

[194] X. Xu and M. Ester. A distribution-based clustering algorithm for mining in large spatial databases. In *Data Engineering, 1998. Proceedings., 14th International Conference on IEEE*, pages 324–331, 1998.

[195] G. Sheikholeslami, S. Chatterjee, and A. Zhang. Wavecluster: A multi-resolution clustering approach for very large spatial databases. In *24th VLDB Conference*, pages 428–439, New York, USA, 1998.

[196] R. Urquhart. Graph theoretical clustering based on limited neighbourhood sets. *Pattern Recognition*, 15(3):173–187, 1982.

[197] L. Rokach and O. Maimon. Distance Measures for Numeric Attributes. In *Data Mining and Knowledge Discovery Handbooknowledge discovery handbook*, pages 322–352. 2010.

[198] G. Sheikholeslami, S. Chatterjee, and A. Zhang. WaveCluster: a wavelet-based clustering approach for spatial data in very large databases. *The VLDB Journal The International Journal on Very Large Data Bases*, 8(3-4):289–304, February 2000.

[199] B. Horn. *Robot Vision.* Mit Press, 1986.

[200] www.krohn-hite.com.

[201] http://www.ni.com/.

[202] http://www.tiepie.com/.

[203] A. Kovalovs, E. Barkanov, and S. Gluhihs. Active control of structures using macro-fiber composite (MFC). *Journal of Physics: Conference Series*, 93(1):12034, 2007.

[204] L. E. Mujica, J. Vehi, M. Ruiz, M. Verleysen, W. Staszewski, and K. Worden. Multivariate statistics process control for dimensionality reduction in structural assessment. *Mechanical Systems and Signal Processing*, 22:155–171, 2008.

[205] G. Rote. Computing the minimum Hausdorff distance between two point sets on a line under translation. *Information Processing Letters*, 38(3):123–127, May 1991.

[206] D. A. Tibaduiza. *Design and validation of a structural health monitoring system for aeronautical structures*. PhD thesis, Technical University of Catalunya, 2013.

[207] F. Gharibnezhad, L. E. Mujica, and J. Rodellar. Damage detection using Andrew plots. In *proceedings of the 8th International Workshop on Structural Health Monitoring*, Stanford University, Stanford, CA, 2011.

[208] H. W. Lilliefors. On the Kolmogorov-Smirnov test for the exponential distribution with mean unknown. *Journal of the American Statistical Association*, 64(325):387–389, March 1969.